frontiers | Research Topics

# Investigating the interplay between tumor mutations, immune evasion, and targeted therapy resistance

**Edited by**
Shanye Yin, Guangchuang Yu and Yinghao Wu

**Published in**
Frontiers in Oncology

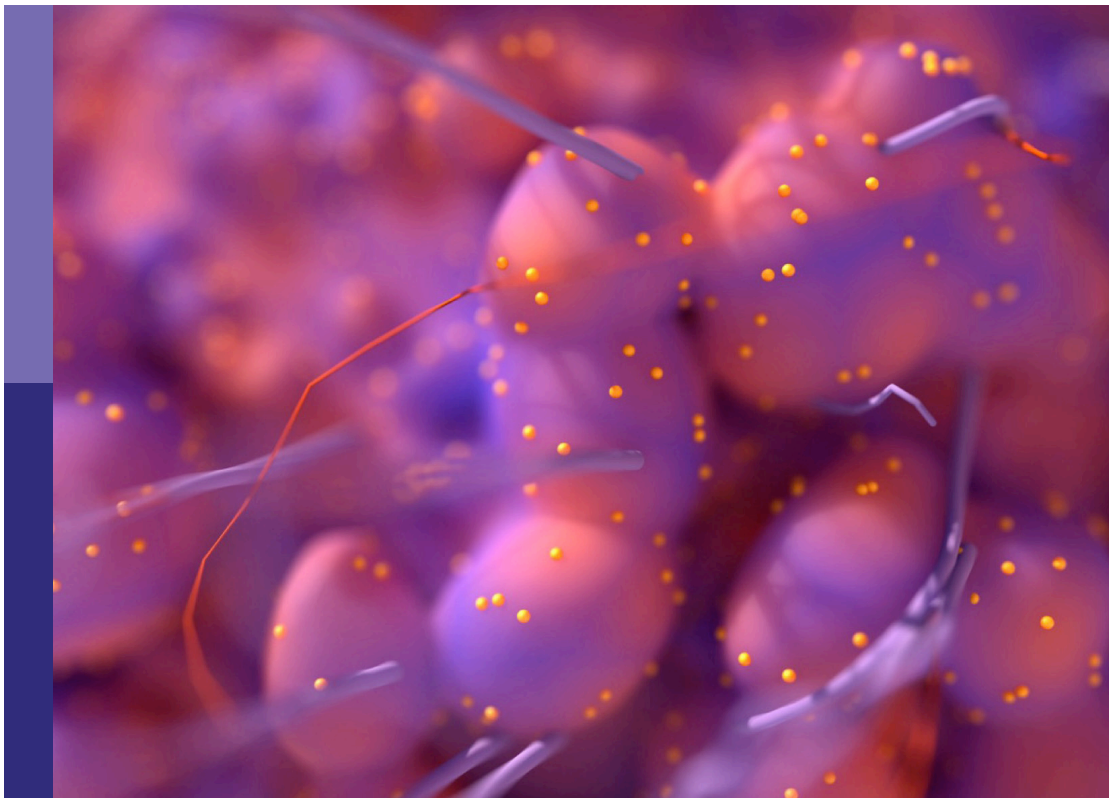

ISSN 1664-8714
ISBN 978-2-8325-6267-3
DOI 10.3389/978-2-8325-6267-3

## About Frontiers

Frontiers is more than just an open access publisher of scholarly articles: it is a pioneering approach to the world of academia, radically improving the way scholarly research is managed. The grand vision of Frontiers is a world where all people have an equal opportunity to seek, share and generate knowledge. Frontiers provides immediate and permanent online open access to all its publications, but this alone is not enough to realize our grand goals.

## Frontiers journal series

The Frontiers journal series is a multi-tier and interdisciplinary set of open-access, online journals, promising a paradigm shift from the current review, selection and dissemination processes in academic publishing. All Frontiers journals are driven by researchers for researchers; therefore, they constitute a service to the scholarly community. At the same time, the *Frontiers journal series* operates on a revolutionary invention, the tiered publishing system, initially addressing specific communities of scholars, and gradually climbing up to broader public understanding, thus serving the interests of the lay society, too.

## Dedication to quality

Each Frontiers article is a landmark of the highest quality, thanks to genuinely collaborative interactions between authors and review editors, who include some of the world's best academicians. Research must be certified by peers before entering a stream of knowledge that may eventually reach the public - and shape society; therefore, Frontiers only applies the most rigorous and unbiased reviews. Frontiers revolutionizes research publishing by freely delivering the most outstanding research, evaluated with no bias from both the academic and social point of view. By applying the most advanced information technologies, Frontiers is catapulting scholarly publishing into a new generation.

## What are Frontiers Research Topics?

Frontiers Research Topics are very popular trademarks of the *Frontiers journals series*: they are collections of at least ten articles, all centered on a particular subject. With their unique mix of varied contributions from Original Research to Review Articles, Frontiers Research Topics unify the most influential researchers, the latest key findings and historical advances in a hot research area.

Find out more on how to host your own Frontiers Research Topic or contribute to one as an author by contacting the Frontiers editorial office: frontiersin.org/about/contact

# Investigating the interplay between tumor mutations, immune evasion, and targeted therapy resistance

**Topic editors**

Shanye Yin — Albert Einstein College of Medicine, United States
Guangchuang Yu — Southern Medical University, China
Yinghao Wu — Albert Einstein College of Medicine, United States

**Citation**

Yin, S., Yu, G., Wu, Y., eds. (2025). *Investigating the interplay between tumor mutations, immune evasion, and targeted therapy resistance*.
Lausanne: Frontiers Media SA. doi: 10.3389/978-2-8325-6267-3

# Table of contents

frontiers | Frontiers in Oncology

TYPE Original Research
PUBLISHED 28 April 2023
DOI 10.3389/fonc.2023.1170122



OPEN ACCESS

EDITED BY
Nan-Shan Chang,
National Cheng Kung University, Taiwan

REVIEWED BY
Brian Stramer,
King's College London, United Kingdom
Xianjue Ma,
Westlake University, China

*CORRESPONDENCE
Ulrich Theopold
uli.theopold@su.se

RECEIVED 20 February 2023
ACCEPTED 05 April 2023
PUBLISHED 28 April 2023

CITATION
Khalili D, Kunc M, Herbrich S, Müller AM and Theopold U (2023) Chitinase-like proteins promoting tumorigenesis through disruption of cell polarity *via* enlarged endosomal vesicles.
*Front. Oncol.* 13:1170122.
doi: 10.3389/fonc.2023.1170122



# Chitinase-like proteins promoting tumorigenesis through disruption of cell polarity *via* enlarged endosomal vesicles

Dilan Khalili, Martin Kunc, Sarah Herbrich, Anna M. Müller and Ulrich Theopold*

Department of Molecular Biosciences, The Wenner-Gren Institute, Stockholm University, Stockholm, Sweden

**Introduction:** Chitinase-like proteins (CLPs) are associated with tissue-remodeling and inflammation but also with several disorders, including fibrosis, atherosclerosis, allergies, and cancer. However, CLP's role in tumors is far from clear.

**Methods:** Here, we utilize *Drosophila melanogaster* and molecular genetics to investigate the function of CLPs (imaginal disc growth factors; Idgf's) in $Ras^{V12}$ dysplastic salivary glands.

**Results and discussion:** We find one of the Idgf's members, *Idgf3*, is transcriptionally induced in a JNK-dependent manner via a positive feedback loop mediated by reactive oxygen species (ROS). Moreover, *Idgf3* accumulates in enlarged endosomal vesicles (EnVs) that promote tumor progression by disrupting cytoskeletal organization. The process is mediated *via* the downstream component, aSpectrin, which localizes to the EnVs. Our data provide new insight into CLP function in tumors and identifies specific targets for tumor control.

KEYWORDS

**Drosophila, immunity, tumor, endosomal vesicles, salivary glands, chitinase, insect immunity**

## 1 Introduction

Chitinase-like protein (CLPs), including human YKL-39 and YKL-40 are synthesized and secreted under various conditions, including tissue injury, inflammatory and regenerative responses. Under pathological conditions they may contribute to asthma, sepsis, fibrosis and tumor progression (1, 2) including ductal tumors, such as the lung, breast, and pancreas (3, 4). CLPs are regulated by growth factors, cytokines, stress and the

extracellular matrix (ECM). However, the causal connection between CLPs' function and disease progression is only partially elucidated (5).

Animal models have been increasingly used in molecular oncology. This includes the fruitfly *Drosophila melanogaster*, where overexpression of dominant-active Ras ($Ras^{V12}$) in proliferating tissue leads to benign tumors and simultaneous reduction of cell polarity genes to progression towards an invasive stage. (6–9). Central to this switch towards increasing malignancy is the C-Jun N-terminal kinase (JNK)-signaling pathway, which becomes activated *via* loss of cell polarity and promotes tumor growth (10). However, the outcome of activated JNK is mediated in a context-dependent manner due to downstream effects several of which are yet to be elucidated (11, 12). Among potential JNK regulators, spectrin family members belong to cytoskeletal proteins which form a spectrin-based membrane skeleton (SBMS) (13). Through the Rac family of small GTPases, cell polarity and SBMS organization are maintained (14, 15). Although the exact relationship between Spectrin and JNK in tumors remains to be established, Rac1 under physiological conditions cooperates with JNK in tissue growth (16–18).

To explore CLPs' tissue autonomous function in a ductal tumor, we utilize the *Drosophila melanogaster* salivary glands (SGs). Generally, *Drosophila* CLPs are endogenously expressed in the larvae and include six members, termed Idgf 1-6 (Imaginal disc growth factors), that are involved in development, establishment of the cuticle, wound healing and restoration of cell organization (19–23). The SGs' epithelial luminal organization and the conserved activation of the tumor-promoting signaling factors make them suitable for dissecting CLP function. Moreover, the lumen separating a single layer of cells can be disrupted by constitutive active *Drosophila Ras* ($Ras^{V12}$) (24) leading to the loss of ECM integrity, the formation of fibrotic lesions and of the loss of secretory activity (25).

Here we investigated the role of *Drosophila* Idgf's in $Ras^{V12}$-expressing SGs. We show that one of the CLP's members, *Idgf3*, is induced in tumor glands, leading to a partial loss of epithelial polarity and promoting a reduction of lumen size. The mechanism is driven through JNK signaling upstream of *Idgf3*. In line with previous work, ROS production *via* JNK mediates induction of *Idgf3*, creating a tumor-promoting signaling loop. Idgf3 further promotes the formation of enlarged endosomal vesicles (EnVs) *via* αSpectrin. Inhibiting EnVs formation by individually knocking-down *Idgf3* and *αSpectrin*, restores cell organization. Similar effects are observed upon expression of human CLP members in $Ras^{V12}$ SGs. Thus, our work identifies a phylogenetically conserved contribution of tumor-induced CLP's towards the dysplasia of ductal organs and supports a role for spectrins as tumor modifiers.

# 2 Materials and methods

## 2.1 *Drosophila* maintenance and larvae staining

Stocks were reared on standard potato meal supplemented with propionic acid and nipagin in a 25°C room with a 12 h light/dark cycle. Female virgins were collected for five days and crossed to the respective males (see supplementary cross-list) after two days. Eggs were collected for six hours and further incubated for 18 h at 29°C. 24 h after egg deposition (AED), larvae were transferred to a vial containing 3 mL food supplemented with antibiotics (see Supplementary Table S1). 96 h and 120 h after egg deposition (AED), larvae were washed out with tap water before being dissected.

## 2.2 Sample preparation and immunohistochemistry

SGs were dissected in 1 x phosphate-buffered saline (PBS) and fixed in 4% paraformaldehyde (PFA) for 20 min. For extracellular protein staining, the samples were washed three times for 10 min in PBS and with PBST (1% TritonX-100) for intracellular proteins. Subsequently, samples stained for H2 were blocked with 0.1% bovine serum albumin (BSA) in PBS, and SG stained for pJNK, Idgf3, Spectrin, Dlg, p62 (ref(2)P), and GFP were blocked with 5% BSA for 20 min. After that, samples were incubated with the respective primary antibodies. Anti-pJNK (1:250), anti-Idgf3 (0.0134 µg/ml), anti-Spectrin (0.135 µg/ml) diluted in PBST were incubated overnight 4°C. anti-GFP (1 µg/ml) in PBST, H2 (1:5), and anti-SPARC (1:3000) in PBS were incubated for one hour at room temperature (RT). Samples were washed three times with PBS or PBST for 10 min and incubated with secondary antibody anti-mouse (4 µg/ml, Thermofisher #A11030) or anti-rabbit (4 µg/ml, Thermofisher #A21069) for one hour at RT. Subsequently, samples were washed three times in PBS or PBST for 10 min and mounted in FluoromountG.

## 2.3 Salivary gland size imaging and analysis

SG samples were imaged with Axioscope II (Objective 4x) (Zeiss, Germany) using AxioVision LE (Version 4.8.2.0). The images were exported as TIF and analyzed in FIJI (ImageJ: Version 1.53j). Representative confocal pictures were selected for figure panels and the complete set of replicate figures processed further for quantification (see below). Region of Interest (ROI) were drawn with the Polygon selection tool, and the scale was set to pixels (Px). The SG area was summarized as a boxplot with whisker length min to max. The bar represents the median. Statistical analysis was done with Prism software (GraphPad Software, 9.1.2, USA), the population was analyzed for normality with D'Agostino-Pearson and p-value quantified with Student's t-test.

## 2.4 Nuclear volume imaging and quantification

Nuclei were stained with DAPI (1 µg/ml, Sigma-Aldrich D9542) in PBST for 1 h at RT. Mounted glands were imaged with Zeiss LSM780 (Zeiss, Germany) using a plan-apochromat 10x/0.45 objective with a pixel dwell 3.15 µs and 27 µm pinhole in z-stack and tile scan mode. Zeiss images were imported into ImageJ and

viewed in Hyperstack. The selection threshold was set individually for each sample, and the analysis was performed with 3D objects counter. The nuclei volume was presented in boxplot, whisker length min to max and bar represent median. P-value quantified with Student's t-test and the scale bar represent $\mu m^3$.

## 2.5 Intensity and hemocyte quantification

The images for quantifying pJNK, TRE, Idgf3, and SPARC intensity and hemocyte recruitment were captured with AxioscopeII (Objective 4x) (Zeiss, Germany). The images were exported as TIF and analyzed in ImageJ. ROI was drawn with the Polygon selection tool, and subsequently, the total intensity was measured (pixel scale). The intensity was quantified according to the equation: Integrated Density – (SG area*Mean gray value). Hemocyte area was selected with Threshold Color and quantified by using the following equation: Ln (Hemocyte area + 1)/Ln (SG size + 1). Representative images were taken with Zeiss LSM780 (Zeiss, Germany). The images were then processed using Affinity Designer (Serif, United Kingdom). Graphs and statistical analysis were generated with Prism software (GraphPad Software, 9.1.2, USA). The population was analyzed for normality with D'Agostino-Pearson. Statistical significance was determined with Student's t-test, One-way ANOVA with Tukey's multiple comparison, and two-way ANOVA with Dunnett's multiple comparison.

## 2.6 Enlarged endosomal vesicles penetrance quantification

The penetrance of the enlarged vesicles was subjectively quantified based on positive actin staining. Samples were analyzed in Axioscope II (Objective 20x) (Zeiss, Germany). At least 15 samples were analyzed with three independent replicates.

## 2.7 Humanized transgenic *Drosophila* lines

Plasmids were generated and transformed at VectorBuilder (https://en.vectorbuilder.com/). Human *CH3L1* and *CH3L2* genes were inserted into *Drosophila Gene Expression Vector pUASTattB* vector generating VB200527-1248haw and VB200518-1121xyy, respectively and transformed into *E. coli*. The bacteria were cultured in 3 ml LB supplemented with ampicillin (AMP: 100 ug/ml) for 15 h, at 37°C. The plasmid was extracted according to the GeneJetTm Plasmid Miniprep Kit #K0503 standard procedure. Plasmids were validated through sequencing at Eurofins (https://www.eurofins.se/: For primer details see Supplementary Table S1). *Drosophila* transgenic lines were generated at thebestgene (https://www.thebestgene.com/). Plasmids were extracted with QIAGEN Plasmid Maxi Kit according to the standard procedure and injected into $w^{1118}$ strains. Expression of the human CLPs was validated with qPCR.

## 2.8 *In situ* hybridization

The Idgf3 (GH07453: DGRC) probe was generated according to (26). The staining procedure is described elsewhere with the following changes (26). The procedure was conducted in 200 µl transwells containing four salivary glands. The procedure included three technical replicates per genotype. Images were aqured with Leica MZ16 (Leica, Germany) microscope and Leica DFC300x FX digital color camera (Leica, Germany). Representative images were taken, and figures were generated in Affinity Designer (Serif, United Kingdom).

## 2.9 qPCR

mRNA isolation and cDNA synthesis were performed according to manufacture instructions (AM1931). qPCR procedures were performed as described earlier (24) with an adjusted Kappa concentration to 0.5x. At least three replicates and two technical replicates were performed for each qPCR. See Supplementary Table S1 for primer list.

# 3 Results

## 3.1 Idgf3 promotes a dysplastic phenotype

Obstruction of SG lumen by the constitutive-active oncogene, $Ras^{V12}$, under *Beadex-Gal4* driver ($Ras^{V12}$) disrupts organ function between 96 h and 120 h after egg deposition (AED) (25). Being that CLPs have been implicated in the loss of cell polarity (27), we investigated whether *Drosophila* CLPs contribute to the observed phenotype. First, to find out whether CLPs were induced in the $Ras^{V12}$ glands, we assessed relative mRNA levels at two different time points, 96 h and 120 h AED. Only one of the *CLP* members, namely *Idgf3*, was significantly upregulated at both time points (Figures 1A, S1A). Therefore, we decided to focus on *Idgf3's* effects on dysplastic glands.

Idgf3 contains an N-terminal signal peptide and has been detected in hemolymph (28). To analyze its subcellular tissue distribution in SGs, we used a C-terminally GFP tagged version of Idgf3 (21). At first we used *in situ* hybridization to show distribution of Idgf3 in salivary glands (Figures S1B-E). At 96 h we could not detect Idgf3 in the whole *WT* or $Ras^{V12}$ animals (Figures S1F-G'), possibly due to limited sensitivity. Likewise, 120 h old *WT* larvae did not show any detectable signal (Figure S1H-H') while a strong Idgf3 signal was detected in $Ras^{V12}$ SGs (Figure S1I-I'). To better understand Idgf3 distribution at a higher resolution, we dissected 120 h AED glands. *WT* glands had a weaker Idgf3::GFP signal in comparison to the $Ras^{V12}$ (Figures 1B, C). Moreover, Idgf3 was unevenly distributed throughout $Ras^{V12}$ SGs (Figure 1C).

The increased level of *Idgf3* between 96 h and 120 h strongly correlated with loss of tissue- and cell-organization and an increased nuclear volume (24). In order to characterize the role of Idgf3 in $Ras^{V12}$ glands, we used a specific *Idgf3 RNA-interference* line ($Idgf^{KD}$). Moreover, we focused on 120 h larvae, unless

10.3389/fonc.2023.1170122

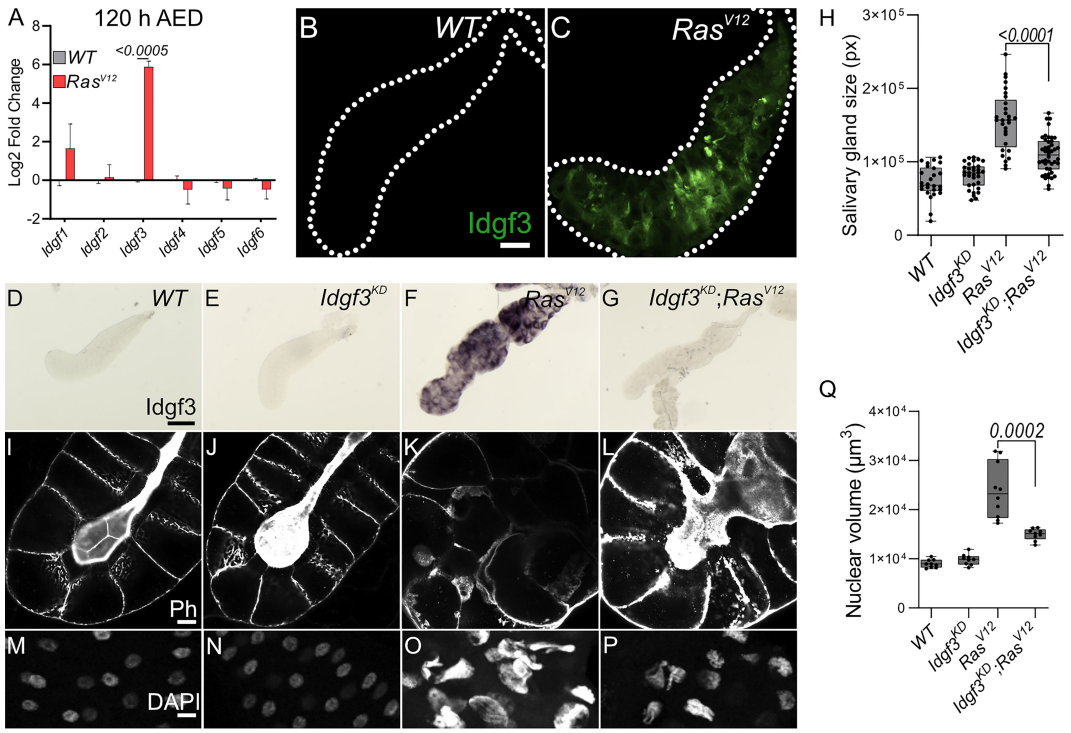


FIGURE 1
Idgf3 promotes growth and disrupts tissue architecture **(A)** qPCR data showing induction of *Idgf3* in 120 h AED $Ras^{V12}$ glands. **(B, C)** Idgf3 tagged with GFP was localized in the dysplastic glands. **(D-G)** Knock-down of *Idgf3* in $Ras^{V12}$ glands confirmed reduced mRNA levels as shown by *in situ* hybridization. **(H)** SG size quantification showing a reduction in tissue size in $Idgf3^{KD};Ras^{V12}$ SG compared to $Ras^{V12}$ alone. **(I-L)** F-actin (Phalloidin) staining revealed partial restoration of the lumen in $Idgf3^{KD};Ras^{V12}$ glands, in comparison to $Ras^{V12}$ alone. **(M-P)** Nuclei in DAPI stained SG displayed a reduced size in $Idgf3^{KD};Ras^{V12}$, quantified in **(Q)**. Scale bars in **(B, C)** represent 100 µm, **(D-G)** represent 0.3 mm and **(I-L)** represent 20 µm **(M-P)** represents 10 µm. Data in **(A)** represent 3 independent replicates summarized as mean ± SD. Boxplot in **(H, Q)** represent at least 20 SG pairs. Whisker length min to max, bar represent median. P-value quantified with Student's t-test.

otherwise stated, since they showed the most robust and developed dysplastic phenotype. Efficient knockdown of *Idgf3* was confirmed using *in situ* hybridization and at the protein level (Figures 1D-G, S1J-M; quantified in N, (21)). Macroscopic inspection showed that $Idgf^{KD};Ras^{V12}$ SGs were smaller than $Ras^{V12}$ SGs (Figure 1H), resembling WT controls. To gain insight into the cellular organization, we stained the glands for F-actin (Phalloidin: Ph) and DNA using DAPI. In $Idgf^{KD}$ the cells retained their cuboidal structure, and the lumen was visible as in *WT*, indicating that Idgf3 on its own does not affect apicobasal polarity (Figures 1I, J). In contrast, in $Ras^{V12}$ glands apicobasal polarity was lost, and the lumen was absent (Figures 1K, (25)). In $Idgf^{KD};Ras^{V12}$ SGs a reversal to the normal distribution of F-actin and partial restoration of the lumen was observed (Figure 1L). Similarly, the nuclear volume, which increased in $Ras^{V12}$ SGs returned to near wild type levels upon $Idgf^{KD}$ (Figure 1M-P, quantified in Figure 1Q). This indicates that $Idgf^{KD}$ can rescue $Ras^{V12}$-induced dysplasia.

In order to unravel the specific effects mediated by Idgf3 we further investigated $Ras^{V12}$ associated phenotypes, including fibrosis and the cellular immune response. As recently reported, $Ras^{V12}$ SGs displayed increased levels of the extracellular matrix components (ECM), including collagen IV and SPARC (BM40, (25)). $Idgf^{KD}$ did not affect SPARC levels in comparison to the *WT* (Figures S1O-P) but *Idgf-KD;*$Ras^{V12}$ SGs displayed significantly reduced SPARC levels in comparison to $Ras^{V12}$ (Figures S1Q-R, quantified in S). To assess whether this led to a reduced inflammatory response, we investigated the recruitment of plasmatocytes, macrophage-like cells previously reported to be recruited towards tumors (9). We found that both control and $Idgf^{KD}$ glands did not show recruitment of hemocytes (Figures S1T-U). In contrast to the effects on ECM components, $Idgf^{KD}$ *in* $Ras^{V12}$ glands did not lead to any changes in hemocyte attachment (Figures S1V-W, quantified in X). Taken together, upon $Ras^{V12}$ overexpression, Idgf3 promotes SG overgrowth, loss of cell organization, and fibrotic-like accumulation of the ECM, but not immune cell recruitment.

## 3.2 Idgf3 induces dysplasia *via* JNK-signaling

Dysplasia is driven by internal and external factors that either work in concert or independently. Similar to what we observed in $Idgf^{KD};Ras^{V12}$ glands blocking the sole *Drosophila* JNK member *basket* reverts many tumor phenotypes (24). Moreover, the dysplastic loss of apical and basolateral polarity between 96 h and 120 h is driven by the JNK-pathway (24). The time frame when we observed upregulation of *Idgf3* (Figures 1A, S1A) coincides with the

period during which blocking JNK restores tissue organization and homeostasis, similar to what occurs in $Idgf^{KD};Ras^{V12}$ tissues (Figures 1L, S1R). Therefore, we decided to test a possible involvement of JNK-signaling in the regulation of Idgf3.

First, we performed a targeted JNK RNAi-screen using Idgf3::GFP intensity in the glands as readout upon KD of JNK signaling components. We first confirmed the sensitivity of the Idgf3::GFP construct by *Idgf3-KD* in $Ras^{V12}$ SGs compared to $Ras^{V12}$ glands (Figures S2A, B, quantified in Figure S2C). Knockdown of the two classical TNF receptors upstream of JNK, *Grnd* (*Grindelwald*) and *Wgn* (*Wengen*) (Figure S2D) similarly reduced Idgf3::GFP intensity (Figures 2A–C, quantified in Figure 2E (29). Similar effects were observed with $Bsk^{KD}$ (Figure 2D, quantified in E). Altogether this suggests that Idgf3 protein levels are regulated downstream of JNK and the TNF members *Grnd* and *Wgn*.

## 3.3 ROS promotes Idgf3 induction *via* JNK

To further dissect Idgf3 regulation, we focused on the positive JNK regulators, reactive oxygen species (ROS) both intra- and extracellularly (9, 30). We previously reported that ROS production in $Ras^{V12}$ SGs increases *via* JNK (24). To inhibit ROS intra- and extracellularly, we separately overexpressed the $H_2O_2$ scavengers Catalase (Cat) and a secreted form of Catalase, IRC (immune-regulated Catalase), and $O_2^-$ scavenger SOD (Superoxide dismutase A), in the $Ras^{V12}$ background and quantified Idgf3::GFP intensity. Reducing levels of intracellular $H_2O_2$ ($Cat^{OE}$), but not $O_2^-$ ($SOD^{OE}$) lowered Idgf3::GFP intensity (Figures S3A-D quantified in E). Similarly, reduction of extracellular $H_2O_2$ by the secreted version of Catalase ($Irc^{OE}$) lowered Idgf3::GFP levels (Figures 3A-D, quantified in Figure 3E) as well as JNK signaling (Figures 3J, K-N', quantified in Figure 3O). We used detection of pJNK and TRE-GFP1b reporter construct, which recapitulates JNK-activation by expressing GFP under control of biding sites for JNK-specific AP-1 transcription factors (31). Confirming JNK-activation, three known JNK targets (puckered, *puc*, a negative feedback regulator of JNK; metalloproteinase 1, *MMP1* and head involution defective, hid (32–34)) as well as Idgf3 itself showed the same dependence on $Irc^{OE}$. In line with the reduced tissue size and improved tissue integrity in $Idgf3^{KD};Ras^{V12}$, overexpression of *IRC* in $Ras^{V12}$ SGs also reduced SG size (Figure 3T), improved tissue integrity and restored the SG lumen (Figure 3F-I, P-S).

In summary, ROSs contribute to pJNK signaling. In addition, overexpression of extracellular and intracellular Catalase but not SOD reduces Idgf3 induction *via* JNK, similar to the feedback loop that has been identified in other tumor models (9).

## 3.4 Idgf3 accumulates in large vesicles, which display markers for endocytosis and macropinocytosis

We previously noted the uneven distribution of Idgf3 in $Ras^{V12}$ SGs (Figure 1C). To further understand how Idgf3 promotes dysplasia, we dissected its subcellular localization (Figure 4A). We stained the glands for F-actin (Phalloidin) and addressed Idgf3::GFP localization at high resolution (Figures 4B, C'). Interestingly, we observed Idgf3::GFP clusters surrounded by F-actin (Figures 4C-C': arrow). Using a different salivary gland driver (*AB-Gal4*) to drive expression of $Ras^{V12}$, we also observed increased expression of Idgf3::GFP and its localization within vesicular structures (Figure S4A-B': arrow). The size of the vesicle-like structures was between 10-43 µm in comparison to secretory *Drosophila* vesicles (3-8µm, Figure 4D) (35). We refer to these as enlarged vesicles (EnVs). Based on the increased Idgf3 levels, we wondered whether the protein was aggregating in EnVs. The aggregation marker p62, which is autophagic adaptor marking cytoplasmic protein aggregates prepared for clearance (36) was strongly bound to the cytoplasm of $Ras^{V12}$ *SGs* unlike from *WT* glands. However, the EnVs did not contain any aggregated proteins (Figure S4C-D'). This may imply that Idgf3 is even taken up from the SG lumen in a soluble state.

Since we had observed a loss of secretion in *RasV12* SGs we next addressed the presence of EnVs within the secretory pathway. We overexpressed two versions of human phosphatidylserine binding protein, MFG-E8 (Milk fat globule-EGF factor), without (referred as non-secreted: Figures 4F, F', I, I') and with a signal peptide (referred as secreted: Figures 4G, G',J, J'37). In controls, the non-secreted form was found in the cytoplasm, whereas the secreted version was detected in the cytoplasm and in the lumen

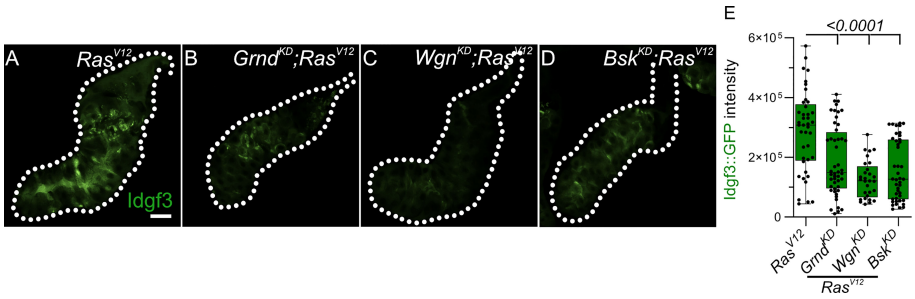


FIGURE 2
Idgf3 dysplasia is mediated through JNK activity **(A-D)** Representative images of Idgf3::GFP in a JNK targeted screen. **(E)** Quantification showing Idgf3::GFP intensity was reduced by $Grnd^{KD}$, $Wgn^{KD}$ and $Bsk^{KD}$ in $Ras^{V12}$ SG. Scale bars in **(A-D)** represent 100 µm. Boxplot in **(E)** represents at least 20 SG pairs. Whisker length min to max, bar represent median. P-value quantified with Student's t-test.

10.3389/fonc.2023.1170122

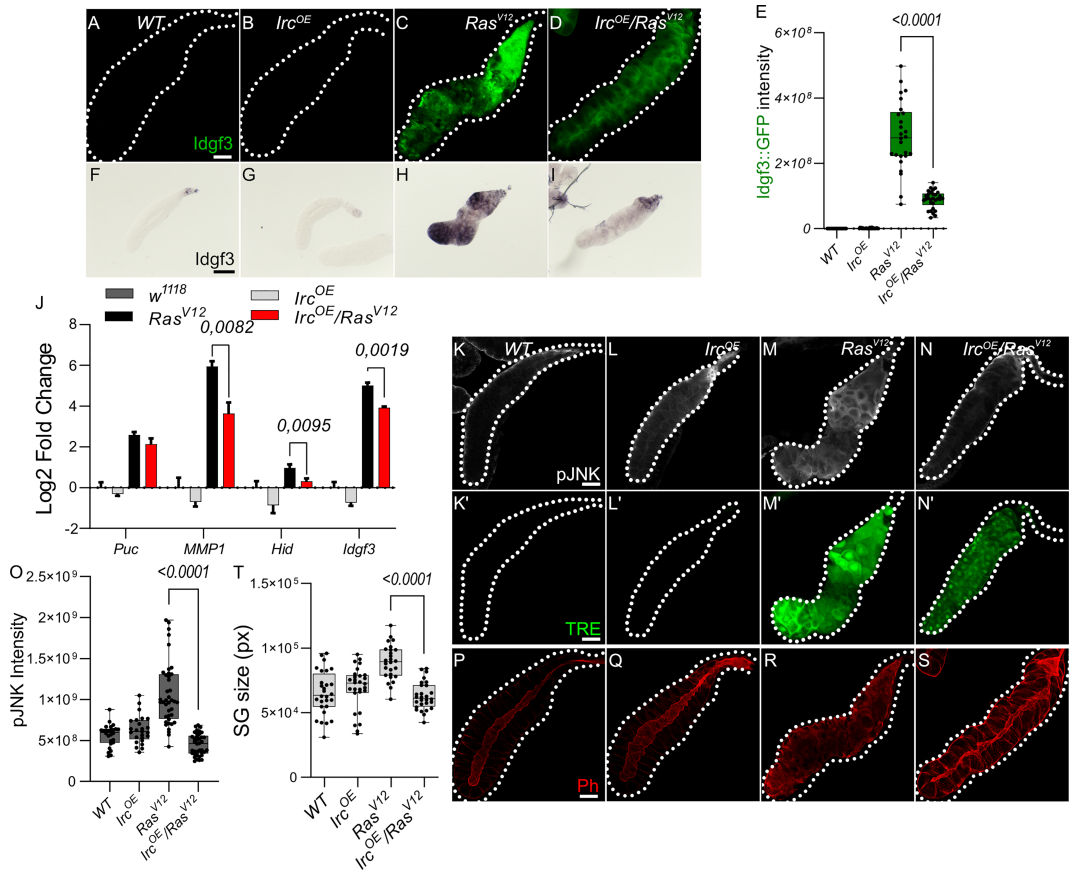


FIGURE 3
Antioxidants overexpression reduce Idgf3 and JNK signaling activity **(A-D)** Reduction of $H_2O_2$ by overexpression of secreted catalase (immune regulated catalase; IRC) lowered Idgf3::GFP levels, quantified in **(E)**. **(F-I)** ISH showing reduced expression of *Idgf3* in *IRC-OE;Ras*$^{V12}$glands. **(J)** qPCR data showing reduction of *Idgf3, puc, MMP1* and *Hid* in *IRC*$^{OE}$*;Ras*$^{V12}$glands. Selection of JNK targets with the most significant induction was partially based on our previous experiments ((24), Figure, S3A). **(K-N')** pJNK staining and TRE reporter constructs showing reduced intensity in *IRC*$^{OE}$*;Ras*$^{V12}$ in comparison to *Ras*$^{V12}$ glands, quantified in **(O)**. **(P-S)** Phalloidin staining showing partially restored lumen in *IRC*$^{OE}$*;Ras*$^{V12}$ glands, quantified in **(T)**. Scale bars in **(A-D, K-S)** represent 100 µm and **(F-I)** represent 0.3 mm. Data in **(J)** represent 3 independent replicates summarized as mean ± SD. Boxplot in **(E, O, T)** represent at least 20 SG pairs. Whisker length min to max, bar represent median. P-value quantified with Student's t-test.

(Figures 4E–E', F–G'). In *Ras*$^{V12}$ SGs, the non-secreted form was surrounding the EnVs (arrow), indicating the presence of phosphatidylserine on their membrane (Figures 4H–H', I, I'). In contrast, the secreted form localized to the inside of the EnVs (Figures 4J, J': arrow). These data suggest that EnVs are surrounded by a lipid membrane and probably derive from the secretory pathway.

In order to further characterize Idgf3-containing EnVs we co-expressed vesicle-specific Rab's coupled with a GFP fluorophore, a lysosomal marker (Atg8), an autophagy marker (Vps35), and a marker for phosphatidylinositol-3-phosphate-(PtdIns3P: *FYVE*)-positive endosomes in *Ras*$^{V12}$ glands (For a complete set, see Figure S4E-M") which marks macroautophagy vesicles. To increase sensitivity and to identify EnVs, we stained with anti-GFP and co-stained with Phalloidin. Localization of Rabs and phalloidin to the same vesicles was observed with endosomal marker (Rab5) and recycling endosomal marker (Rab11) but not endosomal marker (Rab7) (Figure S4E-H", S4M-M"). Moreover, EnVs were also positive for PtdIns3 (Figure S4L-L"). In line with their dependence on secretion, this potentially identifies EnVs as enlarged recycling endosomes. EnV accumulation in *Ras*$^{V12}$ glands between 96 h and 120 h implies that (i) endosome formation is either increased compared to *WT* or (ii) that endosomes are not normally recycled leading to their accumulation. The latter hypothesis correlates with the loss of apico-basolateral polarity and the disruption of secretion due to a lack of a luminal structure in *Ras*$^{V12}$ glands (25). To test the first hypothesis, we blocked the formation of early endosomes with *Rab5*$^{DN}$. Apico-basolateral polarity, detected by a visible lumen, was not affected by *Rab5*$^{DN}$. Moreover, *Rab5*$^{DN}$*;Ras*$^{V12}$ did not block EnV formation and restoration of apicobasal polarity (Figure S4N-Q). Halting the recycling endosome pathway *via Rab11*$^{DN}$ increases the endosomes' accumulation without affecting cell polarity (Figure S4R). In contrast, in *Rab11*$^{DN}$*;Ras*$^{V12}$ SGs, endosomes were not accumulating, and EnVs were still detected (Figure S4S). Taken together, EnV formation is independent of the classical recycling pathway, suggesting other candidates are involved in their generation.

In SGs, overexpression of Rac generates enlarged vesicles with similarity to the EnVs described here (14). Supporting a role in dysplasia in our system, *Ras*$^{V12}$ SGs showed stronger Rac1 expression in comparison to the control. Due to the pleiotropic effects of the *Rac1*$^{DN}$ construct, we addressed Rac1 function by

10.3389/fonc.2023.1170122

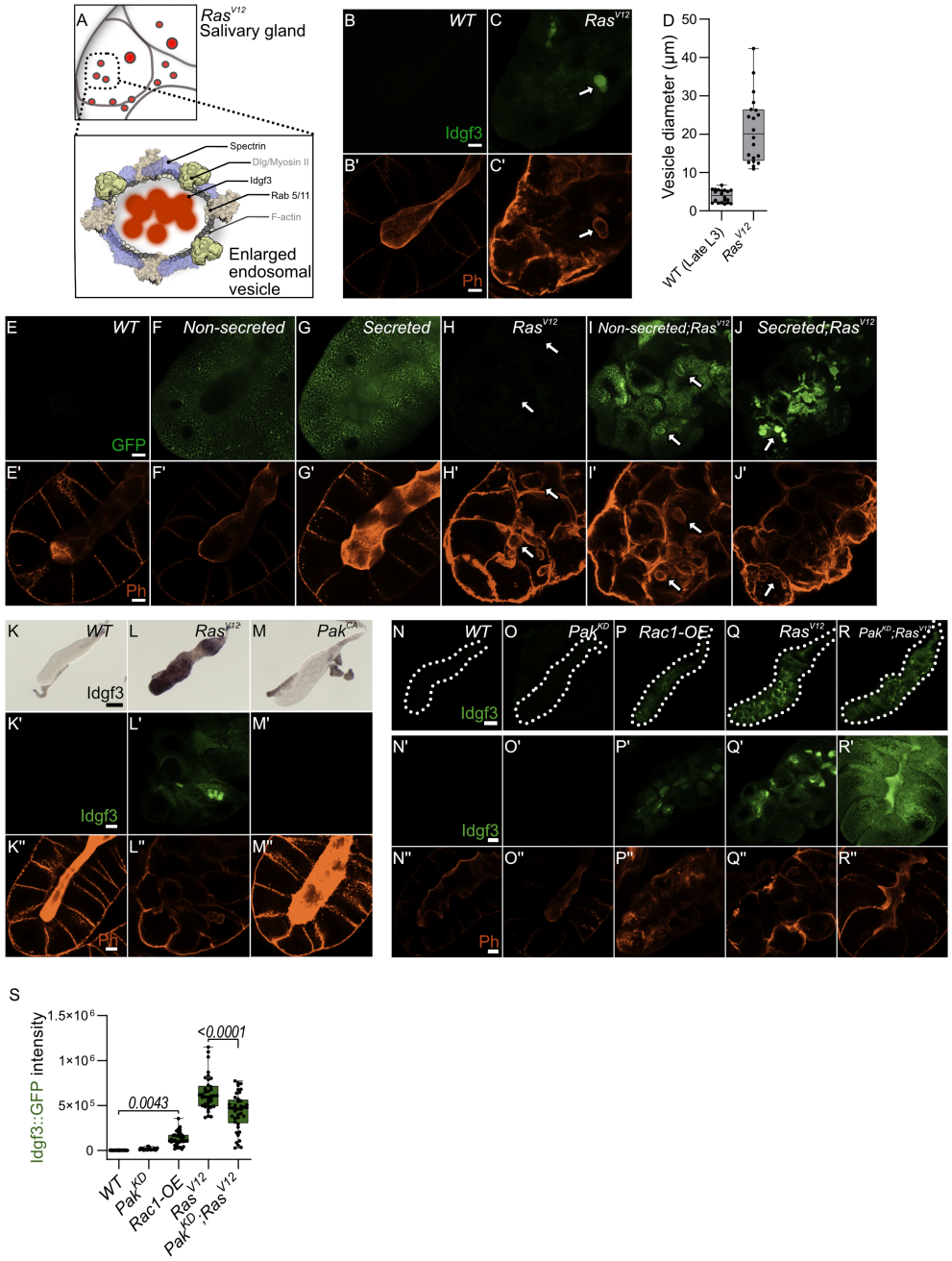


FIGURE 4
*Idgf3* promotes formation of enlarged endosomes in the Ras$^{V12}$ background **(A)** The overall figure shows Ras$^{V12}$ salivary gland with EnVs marked by red color. The inlet depict Idgf3 enclosed by enlarged vesicles (EnVs) coated by cytoskeletal and cell polarity proteins. **(B-C')** Idgf3::GFP clusters coated with Phalloidin. **(D)** Vesicle size quantification showing *Ras$^{V12}$* enlarged vesicles in comparison to prepupae SG vesicles. **(E-J')** Non secreted MFGE8 localizes to the surface of EnVs, co-stained with phalloidin. The secreted MFGE8 is packaged into EnVs in *Ras$^{V12}$*glands. **(K-M)** ISH showing no induction of *Idgf3* by constitutively active Pak. **(K'-M'')** Idgf3::GFP is not detectable in the *Pak$^{CA}$* glands and the lumen is detectable (Phalloidin). **(N-R'')** Restoration of the lumen packed with Idgf3::GFP, no formation of EnVs and Idgf3 in *Pak$^{KD}$;Ras$^{V12}$* glands. Scale bars in **(B-C', E-J', K'-M'', N'-R'')** represent 20 µm, **(K-M)** represents 0.3 mm and **(N-R)** represents 100 µm. Boxplot in **(D)** represents 20 EnVs and **(S)** represents at least 20 SG pairs. Whisker length min to max, bar represent median. P-value quantified with Student's t-test.

modulating the expression of the Rac1 effector molecule, *Pak* (14). Overexpression of *Pak$^{CA}$* did not increase *Idgf3* levels and had no detectable effect on F-actin distribution (Figures 4K-M''). In contrast, Rac1 activity *via* Pak does affect *Ras$^{V12}$* SG integrity: Idgf3::GFP levels were increased in *Rac1-OE* SGs and F-actin was disorganized (Figures 4N-P'' quantified in S). However, the *Rac1-OE* glands did not grow larger compared to *Ras$^{V12}$*,indicating additional signals are necessary for gland overgrowth. Also, *Pak$^{KD}$;Ras$^{V12}$* SGs displayed a more regular F-actin distribution leading to restoration of the lumen and proper secretion of Idgf3 (Figures 4Q-R'' quantified in S). Moreover, we observed Rac1 also localized to EnVs (Figure S4T-U'). Decoration with Rac1 and actin

as well as their dependence on Ras activation potentially identifies EnVs as macropinocytotic vesicles ((38), see also discussion). The enlarged vesicles that form upon Rac overexpression in SGs (14) also stain positive for Spectrins identifying them as additional candidates for EnVs formation. Of note, Spectrins under physiological settings are involved in the maintenance of cellular integrity including epithelial organization, which is lost in $Ras^{V12}$ SGs.

## 3.5 JNK promotes EnVs formation *via* Idgf3 upstream of αSpectrin

To analyze Spectrin contribution to EnVs formation, we stained for αSpectrin, one of the three members in flies (39) and found it to be induced in $Ras^{V12}$ SGs and to localize to the EnVs (Figure S5A-B"). Knockdown of *Idfg3* in $Ras^{V12}$ SGs reduced both αSpectrin levels and EnVs formation (Figures 5A-D'). Despite efficient $Idfg3^{KD}$, transcript levels for both α- and $\beta_{Heavy}$Spectrin as well as for Rac1 were not affected indicating regulation at the posttranscriptional level (Figure 5E). Moreover, we found markers for cell polarity including Dlg, and Myosin II also decorate the EnVs (Figure S4V-Y': arrow). In contrast, $\alpha Spectrin^{KD}$ (Figure S5C-F quantified G) reduced Idgf3 levels (Figures 5F-I' quantified Figure 5J) as well as JNK signaling upstream of Idgf3 (Figures 5U, V). Further supporting a role for Spectrins in SG dysplasia, knockdown of αSpectrin in $Ras^{V12}$ glands abolished EnVs formation and partially restored the SG lumen (Figure 5I").

Taken together this suggests that Idgf3 promotes EnVs formation (Figures 5C, C') most likely post-transcriptionally (Figure 5E). In line, overexpression of Idgf3 throughout the whole gland, at 96 h, as shown by ISH (Figure S5I-L), led to an increase in the number of glands with endosomes (Figure S5M-P"', quantified in Q). To address epistasis between Idgf3 and JNK we calculated the penetrance of EnVs formation. In $Ras^{V12}$ SGs we observed EnVs in 100% of the glands, an effect that was strongly blocked in $Bsk^{DN}$; $Ras^{V12}$ (Figures 5O, S, quantified in Figure 5T). Blocking JNK and overexpressing *Idgf3* in $Ras^{V12}$ strongly reverted the $Bsk^{DN}$;$Ras^{V12}$ phenotype, a lumen could not be detected, and around 98% of the glands contained enlarged endosomes (Figures 5O–S quantified in Figure 5T) while control SGs using RFP-overexpression retained the $Bsk^{DN}$;$Ras^{V12}$ phenotype. Overexpression of Idgf3 alone did not result in EnVs formation (Figures 5K–N). In conclusion, the data suggest that Idgf3 acts downstream of JNK and - through formation of EnV's - disrupts luminal integrity. The proposed activity of Idgf3 in EnVs formation is summarized in Figure 5W.

## 3.6 Human CLP members enhance dysplasia in *Drosophila* SGs

Finally, we wished to determine whether the tumor-modulating effects we had observed for *Drosophila* Idgf3 also applies to human CLP members. For this we expressed two human *CLPs* (*Ch3L1* or *Ykl-40*; 29% amino acid identity to Idgf3 and *Ch3L2* or *Ykl-39*; 26% amino acid identity, Figure 6A) in SGs, both on their own and in combination with $Ras^{V12}$. Overexpression of CLPs in salivary glands was confirmed by qPCR (Figure 6B). Similar to Idgf3, both CLPs enhanced the hypertrophy observed in $Ras^{V12}$ SGs (Figures 6C-H quantified in Figure 6I). The lumen integrity stayed highly disturbed when CLPs were overexpressed in $Ras^{V12}$ background (Figures 6J–O). Additionally, *Ch3L1* enhanced the prevalence of EnVs in the Ras mutant background (Figure 6P). Taken together this means that the tumor-promoting effect of CLPs is conserved between *Drosophila* and humans and may affect different phenotypes of dysplasia depending on the CLP under study.

# 4 Discussion

The levels of Chitinase-like proteins (CLPs) are elevated during a wide range of inflammatory processes as well as neoplastic disorders. Their physiological function has been more elusive but includes the formation of extracellular assemblages (40) including the insect cuticle (22), wound healing and in both mammals (40) and insects (41) and the restoration of cell integrity after oxidative damage (42). Conversely, induction of CLPs has been associated with the development of fibrotic lesions and cancer development with poor prognosis (reviewed in (40)). We used *Drosophila* as a tumor model to dissect CLP (*Idgf3*) function genetically in a secretory ductal organ, the salivary glands. We show that Idgf3 promotes tumor overgrowth through the disruption of cell polarity. The induction of *Idgf3* disrupts cell organization and leads to the formation of enlarged endosome vesicles (EnVs) which accumulate in the cytoplasm. Genetically, *Idgf3* is induced *via* a pro-tumorigenic JNK and ROS signaling feedback loop. Consequently, Idgf3 recruits the spectrin-based membrane skeleton (SBMS) for the formation of EnVs. Significantly, KD of *Idgf3* inhibits overgrowth, restores cell polarity, reduces ECM size and blocks EnV formation.

Our identification of a contribution of JNK signaling and both extra- and intracellular ROS to dysplasia is in line with previous findings from other *Drosophila* tumor models (43). Similarly, like others (43) we observe an amplification loop between ROS and JNK signaling, which augments the dysplastic phenotype (24). Several studies have demonstrated that activation of JNK signaling in mammals promotes the progression of ductal tumors (44–46). Here we identify Idgf3 as an additional component that feeds into JNK signaling. Ultimately in $Ras^{V12}$-expressing SGs this leads to the formation of EnVs involving Spectrins. Under physiological conditions, members of the Spectrin family have a supporting role in maintaining cellular architecture through interaction with phospholipids and actively promoting polymerization of F-actin (47–49). Moreover, the secretory activity of ductal organs has been shown to be facilitated by Spectrins (50).

During *Drosophila* development and under physiological conditions, the pathway that involves Spectrins, Rac1 and Pak1 has been shown to be required for the maintenance of cell polarity while when deregulated it leads to the formation of enlarged vesicles similar to the EnVs (14). Thus, our results provide a possible link between the observed induction of CLPs in a range of tumors and

10.3389/fonc.2023.1170122

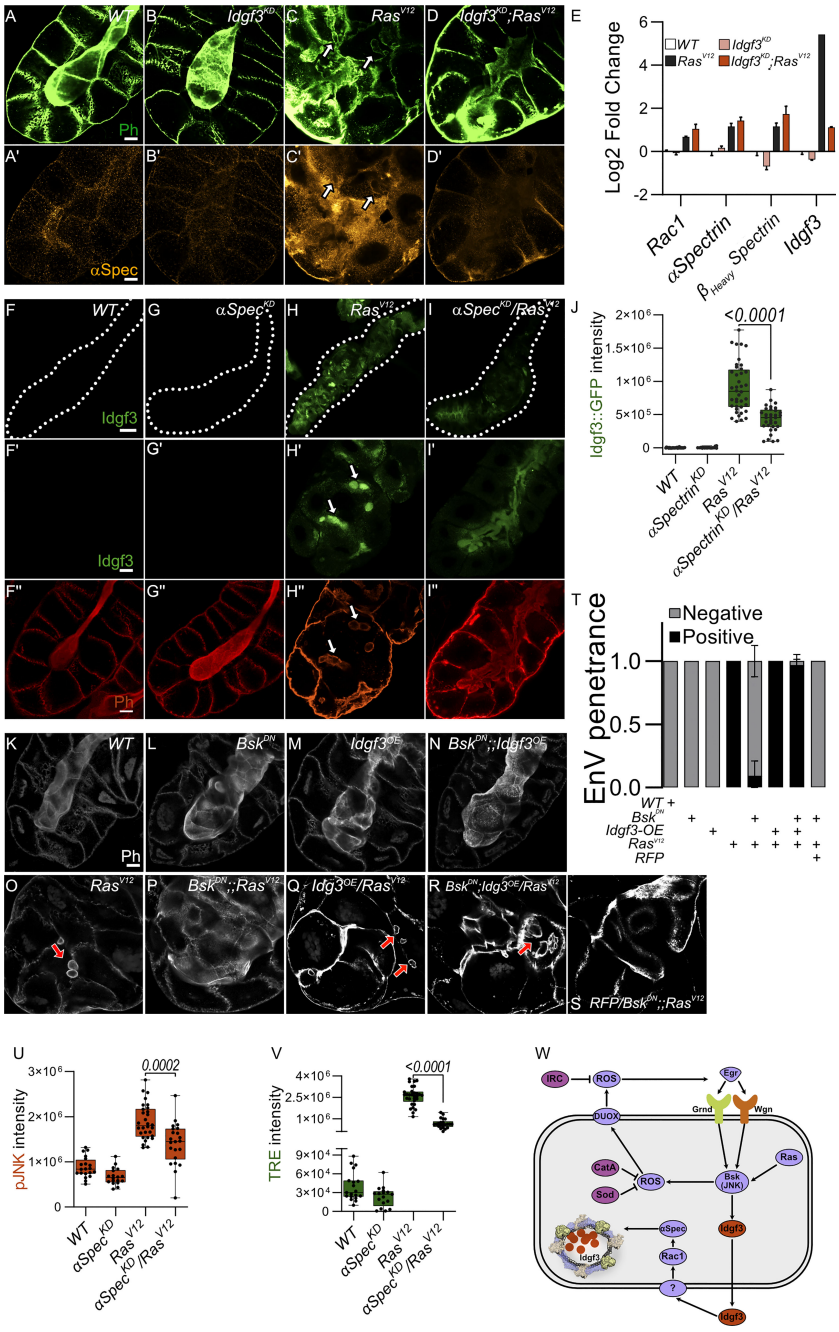


FIGURE 5
JNK promotes EnVs formation *via* Idgf3 upstream of αSpectrin **(A-D')** αSpectrin staining showing restoration of normal distribution in *Idgf3*$^{KD}$;*Ras*$^{V12}$glands. **(E)** qPCR data showing no reduction of *αSpectrin* and $\beta_{Heavy}$*Spectrin* in *Idgf3*$^{KD}$;*Ras*$^{V12}$. **(F-I'')** Reduced levels of αSpectrin (αSpectrin$^{KD}$/*Ras*$^{V12}$) reduces Idgf3::GFP levels quantified in **(J)**, prevents formation of EnVs and largely restores the SG lumen (arrows indicate EnVs). **(K-S)** Phalloidin staining showing epistasis of EnVs formation in which Idgf3 acts downstream of JNK. **(T)** EnVs penetrance quantification showing a strong induction of EnVs in *JNK*$^{DN}$;*Idgf3*$^{OE}$/*Ras*$^{V12}$ glands. **(U)** pJNK intensity quantification showing reduced levels in *aSpectrin*$^{KD}$/*Ras*$^{V12}$. **(V)** TRE intensity quantification showing reduced levels in *aSpectrin*$^{KD}$/*Ras*$^{V12}$. **(W)** Idgf3 promotes formation of EnVs, upstream of Rac1. Scale bars in **(A-D', F'-I'', K-S')** represent 20 µm, **(F-I)** represents 100 µm. Data in **(E)** represent 3 independent replicates summarized as mean ± SD. Barplot in **(T)** represent 3 independent replicates with at least 10 SG pairs, summarized as mean ± SD. Boxplot in **(J, U, V)** represent at least 20 SG pairs. Whisker length min to max, bar represent median. P-value quantified with Student's t-test.

the effects of Spectrins and their deregulation in tumors (51, 52). In addition to the genetic interaction we find, previous work suggests an additional mechanical link *via* a Spectrin binding protein (Human spectrin Src homology domain binding protein1; Hssh3bp1, (53)) the loss of which has been associated with prostatic tumors (54). Hhh3bp1 may influence tumor progression possibly through interaction with tyrosine kinases such as Abelson kinase (54). Interestingly Hhh3bp1 is a marker and possible regulator of macropinocytosis (55), a recycling pathway that is known to be hijacked by Ras-transformed tumor cells to acquire

10.3389/fonc.2023.1170122

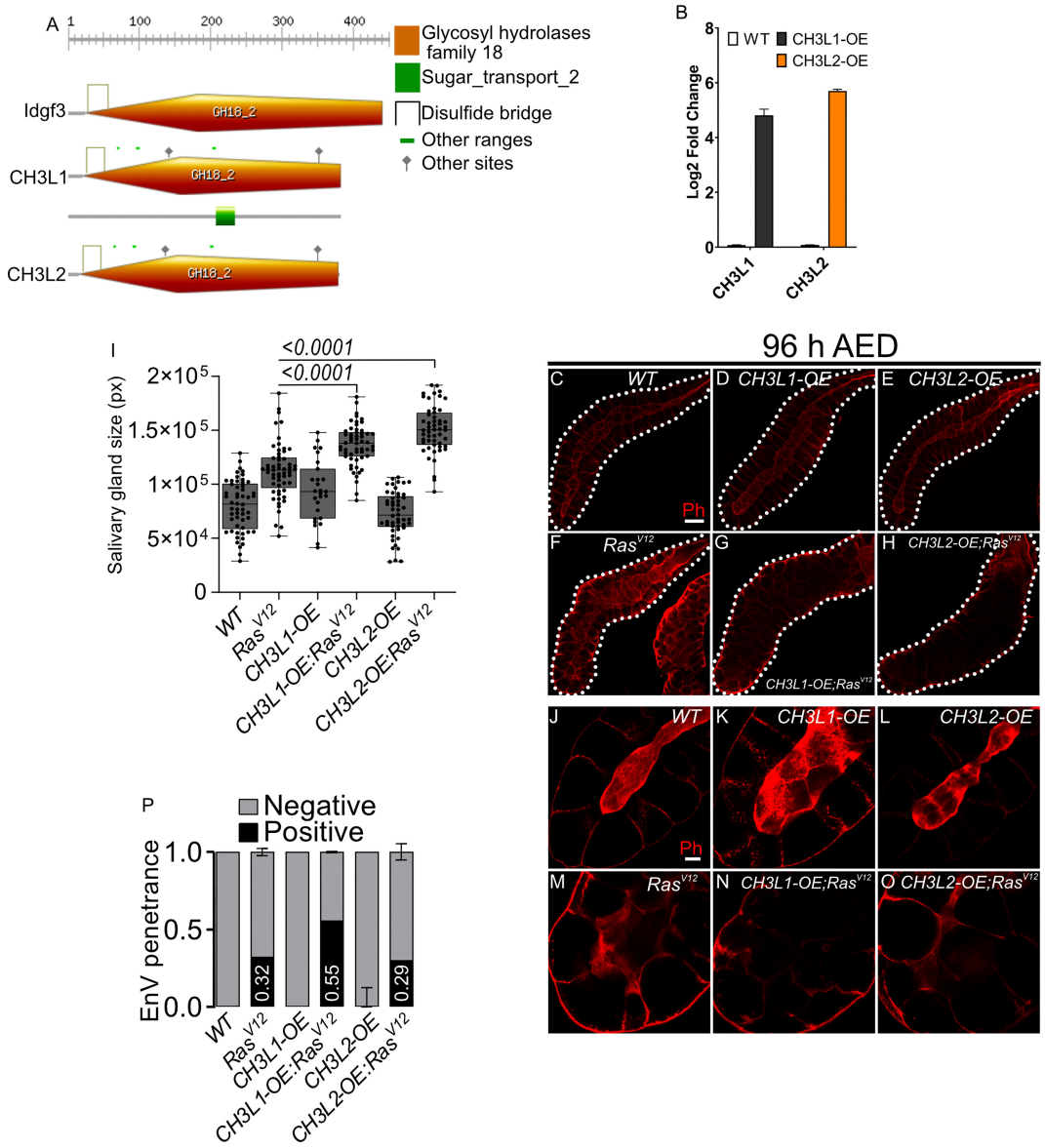


FIGURE 6
Human Chitinase-like proteins similarly to Idgf3 promotes EnVs formation **(A)** Comparison of Idgf3, CH3L1 and CH3L2 protein motifs (https://prosite.expasy.org). **(B)** qPCR confirmation of CH3L1 and CH3L2 expression in SG. **(C-H)** Representative images of phalloidin staining used for size quantification. **(I)** SG size quantification showing an increase in tissue size in $CH3L1^{OE}$;$Ras^{V12}$ and $CH3L2^{OE}$;$Ras^{V12}$ SG compared to $Ras^{V12}$ alone. **(J-O)** Phalloidin staining depicting disrupted lumen integrity in $Ras^{V12}$ glands. **(P)** EnVs penetrance quantification showing an induction of EnVs in $CH3L1^{OE}$;$Ras^{V12}$ glands. Barplot in **(B)** represent 4 independent replicates with at least 10 SG pairs, summarized as mean ± SD. Scale bars in **(C-H)** represent 100 µm and **(J-O)** 20 µm. Boxplot in **(I)** represent at least 20 SG pairs. Whisker length min to max, bar represent median. P-value quantified with Student's t-test. Barplot in **(P)** represent 3 independent replicates with at least 10 SG pairs, summarized as mean ± SD.

nutrients (38) and also leads to the formation of large intracellular vesicles (56). In favor of this hypothesis macropinocytosis is known to depend on Rac1/Pak1 signaling although the resulting vesicles are usually smaller (0.2-5 micrometers) than EnVs (57). We find that - like macropinocytosis - EnV-formation depends on the activity of growth factors (38), in this case Idgf3, much in line with its original description as an *in vitro* mediator of insulin signaling (20). *In vivo*, under normal conditions Idgf3 is required for proper formation of chitin-containing structures, wound healing and cellular integrity (22). Thus, under these circumstances Idgf3 acts to preserve cellular integrity including the epithelial character of SG cells upstream of spectrins. We propose that in a non-physiological setting such as upon overexpression of $Ras^{V12}$, this mechanism is overwhelmed leading to the breakdown of homeostasis, loss of cell polarity and the gland lumen, loss of secretory activity and the formation of EnVs larger than macropinocytotic vesicles. Large vesicles accompany several scenarios of non-apoptotic programed cell death, which occurs a.o. in apoptosis-resistant tumors (58, 59). Such modes of cell death include methuosis, a deregulated form of macropinocytosis (56, 58). Of note, apoptotic cell death is inhibited in *Drosophila* polytenic SGs to account for the increased number of DNA breaks that occur

during endoreplication, which in mitotic cells induce apoptosis in both a p53-dependent and independent manner (60, 61). In line, despite the activation of caspase activity and nuclear fragmentation, which are considered hallmarks of apoptosis, $Ras^{V12}$ SG cells don't disintegrate to produce apoptotic bodies (24). This may also explain the difference to mitotically cycling tumor models, which also activate JNK – yet with apoptosis as an outcome (32, 62, 63). Thus, SGs provide a suitable model for apoptosis-resistant tumors. In a mammalian setting, the phenotypes that are associated with non-apoptotic cell death such as disruption of cellular polarity and reorganization of the ECM provide potential targets for therapeutic treatments (46). Our work adds CLPs and spectrins to this list. Depending on the tissue environment and similar to JNK signaling, CLP's may have varying roles in a context-dependent manner. Overexpression of *Idgf3* alone is not sufficient for the loss of cell polarity, overgrowth, and fibrosis. Collectively, this suggests a tumor-specific phenotype for Idgf3 (Figures 6C-H), in line with mammalian CLPs (reviewed in (40)). Due to their pleiotropic effects, further investigation of CLPs role will be required to dissect their molecular function in a given tissue and to ultimately design tumor-specific treatments (64).

Taken together our findings provide new insight into the loss of tissue integrity in a neoplastic tumor model including the contribution of CLPs, Spectrins and alternative forms of cell death. This may provide further ways to test how developmentally and physiologically important conserved mechanisms that maintain cellular hemostasis - when deregulated - contribute to tumor progression.

## Data availability statement

The original contributions presented in the study are included in the article/Supplementary Material. Further inquiries can be directed to the corresponding author.

## Author contributions

DK, UT and MK conceived the research and designed the experiments. DK, MK, SH and AM performed experiments and data analysation. DK, UT and MK wrote the paper and participated in the revisions. All authors contributed to the article and approved the submitted version.

## Funding

This work was supported by Swedish Cancer Foundation (CAN 2015-546), Wenner-Gren Foundation (UPD2020-0094 and UPD2021-0095 to MK), Swedish Research Council (VR 2016-04077 and VR 2021-04841).

## Acknowledgments

We would like to thank Chris Molenaar, Roger Karlsson, Stina Höglund and the Imaging facility at Stockholm University for support with all aspects of microscopy. We would also like to thank Vasilios Tsarouhas for his critical feedback. This work was supported by grants from the Swedish Cancer Foundation (CAN 2015-546), the Wenner-Gren Foundation (UPD2020-0094 and UPD2021-0095 to MK) and the Swedish Research Council (VR 2016-04077 and VR 2021-04841).

## Conflict of interest

The authors declare that the research was conducted in the absence of any commercial or financial relationships that could be construed as a potential conflict of interest.

## Publisher's note



## Supplementary material

The Supplementary Material for this article can be found online at: https://www.frontiersin.org/articles/10.3389/fonc.2023.1170122/full#supplementary-material

## References

1. Roslind A, Johansen JS. YKL-40: a novel marker shared by chronic inflammation and oncogenic transformation. *Methods Mol Biol* (2009) 511:159–84. doi: 10.1007/978-1-59745-447-6_7

2. Shao R, Hamel K, Petersen L, Cao QJ, Arenas RB, Bigelow C, et al. YKL-40, a secreted glycoprotein, promotes tumor angiogenesis. *Oncogene* (2009) 28:4456–68. doi: 10.1038/onc.2009.292

3. Johansen JS, Jensen BV, Roslind A, Nielsen D, Price PA. Serum YKL-40, a new prognostic biomarker in cancer patients? *Cancer Epidemiol Biomarkers Prev* (2006) 15:194–202. doi: 10.1158/1055-9965.EPI-05-0011

4. Uhlen M, Zhang C, Lee S, Sjostedt E, Fagerberg L, Bidkhori G, et al. A pathology atlas of the human cancer transcriptome. *Science* (2017) 357(6352):357. doi: 10.1126/science.aan2507

5. Park KR, Yun HM, Yoo K, Ham YW, Han SB, Hong JT. Chitinase 3 like 1 suppresses the stability and activity of p53 to promote lung tumorigenesis. *Cell Commun Signal* (2020) 18:5. doi: 10.1186/s12964-019-0503-7

6. Brumby AM, Richardson HE. Scribble mutants cooperate with oncogenic ras or notch to cause neoplastic overgrowth in drosophila. *EMBO J* (2003) 22:5769–79. doi: 10.1093/emboj/cdg548

7. Pagliarini RA, Xu T. A genetic screen in drosophila for metastatic behavior. *Science* (2003) 302:1227–31. doi: 10.1126/science.1088474

8. Igaki T, Pagliarini RA, Xu T. Loss of cell polarity drives tumor growth and invasion through JNK activation in drosophila. *Curr Biol* (2006) 16:1139–46. doi: 10.1016/j.cub.2006.04.042

9. Perez E, Lindblad JL, Bergmann A. Tumor-promoting function of apoptotic caspases by an amplification loop involving ROS, macrophages and JNK in drosophila. *Elife* (2017) 6:e26747. doi: 10.7554/eLife.26747

10. Zhu M, Xin T, Weng S, Gao Y, Zhang Y, Li Q, et al. Activation of JNK signaling links lgl mutations to disruption of the cell polarity and epithelial organization in drosophila imaginal discs. *Cell Res* (2010) 20:242–5. doi: 10.1038/cr.2010.2

11. Ciapponi L, Jackson DB, Mlodzik M, Bohmann D. Drosophila fos mediates ERK and JNK signals *via* distinct phosphorylation sites. *Genes Dev* (2001) 15:1540–53. doi: 10.1101/gad.886301

12. Zeke A, Misheva M, Remenyi A, Bogoyevitch MA. JNK signaling: regulation and functions based on complex protein-protein partnerships. *Microbiol Mol Biol Rev* (2016) 80:793–835. doi: 10.1128/MMBR.00043-14

13. Bennett V, Baines AJ. Spectrin and ankyrin-based pathways: metazoan inventions for integrating cells into tissues. *Physiol Rev* (2001) 81:1353–92. doi: 10.1152/physrev.2001.81.3.1353

14. Lee SK, Thomas GH. Rac1 modulation of the apical domain is negatively regulated by beta (Heavy)-spectrin. *Mech Dev* (2011) 128:116–28. doi: 10.1016/j.mod.2010.11.004

15. Fletcher GC, Elbediwy A, Khanal I, Ribeiro PS, Tapon N, Thompson BJ. The spectrin cytoskeleton regulates the hippo signalling pathway. *EMBO J* (2015) 34:940–54. doi: 10.15252/embj.201489642

16. Baek SH, Kwon YC, Lee H, Choe KM. Rho-family small GTPases are required for cell polarization and directional sensing in drosophila wound healing. *Biochem Biophys Res Commun* (2010) 394:488–92. doi: 10.1016/j.bbrc.2010.02.124

17. Wertheimer E, Gutierrez-Uzquiza A, Rosemblit C, Lopez-Haber C, Sosa MS, Kazanietz MG. Rac signaling in breast cancer: a tale of GEFs and GAPs. *Cell Signal* (2012) 24:353–62. doi: 10.1016/j.cellsig.2011.08.011

18. Archibald A, Mihai C, Macara IG, McCaffrey L. Oncogenic suppression of apoptosis uncovers a Rac1/JNK proliferation pathway activated by loss of Par3. *Oncogene* (2015) 34:3199–206. doi: 10.1038/onc.2014.242

19. Kirkpatrick RB, Matico RE, McNulty DE, Strickler JE, Rosenberg M. An abundantly secreted glycoprotein from drosophila melanogaster is related to mammalian secretory proteins produced in rheumatoid tissues and by activated macrophages. *Gene* (1995) 153:147–54. doi: 10.1016/0378-1119(94)00756-I

20. Kawamura K, Shibata T, Saget O, Peel D, Bryant PJ. A new family of growth factors produced by the fat body and active on drosophila imaginal disc cells. *Development* (1999) 126:211–9. doi: 10.1242/dev.126.2.211

21. Kucerova L, Kubrak OI, Bengtsson JM, Strnad H, Nylin S, Theopold U, et al. Slowed aging during reproductive dormancy is reflected in genome-wide transcriptome changes in drosophila melanogaster. *BMC Genomics* (2016) 17:50. doi: 10.1186/s12864-016-2383-1

22. Pesch YY, Riedel D, Patil KR, Loch G, Behr M. Chitinases and imaginal disc growth factors organize the extracellular matrix formation at barrier tissues in insects. *Sci Rep* (2016) 6:18340. doi: 10.1038/srep18340

23. Yadav S, Eleftherianos I. The imaginal disc growth factors 2 and 3 participate in the drosophila response to nematode infection. *Parasite Immunol* (2018) 40:e12581. doi: 10.1111/pim.12581

24. Krautz R, Khalili D, Theopold U. Tissue-autonomous immune response regulates stress signalling during hypertrophy. *Elife* (2020) 9:e64919. doi: 10.7554/eLife.64919

25. Khalili D, Kalcher C, Baumgartner S, Theopold U. Anti-fibrotic activity of an antimicrobial peptide in a drosophila model. *J Innate Immun* (2021) 13:376–90. doi: 10.1159/000516104

26. Hauptmann G, Söll I, Krautz R, Theopold U. Multi-target Chromogenic Whole-mount In Situ Hybridization for Comparing Gene Expression Domains in Drosophila Embryos. *J Vis Exp* (2016) 107:e53830. doi: 10.3791/53830

27. Morera E, Steinhauser SS, Budkova Z, Ingthorsson S, Kricker J, Krueger A, et al. YKL-40/CHI3L1 facilitates migration and invasion in HER2 overexpressing breast epithelial progenitor cells and generates a niche for capillary-like network formation. *In Vitro Cell Dev Biol Anim* (2019) 55:838–53. doi: 10.1007/s11626-019-00403-x

28. Karlsson C, Korayem AM, Scherfer C, Loseva O, Dushay MS, Theopold U. Proteomic analysis of the drosophila larval hemolymph clot. *J Biol Chem* (2004) 279:52033–41. doi: 10.1074/jbc.M408220200

29. Palmerini V, Monzani S, Laurichesse Q, Loudhaief R, Mari S, Cecatiello V, et al. Drosophila TNFRs grindelwald and wengen bind eiger with different affinities and promote distinct cellular functions. *Nat Commun* (2021) 12:2070. doi: 10.1038/s41467-021-22080-9

30. Diwanji N, Bergmann A. The beneficial role of extracellular reactive oxygen species in apoptosis-induced compensatory proliferation. *Fly (Austin)* (2017) 11:46–52. doi: 10.1080/19336934.2016.1222997

31. Chatterjee N, Bohmann D. A versatile PhiC31 based reporter system for measuring AP-1 and Nrf2 signaling in drosophila and in tissue culture. *PloS One* (2012) 7:e34063. doi: 10.1371/journal.pone.0034063

32. Uhlirova M, Bohmann D. JNK- and fos-regulated Mmp1 expression cooperates with ras to induce invasive tumors in drosophila. *EMBO J* (2006) 25:5294–304. doi: 10.1038/sj.emboj.7601401

33. La Marca JE, Richardson HE. Two-faced: roles of JNK signalling during tumourigenesis in the drosophila model. *Front Cell Dev Biol* (2020) 8:42. doi: 10.3389/fcell.2020.00042

34. Bilder D, Ong K, Hsi TC, Adiga K, Kim J. Tumour-host interactions through the lens of drosophila. *Nat Rev Cancer* (2021) 21:687–700. doi: 10.1038/s41568-021-00387-5

35. Tran DT, Kelly G. Ten Hagen Real-time insights into regulated exocytosis. *J Cell Sci* (2017) 130 (8):1355–1363. doi: 10.1242/jcs.193425

36. Bartlett BJ, Isakson P, Lewerenz J, Sanchez H, Kotzebue RW, Cumming RC, et al. p62, Ref(2)P and ubiquitinated proteins are conserved markers of neuronal aging, aggregate formation and progressive autophagic defects. *Autophagy* (2011) 7:572–83. doi: 10.4161/auto.7.6.14943

37. Asano K, Miwa M, Miwa K, Hanayama R, Nagase H, Nagata S, et al. Masking of phosphatidylserine inhibits apoptotic cell engulfment and induces autoantibody production in mice. *J Exp Med* (2004) 200 (4):459–467. doi: 10.1084/jem.20040342

38. Recouvreux MV, Commisso C. Macropinocytosis: a metabolic adaptation to nutrient stress in cancer. *Front Endocrinol (Lausanne)* (2017) 8:261. doi: 10.3389/fendo.2017.00261

39. Williams ST, Smith AN, Cianci CD, Morrow JS, Brown TL. Identification of the primary caspase 3 cleavage site in alpha II-spectrin during apoptosis. *Apoptosis* (2003) 8:353–61. doi: 10.1023/A:1024168901003

40. Zhao T, Su Z, Li Y, Zhang X, You Q. Chitinase-3 like-protein-1 function and its role in diseases. *Signal Transduct Target Ther* (2020) 5:201. doi: 10.1038/s41392-020-00303-7

41. Kucerova L, Broz V, Arefin B, Maaroufi HO, Hurychova J, Strnad H, et al. The drosophila chitinase-like protein IDGF3 is involved in protection against nematodes and in wound healing. *J Innate Immun* (2015) 8:199–210. doi: 10.1159/000442351

42. Lee CG, Da Silva CA, Dela Cruz CS, Ahangari F, Ma B, Kang MJ, et al. Role of chitin and chitinase/chitinase-like proteins in inflammation, tissue remodeling, and injury. *Annu Rev Physiol* (2011) 73:479–501. doi: 10.1146/annurev-physiol-012110-142250

43. Fogarty CE, Bergmann A. Killers creating new life: caspases drive apoptosis-induced proliferation in tissue repair and disease. *Cell Death Differ* (2017) 24:1390–400. doi: 10.1038/cdd.2017.47

44. Yeh YT, Hou MF, Chung YF, Chen YJ, Yang SF, Chen DC, et al. Decreased expression of phosphorylated JNK in breast infiltrating ductal carcinoma is associated with a better overall survival. *Int J Cancer* (2006) 118:2678–84. doi: 10.1002/ijc.21707

45. Tang H, Sun Y, Shi Z, Huang H, Fang Z, Chen J, et al. YKL-40 induces IL-8 expression from bronchial epithelium *via* MAPK (JNK and ERK) and NF-kappaB pathways, causing bronchial smooth muscle proliferation and migration. *J Immunol* (2013) 190:438–46. doi: 10.4049/jimmunol.1201827

46. Insua-Rodriguez J, Pein M, Hongu T, Meier J, Descot A, Lowy CM, et al. Stress signaling in breast cancer cells induces matrix components that promote chemoresistant metastasis. *EMBO Mol Med* (2018) 10:e9003. doi: 10.15252/emmm.201809003

47. Juliano RL, Kimelberg HK, Papahadjopoulos D. Synergistic effects of a membrane protein (spectrin) and Ca 2+ on the Na + permeability of phospholipid vesicles. *Biochim Biophys Acta* (1971) 241:894–905. doi: 10.1016/0005-2736(71)90017-4

48. Pinder JC, Bray D, Gratzer WB. Actin polymerisation induced by spectrin. *Nature* (1975) 258:765–6. doi: 10.1038/258765a0

49. Hardy B, Schrier SL. The role of spectrin in erythrocyte ghost endocytosis. *Biochem Biophys Res Commun* (1978) 81:1153–61. doi: 10.1016/0006-291X(78)91257-3

50. Lattner J, Leng W, Knust E, Brankatschk M, Flores-Benitez D. Crumbs organizes the transport machinery by regulating apical levels of PI(4,5)P2 in drosophila. *Elife* (2019) 8:e50900. doi: 10.7554/eLife.50900

51. Ackermann A, Brieger A. The role of nonerythroid spectrin alphaII in cancer. *J Oncol* (2019) 2019:7079604. doi: 10.1155/2019/7079604

52. Yang P, Yang Y, Sun P, Tian Y, Gao F, Wang C, et al. betaII spectrin (SPTBN1): biological function and clinical potential in cancer and other diseases. *Int J Biol Sci* (2021) 17:32–49. doi: 10.7150/ijbs.52375

53. Ziemnicka-Kotula D, Xu J, Gu H, Potempska A, Kim KS, Jenkins EC, et al. Identification of a candidate human spectrin src homology 3 domain-binding protein suggests a general mechanism of association of tyrosine kinases with the spectrin-based membrane skeleton. *J Biol Chem* (1998) 273:13681–92. doi: 10.1074/jbc.273.22.13681

54. Macoska JA, Xu J, Ziemnicka D, Schwab TS, Rubin MA, Kotula L. Loss of expression of human spectrin src homology domain binding protein 1 is associated with 10p loss in human prostatic adenocarcinoma. *Neoplasia* (2001) 3:99–104. doi: 10.1038/sj.neo.7900145

55. Dubielecka PM, Cui P, Xiong X, Hossain S, Heck S, Angelov L, et al. Differential regulation of macropinocytosis by Abi1/Hssh3bp1 isoforms. *PloS One* (2010) 5:e10430. doi: 10.1371/journal.pone.0010430

56. Ritter M, Bresgen N, Kerschbaum HH. From pinocytosis to methuosis-fluid consumption as a risk factor for cell death. *Front Cell Dev Biol* (2021) 9:651982. doi: 10.3389/fcell.2021.651982

57. Maxson ME, Sarantis H, Volchuk A, Brumell JH, Grinstein S. Rab5 regulates macropinocytosis by recruiting the inositol 5-phosphatases OCRL and Inpp5b that hydrolyse PtdIns(4,5)P2. *J Cell Sci* (2021) 134(7):jcs252411. doi: 10.1242/jcs.252411

58. Shubin AV, Demidyuk IV, Komissarov AA, Rafieva LM, Kostrov SV. Cytoplasmic vacuolization in cell death and survival. *Oncotarget* (2016) 7:55863–89. doi: 10.18632/oncotarget.10150

59. Yan G, Dawood M, Bockers M, Klauck SM, Fottner C, Weber MM, et al. Multiple modes of cell death in neuroendocrine tumors induced by artesunate. *Phytomedicine* (2020) 79:153332. doi: 10.1016/j.phymed.2020.153332

60. Mehrotra S, Maqbool SB, Kolpakas A, Murnen K, Calvi BR. Endocycling cells do not apoptose in response to DNA rereplication genotoxic stress. *Genes Dev* (2008) 22:3158–71. doi: 10.1101/gad.1710208

61. Zhang B, Mehrotra S, Ng WL, Calvi BR. Low levels of p53 protein and chromatin silencing of p53 target genes repress apoptosis in drosophila endocycling cells. *PloS Genet* (2014) 10:e1004581. doi: 10.1371/journal.pgen.1004581

62. Araki M, Kurihara M, Kinoshita S, Awane R, Sato T, Ohkawa Y, et al. Anti-tumour effects of antimicrobial peptides, components of the innate immune system, against haematopoietic tumours in drosophila mxc mutants. *Dis Model Mech* (2019) 12 (6):dmm037721. doi: 10.1242/dmm.037721

63. Parvy JP, Yu Y, Dostalova A, Kondo S, Kurjan A, Bulet P, et al. The antimicrobial peptide defensin cooperates with tumour necrosis factor to drive tumour cell death in drosophila. *Elife* (2019) 8:e45061. doi: 10.7554/eLife.45061

64. Kzhyshkowska J, Larionova I, Liu T. YKL-39 as a potential new target for anti-angiogenic therapy in cancer. *Front Immunol* (2019) 10:2930. doi: 10.3389/fimmu.2019.02930

frontiers | Frontiers in Oncology

TYPE Original Research
PUBLISHED 03 May 2023
DOI 10.3389/fonc.2023.1200203



OPEN ACCESS

EDITED BY
Zhiqian Zhang,
Southern University of Science and Technology, China

REVIEWED BY
Yi Li,
Nanjing Medical University, China
Aierpati Maimaiti,
First Affiliated Hospital of Xinjiang Medical University, China

*CORRESPONDENCE
Zhi-qiang Wei
zhiqiang20088@126.com
Yan-cai Yang
yangyancai2008@sina.com

RECEIVED 04 April 2023
ACCEPTED 24 April 2023
PUBLISHED 03 May 2023

CITATION
Wei Z-q, Ding S and Yang Y-c (2023) TYROBP-positive endothelial cell-derived TWEAK as a promoter of osteosarcoma progression: insights from single-cell omics.
*Front. Oncol.* 13:1200203.
doi: 10.3389/fonc.2023.1200203



# TYROBP-positive endothelial cell-derived TWEAK as a promoter of osteosarcoma progression: insights from single-cell omics

Zhi-qiang Wei*, Sheng Ding and Yan-cai Yang*

The Department of Pediatric Surgery, The Ningbo Women and Children's Hospital, Ningbo, China

**Background:** Endothelial cells (ECs) play a vital role in promoting the progression of malignant cells, and they exhibit heterogeneity in their phenotypic characteristics. We aimed to explore the initiating cells of ECs in osteosarcoma (OS) and investigate their potential interaction with malignant cells.

**Method:** We obtained scRNA-seq data from 6 OS patients, and datasets were batch-corrected to minimize variations among samples. Pseudotime analysis was performed to investigate the origin of differentiation of ECs. CellChat was employed to examine the potential communication between endothelial cells and malignant cells, and gene regulatory network analysis was performed to identify transcription factor activity changes during the conversion process. Importantly, we generated TYROBP-positive ECs *in vitro* and investigated its role in OS cell lines. Finally, we explored the prognosis of specific ECs cluster and their impact on the tumor microenvironment (TME) at the bulk transcriptome level.

**Results:** The results showed that TYROBP-positive ECs may play a crucial role in initiating the differentiation of ECs. TYROBOP-positive endothelial cells (ECs) exhibited the strongest crosstalk with malignant cells, likely mediated by TWEAK, a multifunctional cytokine. TYROBP-positive ECs exhibited significant expression of TME-related genes, unique metabolic and immunological profiles. Importantly, OS patients with low enrichment of TYROBP-positive ECs had better prognoses and a lower risk of metastasis. Finally, vitro assays confirmed that TWEAK was significantly increased in ECs-conditioned medium (ECs-CM) when TYROBP was over-expressed in EC cells, and could promote the proliferation and migration of OS cells.

**Conclusion:** We concluded that TYROBP-positive ECs may be the initiating cells and play a crucial role in the promotion of malignant cell progression. TYROBP-positive ECs have a unique metabolic and immunological profile and may interact with malignant cells through the secretion of TWEAK.

KEYWORDS

**TWEAK, osteosarcoma, TYROBP, tumor microenvironment, prognosis, endothelial cells**

# Introduction

Osteosarcoma (OS) is a highly malignant bone tumor, mainly affecting children and adolescents (1). With the development of multimodal therapy, including surgery, chemotherapy, and radiation therapy, the survival rate of OS patients has improved significantly over the past few decades (2). Current research efforts on OS treatment are mainly focused on two aspects: identifying novel therapeutic targets and improving the effectiveness of existing therapies (3). Several potential therapeutic targets for OS have been identified, including receptor tyrosine kinases, immune checkpoints, and metabolic pathways (4, 5). Moreover, advances in genomics and transcriptomics have led to the identification of several molecular subtypes of OS, which may have different treatment responses and prognoses (6). Understanding the molecular characteristics of OS can help to develop personalized treatment strategies and improve patient outcomes.

The tumor microenvironment (TME) plays a crucial role in the progression of OS (7). For example, studies have shown that the TME can affect the behavior of OS cells by promoting angiogenesis, remodeling of the extracellular matrix, and immune evasion (8). Additionally, studies have shown that the TME can influence the response of OS to chemotherapy and radiation therapy (9). Endothelial cells (ECs), the major component of vascular endothelium, have important impacts on tumor growth and metastasis in cancer (10). In cancer, ECs can be classified into multiple subtypes with different transcriptional profiles, phenotypes, and functions (7). The expression profiles and distribution of endothelial cell subtypes are closely associated with different tumor types and microenvironments. Specific proteins expressed by ECs in tumor vasculature can be used for screening potential therapeutic targets, and different subtypes of ECs may respond differently to therapeutic drugs (7). In some cases, ECs can suppress tumor immune responses by expressing immune checkpoint molecules such as PD-L1 (11), and some studies have suggested that tumor vasculature ECs can promote tumor immune evasion and metastasis (12). Therefore, a deeper understanding of endothelial cell heterogeneity in cancer can not only promote the understanding of the tumor microenvironment but also provide valuable insights for the development of novel cancer therapeutic strategies.

The impact of single-cell omics methods on OS and other tumors in the introduction. Indeed, single-cell omics methods have revolutionized our ability to study tumors at the single-cell level, providing unprecedented insights into tumor heterogeneity, cell-to-cell communication, and cellular plasticity (13). Single-cell RNA sequencing (scRNA-seq) is particularly powerful, allowing us to identify rare cell populations and study their transcriptional profiles in depth. In this study, we analyzed scRNA-seq data from OS patients and identified heterogeneity of ECs across different patients. Specifically, we observed that TYROBP-positive ECs showed the strongest interaction with malignant cells and may serve as initiating cells by secreting TWEAK and other proteins that influence tumor progression. We also found that patients with low enrichment of TYROBP-positive ECs had better prognoses and a lower risk of metastasis.

# Materials and methods

## Pre-processing of the scRNA-seq datasets

We obtained the scRNA-seq dataset for osteosarcoma comprising of 6 samples (GSE162454) and the corresponding meta information from the Tumor Immune Single-cell Hub (TISCH) database (14). To ensure the quality of the data, we conducted quality control (QC), normalization, scaling, and principal component analysis (PCA) using the Seurat package (v4.0.5). We then performed clustering using the "Find Neighbors" and "Find Clusters" functions at a resolution of 0.7. The resulting clusters were visualized by t-distributed stochastic neighbor embedding (tSNE) and identified using the meta information files from TISCH database. Subsequently, we extracted the data for ECs from the Seurat object and repeated the aforementioned process with LogFC = 0.5 and min.pct = 0.35 to identify markers for different clusters.

## Cell culture and conditioned medium collection

As EC cells are difficult to extract from OS tissues, we selected the Human umbilical vein endothelial cells (HUVECs) as an *in vitro* model, based on previous references. The HUVECs were cultured in an endothelial growth medium supplemented with 10% fetal bovine serum and penicillin-streptomycin, as well as all the supplied endothelial growth medium supplements (Procel, Wuhan, China). For the preparation of endothelial cell-conditioned medium (ECs-CM), $1 \times 10^6$ cells were seeded onto T25 culture flasks and incubated for 48 hours. The medium was then replaced with 5mL of serum-free DMEM/F12 (keyGEN, China) and further incubated for 24 h. The resulting CM was collected, filtered, and stored at −80° C. The human OS cell lines U2-OS and 143B (Procel, Wuhan, China) were cultured in DMEM/F12 supplemented with 10% FBS. All cells were cultured at 37°C in a humidified atmosphere of 95% air/5% $CO_2$.

## Lentiviral transfection

LV-TYROBP and LV-NC were purchased from Sangon Biotech (Shanghai, China). HUVECs cells stably expressing TYROBP were established by transfecting the lentivirus.

## Enzyme-linked immunosorbent assay

Cell culture supernatants from normal HUVECs and TYROBP-positive HUVECs were collected to assess TWEAK secretion levels using a specific TWEAK ELISA kit (R&D Systems Inc., Minneapolis, MN). The color intensity of the wells was measured using a microplate reader (BioTek, Winooski, VT) at 450 nm after color development was stopped.

## Migration assay and Cell Counting Kit-8

We utilized Transwell chambers (8-μm pores) in a 24-well plate (Corning, MA, USA) to evaluate the migration of U2-OS and 143B. In the upper chamber, serum-free F12/DMEM containing tumor cells was added, while the lower chamber contained ECs-CM supplemented with 20% FBS. After culturing for 24 h, the migrated cells were fixed with 4% paraformaldehyde, stained with crystal violet, and enumerated using bright-field microscopy. The proliferation of U2-OS and 143B was assessed using a 96-well plate, with 2000 cells per well, and various concentrations of ECs-CM derived from normal HUVECs and TYROBP-positive HUVECs. The plate was incubated for two hours at 37°C, and the Cell Counting Kit-8 (CCK-8) reagent (Dojindo, Japan) was added before measuring absorbance at 450 nm. Assays were performed every 24 h.

## RNA extraction and real-time polymerase chain reaction (PCR) assay

RNA isolation was performed using the FastPure Cell/Tissue Total RNA Isolation Kit V2 (Vazyme, Nanjing, China) according to the manufacturer's protocol. Complementary DNA (cDNA) was synthesized from the isolated RNA using the HiScript III All-in-one RT SuperMix Perfect for qPCR Kit (Vazyme, Nanjing, China). Real-time PCR was carried out on the synthesized cDNA using the Taq Pro Universal SYBR qPCR Master Mix Kit (Vazyme, Nanjing, China) in an ABI7500 real-time PCR system (Applied Biosystems). The primer sequence was from the previous references (15).

## Gene regulatory network analysis and pseudotime analysis

In order to identify the gene regulatory network of each cluster of ECs, we employed the single-cell regulatory network inference and clustering (SCENIC) approach using the SCENIC package (v1.3.1). The method infers potential transcription factor targets based on the expression data and evaluates the activity of regulons in individual cells. The differentially activated regulons of each cluster of ECs were identified by constructing a heatmap. Pseudotime analysis was conducted using the Monocle package (v2.22.0). Single-cell trajectories were calculated using the functions "order_cells" based on ECs cluster from Seurat.

## Cell–cell communication analysis

Cell-Cell Communication (CCC) Analysis serves as an essential reference database for establishing ligand-receptor pairs and secretory signaling pathways via the CellChat package (v1.1.3). The principal focus of CCC is to explore the relationship between malignant cells and ECs. To this end, the analytical suite, including "netAnalysis signalingRole scatter," "netAnalysis signalingRole heatmap," and "netVisual circle," was utilized to gain valuable insight into the complex interplay between these cells.

## Gene set variation analysis and metabolic analysis

Gene set variation analysis (GSVA) (16) was executed utilizing the GSVA package (v1.40.1). Specifically, in the single-cell RNA sequencing dataset, the pathway activation was calculated for each cluster using "hallmark" gene sets. In addition, in the bulk RNA data, the score for each sample was evaluated using "KEGG.v7.4" gene sets, and a list of 29 immune cell-associated genes previously reported in the references was also considered. Metabolic analysis was executed utilizing the scMetabolism package (v0.2.1). The package was pre-populated with a human metabolic gene set, including 85 KEGG pathways and 82 REACTOME entries, based on the mean of the above gene sets values for metabolic activity analysis. These approaches provide a comprehensive and in-depth understanding of the gene expression pattern in these datasets.

## Pre-processing of the bulk transcriptome datasets

We utilized RNA-seq data from the TARGET database, including 88 OS samples, with non-coding RNAs excluded for downstream analysis. To ensure robustness of our modeling, we finally included 84 osteosarcoma samples without duplicate sequencing. To complement our findings, we also obtained the GSE21257 dataset from the GEO database, with samples screened using the same inclusion and exclusion criteria. An external validation cohort of 53 OS patients was included in our study. Finally, the specific endothelial cell cluster's score of the bulk transcriptome sample was calculated using ssGSEA algorithm based on the marker genes derived from the scRNA-seq data. Overall patients were divided into high-score and low-score groups based on the cut-off of endothelial cell scores in survival analysis.

## ESTIMATE algorithm

We employed the ESTIMATE package (v1.0.13) to estimate stromal score and immune score of tumor samples based on their expression data. Furthermore, differential comparisons were conducted based on specific epithelial cells score.

## Construction and validation of the ECs-derived risk score

We used the limma package (v3.50.3) to calculate the differentially expressed genes (DEGs) between different epithelial cell score in the TARGET cohort. An adjusted p-value <0.05, and an absolute value of logFC greater than 1 were used as thresholds for

selecting DEGs. We conducted a series of analyses to identify genes with prognostic value for our study. Initially, we performed univariate Cox regression analysis on the previously identified genes (p-value <0.05). Next, we applied a least absolute shrinkage and selection operator (LASSO) model to eliminate genes that were not useful for prognosis. We then constructed risk score formulas by integrating gene expression values weighted by their LASSO-Cox coefficients, as recommended in previous references's pipline (17, 18). Finally, we assessed the independent prognostic value of the risk score in our dataset using multivariate Cox regression analysis. Additionally, we employed time-dependent subject operating characteristic (ROC) curves to compare the predictive accuracy of the risk score in different survival time. Finally, all patients were divided into high and low risk groups according to the cut-off value of risk score. For nomogram, based on our previous references, we utilized the regplot package (v1.1) to develop a nomogram that combined risk scores with significant clinical indicators identified by multivariate Cox regression analysis (19). To validate the prognostic predictive ability of the newly generated scores, we employed several packages, including survminer (v3.3-1), timeROC (v0.4), rms (v6.3-0), and rmda (v1.6). These packages were instrumental in assessing the performance of the scores and determining their usefulness in predicting outcomes.

## Drug sensitivity

The compDrugsen function of MOVICS package (v0.99.17) was used to compare the IC50 of drug of different groups by constructing ridge regression model.

## Statistical analysis

We conducted statistical analysis using R software (v4.1.2). For most cases, the significance of differences was tested using the Wilcoxon rank-sum test. The level of statistical significance was set at a p-value < 0.05, denoted by *p < 0.05, **p < 0.01, or ***p <0.001, while results without significant differences were marked as ns (not significant). We also performed overall survival analysis using the log-rank test.Results

## TYROBP-positive endothelial cells may be the initiating cells

We obtained the GSE162454 dataset from the TISCH database, which had been batch-corrected to minimize variations among samples. The dataset comprised of scRNA data from 6 OS patients, and these cells were clustered to yield 29 subgroups (Figure 1A). Using the annotation information provided in the TISCH database, the cells were classified into eight different cell types, namely, plasma cells, conventional $CD4^+$ T cells (CD4Tconv), exhausted $CD8^+$ T cells (CD8Tex), ECs, epithelial cells, fibroblasts, monocytes/macrophages (mono/macro), and osteoblasts (Figure 1B). As ECs are known to promote the progression of malignant cells (10), the original data was extracted from the endothelial cell clusters and re-clustered to construct an endothelial cell atlas, and the final ECs were divided into four clusters. The highly expressed genes in each cluster were identified as EDNBR (endothelial_0), FABP4 (endothelial_1), MKI67 (endothelial_2), and TYROBP (endothelial_3), as depicted in Figure 1C. To explore the specificity of different ECs, we determined the percentage of different ECs in six patients. For instance, endothelial_0 accounted for 62.2% in GSM4952363, endothelial_0 accounted for 66.2% in GSM4952364, endothelial_1 accounted for 63.6% in patient GSM4952365, endothelial_0 accounted for 77.3% in patient GSM5155198, endothelial_0 accounted for 60.1% in patient GSM5155199, and endothelial_1 accounted for 78.9% in patient GSM5155200 (Figure 1D). These results indicated that endothelial_0 and endothelial_1 was predominant in different patients, and there was heterogeneity in the distribution of other ECs among patients. To investigate the origin of differentiation of ECs, pseudotime analysis was performed, and interestingly, four nodes were identified in the trajectory in two-dimensional space after sorting the cells, with endothelial_3 being the initiating cells at the beginning (Figure 1E). Therefore, we speculate that TYROBP-positive ECs (endothelial_3) may play a crucial role in initiating the differentiation of ECs.

## TYROBP-positive endothelial cells generate the strongest crosstalk with malignant cells

We have re-annotated and visualized ECs using highly expressed markers of different subsets of ECs. Our analysis identified four renamed subclusters of endothelial cells, namely TYROBP-positive ECs, EDNRB-positive ECs, FABP4-positive ECs, and MKI67-positive ECs, as shown in the t-sne plot in Figure 2A. Interestingly, TYROBP-positive ECs displayed the highest incoming and outgoing signal strength, indicating that they may play a critical role in the communication between endothelial cell clusters and malignant cells (Figure 2B). We further examined the strength of secretory signals in different cell types using heatmaps, and our results demonstrated significant activation of key efferent signals such as VEGF and CCL (Figure 2C). Moreover, we used a network to calculate the weight and strength ratio of the interactions, and our findings revealed major interactions between malignant cells and TYROBP-positive ECs, MKI67-positive ECs, and EDNRB-positive ECs, as well as interconnections between different ECs (Figure 2D).

## Overexpression of TYROBP results in increased TWEAK production by endothelial cells

We investigated the potential mechanism by which TYROBP-positive ECs may interact with malignant cells through the secretion of chemokines, such as TNFSF12, TNF, RETN, and PDGFB, among others (Figure 3A). It is worth noting that TNSF12 showed the strongest communication scores. TNFSF12, also known as TNF-related weak inducer of apoptosis (TWEAK), is a cytokine that has been implicated in a variety of physiological and pathological

processes. TNFSF12 is expressed by a range of cell types, including endothelial cells, and has been shown to interact with its receptor, fibroblast growth factor-inducible 14 (Fn14), to activate downstream signaling pathways. To investigate the impact of TYROBP overexpression in endothelial cells, we attempted to transfect TYROBP into HUVECs cell lines. However, due to the inherent characteristics of HUVECs, we encountered suboptimal transfection efficiency (Figure 3B). Nevertheless, we successfully confirmed the presence of TYROBP-positive endothelial cells through the detection of TYROBP mRNA (Figure 3C), which was further validated by ELISA data showing a significant increase in TWEAK production in the conditioned medium (Figure 3D). Notably, the conditioned medium from TYROBP-positive endothelial cells induced significant changes in the proliferation and migration of osteosarcoma cell lines (Figures 3E–G). Mechanistically, our data suggest that the elevated expression of

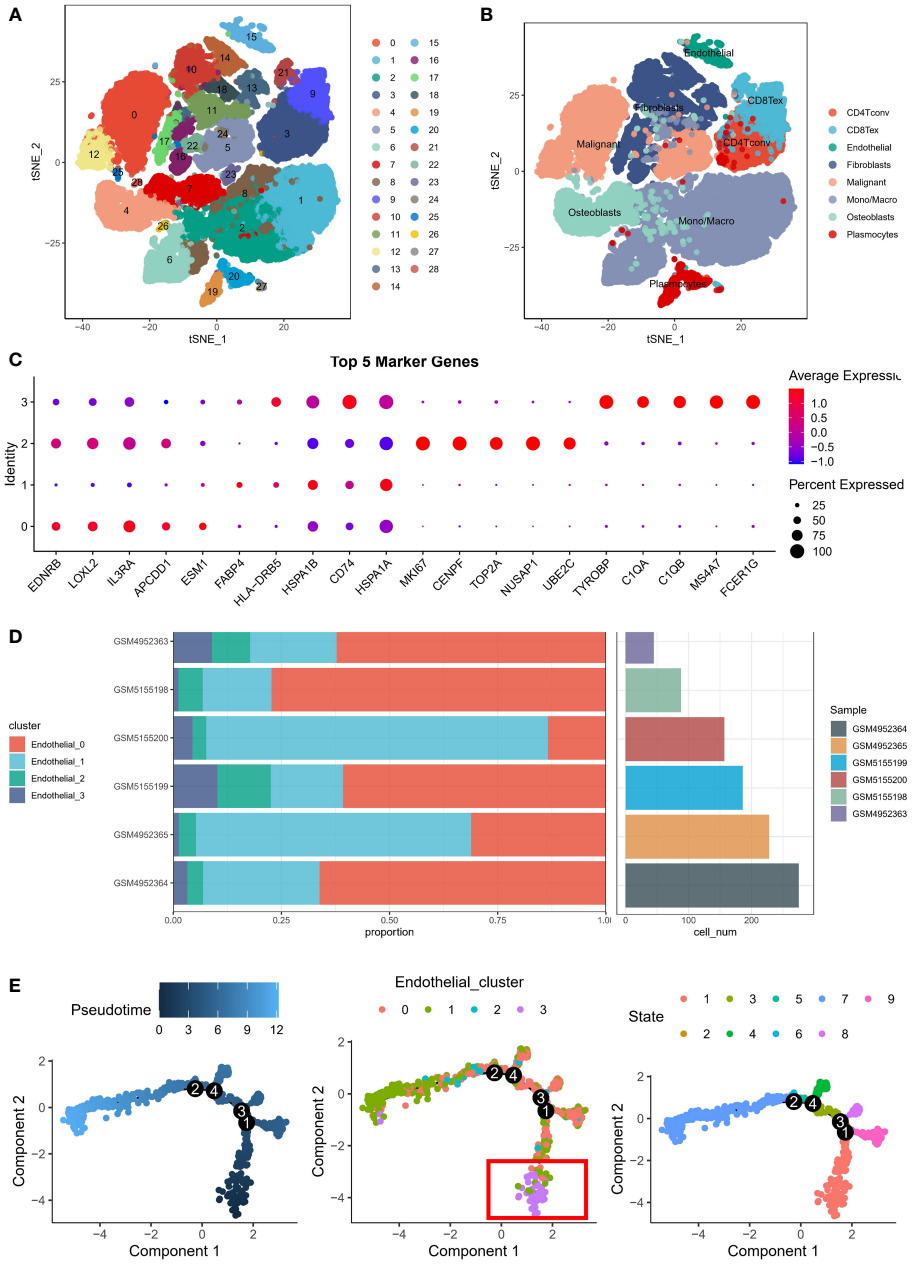


FIGURE 1
Endothelial cell atlas of osteosarcoma. **(A)** Clustering analysis of scRNA data from 6 osteosarcoma patients, which generated 29 subgroups. **(B)** Classification of cells into eight different cell types: plasma cells, conventional CD4+ T cells (CD4Tconv), exhausted CD8+ T cells (CD8Tex), endothelial cells, epithelial cells, fibroblasts, monocytes/macrophages (mono/macro), and osteoblasts. **(C)** Expression of highly expressed genes in four endothelial cell clusters: EDNBR (endothelial_0), FABP4 (endothelial_1), MKI67 (endothelial_2), and TYROBP (endothelial_3). **(D)** Percentage of different endothelial cells in six patients, with endothelial_0 and endothelial_1 being predominant in different patients. **(E)** Pseudotime analysis of endothelial cells, showing four nodes in the trajectory in two-dimensional space, with TYROBP-positive endothelial cells (endothelial_3) being the initiating cells.

TWEAK and other proteins in the TYROBP-positive endothelial cell-conditioned medium promoted the malignant phenotype of OS cells.

## TYROBP-positive endothelial cells have a unique metabolic and immunological profile

Notably, TYROBP-positive ECs exhibited significant expression of TME-related genes, including those regulating chemokine expression, such as CXCL12 and CXCL3, as demonstrated in Figure 4A. Additionally, differential expression of immune checkpoints (ICI) on ECs clusters was observed, with LAG3, CD48, PDCD1LG2, CD244, SLAMF7, and HAVCR2 being highly expressed in TYROBP-positive ECs, while IDO1, TIGIT, CD95, CD160, and CTLA4 were highly expressed in FABP4-positive ECs, as depicted in Figure 4B. Subsequently, we examined the gene regulatory network to elucidate the transcription factors (TFs) activity changes during the conversion process. Our findings revealed that TYROBP-positive ECs exhibited high activity of FOS, FOSB, HES1, and JUNB, indicating that these TFs may

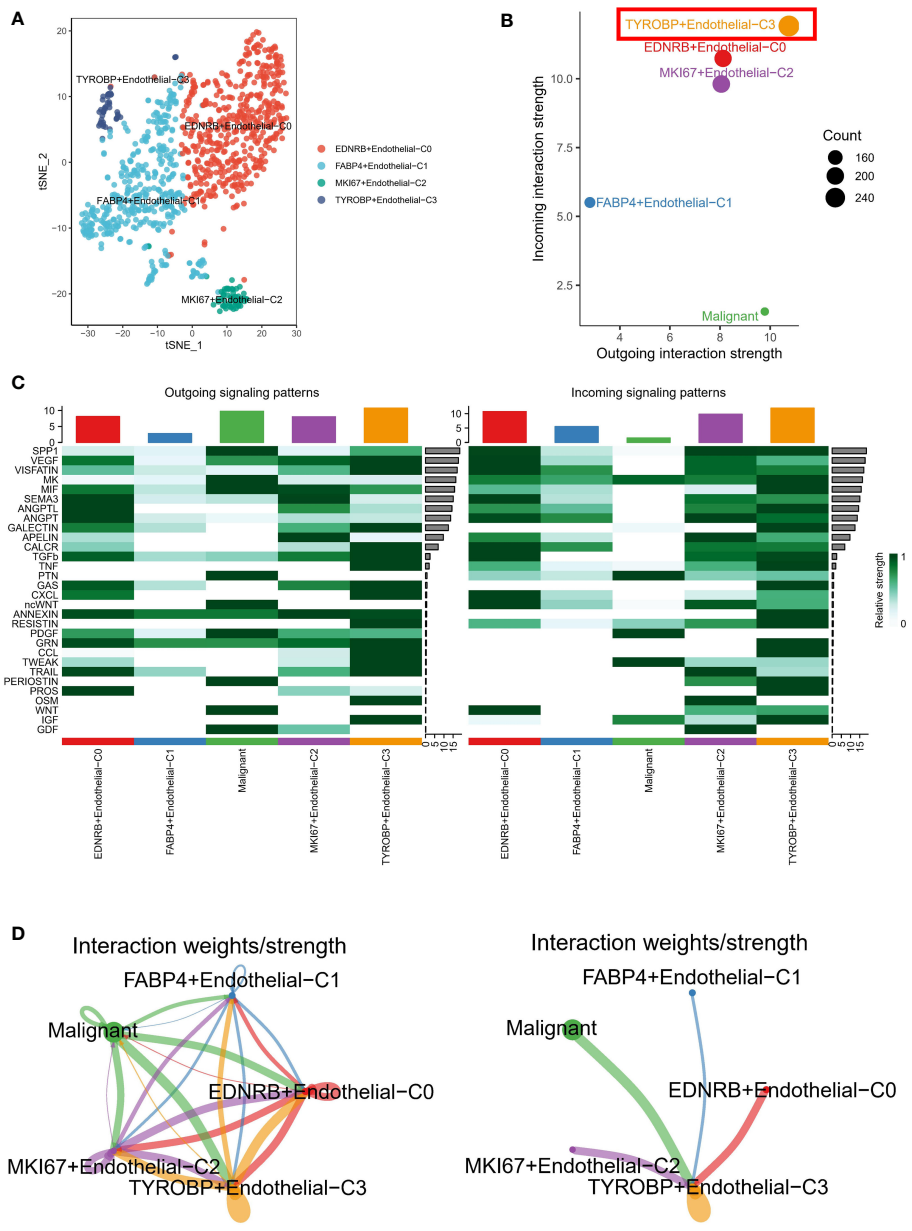


FIGURE 2
Analysis of endothelial cell subsets and interactions with malignant cells. **(A)** Tsne plot showing the four renamed subclusters of endothelial cells based on highly expressed markers. **(B)** TYROBP-positive ECs exhibit the highest incoming and outgoing signal strength, suggesting a critical role in communication between endothelial cell clusters and malignant cells. **(C)** Heatmap analysis demonstrates significant activation of key efferent signals, such as VEGF and CCL, in different cell types. **(D)** Network analysis reveals major interactions between malignant cells and TYROBP-positive ECs, MKI67-positive ECs, and EDNRB-positive ECs, as well as interconnections between different ECs.

promote the differentiation of initiating cells (TYROBP-positive ECs) to other isoforms, as illustrated in Figure 4C. Pathway analysis demonstrated that TYROBP-positive ECs were highly activated in fatty acid metabolic signaling pathways, inflammatory responses, and pro-oncogenic pathways, such as p53 and KRAS, as presented in Figure 4D. Therefore, we further investigated the differences in metabolic pathways between ECs clusters and found that they were distinct. The heat map of the top 10 activated metabolism-related pathways showed that FABP4-positive ECs were in a metabolic silent state, while MKI67-positive ECs were dominated by pyruvate metabolism, and TYROBP-positive ECs were primarily engaged in starch and sucrose metabolism (Figure 4E).

## High enrichment of TYROBP-positive endothelial cells indicates a better prognosis

We utilized the ssGSEA algorithm to assess different ECs scores per patient from bulk transcriptome data. Remarkably, only

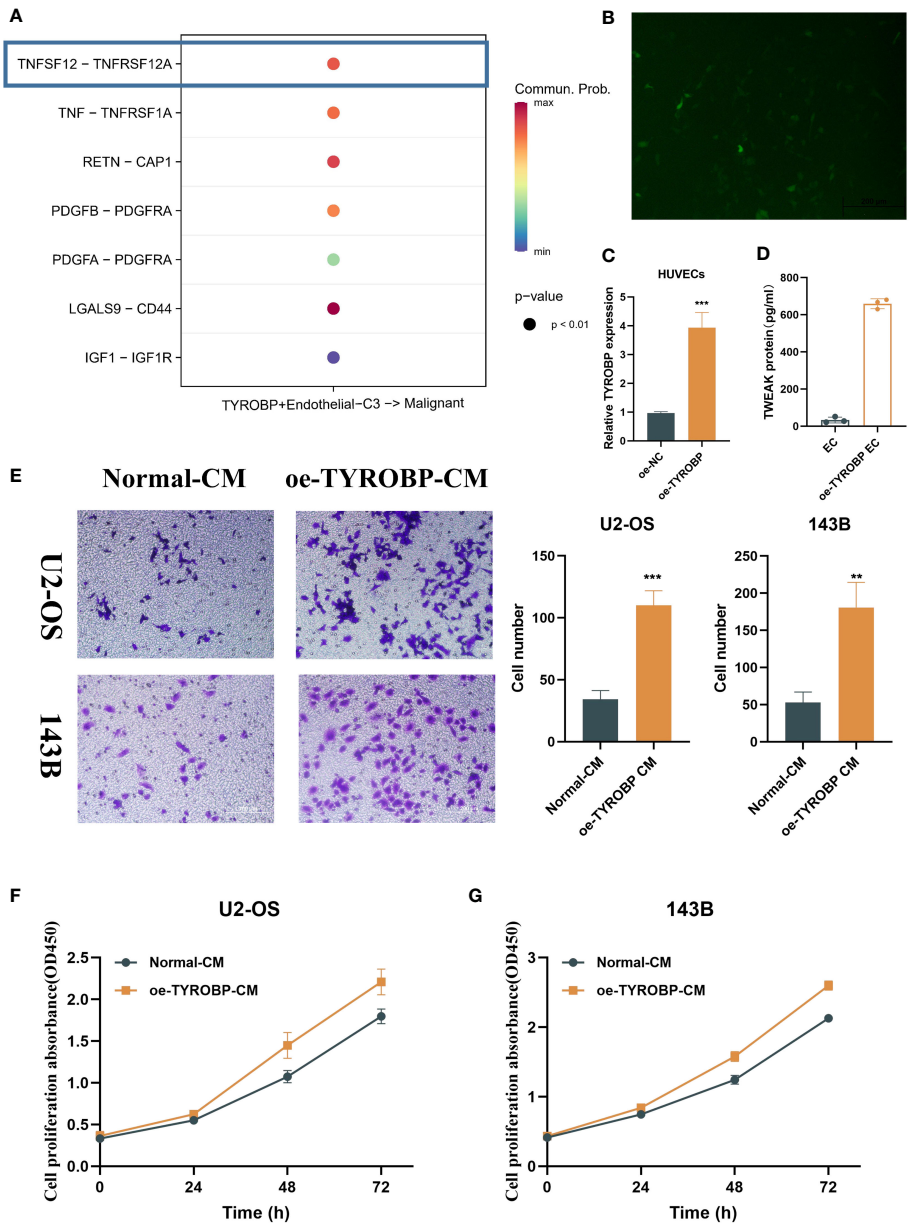


FIGURE 3
TYROBP-positive endothelial cells-derived TWEAK promote proliferation and migration of osteosarcoma. **(A)** Potential mechanism of interaction between TYROBP-positive ECs and malignant cells through the secretion of chemokines, including TNFSF12, TNF, RETN, and PDGFB, among others. **(B)** Fluorescence image 48h after transfection. **(C)** Relative mRNA expression of TYROBP in HUVECs cell lines after TYROBP overexpression. **(D)** TWEAK concentration in different conditioned medium. **(E)** Migration images of OS cell lines (U2-OS and 143B) treated with different conditioned medium. **(F)** The change of proliferative ability of U2-OS cell line under different conditioned medium. **(G)** The change of proliferative ability of 143B cell line under different conditioned medium. **P < 0.01; ***P < 0.001.

10.3389/fonc.2023.1200203

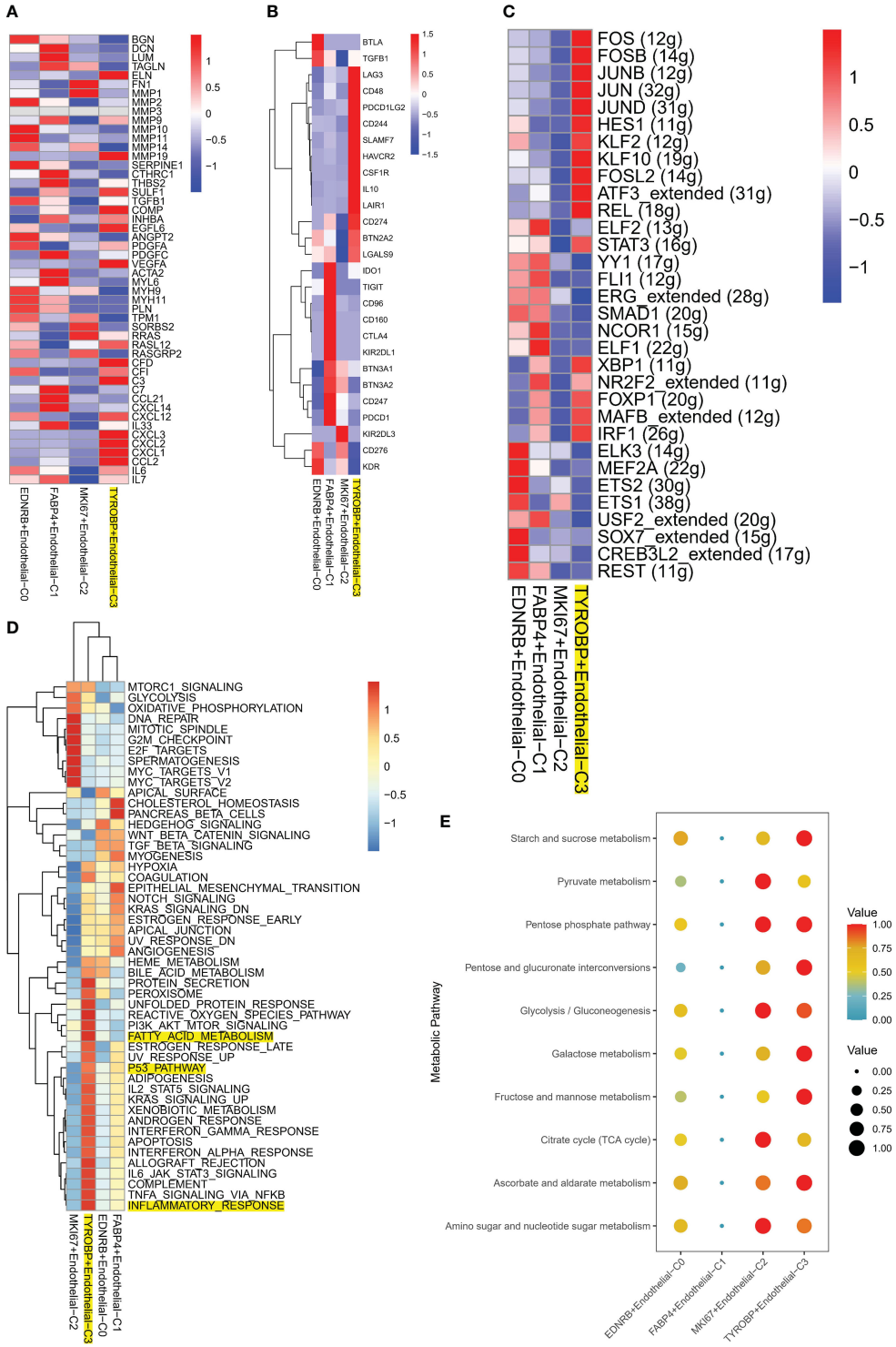


FIGURE 4
Molecular characteristics of TYROBP-positive endothelial cells in the tumor microenvironment. **(A)** TYROBP-positive endothelial cells showed significant expression of tumor microenvironment-related genes, including those involved in chemokine regulation such as CXCL12 and CXCL3. **(B)** Endothelial cell clusters exhibited differential expression of immune checkpoints, with TYROBP-positive endothelial cells expressing high levels of LAG3, CD48, PDCD1LG2, CD244, SLAMF7, and HAVCR2, while IDO1, TIGIT, CD95, CD160, and CTLA4 were highly expressed in FABP4-positive endothelial cells. **(C)** Analysis of gene regulatory networks revealed high activity of FOS, FOSB, HES1, and JUNB in TYROBP-positive endothelial cells, suggesting that these transcription factors may promote the differentiation of initiating cells to other isoforms. **(D)** Pathway analysis showed that TYROBP-positive endothelial cells were highly activated in fatty acid metabolic signaling pathways, inflammatory responses, and pro-oncogenic pathways, such as p53 and KRAS. **(E)** A heatmap of the top 10 activated metabolism-related pathways showed that FABP4-positive endothelial cells were in a metabolic silent state, while MKI67-positive endothelial cells were dominated by pyruvate metabolism. In contrast, TYROBP-positive endothelial cells were primarily engaged in starch and sucrose metabolism, highlighting distinct metabolic pathway utilization between different endothelial cell clusters in the tumor microenvironment.

TYROBP-positive ECs were found to be downregulated in metastatic samples in the TARGET-OS cohort, indicating its potential role in inhibiting tumor metastasis (Figures 5A–D). Additionally, we evaluated the prognostic impact of different ECs on patient outcomes in the TARGET-OS cohort, and only TYROBP-positive ECs exhibited significant prognostic implications. Specifically, patients with low levels of enriched TYROBP-positive ECs had a poorer prognosis (Figures 5E–H). Notably, the prognostic power of TYROBP-positive ECs was consistently observed in the validation cohort GSE21257 (Figure 5I).

## High enrichment of TYROBP-positive endothelial cells represents the "hot" tumor state

Using the GSVA algorithm, we observed differences in the immune microenvironment among patients with varying enrichment levels of TYROBP-positive ECs. Interestingly, patients with high enrichment of TYROBP-positive ECs had greater numbers of activated $CD4^+$ T cells, $CD8^+$ T cells, and natural killer cells (Figure 6A). To ensure the robustness of our

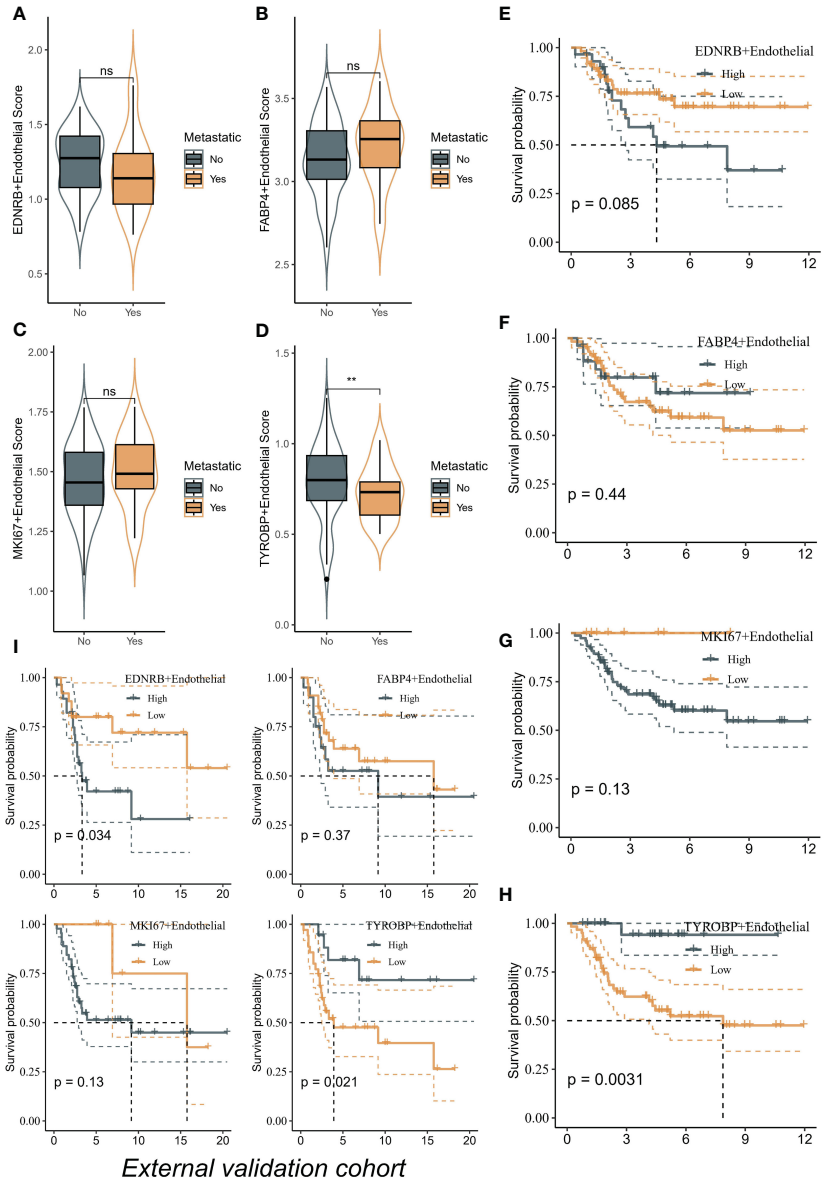


FIGURE 5
TYROBP-positive endothelial cells as potential suppressors of tumor metastasis and prognostic indicators in osteosarcoma. **(A)** The scores of EDNRB-positive ECs in metastatic samples and no-metastatic samples. **(B)** The scores of FABP4-positive ECs in metastatic samples and no-metastatic samples. **(C)** The scores of MKI67-positive ECs in metastatic samples and no-metastatic samples. **(D)** The scores of TYROBP-positive ECs in metastatic samples and no-metastatic samples. TYROBP-positive endothelial cells were found to be downregulated in metastatic samples in the TARGET-OS cohort. Kaplan-Meier plots of the prognostic impact of different endothelial cell types on patient outcomes in the TARGET-OS cohort, including EDNRB-positive ECs **(E)**, FABP4-positive ECs **(F)**, and MKI67-positive ECs **(G)** and TYROBP-positive ECs **(H)**. **(I)** Kaplan-Meier plots of the prognostic impact of different endothelial cell types on patient outcomes in the GSE21257 cohort. **p < 0.01, ns (not significant).

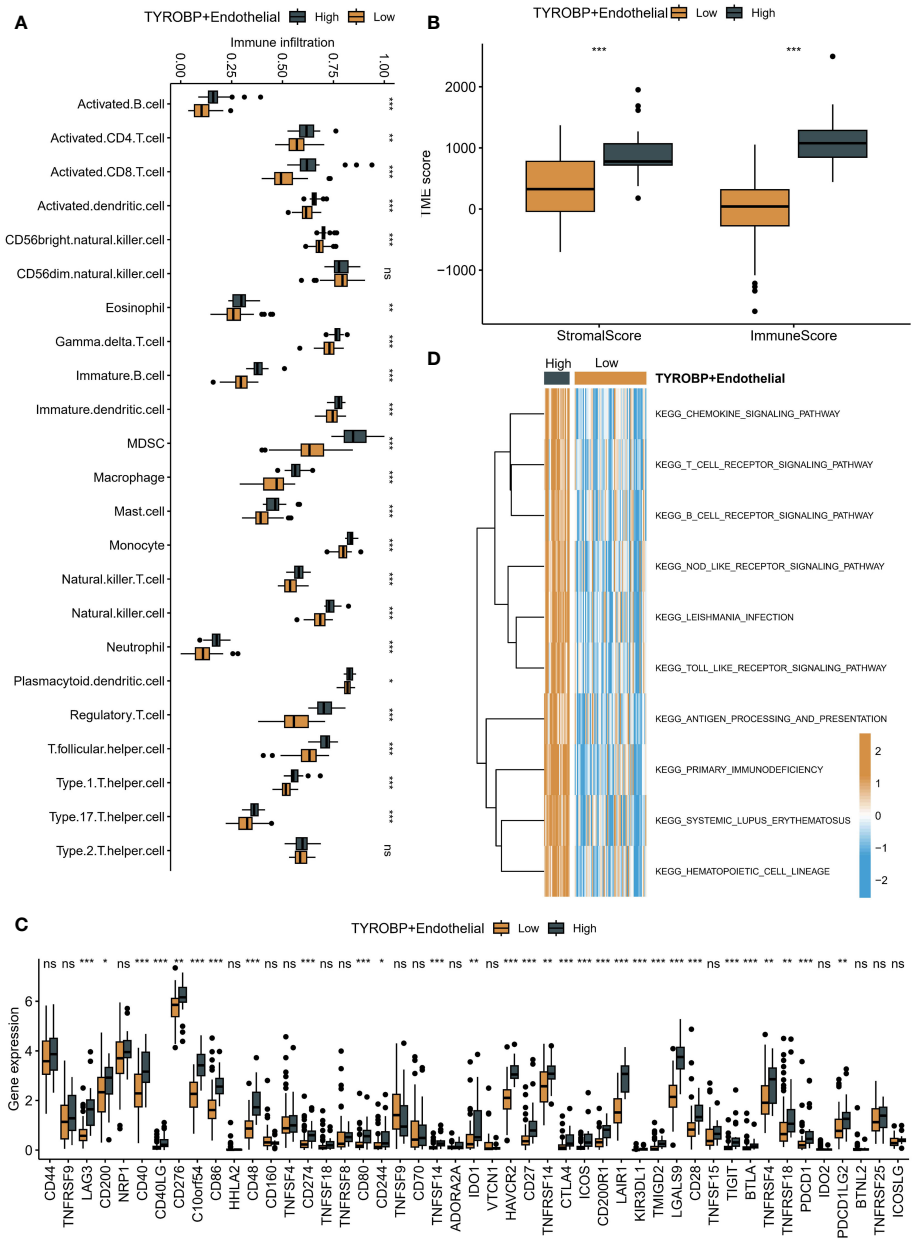


FIGURE 6
Immune microenvironment differences in patients with varying TYROBP-positive EC enrichment levels. **(A)** Patients with high enrichment of TYROBP-positive ECs had increased numbers of activated CD4+ T cells, CD8+ T cells, and natural killer cells. **(B)** Patients with highly enriched TYROBP-positive ECs also exhibited higher immune scores, indicative of a "hot" tumor state, as determined by the ESTIMATE algorithm. **(C)** Patients with highly enriched ECs had higher expression of classical immune checkpoint inhibitors (ICIs). **(D)** High enrichment of TYROBP-positive ECs was associated with significantly activated chemokine, T cell receptor, B cell receptor, and Nod-like receptor signaling pathways, indicating a "hot" tumor state. *P < 0.05; **P < 0.01; ***P < 0.001; ns represents no statistical significance.

findings, we further used the ESTIMATE algorithm to determine that patients with highly enriched TYROBP-positive ECs also exhibited higher immune scores, indicative of a "hot" tumor state (Figure 6B). Additionally, we compared the mRNA expression levels of immune checkpoint inhibitors (ICIs) in patients with different EC enrichments and found that those with highly enriched ECs had higher expression of classical ICIs, such as CD276 and CD274 (Figure 6C). Finally, we evaluated the activation of KEGG pathways among different patients and found that high enrichment of TYROBP-positive ECs was associated with significantly activated chemokine, T cell receptor, B cell receptor, and Nod-like receptor signaling pathways, further supporting our conclusion that it corresponds to a "hot" tumor state. (Figure 6D).

## TYROBP-positive endothelial cell-derived risk signature can be used for prognostic prediction and medication guidance

We identified 213 differential expression genes (DEGs) between patients with varying levels of TYROBP-positive EC enrichment (Figure 7A). Further KEGG enrichment analysis revealed a significant association between TYROBP-positive ECs and immunity, with cytokine-cytokine receptor interaction being the most enriched pathway (Figure 7B). Using LASSO-Cox model, we identified 35 overlapping prognostic genes from the validation cohort, and subsequently selected 6 TYROBP-positive endothelial cell-derived genes for risk score construction (Figure 7C). We divided patients into high-risk and low-risk groups using a cut-off value, and found that

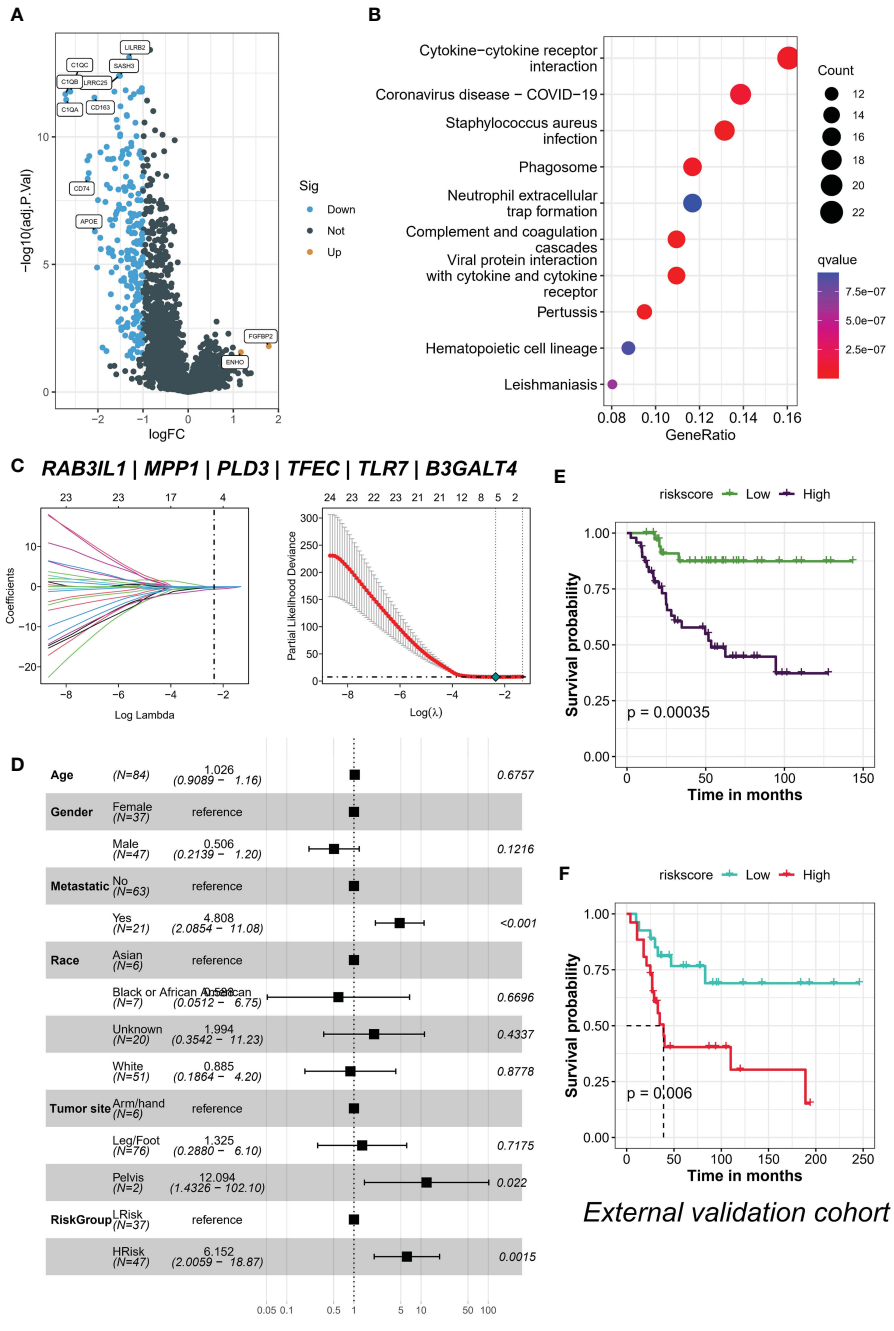


FIGURE 7
TYROBP-positive endothelial cell enrichment is associated with immunity and is an independent prognostic factor. **(A)** Volcano plot depicting the 213 differentially expressed genes (DEGs) identified between patients with varying levels of TYROBP-positive ECs enrichment. **(B)** KEGG enrichment analysis demonstrating that cytokine-cytokine receptor interaction is the most enriched pathway associated with TYROBP-positive ECs. **(C)** LASSO regression model selecting 6 TYROBP-positive endothelial cell-derived genes for risk score construction. **(D)** Multifactorial Cox regression analysis showing that risk grouping based on the constructed risk score is an independent prognostic factor, even after adjusting for clinicopathological variables. Kaplan-Meier curves depicting the survival of patients in different cohorts, such as TARGERT-OS cohort **(E)** and GSE21257 **(F)**, divided into high-risk and low-risk groups based on the constructed risk score.

risk grouping was an independent prognostic factor, even after adjusting for clinicopathological variables (Figure 7D). The high-risk group had a better prognosis in different cohorts (Figures 7E, F). To aid clinical use, we developed nomograms based on meaningful clinical variables and risk scores, which demonstrated clinical benefit in ROC curve, calibration curve, and clinical impact curve analyses (Figures 8A–E). Additionally, we performed drug sensitivity analysis using three targeted drugs with therapeutic OS potential, including BMS-536924, KIN001, and PHA-665752. Our findings showed that the IC50 of the high-risk array was significantly lower than that of the low-risk array, indicating greater sensitivity to these drugs in the high-risk group (Figures 8F–H).

In summary, our findings suggest that TYROBP-positive EC enrichment plays a critical role in promoting immunity and can be used as an independent prognostic feature to predict patient outcomes. The development of visualized nomograms and drug

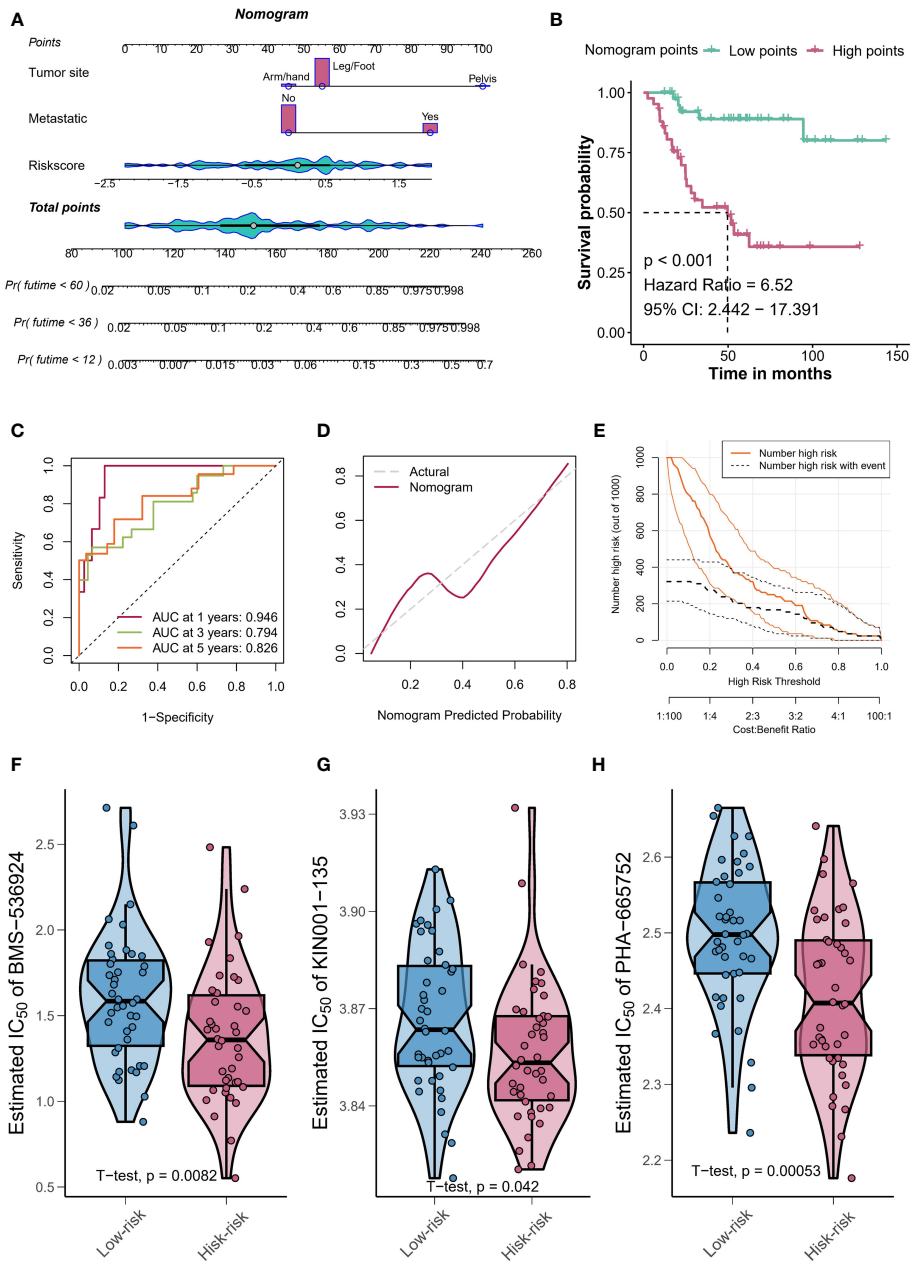


FIGURE 8
Nomograms and drug sensitivity analysis. **(A)** Nomograms based on clinical variables and risk scores demonstrate clinical benefit. **(B)** Kaplan-Meier curves depicting the survival of patients with different nomogram's points. **(C)** The calibration curve shows the agreement between predicted and actual outcomes, further validating the clinical benefit of using the points-based classification scheme. **(D)** The clinical impact curve demonstrates the clinical benefit of using the points-based classification scheme. **(E)** The clinical impact curve demonstrates the clinical benefit of using the points-based classification scheme. Drug sensitivity analysis using BMS-536924 **(F)**, KIN001 **(G)**, and PHA-665752 **(H)** reveals greater sensitivity to these drugs in the high-risk group.

sensitivity analysis further demonstrate the clinical benefit of using this classification scheme.

## Discussion

ECs play a critical role in the TME and have been shown to promote tumor progression by providing oxygen and nutrients to tumor cells, regulating immune cell infiltration, and mediating tumor cell intravasation and extravasation during metastasis (20). In this study, we utilized scRNA-seq and bulk transcriptome to investigate the heterogeneity of ECs in OS and identify potential initiating cells and their role in tumor progression.

TYROBP, also known as DAP12, is a human gene located on chromosome 19q13.1. It encodes a transmembrane adaptor protein that is mainly expressed in cells, and the protein product of TYROBP is involved in a variety of immune responses, including regulating the activation and function of natural killer cells and dendritic cells (21). It forms complexes with cell surface receptors, such as triggering receptor expressed on myeloid cells 1 (TREM1), which activate downstream signaling pathways (22). Mutations in TYROBP have been associated with various diseases, including Nasu-Hakola disease, which is a rare neurodegenerative disorder that affects the brain and bones (23). Additionally, TYROBP has been implicated in the pathogenesis of Alzheimer's disease and other neurodegenerative diseases (24, 25). Overall, TYROBP plays a crucial role in immune system function and has implications for various diseases, particularly those affecting the brain and immune system. Our results revealed that TYROBP-positive ECs displayed the highest incoming and outgoing signal strength when communicating with malignant cells. We also found that TYROBP-positive ECs exhibited significant expression of TME-related genes, including those regulating chemokine expression, and had high activity of transcription factors FOS, FOSB, HES1, and JUNB. These findings suggest that TYROBP-positive ECs may play a crucial role in regulating immune cell infiltration and promoting tumor progression through their interactions with malignant cells. Moreover, our analysis identified differential expression of immune checkpoints (ICI) on ECs clusters. LAG3, CD48, PDCD1LG2, CD244, SLAMF7, and HAVCR2 were highly expressed in TYROBP-positive ECs, while IDO1, TIGIT, CD95, CD160, and CTLA4 were highly expressed in FABP4-positive ECs. This differential expression of ICIs suggests that TYROBP-positive ECs may play a unique role in immune evasion in the TME.

There have been successful precedents for converting "cold" tumors to "hot" tumors and improving the efficacy of immunotherapy. "Cold" tumors are characterized by a lack of T cell infiltration, whereas "hot" tumors are characterized by high levels of T cell infiltration and activity (26). Immunotherapy, such as immune checkpoint inhibitors, can be highly effective in treating "hot" tumors, but has limited efficacy in "cold" tumors. We evaluated the activation of KEGG pathways among different patients and found that high enrichment of TYROBP-positive ECs was associated with significantly activated chemokine, T cell receptor, B cell receptor, and Nod-like receptor signaling pathways, further supporting our conclusion that it corresponds to a "hot" tumor state.

Studies have shown that the TYROBP gene may play a role in the development and progression of certain cancers. For example, TYROBP expression has been found to be increased in several types of cancer, including breast cancer (27), lung cancer (28), and low-grade glioma (8). In breast cancer, higher levels of TYROBP expression have been associated with worse clinical outcomes, including shorter overall survival and disease-free survival (27). In low-grade glioma, TYROBP has been shown to promote tumor growth and metastasis through its interaction with other proteins involved in cell signaling pathways (8). Although the exact mechanisms by which TYROBP contributes to tumorigenesis are not yet fully understood, these findings suggest that TYROBP may be a potential target for cancer therapy and highlight the need for further research into its role in cancer development and progression.

Currently, numerous studies have investigated the relationship between ECs and osteosarcoma; however, a specific subtype of ECs has not been the primary focus of most of these reports. ECs promote osteosarcoma progression by secreting Von Willebrand factor (VWF) and activating NF-κB signaling, which contributes to epithelial-mesenchymal transition (EMT) and metastasis; OS cells in turn activate phospholipase D1 signaling to promote VWF release by ECs, resulting in further tumor deterioration (29). Kanako Minami and his colleagues found that Free fatty acid receptor 1 (FFA1) and FFA4, which regulate various malignant properties in cancer cells, may play a significant role in the modulation of cellular functions by ECs in OS, with higher expression levels of FFAR1 and FFAR4 genes in highly migratory MG63-CR7(F2) cells than in MG-63 cells, and knockdown of FFA1 or FFA4 inhibiting cell survival in the presence of cisplatin (30). Filomena de Nigris a suggests that Cyclin-dependent kinase 2 and 5 (Cdk2, Cdk5) are important mediators of neoangiogenesis in osteosarcoma, and a specific Yin Yang 1 (YY1) protein-dependent signal from tumor cells determines proliferation of human ECs, with Roscovitine inhibiting Cdk2 and Cdk5 activity, decreasing ECs proliferation and angiogenesis, and potentially serving as a pharmacologically accessible target for both antiangiogenic and antitumor therapy (31). However, we concluded that TYROBP-positive ECs may be the initiating cells and target specific subgroups of ECs that may benefit patients with OS.

It is worth noting that our study has several limitations. About vitro experiment, the main limitation is the suboptimal transfection efficiency of HUVECs cell lines, which may have resulted in incomplete TYROBP overexpression. Additionally, the study did not investigate the specific mechanisms underlying the changes in osteosarcoma cell proliferation and migration induced by the TYROBP-positive endothelial cell-conditioned medium. Finally, while the data suggests a role for TWEAK and other proteins in promoting the malignant phenotype of osteosarcoma cells, the study did not provide conclusive evidence regarding the specific proteins or pathways involved. Moreover, our sample size is

relatively small and that it may limit the generalizability of our findings. Our analysis was based on a single scRNA-seq dataset from the TISCH database, which may not fully represent the heterogeneity of ECs in OS. Further validation with additional datasets is necessary to confirm our findings. Second, we focused on the role of TYROBP-positive ECs in tumor progression, but other EC clusters may also play important roles in the TME. Finally, our study was based on computational analysis and further experimental validation is necessary to confirm our findings.

## Conclusions

In conclusion, our study identified TYROBP-positive ECs as the initiating cells of differentiation in ECs clusters in OS, and suggested that they may play a crucial role in promoting tumor progression through their interactions with malignant cells and regulating immune cell infiltration in the TME. In the future, targeting TYROBP-positive ECs maybe represent a promising approach for the treatment of OS and holds great potential for improving patient outcomes.

## Data availability statement

The original contributions presented in the study are included in the article/supplementary material. Further inquiries can be directed to the corresponding authors.

## Author contributions

Z-QW conceived and designed the study. SD drafted the article. Y-CY revised the article critically. All authors contributed to the article and approved the submitted version.

## Funding

This research was supported by Key supporded disciplines of Ningbo City under Grant No. 2022-F25.

## Conflict of interest

The authors declare that the research was conducted in the absence of any commercial or financial relationships that could be construed as a potential conflict of interest.

## Publisher's note



## References

1. Eaton BR, Schwarz R, Vatner R, Yeh B, Claude L, Indelicato DJ, et al. Osteosarcoma. *Pediatr Blood Cancer* (2021) 68 Suppl 2:e28352. doi: 10.1002/pbc.28352

2. Cole S, Gianferante DM, Zhu B, Mirabello L. Osteosarcoma: a surveillance, epidemiology, and end results program-based analysis from 1975 to 2017. *Cancer* (2022) 128:2107–18. doi: 10.1002/cncr.34163

3. Kong C, Hansen MF. Biomarkers in osteosarcoma. *Expert Opin Med Diagn* (2009) 3:13–23. doi: 10.1517/17530050802608496

4. Dana PM, Sadoughi F, Asemi Z, Yousefi B. Molecular signaling pathways as potential therapeutic targets in osteosarcoma. *Curr Med Chem* (2022) 29:4436–44. doi: 10.2174/0929867329666220209110009

5. Harrison DJ, Geller DS, Gill JD, Lewis VO, Gorlick R. Current and future therapeutic approaches for osteosarcoma. *Expert Rev Anticancer Ther* (2018) 18:39–50. doi: 10.1080/14737140.2018.1413939

6. Rickel K, Fang F, Tao J. Molecular genetics of osteosarcoma. *Bone* (2017) 102:69–79. doi: 10.1016/j.bone.2016.10.017

7. Amersfoort J, Eelen G, Carmeliet P. Immunomodulation by endothelial cells - partnering up with the immune system? *Nat Rev Immunol* (2022) 22:576–88. doi: 10.1038/s41577-022-00694-4

8. Lu J, Peng Y, Huang R, Feng Z, Fan Y, Wang H, et al. Elevated TYROBP expression predicts poor prognosis and high tumor immune infiltration in patients with low-grade glioma. *BMC Cancer* (2021) 21:723. doi: 10.1186/s12885-021-08456-6

9. Huang Q, Liang X, Ren T, Huang Y, Zhang H, Yu Y, et al. The role of tumor-associated macrophages in osteosarcoma progression - therapeutic implications. *Cell Oncol (Dordr)* (2021) 44:525–39. doi: 10.1007/s13402-021-00598-w

10. Maishi N, Hida K. Tumor endothelial cells accelerate tumor metastasis. *Cancer Sci* (2017) 108:1921–6. doi: 10.1111/cas.13336

11. Liu S, Qin T, Liu Z, Wang J, Jia Y, Feng Y, et al. Anlotinib alters tumor immune microenvironment by downregulating PD-L1 expression on vascular endothelial cells. *Cell Death Dis* (2020) 11:309. doi: 10.1038/s41419-020-2511-3

12. Xia Y, Wang WC, Shen WH, Xu K, Hu YY, Han GH, et al. Thalidomide suppresses angiogenesis and immune evasion via lncRNA FGD5-AS1/miR-454-3p/ZEB1 axis-mediated VEGFA expression and PD-1/PD-L1 checkpoint in NSCLC. *Chem Biol Interact* (2021) 349:109652. doi: 10.1016/j.cbi.2021.109652

13. Nam AS, Chaligne R, Landau DA. Integrating genetic and non-genetic determinants of cancer evolution by single-cell multi-omics. *Nat Rev Genet* (2021) 22:3–18. doi: 10.1038/s41576-020-0265-5

14. Sun D, Wang J, Han Y, Dong X, Ge J, Zheng R, et al. TISCH: a comprehensive web resource enabling interactive single-cell transcriptome visualization of tumor microenvironment. *Nucleic Acids Res* (2021) 49:D1420–30. doi: 10.1093/nar/gkaa1020

15. Li S, Zhang Q, Huang Z, Tao W, Zeng C, Yan L, et al. Comprehensive analysis of immunocyte infiltration and the key genes associated with intraplaque hemorrhage in carotid atherosclerotic plaques. *Int Immunopharmacol* (2022) 106:108633. doi: 10.1016/j.intimp.2022.108633

16. Hanzelmann S, Castelo R, Guinney J. GSVA: gene set variation analysis for microarray and RNA-seq data. *BMC Bioinf* (2013) 14:7. doi: 10.1186/1471-2105-14-7

17. Feng S, Xu Y, Dai Z, Yin H, Zhang K, Shen Y. Integrative analysis from multicenter studies identifies a WGCNA-derived cancer-associated fibroblast signature for ovarian cancer. *Front Immunol* (2022) 13:951582. doi: 10.3389/fimmu.2022.951582

18. Feng S, Yin H, Zhang K, Shan M, Ji X, Luo S, et al. Integrated clinical characteristics and omics analysis identifies a ferroptosis and iron-metabolism-related lncRNA signature for predicting prognosis and therapeutic responses in ovarian cancer. *J Ovarian Res* (2022) 15:10. doi: 10.1186/s13048-022-00944-y

19. Zhang K, Feng S, Ge Y, Ding B, Shen Y. A nomogram based on SEER database for predicting prognosis in patients with mucinous ovarian cancer: a real-world study. *Int J Womens Health* (2022) 14:931–43. doi: 10.2147/IJWH.S372328

20. Nagl L, Horvath L, Pircher A, Wolf D. Tumor endothelial cells (TECs) as potential immune directors of the tumor microenvironment - new findings and future perspectives. *Front Cell Dev Biol* (2020) 8:766. doi: 10.3389/fcell.2020.00766

21. Tomasello E, Vivier E. KARAP/DAP12/TYROBP: three names and a multiplicity of biological functions. *Eur J Immunol* (2005) 35:1670–7. doi: 10.1002/eji.200425932

22. Chen B, Zhou M, Zhang H, Wang C, Hu X, Wang B, et al. TREM1/Dap12-based CAR-T cells show potent antitumor activity. *Immunotherapy* (2019) 11:1043–55. doi: 10.2217/imt-2019-0017

23. Satoh JI, Yanaizu M, Tosaki Y, Sakai K, Kino Y. Targeted sequencing approach to identify genetic mutations in nasu-hakola disease. *Intractable Rare Dis Res* (2016) 5:269–74. doi: 10.5582/irdr.2016.01064

24. Ma J, Jiang T, Tan L, Yu JT. TYROBP in alzheimer's disease. *Mol Neurobiol* (2015) 51:820–6. doi: 10.1007/s12035-014-8811-9

25. Haure-Mirande JV, Audrain M, Ehrlich ME, Gandy S. Microglial TYROBP/DAP12 in alzheimer's disease: transduction of physiological and pathological signals across TREM2. *Mol Neurodegener* (2022) 17:55. doi: 10.1186/s13024-022-00552-w

26. Zhang J, Huang D, Saw PE, Song E. Turning cold tumors hot: from molecular mechanisms to clinical applications. *Trends Immunol* (2022) 43:523–45. doi: 10.1016/j.it.2022.04.010

27. Shabo I, Olsson H, Stal O, Svanvik J. Breast cancer expression of DAP12 is associated with skeletal and liver metastases and poor survival. *Clin Breast Cancer* (2013) 13:371–7. doi: 10.1016/j.clbc.2013.05.003

28. Kettunen E, Anttila S, Seppanen JK, Karjalainen A, Edgren H, Lindstrom I, et al. Differentially expressed genes in nonsmall cell lung cancer: expression profiling of cancer-related genes in squamous cell lung cancer. *Cancer Genet Cytogenet* (2004) 149:98–106. doi: 10.1016/S0165-4608(03)00300-5

29. Ling J, Sun Y, Pan J, Wang H, Ma Z, Yin J, et al. Feedback modulation of endothelial cells promotes epithelial-mesenchymal transition and metastasis of osteosarcoma cells by Von willebrand factor release. *J Cell Biochem* (2019) 120:15971–9. doi: 10.1002/jcb.28875

30. Minami K, Ueda N, Ishimoto K, Tsujiuchi T. Regulation of cell survival through free fatty acid receptor 1 (FFA1) and FFA4 induced by endothelial cells in osteosarcoma cells. *J Recept Signal Transduct Res* (2020) 40:181–6. doi: 10.1080/10799893.2020.1725047

31. de Nigris F, Mancini FP, Schiano C, Infante T, Zullo A, Minucci PB, et al. Osteosarcoma cells induce endothelial cell proliferation during neo-angiogenesis. *J Cell Physiol* (2013) 228:846–52. doi: 10.1002/jcp.24234

frontiers | Frontiers in Oncology

TYPE Brief Research Report
PUBLISHED 10 May 2023
DOI 10.3389/fonc.2023.1156111



OPEN ACCESS

EDITED BY
Shihori Tanabe,
National Institute of Health Sciences (NIHS), Japan

REVIEWED BY
Jogendra Singh Pawar,
The Ohio State University, United States
Anabel Sorolla,
Lleida Institute for Biomedical Research (IRBLleida), Spain

*CORRESPONDENCE
Kohei Kumegawa
kohei.kumegawa@jfcr.or.jp

†These authors have contributed equally to this work

RECEIVED 01 February 2023
ACCEPTED 28 April 2023
PUBLISHED 10 May 2023

CITATION
Kumegawa K, Yang L, Miyata K and Maruyama R (2023) FOXD1 is associated with poor outcome and maintains tumor-promoting enhancer–gene programs in basal-like breast cancer. *Front. Oncol.* 13:1156111. doi: 10.3389/fonc.2023.1156111



# FOXD1 is associated with poor outcome and maintains tumor-promoting enhancer–gene programs in basal-like breast cancer

Kohei Kumegawa[1*†], Liying Yang[2†], Kenichi Miyata[2] and Reo Maruyama[1,2]

[1]Cancer Cell Diversity Project, NEXT-Ganken Program, Japanese Foundation for Cancer Research, Tokyo, Japan, [2]Project for Cancer Epigenomics, Cancer Institute, Japanese Foundation for Cancer Research, Tokyo, Japan

Breast cancer biology varies markedly among patients. Basal-like breast cancer is one of the most challenging subtypes to treat because it lacks effective therapeutic targets. Despite numerous studies on potential targetable molecules in this subtype, few targets have shown promise. However, the present study revealed that *FOXD1*, a transcription factor that functions in both normal development and malignancy, is associated with poor prognosis in basal-like breast cancer. We analyzed publicly available RNA sequencing data and conducted *FOXD1*-knockdown experiments, finding that *FOXD1* maintains gene expression programs that contribute to tumor progression. We first conducted survival analysis of patients grouped via a Gaussian mixture model based on gene expression in basal-like tumors, finding that *FOXD1* is a prognostic factor specific to this subtype. Then, our RNA sequencing and chromatin immunoprecipitation sequencing experiments using the basal-like breast cancer cell lines BT549 and Hs578T with *FOXD1* knockdown revealed that *FOXD1* regulates enhancer–gene programs related to tumor progression. These findings suggest that *FOXD1* plays an important role in basal-like breast cancer progression and may represent a promising therapeutic target.

KEYWORDS

**FOXD1, TCGA, gaussian mixture model, enhancer, basal-like breast cancer**

## Introduction

The biology of breast cancer, a leading cause of cancer-related death among women worldwide, varies greatly among patients (1, 2), and studies on gene expression profiles have revealed several intrinsic subtypes, e.g., luminal A, luminal B, HER2-enriched, normal-like, and basal-like (3–6). The most aggressive subtype, basal-like breast cancer, is characterized by a gene expression profile similar to that of basal or myoepithelial cells. However, basal-like breast cancer tumors often lack established therapeutic targets, such as

hormone receptors or HER2, making their treatment challenging (7). Moreover, the heterogeneity of basal-like tumors makes identifying optimized therapeutic targets difficult.

In the epigenetic landscape of cancer, the complex and dynamic interplay between genetic and environmental factors has profound implications on the initiation, progression, and metastasis of malignant neoplasms (8). The aberrant regulation of cis-regulatory elements and transcription factors (TFs) is a key mechanism underlying reprogramming of the gene regulatory circuit in cancer and leads to the emergence of distinct phenotypic and functional states (9). Enhancers, a class of noncoding cis-regulatory elements, are characterized by specific histone modifications, such as acetylation of histone H3 lysine 27 (H3K27ac), which confer a permissive chromatin environment and promote the transcriptional activity of target genes. The aberrant activation of TFs, particularly those associated with oncogenic pathways, is one of the most common mechanisms underlying enhancer reprogramming in cancer (10). For example, in breast cancer, abnormal upregulation of the luminal-lineage TF *FOXA1* modifies genome-wide enhancer activity and induces transcriptional reprogramming to establish an endocrine-resistant state in metastatic tumors (11).

Previous studies have found that *FOXD1*, a member of the forkhead TF family, plays a critical role in regulating various cellular and molecular processes in both normal and malignant tissues (12–16). The expression of *FOXD1* is upregulated in primary breast cancer and promotes tumor proliferation and chemoresistance in the MDA-MB-231 (basal-like) and MCF7 (luminal) cell lines (17). However, the specific effects of *FOXD1* in basal-like tumors, mechanisms underlying these effects, and association with enhancer–gene regulation have not been elucidated.

In the present study, we conducted integrative analysis of publicly available expression data and multiomics data from cell line experiments to identify potential therapeutic targets for basal-like breast cancer. We stratified patients with basal-like tumors in The Cancer Genome Atlas Breast Invasive Carcinoma (TCGA-BRCA) data using a Gaussian mixture model (GMM) according to the expression level of each gene. We then performed survival analysis to identify genes associated with poor prognosis in basal-like breast cancer, finding that *FOXD1* was associated with poor prognosis in basal-like breast cancer but not in other subtypes. RNA sequencing (RNA-seq) and H3K27ac chromatin immunoprecipitation sequencing (ChIP-seq) experiments in basal-like cell lines with *FOXD1* knockdown revealed that *FOXD1* maintains distinct enhancer-gene programs associated with tumor progression. Collectively, our findings suggest that *FOXD1* plays a critical role in establishing an aggressive phenotype in a basal-like breast cancer subset by maintaining tumor-promoting epigenetic features and gene expression patterns.

# Materials and methods

## Quantification of FOXD1 expression in breast cancer cell lines

Breast cancer cell lines were either purchased from the Japanese Collection of Research Bioresources (JCRB) or American Type Culture Collection (ATCC) or were kindly gifted by Drs. Hitoshi Zembutsu and Yoshio Miki. The cells were maintained in accordance with the manufacturer's instructions, and details were provided in Supplementary Table 1. Total RNA was extracted from the cells using QIAGEN RNeasy Plus Mini Kit (QIAGEN). Subsequently, cDNA was synthesized from 500 ng of total RNA using PrimeScript RT Master Mix Perfect Realtime (TaKaRa) and then diluted to 200 µL. Reverse transcription real-time polymerase chain reaction (RT–qPCR) was performed using 2 µL of cDNA per reaction with PowerUp™ SYBR™ Green Master Mix (ThermoFisher) via 7500 Fast Real-Time PCR System (Applied Biosystems). The relative expression levels of *FOXD1* were determined using the delta-delta Ct method, with normal human breast tissue RNA (BioChain) as a reference, and the endogenous housekeeping gene ACTB serving as an internal control. The primers used in this study included FOXD1-F (GGACTCTGCACCAAGGGA), FOXD1-R(AAACACC GAACCACCAAGAC), ACTB-F(GCCAACCGCGAG AAGATGA), and ACTB-R(AGCACAGCCTGGATAGCAAC).

## Small interfering RNA transfection

BT549 and Hs578T cells were seeded onto 6-well plates at a density of $1.6 \times 10^5$ cells per well and cultured for 24 h. Cells were transfected with FOXD1 small interfering RNA (siRNA) (Ambion, s5229 or s5230) and negative siRNA control (Ambion, Negative Control siRNA) at a final concentration of 16 nM using Lipofectamine RNAiMAX Transfection Reagent (Invitrogen) and Opti-MEM Reduced Serum Medium (Gibco) following the manufacturer's instructions. Cells were subjected to RNA-seq and ChIP-seq 48 h after transfection. Knockdown efficiency was confirmed by quantifying FOXD1 mRNA as described above.

## RNA-seq

Total RNA was extracted from BT549 and Hs578T cells that had been treated with siRNA for 48 h, using the method described previously. RNA-seq libraries were prepared with 10 ng of total RNA, as a technical duplicate, using a SMARTer Stranded Total RNA-Seq Kit v2-Pico Input Mammalian (Takara) following the manufacturer's instructions. The resulting gene expression libraries were sequenced via an Illumina NextSeq 550 platform with paired-end reads (read1, 75 bp; index1 8 bp; read2, 75 bp).

## ChIP-seq

BT549 and Hs578T cells treated with siRNA for 48 h were subjected to ChIP-seq. ChIP-seq was performed as described in our previous report with slight modifications (18). Briefly, approximately $3 \times 10^5$ cells were fixed with 0.5% formaldehyde for 10 min at room temperature, quenched with 1.25 M glycine, washed, and lysed. The chromatin was sheared using an S220 Focused-ultrasonicator (Covaris). The complex of anti-H3K27ac antibody (Cell Signaling Technology, 8173S) and protein G Dynabeads (Invitrogen) was mixed with sheared chromatin. After overnight incubation, the complex was washed and incubated at 65°

C for 4 h for reverse cross-linking. The released DNA was purified using AMPure XP (Beckman). ChIP-seq libraries were prepared as a technical duplicate using ThruPLEX DNA-seq Kit (Takara) and were sequenced via Illumina NextSeq.

## Cell growth assay

BT549 and Hs578T cells were seeded onto 96-well plates at a density of $3 \times 10^3$ cells per well. After 24 h, siRNA was transfected into the cells using the same method and concentration as described previously. After 5 h, RealTime-Glo™ MT Cell Viability Assay (Promega) reagent was added to the cells, and luminescence was quantified at 48 h using ARVO2 (PerkinElmer).

## The cancer genome atlas breast invasive carcinoma data analysis

We downloaded TCGA-BRCA RNA-seq data as a SummarizedExperiment object via the R package TCGAbiolinks (19) using "GDCquery(project = "TCGA-BRCA," data.category = "Transcriptome Profiling," data.type = "Gene Expression Quantification," workflow.type = "STAR–Counts")," "GDCdownload()," and "GDCprepare()." GMM clustering was performed using the "Mclust()" function in the mclust package with the option modelNames = "V." For survival analysis, we used the "survfit()" function of the survival package and "ggsurvplot()" function of the survminer package.

## RNA-seq analysis

To generate an expression count matrix, row reads were trimmed to remove adaptor sequences using Skewer (v0.2.2) and mapped to the hg38 genome using STAR (v.2.7.8a). The mapped reads were then counted using featureCounts (v.2.0.10). To quantify differential gene expression, we utilized edgeR's glmQLFTest (v3.32.1). We used control and intervention experiments as input groups with a simple design using a 0 intercept '~0 + Group.' First, we normalized the library sizes by calculating scaling factors using 'calcNormFactors(y, method = TMM).' We next estimated dispersions via 'estimateDisp(y, design = design, robust = TRUE)' and fitted the generalized linear model using 'glmQLFit(y, design = design).' Finally, we determined log2 fold changes and false discovery rates (FDRs) using glmQLFTest. Genes with an FDR of <0.01 and log2FC of >1 (upregulated) or <−1 (downregulated) were considered differentially expressed genes. Gene Ontology enrichment analysis was performed via Enrichr (20).

## ChIP-seq analysis

The sequenced reads were mapped to the hg38 genome using bowtie2 (v.2.4.2). Multi-mapped reads and PCR duplicates were removed using Picard (v.2.25.3). Overlapping reads according to the ENCODE blacklist were filtered out using bedtools (2.30.0). MACS2 (v.2.2.7.1) was used for calling peaks with the "–keep-dup auto -q 0.1" parameter. After calling peaks, the peak summits were extended by 250 bp on both sides to a final width of 501 bp. Then, the regions of ENCODE hg38 blacklist were filtered out. Overlapping peaks within a single sample were removed using an iterative removal procedure that preserved the most significant peaks based on MACS2 'score' values, thus identifying "a sample peak set." The "score per million" was calculated by dividing individual peak score by the sum of all peak scores in each sample divided by 1 million. This iterative removal procedure was repeated across sample peak sets based on the score per million. The reproducible peak set was identified by selecting peaks with a score per million of ≥5 and overlaps between at least two samples; in addition, the peaks on chromosome Y were removed. Finally, we generated a reproducible high-quality set of 501 bp fixed-width peaks. To obtain the number of fragments in each peak, bam files were read as Genomic Ranges object via R using Rsamtool's "scambam()." Each fragment per peak was estimated using "countOverlaps()." The counts matrix was normalized using edgeR's "cpm(log = TRUE, prior.count = 1)." The motif enrichment score was calculated using ChromVAR (21) as follows: (i) adding GC bias information using "addGCBias()," (ii) identifying elements with motifs via "matchMotifs()" using the motif annotation of the R package chromVARmotif's "homer_pwms," (iii) obtaining background peaks via "getBackgroundPeaks(),"and (iv) calculating motif deviations using "computeDeviations()." The Z-scores of motif deviations (i.e., Motif scores) were used for analysis. To perform differential peak analysis, we used edgeR as previously described for RNA-seq analysis. Peaks with an FDR of <0.1 and log2FC of >0 (upregulated) or <0 (downregulated) were determined as differential peaks. To annotate peaks and determine peak–gene association, Genomic Regions Enrichment of Annotations Tool (GREAT) was used with default settings.

# Results

## GMM based approach reveals genes associated with overall survival in basal-like breast cancer

RNA-seq data from 193 basal-like tumors in the TCGA-BRCA dataset were analyzed to identify prognosis-associated genes in basal-like breast cancer. Genes were screened using three steps: (1) filtering genes with low average expression and variance of expression, (2) classifying tumors based on the expression level of each gene using the GMM, and (3) comparing the survival rates between different GMM classifications via Kaplan–Meier analysis (Figure 1A).

Of 60,660 genes, 5,755 genes had both an average expression and variance of expression of ≥0.5 across basal-like tumors (Figure 1B). Using GMM classification, we stratified the patients into one group (not stratified) for 3,008 genes, two groups for 1,584

genes, three groups for 756 genes, four groups for 311 genes, five groups for 85 genes, and six groups for 11 genes (Figure 1C). For 2,394 genes with ≥2 GMM groups that contained at least 10 patients per group, we conducted survival analysis, identifying 43 genes for which expression groups were associated with overall survival (log-rank P-value <0.01; Figure 1D and Supplementary Table 2). For example, *YTHDF3-AS1* and *KCNK6* were the top significant genes associated with poor prognosis. According to their expression levels, the patients were stratified into two groups, i.e., the low and high expression groups (Figure 1E), of which the high expression group exhibited shorter overall survival (Figure 1F). Although *YTHDF3-AS1* has not been well-characterized, its antisense gene, *YTHDF3*, is involved in the progression and metastasis of triple-negative tumors (22). *KCNK6* is as an overexpressed gene that promotes breast cancer cell proliferation, invasion, and migration (23). Overall, these results indicate that the GMM-based approach is useful for identifying genes associated with patient outcomes.

## *FOXD1* expression is associated with poor outcome in basal-like breast cancer but not in other subtypes

Of the 43 prognosis-related genes identified, we focused on *FOXD1*, a TF involved in breast cancer proliferation and drug resistance. According to *FOXD1* expression levels, the GMM classified patients into four groups (Figure 2A), of which the groups with higher *FOXD1* expression levels (groups 3 and 4) exhibited poorer outcomes (Figure 2B). According to GMM

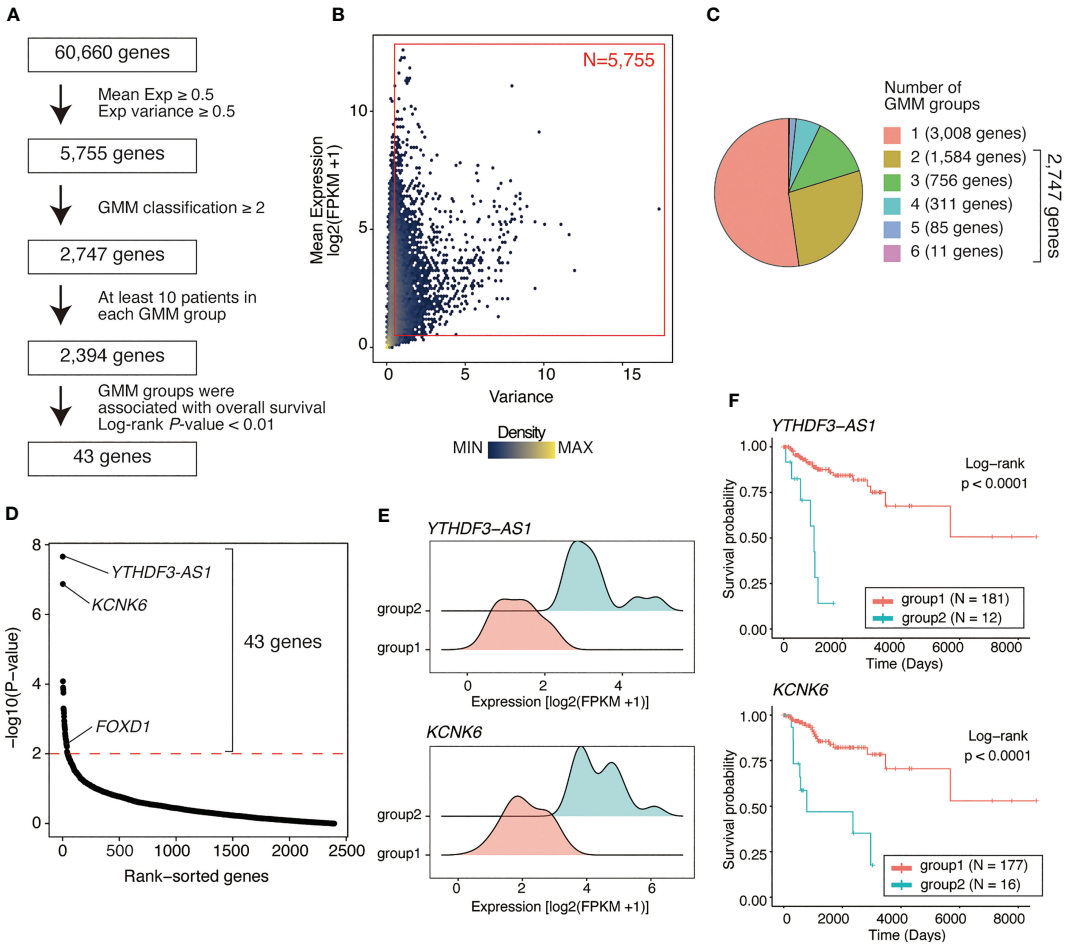


FIGURE 1
Identifying genes associated with poor outcome in basal-like breast cancer using a Gaussian mixture model. **(A)** Flow chart of gene identification. First, genes with low mean expression or low variance (both mean expression [log2(FPKM+1)] and variance of <0.5) across basal-like breast cancer samples were filtered out, leaving 5755 genes. Using GMM classification, 2747 genes that divided the patients into ≥2 expression groups were selected. Thus, based on gene expression, 2394 genes covering ≥2 GMM groups containing ≥10 patients were selected. Finally, 43 were identified as the genes whose expression level were associated with poor prognosis (Kaplan–Meier analysis; log-rank P-value of <0.01). **(B)** Scatter plot showing mean expression level and variance of expression of each gene. Each dot represents a gene. Red box represents the selected genes (N = 5755, average expression ≥ 0.5; variance ≥ 0.5). **(C)** Pie chart showing the distribution of the number of GMM groups. Overall, 2747 genes were selected covering ≥2 expression level-based GMM groups. **(D)** Dot plot showing log-rank test *P*-values of each filtered gene (2,394 genes) calculated via Kaplan–Meier analysis between GMM clusters. Red line represents filtering criteria ($P < 0.01$), and 43 genes were finally selected as the prognostic factors in basal-like breast cancer. **(E)** Ridge plots representing the distribution of *YTHDF3-AS1* and *KCNK6* expression in GMM groups. **(F)** Kaplan–Meier plots of patient groups stratified by the GMM for *YTHDF3-AS1* and *KCNK6* expression. *P*-values were calculated using log-rank test.

classification by *FOXD1* expression and survival analysis in the other subtypes, there was no significant difference across the GMM classification for luminal A, luminal B, Her2-enriched, and normal-like tumors (Supplementary Figure 1). These results suggest that elevated *FOXD1* expression is associated with poor outcome specifically in basal-like breast cancer.

## *FOXD1* regulates distinct gene expression in basal-like breast cancer cell lines

To confirm our findings, we examined *FOXD1* expression levels in a panel of breast cancer cell lines, including three luminal lines (MCF7, T47D, and YMB1), four HER2-amplified lines (BT474, SKBR3, MDA-MB-361, and MDA-MB-453), and six basal lines (BT549, Hs578T, MDA-MB-231, BT20, HCC1954, and HCT1937). We found that *FOXD1* expression levels were low in all luminal lines, with high expression levels observed only in one HER2-amplified line (MDA-MB-361) and two basal cell lines (BT549 and HS578T) (Figure 3A). These results were consistent with the heterogeneity of *FOXD1* expression found among basal-like tumors in our analysis of TCGA-BRCA data (Figure 2A).

To investigate the impact of *FOXD1* on gene expression, we conducted *FOXD1*-knockdown (*FOXD1*-KD) experiments using siRNA in BT549 and Hs578T cells, followed by RNA-seq analysis. First, we validated the effectiveness of two different siRNAs against FOXD1 (siFOXD1#1 and siFOXD1 #2) (Figure 3B). Subsequently, we performed RNA-seq analysis and identified 56 genes in BT549 cells and 142 genes in Hs578T cells that were commonly downregulated by *FOXD1*-KD using two siRNAs (Figures 3C–E and Supplementary Table 3). We performed gene annotation analysis using The Molecular Signature Database Hallmark gene set and found that the genes downregulated by *FOXD1*-KD in BT549 cells were associated with myogenesis, and those in Hs578T cells were associated with the G2–M checkpoint (Figures 3F, G), suggesting that FOXD1 has a different effect on the gene expression program of each cell line. Interestingly, cell proliferation assays following *FOXD1*-KD did not indicate significant inhibition of cell growth in either cell line (Supplementary Figure 2). This suggests that although FOXD1 plays a role in tumor progression and shorter prognosis, it may not be involved in cell cycle regulation.

## *FOXD1* regulates enhancer–gene programs potentially associated with tumor progression

Enhancers play a critical role in maintaining gene expression programs in various tumors. To examine the impact of FOXD1 on enhancer activity, we conducted *FOXD1*-KD in BT549 and Hs578T cells, followed by H3K27ac ChIP-seq assays. Our analysis identified 25,669 and 53,794 consensus peaks in BT549 and Hs578T cells, respectively. Using principal component analysis, we observed distinct patterns of enhancer activity in both cells treated with control siRNA (siNC), siFOXD1#1, and siFOXD1#2 (Supplementary Figure 3).

To identify TFs that regulate FOXD1-associated enhancers, we used ChromVAR to calculate TF motif scores and found that EBF1, SNAI1, and SNAI2 were less enriched in both cell lines after *FOXD1*-KD (Figure 4A and Supplementary Table 4). EBF1 is a tumor-promoting TF in triple-negative breast cancer (24), whereas SNAI1/2 are master regulatory TFs for organogenesis and wound healing in normal tissue as well as for the epithelial–mesenchymal transition (EMT) in cancer cells (25). Interestingly, enhancers containing FOXD1 motifs themselves were not downregulated, indicating an indirect effect of FOXD1 for maintaining enhancer

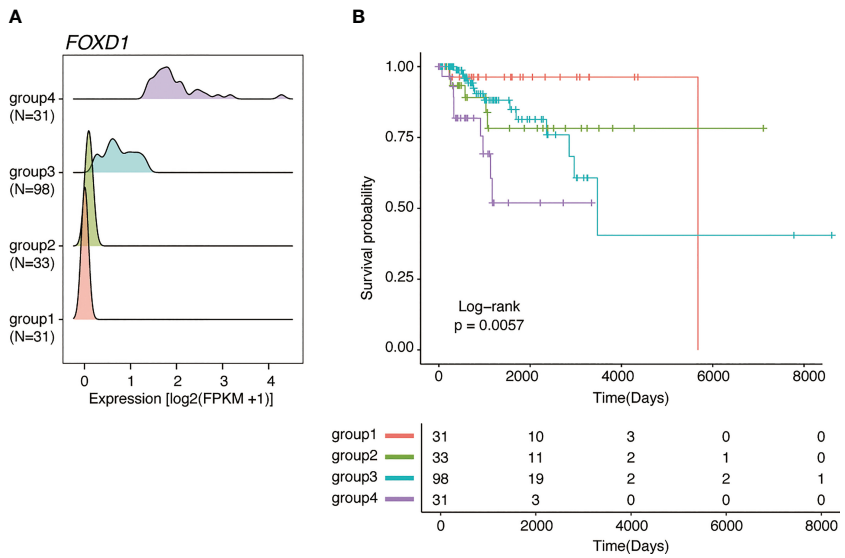


FIGURE 2
*FOXD1* is associated with poor prognosis specifically in basal-like breast cancer. **(A)** Ridge plots representing the distribution of *FOXD1* expression for GMM groups (group1, N=31; group2, N=33; group3, N=98; group4, N = 31). **(B)** Kaplan–Meier plot of *FOXD1* expression-based GMM groups stratified by GMM for *FOXD1* expression. *P*-values were calculated using log-rank test.

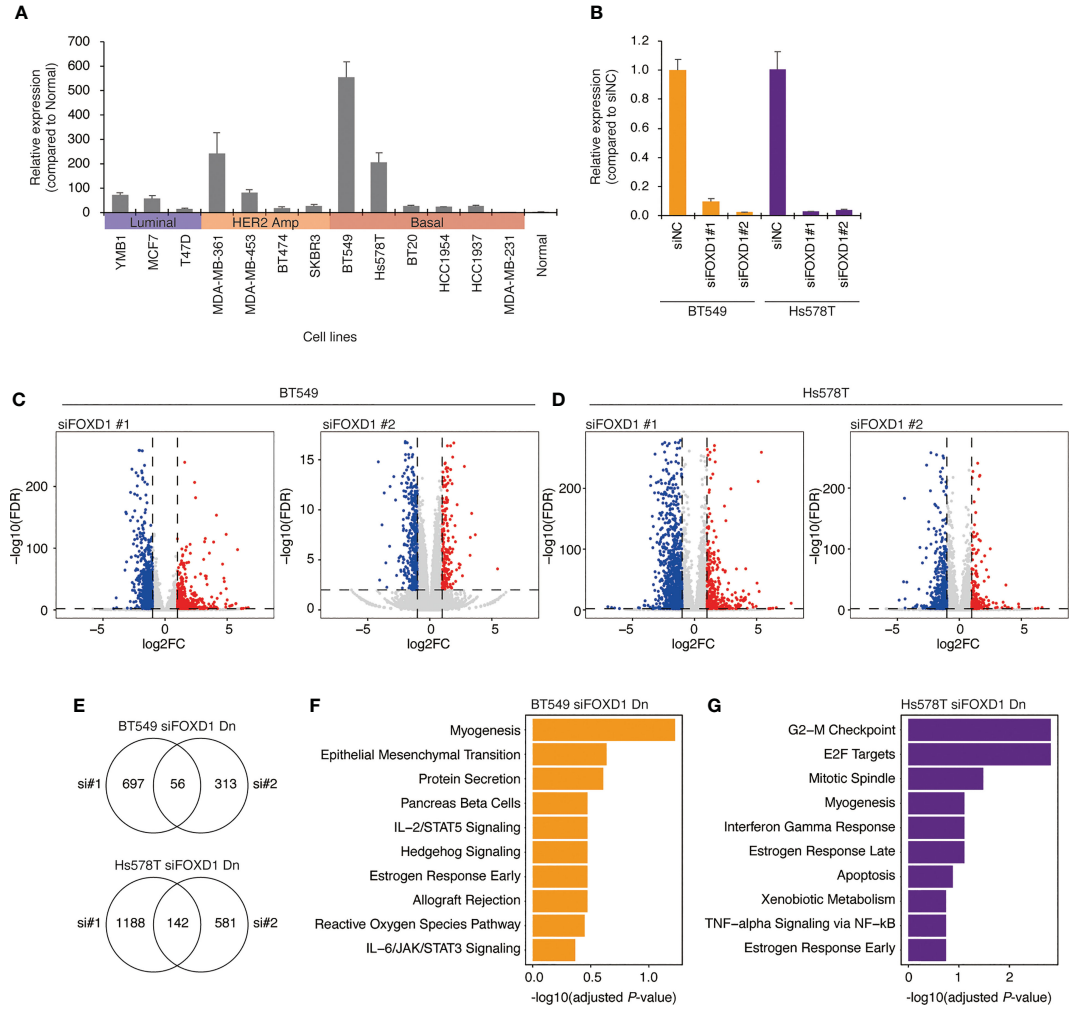


FIGURE 3
Gene expression changes induced by *FOXD1*-KD in basal-like breast cancer cell lines BT549 and Hs578T. **(A)** Bar chart showing *FOXD1* expression levels in breast cancer cell lines (three luminal, four HER2 amplification, six basal-like lines) and normal breast tissue examined *via* qPCR. Error bars represent standard deviation. **(B)** Bar chart showing *FOXD1* expression levels in BT549 and Hs578T cells transfected with control siRNA (siNC) or two siRNA against FOXD1 (siFOXD1#1 and siFOXD1#2). Error bars represent standard deviation. **(C)** Volcano plot showing differential expression analysis in BT549 cells between siNC and siFOXD1#1 (left) or siFOXD1#2 (right). Each dot represents a gene. The upregulated or downregulated genes are indicated in red or blue, respectively. **(D)** Volcano plot showing differential expression analysis in Hs578T cells between siNC and siFOXD1#1 (left) or siFOXD1#2 (right). Each dot represents a gene. The upregulated or downregulated genes are indicated in red or blue, respectively. **(E)** Venn diagram showing overlaps between the genes downregulated by siFOXD1#1 and siFOXD1#2 in BT549 (up) or Hs578T (bottom) cells. **(F, G)** Bar chart showing gene enrichment analysis (MSigDB Hallmark gene set) for the overlap of the downregulated genes by two siRNAs in BT549 **(F)** and Hs578T **(G)** cells.

activity. These results suggest that FOXD1 is involved in maintaining the activity of the enhancers targeted by tumor-promoting TFs.

Next, we performed differential analysis of the control and *FOXD1*-KD groups, where siFOXD1#1 and siFOXD1#2 identified 1,913 and 485 downregulated peaks in BT549 cells (Figure 4B and Supplementary Figure 4A) and 5,408 and 1,133 downregulated peaks in Hs578T cells, respectively (Figure 4C and Supplementary Figure 4B). GREAT Gene Ontology analysis revealed that these regions were associated with tumor microenvironment features such as extracellular structure organization, hemopoiesis regulation, and blood vessel morphogenesis (Figures 4D, E and Supplementary Figures 4C, D). In BT549 cells, the downregulated peaks were also associated with wound healing (Figure 1D), which was consistent with the lower SNAI1/2 motif enrichment in *FOXD1*-KD (Figure 4A).

To identify enhancer–gene pairs that could be regulated by FOXD1, we identified genes that were transcriptionally downregulated and were associated with the downregulated peaks in *FOXD1*-KD identified via GREAT analysis (Figure 4F). We found that 14 and 82 enhancer–gene pairs were downregulated by *FOXD1*-KD (at least one of the siRNAs) in BT549 or Hs578T cells, respectively (Figures 4G, H; Supplementary Tables 5, 6). Interestingly, we observed that these pairs were largely distinct between the two cell lines (Figure 4I; Supplementary Tables 5 and 6), indicating that the function of FOXD1 depends on the context. Both gene lists contained genes associated with tumor progression and metastasis, such as *CDK6*, *SNED1*, and *MTDH* (26–28). Taken

10.3389/fonc.2023.1156111

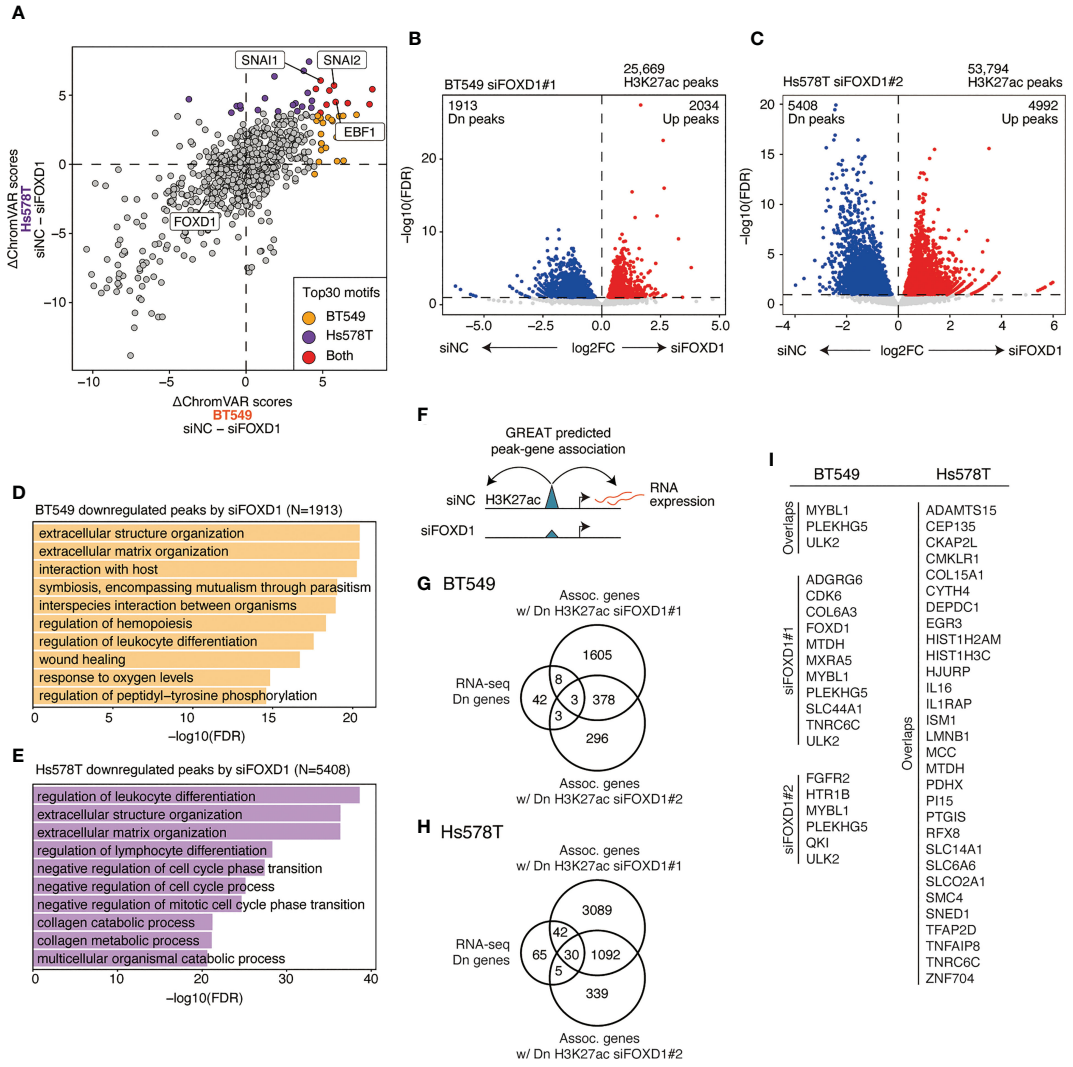


FIGURE 4
Changes in enhancer activity induced by *FOXD1*-KD and enhancer–gene pairs maintained by FOXD1. **(A)** Scatter plot of ΔChromVAR motif scores (siNC – siFOXD1) calculated using H3K27ac ChIP-seq data. A high ΔChromVAR score indicates reduced motif enrichment in H3K27ac peaks by *FOXD1*-KD. Each dot represents a CISBP motif. The top 30 enriched motifs in each cell line are indicated in orange (BT549), purple (Hs578T), or red (both). **(B)** Volcano plot showing differential peak analysis in BT549 cells between siNC and siFOXD1#1. Each dot represents a peak. Upregulated or downregulated peaks are indicated in red or blue, respectively. **(C)** Volcano plot showing differential peak analysis in Hs578T cells between siNC and siFOXD1#1. Each dot represents a peak. Upregulated or downregulated peaks are indicated in red or blue, respectively. **(D)** Bar plot showing the GREAT GO Biological Process for H3K27ac peaks downregulated by siFOXD1#1 in BT549 cells. **(E)** Bar plot showing the GREAT GO Biological Process for H3K27ac peaks downregulated by siFOXD1#1 in Hs578T cells. **(F)** Schema representing the identification for downregulated peak–gene associations via *FOXD1*-KD. **(G)** Venn diagram showing overlaps between the genes downregulated by *FOXD1*-KD and the genes associated with the downregulated H3K27ac peaks by siFOXD1#1 and siFOXD1#2 in BT549 cells. **(H)** Venn diagram showing overlaps between the genes downregulated by *FOXD1*-KD and the genes associated with the downregulated H3K27ac peaks by siFOXD1#1 and siFOXD1#2 in Hs578T cells. **(I)** List of enhancer–gene pairs. For Hs578T cells, only overlapping genes are included (other pairs are shown in Supplementary Table 6).

together, these findings suggest that *FOXD1* modulates gene expression programs involved in tumor progression.

## Discussion

Forkhead box TFs are involved in various processes of cancer progression such as metastasis, hormone regulation, therapeutic resistance, and reprogramming metabolism (29). FOXA1 is a central regulator of gene expression programs in ER+ breast cancer (30), FOXC1 is associated with EMT and poor prognosis in basal-like breast cancer (31), and FOXO3 is often dysregulated and plays both tumor-suppressive and oncogenic roles (32, 33). FOXD1 plays a role in both normal development and cancer progression. In normal development, FOXD1 controls kidney morphogenesis (34, 35) and appropriate formation of the optic chiasm (36). FOXD1 also contributes to the successful reprogramming of cells during the establishment of induced pluripotent stem cells (37). Moreover, it has been suggested that FOXD1 plays critical roles in cell proliferation, invasion, metastasis, and poor prognosis in various cancer types. In glioma, FOXD1 has been found to activate signaling pathways that contribute to the

tumorigenicity of mesenchymal glioma stem cells by activating *ALDH1A3* transcription (38). A recent report also suggested that FOXD1 enhances GLUT1 expression, leading to cell proliferation, invasion, and metastasis by modulating aerobic glycolysis in pancreatic cancer (15). Similarly, FOXD1 regulates histone modification to promote tumor growth in clear cell renal cell carcinoma (16). These results suggest that FOXD1 is involved in tumor progression and is a promising target for multiple cancer types.

In this study, we analyzed publicly available expression data from clinical specimens, finding that elevated expression of *FOXD1* is associated with poor outcomes in basal-like breast cancer but not in other subtypes. Therefore, FOXD1 may be a lineage-specific tumor-promoting TF in basal-like breast cancer. We also analyzed gene expression and enhancer profiles in the BT549 and Hs578T cell lines, finding that some enhancer-genes were regulated by FOXD1. The binding motifs of EMT-associated TFs SNAI1/2 were enriched in the potential enhancers regulated by FOXD1, suggesting that FOXD1 can modulate the enhancer activity regulating dedifferentiation. These enhancer–gene pairs included *CDK6*, [a key regulator of cell cycle and other tumor-promoting programs (26)], *SNED1* [a metastasis-promoting gene associated with poor prognosis of triple-negative breast cancer (27)], and MTDH [a gene involved in breast cancer initiation, metastasis, and drug resistance (28)]. These findings are consistent with those of previous reports regarding FOXD1 function associated with tumor progression and metastasis. Further, they highlight that FOXD1 may be an oncogenic TF that activates tumor-promoting gene expression programs by modulating enhancers. Although FOXD1-KD downregulated cancer-associated enhancer–gene pairs, we did not observe any effect on the proliferation of either of the cell lines (Supplementary Figure 2). This result may seem contradictory to the RNA-seq results in Hs578T cells, which showed that *FOXD1*-KD downregulated the expression of cell cycle-associated genes (Figure 3G). However, we also observed that enhancers downregulated by *FOXD1*-KD were associated with EMT-related TFs (Figure 4A), suggesting that FOXD1 is more closely related to metastatic features than to cell proliferation.

The present study and other studies suggest that targeting FOXD1 is an attractive therapeutic approach for basal-like breast cancer. Accordingly, inhibiting FOXD1 could potentially reduce breast cancer metastasis by inactivating the enhancers associated with EMT. Furthermore, recent studies have shown that molecular targeting therapies can increase the sensitivity of established treatments, such as chemotherapy and radiotherapy, in various types of cancer (39–41). One of the primary challenges in developing FOXD1-targeting therapies is the lack of available FOXD1 inhibitors. TFs are generally not considered druggable, but recent progress in developing proteolysis-targeting chimera (PROTAC) technology has made it possible to target certain TFs. For example, a clinical trial for ARV-471, an estrogen receptor (ER) degrader, demonstrated significant clinical efficacy in patients with ER-positive breast cancer (42). This implicates that FOXD1 specific inhibitors could be developed using PROTAC technology. Therefore, further research is warranted to develop specific FOXD1 inhibitors and determine the precise role of FOXD1 in cancer using breast cancer preclinical models.

This study has a limitation of using only cell line models for investigating FOXD1 function. Although cell lines are useful tools for cancer biology, they may exhibit distinct features compared with primary tumors. To address this limitation, further research should focus on manipulating patient-derived models, such as patient-derived organoids and xenografts. Despite this limitation, our study is clinically relevant because it reveals the correlation between poor prognosis and *FOXD1* expression levels in basal-like primary tumors and indicates that FOXD1 maintains specific enhancer–gene programs associated with tumor progression.

In summary, we used integrative analysis of TCGA-BRCA RNA-seq data and cell line experiments to highlight the intertumor heterogeneity of gene expression in basal-like tumors and identify a gene set associated with poor prognosis in basal-like breast cancer. *FOXD1* knockdown experiments revealed that FOXD1 maintains the regulation of enhancers associated with tumor-promoting gene expression in basal-like cell lines. Based on our findings, we postulate that FOXD1 is a critical TF that influences the epigenetic machinery underlying tumor progression and may be a potential therapeutic target.

## Data availability statement

Sequencing data have been deposited at GEO (GSE230119) and are publicly available as of the date of publication. R code for reproducing the analysis is available at https://github.com/KoheiKumegawa/BasalBC_GMM.

## Author contributions

KK and KM performed data analysis. LY performed cell line and sequencing experiments RM supervised all the work. KK and RM wrote the manuscript. All authors contributed to the article and approved the submitted version.

## Funding

This work was supported in part by JSPS KAKENHI grant numbers JP20K07708 [to RM], JP17K18336 [to RM], the Research Program on Hepatitis from Japan Agency for Medical Research and Development, AMED (JP21fk0210054, JP21fk0210092) [to RM], and the Vehicle Racing Commemorative Foundation [to RM, LY].

## Acknowledgments

The authors would like to thank Hajime Mihara for his helpful advice. We also would like to thank Enago (www.enago.jp) for the English language review. The results shown here are in part based upon data generated by the TCGA Research Network: https://www.cancer.gov/tcga.

## Conflict of interest

The authors declare that the research was conducted in the absence of any commercial or financial relationships that could be construed as a potential conflict of interest.

## Publisher's note

All claims expressed in this article are solely those of the authors and do not necessarily represent those of their affiliated organizations, or those of the publisher, the editors and the reviewers. Any product that may be evaluated in this article, or claim that may be made by its manufacturer, is not guaranteed or endorsed by the publisher.

## Supplementary material

The Supplementary Material for this article can be found online at: https://www.frontiersin.org/articles/10.3389/fonc.2023.1156111/full#supplementary-material

## References


1. DeSantis CE, Ma J, Gaudet MM, Newman LA, Miller KD, Goding Sauer A, et al. Breast cancer statistics, 2019. *CA Cancer J Clin* (2019) 69:438–51. doi: 10.3322/caac.21583

2. Sung H, Ferlay J, Siegel RL, Laversanne M, Soerjomataram I, Jemal A, et al. Global cancer statistics 2020: GLOBOCAN estimates of incidence and mortality worldwide for 36 cancers in 185 countries. *CA Cancer J Clin* (2021) 71:209–49. doi: 10.3322/caac.21660

3. Sotiriou C, Pusztai L. Gene-expression signatures in breast cancer. *New Engl J Med* (2009) 360:790–800. doi: 10.1056/NEJMra0801289

4. Sørlie T, Tibshirani R, Parker J, Hastie T, Marron JS, Nobel A, et al. Repeated observation of breast tumor subtypes in independent gene expression data sets. *Proc Natl Acad Sci* (2003) 100:8418–23. doi: 10.1073/pnas.0932692100

5. Sørlie T, Perou CM, Tibshirani R, Aas T, Geisler S, Johnsen H, et al. Gene expression patterns of breast carcinomas distinguish tumor subclasses with clinical implications. *Proc Natl Acad Sci* (2001) 98:10869–74. doi: 10.1073/pnas.191367098

6. Perou CM, Sørlie T, Eisen MB, van de Rijn M, Jeffrey SS, Rees CA, et al. Molecular portraits of human breast tumours. *Nature* (2000) 406:747–52. doi: 10.1038/35021093

7. Rakha EA, Reis-Filho JS, Ellis IO. Basal-like breast cancer: a critical review. *J Clin Oncol* (2008) 26:2568–81. doi: 10.1200/JCO.2007.13.1748

8. Hanahan D. Hallmarks of cancer: new dimensions. *Cancer Discovery* (2022) 12:31–46. doi: 10.1158/2159-8290.CD-21-1059

9. Sur I, Taipale J. The role of enhancers in cancer. *Nat Rev Cancer* (2016) 16:483–93. doi: 10.1038/nrc.2016.62

10. Okabe A, Kaneda A. Transcriptional dysregulation by aberrant enhancer activation and rewiring in cancer. *Cancer Sci* (2021) 112:2081–8. doi: 10.1111/cas.14884

11. Fu X, Pereira R, de Angelis C, Veeraraghavan J, Nanda S, Qin L, et al. FOXA1 upregulation promotes enhancer and transcriptional reprogramming in endocrine-resistant breast cancer. *Proc Natl Acad Sci* (2019) 116:26823–34. doi: 10.1073/pnas.1911584116

12. Kobayashi A, Mugford JW, Krautzberger AM, Naiman N, Liao J, McMahon AP. Identification of a multipotent self-renewing stromal progenitor population during mammalian kidney organogenesis. *Stem Cell Rep* (2014) 3:650–62. doi: 10.1016/j.stemcr.2014.08.008

13. Hernández-Bejarano M, Gestri G, Monfries C, Tucker L, Dragomir EI, Bianco IH, et al. Foxd1-dependent induction of a temporal retinal character is required for visual function. *Development* (2022) 149. doi: 10.1242/dev.200938

14. Sun Q, Novak D, Hüser L, Poelchen J, Wu H, Granados K, et al. FOXD1 promotes dedifferentiation and targeted therapy resistance in melanoma by regulating the expression of connective tissue growth factor. *Int J Cancer* (2021) 149:657–74. doi: 10.1002/ijc.33591

15. Cai K, Chen S, Zhu C, Li L, Yu C, He Z, et al. FOXD1 facilitates pancreatic cancer cell proliferation, invasion, and metastasis by regulating GLUT1-mediated aerobic glycolysis. *Cell Death Dis* (2022) 13:765. doi: 10.1038/s41419-022-05213-w

16. Bond KH, Fetting JL, Lary CW, Emery IF, Oxburgh L. FOXD1 regulates cell division in clear cell renal cell carcinoma. *BMC Cancer* (2021) 21:312. doi: 10.1186/s12885-021-07957-8

17. Zhao Y-F, Zhao J-Y, Yue H, Hu K-S, Shen H, Guo Z-G, et al. FOXD1 promotes breast cancer proliferation and chemotherapeutic drug resistance by targeting p27. *Biochem Biophys Res Commun* (2015) 456:232–7. doi: 10.1016/j.bbrc.2014.11.064

18. Maruyama R, Choudhury S, Kowalczyk A, Bessarabova M, Beresford-Smith B, Conway T, et al. Epigenetic regulation of cell type–specific expression patterns in the human mammary epithelium. *PloS Genet* (2011) 7:e1001369. doi: 10.1371/journal.pgen.1001369

19. Colaprico A, Silva TC, Olsen C, Garofano L, Cava C, Garolini D, et al. TCGAbiolinks: an R/Bioconductor package for integrative analysis of TCGA data. *Nucleic Acids Res* (2016) 44(8):e71. doi: 10.1093/nar/gkv1507

20. Xie Z, Bailey A, Kuleshov MV, Clarke DJB, Evangelista JE, Jenkins SL, et al. Gene set knowledge discovery with enrichr. *Curr Protoc* (2021) 1. doi: 10.1002/cpz1.90

21. Schep AN, Wu B, Buenrostro JD, Greenleaf WJ. ChromVAR: inferring transcription-factor-associated accessibility from single-cell epigenomic data. *Nat Methods* (2017) 14:975–8. doi: 10.1038/nmeth.4401

22. Lin Y, Jin X, Nie Q, Chen M, Guo W, Chen L, et al. YTHDF3 facilitates triple-negative breast cancer progression and metastasis by stabilizing ZEB1 mRNA in an m6A-dependent manner. *Ann Transl Med* (2022) 10:83–3. doi: 10.21037/atm-21-6857

23. Hou X, Tang L, Li X, Xiong F, Mo Y, Jiang X, et al. Potassium channel protein KCNK6 promotes breast cancer cell proliferation, invasion, and migration. *Front Cell Dev Biol* (2021) 9:616784. doi: 10.3389/fcell.2021.616784

24. Qiu Z, Guo W, Dong B, Wang Y, Deng P, Wang C, et al. EBF1 promotes triple-negative breast cancer progression by surveillance of the HIF1α pathway. *Proc Natl Acad Sci* (2022) 119(28):e2119518119. doi: 10.1073/pnas.2119518119

25. Georgakopoulos-Soares I, Chartoumpekis DV, Kyriazopoulou V, Zaravinos A. EMT factors and metabolic pathways in cancer. *Front Oncol* (2020) 10:499. doi: 10.3389/fonc.2020.00499

26. Fassl A, Geng Y, Sicinski P. CDK4 and CDK6 kinases: from basic science to cancer therapy. *Sci (1979)* (2022) 375:eabc1495. doi: 10.1126/science.abc1495

27. Naba A, Clauser KR, Lamar JM, Carr SA, Hynes RO. Extracellular matrix signatures of human mammary carcinoma identify novel metastasis promoters. *Elife* (2014) 3:e01308. doi: 10.7554/eLife.01308

28. Shen M, Wei Y, Kim H, Wan L, Jiang Y-Z, Hang X, et al. Small-molecule inhibitors that disrupt the MTDH–SND1 complex suppress breast cancer progression and metastasis. *Nat Cancer* (2021) 3:43–59. doi: 10.1038/s43018-021-00279-5

29. Castaneda M, den Hollander P, Mani SA. Forkhead box transcription factors: double-edged swords in cancer. *Cancer Res* (2022) 82:2057–65. doi: 10.1158/0008-5472.CAN-21-3371

30. Seachrist DD, Anstine LJ, Keri RA. FOXA1: a pioneer of nuclear receptor action in breast cancer. *Cancers (Basel)* (2021) 13:5205. doi: 10.3390/cancers13205205

31. Han B, Bhowmick N, Qu Y, Chung S, Giuliano AE, Cui X. FOXC1: an emerging marker and therapeutic target for cancer. *Oncogene* (2017) 36:3957–63. doi: 10.1038/onc.2017.48

32. Yao S, Fan LY-N, Lam EW-F. The FOXO3-FOXM1 axis: a key cancer drug target and a modulator of cancer drug resistance. *Semin Cancer Biol* (2018) 50:77–89. doi: 10.1016/j.semcancer.2017.11.018

33. Khan MA, Ahmad I, Aloliqi AA, Eisa AA, Najm MZ, Habib M, et al. FOXO3 gene hypermethylation and its marked downregulation in breast cancer cases: a study on female patients. *Front Oncol* (2023) 12:1078051. doi: 10.3389/fonc.2022.1078051

34. Hatini V, Huh SO, Herzlinger D, Soares VC, Lai E. Essential role of stromal mesenchyme in kidney morphogenesis revealed by targeted disruption of winged helix transcription factor BF-2. *Genes Dev* (1996) 10:1467–78. doi: 10.1101/gad.10.12.1467

35. Levinson RS, Batourina E, Choi C, Vorontchikhina M, Kitajewski J, Mendelsohn CL. Foxd1-dependent signals control cellularity in the renal capsule, a structure required for normal renal development. *Development* (2005) 132:529–39. doi: 10.1242/dev.01604

36. Herrera E, Marcus R, Li S, Williams SE, Erskine L, Lai E, et al. Foxd1 is required for proper formation of the optic chiasm. *Development* (2004) 131:5727–39. doi: 10.1242/dev.01431

37. Koga M, Matsuda M, Kawamura T, Sogo T, Shigeno A, Nishida E, et al. Foxd1 is a mediator and indicator of the cell reprogramming process. *Nat Commun* (2014) 5:3197. doi: 10.1038/ncomms4197

38. Cheng P, Wang J, Waghmare I, Sartini S, Coviello V, Zhang Z, et al. FOXD1–ALDH1A3 signaling is a determinant for the self-renewal and tumorigenicity of mesenchymal glioma stem cells. *Cancer Res* (2016) 76:7219–30. doi: 10.1158/0008-5472.CAN-15-2860

39. Pawar JS, Al-Amin M, Hu C-D. JNJ-64619178 radiosensitizes and suppresses fractionated ionizing radiation-induced neuroendocrine differentiation (NED) in prostate cancer. *Front Oncol* (2023) 13:1126482. doi: 10.3389/fonc.2023.1126482

40. Owens JL, Beketova E, Liu S, Shen Q, Pawar JS, Asberry AM, et al. Targeting protein arginine methyltransferase 5 suppresses radiation-induced neuroendocrine differentiation and sensitizes prostate cancer cells to radiation. *Mol Cancer Ther* (2022) 21:448–59. doi: 10.1158/1535-7163.MCT-21-0103

41. Shu S, Wu HJ, Ge JY, Zeid R, Harris IS, Jovanović B, et al. Synthetic lethal and resistance interactions with BET bromodomain inhibitors in triple-negative breast cancer. *Mol Cell* (2020) 78:1096–1113.e8. doi: 10.1016/j.molcel.2020.04.027

42. Békés M, Langley DR, Crews CM. PROTAC targeted protein degraders: the past is prologue. *Nat Rev Drug Discovery* (2022) 21:181–200. doi: 10.1038/s41573-021-00371-6

frontiers | Frontiers in Oncology

TYPE Original Research
PUBLISHED 09 June 2023
DOI 10.3389/fonc.2023.1130380



OPEN ACCESS

EDITED BY
Tao Liu,
University of New South Wales, Australia

REVIEWED BY
Rodolfo Chavez,
National Autonomous University of Mexico, Mexico
Dolores Aguilar-Cazares,
National Institute of Respiratory Diseases-Mexico (INER), Mexico
Francesco Pezzella,
University of Oxford, United Kingdom

*CORRESPONDENCE
Divya P. Kumar
divyapk243@gmail.com
divyapkumar@jssuni.edu.in

RECEIVED 23 December 2022
ACCEPTED 26 May 2023
PUBLISHED 09 June 2023

CITATION
Suresh D, Srinivas AN, Prashant A, Satish S, Vishwanath P, Nataraj SM, Koduru SV, Santhekadur PK and Kumar DP (2023) AATF inhibition exerts antiangiogenic effects against human hepatocellular carcinoma. *Front. Oncol.* 13:1130380. doi: 10.3389/fonc.2023.1130380



# AATF inhibition exerts antiangiogenic effects against human hepatocellular carcinoma

Diwakar Suresh[1], Akshatha N. Srinivas[1], Akila Prashant[1], Suchitha Satish[2], Prashant Vishwanath[1], Suma M. Nataraj[1], Srinivas V. Koduru[3], Prasanna K. Santhekadur[1] and Divya P. Kumar[1]*

[1]Department of Biochemistry, CEMR, JSS Medical College, JSS Academy of Higher Education and Research, Mysuru, Karnataka, India, [2]Department of Pathology, JSS Medical College and Hospital, JSS Academy of Higher Education and Research, Mysuru, India, [3]Gene Arrays, Omelette Inc., New York, NY, United States

**Background and aims:** Angiogenesis is a key factor in the growth and metastasis of hepatic tumors and thus a potential therapeutic target in hepatocellular carcinoma (HCC). In this study, we aim to identify the key role of apoptosis antagonizing transcription factor (AATF) in tumor angiogenesis and its underlying mechanisms in HCC.

**Methods:** HCC tissues were analyzed for AATF expression by qRT-PCR and immunohistochemistry. Stable clones of control and AATF knockdown (KD) were established in human HCC cells. The effect of AATF inhibition on the angiogenic processes was determined by proliferation, invasion, migration, chick chorioallantoic membrane (CAM) assay, zymography, and immunoblotting techniques.

**Results:** We identified high levels of AATF in human HCC tissues compared to adjacent normal liver tissues, and the expression was found to be correlated with the stages and tumor grades of HCC. Inhibiting AATF in QGY-7703 cells resulted in higher levels of pigment epithelium-derived factor (PEDF) than controls due to decreased matric metalloproteinase activity. Conditioned media from AATF KD cells inhibited the proliferation, migration, and invasion of human umbilical vein endothelial cells as well as the vascularization of the chick chorioallantoic membrane. Furthermore, the VEGF-mediated downstream signaling pathway responsible for endothelial cell survival and vascular permeability, cell proliferation, and migration favoring angiogenesis was suppressed by AATF inhibition. Notably, PEDF inhibition effectively reversed the anti-angiogenic effect of AATF KD.

**Conclusion:** Our study reports the first evidence that the therapeutic strategy based on the inhibition of AATF to disrupt tumor angiogenesis may serve as a promising approach for HCC treatment.

KEYWORDS

**apoptosis antagonizing transcription factor, angiogenesis, hepatocellular carcinoma, knockdown (KD), human umbilic vein endothelial cells (HUVEC), pigment epithelium derived factor**

# 1 Introduction

Hepatocellular carcinoma (HCC), which makes up 80% of primary liver malignancies, has become a severe public health issue. It is estimated that in the next two decades, there will be a 55% increase in the incidence rate of liver cancer, posing a challenge worldwide (1). The underlying causes of HCC development have been identified as viral infections (Hepatitis B virus and Hepatitis C virus), as well as additional risk factors including metabolic syndrome, carcinogens, fatty liver disease, and cirrhosis (2). Hepatic injury and chronic liver inflammation cause hepatocyte necrosis, regeneration, and the progression to fibrosis, cirrhosis, resulting in the onset and progression of HCC (3). The pathophysiology of HCC is multifactorial and highly complex owing to its molecular and immune heterogeneity, and thus, understanding the molecular processes could facilitate the development of preventive measures, early diagnostic techniques, and improved therapeutic options (4, 5). HCC being a highly vascular tumor underscores the importance of angiogenesis in the process of tumor growth and metastasis, which is responsible for the rapid recurrence and poor survival rates of HCC (6).

Inducing or accessing the vasculature is one of the hallmarks of cancer and plays a crucial role in the development of solid malignancies (7). The process of inducing new blood vessel formation (angiogenesis) aids cancer cells in creating a local vascular ecology to deliver nutrients and growth factors, remove potentially toxic metabolites, and thereby promote cancer cell proliferation and metastasis (6, 7). Angiogenesis is stimulated by various proangiogenic factors such as vascular endothelial growth factor (VEGF), platelet-derived growth factor (PDGF), fibroblast growth factor (FGF), and angiopoietins (8). The molecular understanding of this intricate and dynamic angiogenic tumor ecosystem has led to the advancement of anti-angiogenic therapy for HCC (9). The "starve a tumor to death" theory has emerged as an appealing anti-angiogenic therapy for a variety of cancers, including HCC (10). Sorafenib, a multikinase inhibitor, exerts an anti-tumor effect by inhibiting angiogenesis. In addition, over the last decade, ramucirumab and bevacizumab have been the FDA-approved drugs that target vascular endothelial growth factors (VEGFs) to treat HCC (11–13). Despite the positive effects of antiangiogenic therapies, their usage is constrained by drawbacks like tumor resistance, cardiovascular damage, and off-target effects on healthy tissues because they may activate various signaling pathways that are favorable to invasion, metastasis, and overall survival (14, 15). The ability to limit sprouting angiogenesis or vessel co-option is known to facilitate acquired resistance to antiangiogenic therapy in HCC (16). However, a mechanistic understanding to overcome tumor resistance and nanoparticle-based delivery techniques are emerging in cancer therapeutics (17). Thus, the novel cellular and molecular strategies targeting angiogenesis have been considered effective in treating HCC development and progression.

Apoptosis antagonizing transcription factor (AATF), also called Che-1, is a transcription factor that controls several genes involved in the regulation of different processes such as cell proliferation, cell cycle arrest, DNA damage response, and apoptosis (18). Previous studies have shown that AATF regulates the transcription of many genes, including nuclear hormone receptor-targeted genes, p53, p21, and the X-linked inhibitor of apoptosis (19–22). AATF plays a role in the pathogenesis of many cancers. AATF levels were found to be elevated in various cancers such as breast cancer, leukemia, lung cancer, Wilm's tumor, osteosarcoma, and neuroblastoma, and their level increased during disease progression (23–28). It is interesting to note that the anti-apoptotic factor AATF, which is an oncogene, is also implicated in growth arrest and cellular checkpoint signaling. AATF is also well studied as a component of the unfolded protein response (UPR), which is an adaptive mechanism activated during endoplasmic reticulum (ER) stress. AATF induced as a resultant of ER stress protects the cells from apoptosis by activating the transcription factor Akt1 (29). An interesting study by Wang et al., has shown that AATF alleviates hypoxia/reoxygenation (H/R)-induced cardiomyocyte apoptosis by upregulating Nrf2 signaling (30). Shimizu et al., recently reported that elevated NRAGE expression is significantly correlated with AATF expression in accelerating cancer proliferation and migration, leading to hepatocarcinogenesis (31). However, the potential role of AATF in HCC pathogenesis has not been investigated.

We have previously, for the first time, unraveled the role of AATF as a potential driver of HCC in NAFLD and demonstrated that the knockdown of AATF inhibited tumor growth and metastasis (32). In the present study, we investigated whether suppression of AATF expression inhibits angiogenesis in HCC and explored its underlying mechanisms. The specific objectives of the study were to (i) confirm the overexpression of AATF in human HCC tissues and correlate AATF expression with different stages and grades of HCC; (ii) define the impact of AATF knockdown on key angiogenic properties of HCC; and (iii) identify the signaling pathway by which AATF inhibition suppresses angiogenesis in HCC. In this study, we showed the overexpression of AATF in human HCC tissues and evaluated the role of AATF in proliferation, migration, invasion of HUVECs, and vascular growth in a chicken embryo by testing the effect of conditioned media from control and AATF knockdown HCC cells. PEDF antibody was used to investigate the effect of PEDF on AATF-mediated angiogenesis in HCC. Our findings demonstrated that AATF inhibition exerts an anti-angiogenic effect in HCC *via* PEDF, and that AATF merits further investigation as a potential therapeutic target, leading to a better

**Abbreviations:** HCC, hepatocellular carcinoma; AATF, apoptosis antagonizing transcription factor; DNA, deoxyribonucleic acid; UPR, unfolded protein response; ER, endoplasmic reticulum; NAFLD, nonalcoholic fatty liver disease; HUVECs, human umbilical vein endothelial cells; VEGF, vascular endothelial growth factor; PDGF, platelet-derived growth factor; FGF, fibroblast growth factor; PEDF, pigment epithelium-derived factor; CAM, chorioallantoic membrane; CM, conditioned media; nrf2, nuclear factor erythroid-related factor 2; NRAGE, neurotrophin receptor-interacting MAGE homolog; MMP, matrix metalloproteinases; ERK1/2, extracellular signal-regulated protein kinase; FAK, focal adhesion kinase; STAT3, signal transducer and activator of transcription 3; VEGFR, vascular endothelial growth factor receptor; siRNA, small interfering ribonucleic acid; AAV, adeno associated virus.

understanding of anti-angiogenic strategies for the treatment of HCC.

# 2 Materials and methods

## 2.1 Reagents

Endothelial cell growth medium (EGM), extracellular matrix gel (ECM), TRIzol, RIPA buffer, collagenase A, and AATF antibody were procured from Sigma-Aldrich (St. Louis, USA). Dulbecco's modified eagle's medium (DMEM), giemsa stain, hematoxylin, 8µm-transwell inserts, and 24- well plates were procured from HiMedia laboratories (India). Lipofectamine 3000, penicillin/streptomycin, glutamine, FBS were from Invitrogen (USA); WST-1 cell proliferation assay kit from Takara Bio Inc. (Shinga, Japan); antibodies to IgG, PEDF, pAkt, pErk1/2, pFAK, Akt, Erk, and control and AATF shRNA from Santa Cruz Biotechnology, Inc. (CA, USA); antibodies to β-actin from Cell Signaling Technologies (USA); verso cDNA synthesis kit, and DyNamo Colorflash SYBR green kit from Thermo Fisher Scientific (USA); western bright ECL HRP substrate from Advansta (USA); western blotting materials were from BioRad; primers from Integrated DNA Technologies (IDT) (Iowa, USA), and all other reagents were obtained from Thermo Fisher Scientific or Sigma.

## 2.2 Subjects and sample collection

Human HCC tissues (n=50) and normal tissues (n=15) were procured from the National Tumor Tissue Repository (NTTR), Tata Memorial Hospital, Mumbai, India. Normal liver tissue adjacent to the tumor will be considered as control. The study was approved by the institutional ethics committees of JSS Medical College, JSS AHER, Mysore, Karnataka, India (JSSMC/IEC/090721/28NCT/2021-22), and Tata Memorial Hospital (Inclusion Criteria: Patients with clinical or histologically documented hepatocellular carcinoma. All stages of HCC were considered; Exclusion Criteria: Patients with non-neoplastic lesions of the liver were excluded from the study). Clinical characteristics and biochemical parameters were evaluated. The demographic and clinicopathological data of the HCC subjects are described in Supplementary Table 1.

The human umbilical cord was procured from Shree Devi Nursing Home, Mysore. Informed consent was obtained from the subjects for the use of cells in clinical research. The study was approved by the institutional ethics committee at JSS Medical College, JSS AHER, Mysore, Karnataka, India. (JSSMC/IEC/260822/37NCT/2022-23).

## 2.3 Isolation and culture of human umbilical vein endothelial cells (HUVECs)

The freshly collected human umbilical cord (40-60 cm long, tied at both ends) from the maternity hospital was washed using 0.09% saline. After confirming the cord is devoid of hematic and physical damage, it is incubated with 2 mg/ml collagenase A solution at $37^0$C. The digested cells were collected into a tube and centrifuged at 750 g for 10 min at $4^0$C. The cells were resuspended with endothelial cell growth medium and cultured by incubating at $37^0$C in 5% $CO_2$. All procedure was carried out in the cell culture hood with laminar airflow under aseptic condition. HUVECs were used from passages 3-5 to ensure their endothelial characteristics and were freshly isolated to perform experiments in duplicate or triplicate (Supplementary Figure 1B).

## 2.4 Cell culture and stable clones preparation

Human HCC cells- QGY-7703 (kind donation from Dr. Devanand Sarkar, Virginia Commonwealth University, USA) and Hep3B (obtained from American Type Culture Collection (ATCC), USA) were cultured in Dulbecco's modified eagle's medium containing 4.5 g/L glucose and supplemented with 10% fetal bovine serum, L-glutamine, and 100 U/ml penicillin-streptomycin incubated at $37^0$C in 5% $CO_2$. The authentication of QGY-7703 cell line was done by short tandem repeats (STR) profiling.

Stable clones expressing AATF shRNA in QGY-7703 cells were prepared as described previously (32). Firstly, the optimal antibiotic concentration for selecting the stable cell colonies was determined using different concentrations of puromycin (1-10 µg/ml). Control and AATF shRNA plasmid containing puromycin resistance gene was transfected to QGY-7703 cells according to the manufacturer's protocol. Individual colonies were isolated, expanded and maintained in 1 µg/ml Puromycin. Stable knockdown of AATF in QGY-7703 cells was confirmed by qRT-PCR and western blot. We have used two clones of AATF control and AATF knockdown cells in the experiments.

## 2.5 Tissue processing and histological analysis

Human normal and HCC tissues were fixed in a 4% (v/v) formaldehyde solution in phosphate buffered saline for 16 h. After formalin fixation, tissues were processed and embedded in standard paraffin blocks. Subsequently, tissue sections of 5 µm thickness were cut from each paraffin block and stained with hematoxylin and eosin (H&E). A pathologist at JSS Hospital performed the histological grading of HCC according to the World Health Organization (WHO) classification: well differentiated, moderately differentiated, or poorly differentiated HCC (33). The various stages of HCC were determined according to the classification criteria of the American Joint Committee on Cancer (AJCC) TNM [primary tumor features (T), presence or absence of nodal involvement (N), and distant metastasis (M) staging systems (34).

## 2.6 Immunohistochemistry

The formalin-fixed, paraffin-embedded (FFPE) tissue sections were deparaffinized and rehydrated following the treatment with xylene and a series of ethanol concentrations. After antigen retrieval

with citrate buffer (pH 6) at 94°C for 15 min, followed by washing with water, the sections were incubated with 3% hydrogen peroxide for 10 min. After incubating the slides with blocking buffer for 1 hr at room temperature, the slides were incubated with AATF antibody (1:100 dilution) overnight at 4°C in a humidified chamber. The signals were developed using the polyexcel HRP/DAB detection system-one step (PathnSitu, Biotechnologies) as per the manufacturer's protocol, and the nucleus was stained using hematoxylin. All the immunohistochemistry images were taken using an Olympus BX53 microscope. The images were quantified using Image J software.

## 2.7 Condition media preparation and neutralization of PEDF

To examine the effect of the biologically active components secreted by HCC cells on angiogenesis, conditioned media was prepared from control and AATF knockdown clones of QGY-7703 cells and then treated on HUVECs. The AATF control and knockdown clones were cultured until cells reached 80-85% confluency. The cells were washed with PBS and then incubated in serum-free DMEM medium for 24 hours. The conditioned medium was collected and centrifuged at 2500 rpm for 5 min at $4^0$C to remove the dead cells and cell debris. The conditioned media was aliquoted and stored at -$80^0$C. The amount of protein in the conditioned media was determined by Bradford's protein assay (Supplementary Figure 3B). For all the experiments, the volume of conditioned media was normalized to have the same protein concentration as the control and AATF knockdown cells.

To neutralize the PEDF in the conditioned media secreted by the control and AATF knockdown QGY-7703 cells, the conditioned media was treated with anti-PEDF antibody. A non-specific antibody was used as an isotype control. The antibodies were used at a concentration of 5 µg/ml.

## 2.8 Enzyme-linked immunosorbent assay)

The concentration of PEDF was measured in the conditioned media collected from control and knockdown QGY-7703 cells by using ELISA kit (R&D Systems, Minnesota, USA) according to the manufacturer's protocol.

## 2.9 Proliferation assay

The HUVECs were seeded in 96 well plates at a density of $10^4$ cells per well and cultured up to 70% confluency. The cells were treated with the conditioned media of control and AATF knockdown QGY-7703 cells for 24 h, 48 h, and 72 h. At the end of the treatment, the proliferation of HUVECs was evaluated using a premix WTS-1 cell proliferation assay mix (Takara Bio Inc., Japan). The absorbance was measured at 450 nm on a multi-mode plate reader (EnSpire™ Multimode Plate Reader, Perkin Elmer) according to the manufacturer's protocol.

## 2.10 Migration assay

The HUVECs were seeded at a density of 5 X$10^5$ cells per well in 6 well plates and allowed to attain 70-80% confluency. A scratch was made using a 1 ml pipette tip across the centre of the well, and the medium was removed to get rid of the detached cells. The HUVECs were incubated with conditioned media of control and knockdown cells with or without IgG and PEDF antibodies (Santa Cruz). The migration ability of the HUVECs was evaluated by measuring the gap widths at time intervals of 0 and 24 h. Images were acquired with a Zeiss Primovert inverted microscope and analyzed for the measurement of gap distance using ImageJ software.

## 2.11 Invasion assay

Transwell inserts of 8 µm pore size were coated with matrigel matrix gel and placed into a 24-well plate. The HUVECs were suspended in the serum-free endothelial cell growth medium at the density of 5X$10^4$ cells and seeded into each pre-coated transwell inserts. In the lower chambers of 24 well plates were added conditioned media from control and knockdown cells with or without IgG and PEDF antibodies. Cells were incubated at $37^0$C for 24 h to analyze the invasive ability of the cells. After the incubation, the non-invasive cells in the precoated transwell inserts were removed with a sterile PBS-soaked cotton swab. The invasive cells at the bottom of the transwell inserts were fixed with paraformaldehyde and stained with Giemsa stain. Images were captured using a Zeiss Primovert inverted microscope and analyzed by comparing the number of cells that had crossed the membrane between the control and knockdown conditioned media groups.

## 2.12 Chick chorioallantoic membrane assay

Fertilized chicken eggs were sterilized and pre-incubated at $37^0$C in 85% humidity. After 7 days of incubation, a small hole was made on the broad side of the shell, and carefully, a window of 1 $cm^2$ was created. The embryos were treated with the conditioned media of control and knockdown cells. The window was sealed, and the eggs were incubated for 48 h in the humidified incubator at $37^0$C. Images were photographed using a Nikon digital camera, and angiogenesis is quantified by comparing the number of blood vessels between the control and knockdown groups.

## 2.13 Zymography

The protease activity of the metalloproteases was detected by gelatin zymography. 7.5% of polyacrylamide gels containing 0.1% gelatin with a Tris-glycine running buffer were used to separate proteins. After electrophoresis, gels were washed in 2.5% TritonX-100 prepared in 50 mM Tris-HCl of pH 7.5 for 1h. Later, gels were incubated in developing buffer (1% TritonX-100, 50 mM Tris-HCl pH 7.5 along with 5 mM Calcium chloride and 1 µM zinc chloride) for 24 h at $37^0$C. After the incubation, gels were stained using

coomassie blue for 1 h and destained using a destaining solution. Images were taken using the Gel Doc system (Genesys) and analyzed in ImageJ software.

## 2.14 RNA isolation and quantitative real-time PCR

Total RNA from the cells and frozen liver tissues was isolated using the TRIzol method. The quality and concentration of the RNA were determined by a nanodrop spectrophotometer. The RNA was reverse transcribed by following the manufacturer's instructions using the Verso cDNA synthesis kit. The real-time PCR reactions were carried out using the DyNamo Colorflash SYBR Green kit with 0.5 mM primers (IDT), and 50 ng of cDNA in a 20 µl reaction volume. The real-time PCR reactions were performed using the Rotor-Gene Q5plex HRM System (Qiagen). The relative quantification of the mRNA fold change was calculated as $2^{-\Delta\Delta Ct}$ and was expressed normalized with endogenous control β-actin. The primers for the qRT-PCR were validated, and the sequences of the primers used in this study are provided in Supplementary Table 2.

## 2.15 Immunoblotting

The lysates were prepared by homogenizing the human liver tissues and HCC cells in RIPA buffer containing protease/phosphatase inhibitors. The supernatant was collected after the homogenized tissue or cell samples were centrifuged at 13000 rpm for 10 minutes at $4^0$C. The protein concentration was determined by using the Bio-Rad protein assay dye reagent (Bio-Rad) of Bradford's protein estimation method. A 30-50 µg of protein was loaded to separate the proteins in the SDS-PAGE and transferred onto a nitrocellulose membrane for all western blots. The membranes were blocked using 5% nonfat skim milk for an hour at room temperature and probed with specific primary antibodies (AATF, β-actin, pErk1/2, Erk1/2, pAkt, Akt, pFak, and PEDF) for overnight incubation at $4^0$C. Furthermore, membranes were washed and incubated for secondary antibodies for 2 h at room temperature. The blots were developed using the Western Bright ECL HRP substrate, and images were captured using the Uvitec Alliance Q9 chemiluminescence imaging system. The bands were quantified using ImageJ software. The intensity of each band was normalized to its respective endogenous control, β-actin.

## 2.16 Gene expression analysis using TCGA database

The RNA sequence and clinical information data of HCC tissues (n= 371) and normal liver tissues (n=50) were downloaded from the TCGA-LIHC website of The Genomic Data Commons (GDC: https://portal.gdc.cancer.gov/repository) up to November 15, 2022. TCGA dataset containing only primary tumors was processed. Different stages of HCC clinical samples as follows: Stage1: n=168; Stage2: n=84; Stage3: n=82 and Stage4: n=6. The expression values of AATF in terms of transcripts per million from the whole transcriptome profile were obtained for which a differential expression analysis was performed on normal and different stages of HCC datasets using limma R package at a significance level of FDR<0.05 along with p<0.05. The graphs were plotted using GraphPad Prism software (version 6).

## 2.17 Statistical analysis

Results were calculated as means ± SEM. Statistical significance was analyzed using Student's t-test. All statistical analyses were performed using the GraphPad Prism software (version 6), and all experiments were considered significant with p<0.05 [p<0.05 (*, #) or <0.001 (**, ##)].

# 3 Results

## 3.1 Upregulation of AATF in human HCC

To investigate the role of AATF in HCC, mRNA and protein levels of AATF were measured in human HCC cell lines and found to be relatively overexpressed in QGY-7703 compared to Hep3B and normal liver tissues (Figures 1A, B). Consistent with these observations, the mRNA expression of AATF in human HCC tissues (n=50) was also found to be significantly upregulated compared to adjacent normal liver tissues (n=15) (Figure 1C). Histological analysis of human HCC tissues revealed distinctive changes in the cell structure and arrangement of the hepatocytes, confirming different grades of HCC (Figure 1D). Furthermore, immunohistochemistry revealed that AATF expression increased gradually from stages I to IV, as well as with the differentiation grades from well differentiated to poorly differentiated HCC (Figure E, Supplementary Figure 1A). These findings show that AATF expression increases with the HCC stage and loss of differentiation, confirming AATF's role in the development and progression of HCC. Next, we analyzed the publicly available TCGA database to evaluate the status of AATF in normal (n=50) and HCC (n=371). In support of our results, the data from the TCGA database provided evidence that there are significantly higher AATF differential transcription levels in HCC compared to normal. The levels of AATF were found to be significantly related to the pathological stages and tumor grades of HCC (Supplemental Figure 2).

## 3.2 AATF knockdown suppresses the angiogenic potential of HCC

We investigated the regulatory role of AATF on angiogenesis, a major hallmark of cancer, which is responsible for the rapid recurrence and poor survival rate in HCC patients (35). The effect of AATF on angiogenesis was determined by assessing the impact of its loss of function. The initial step towards achieving this was the establishment of stable QGY-7703 cell lines. The expression of

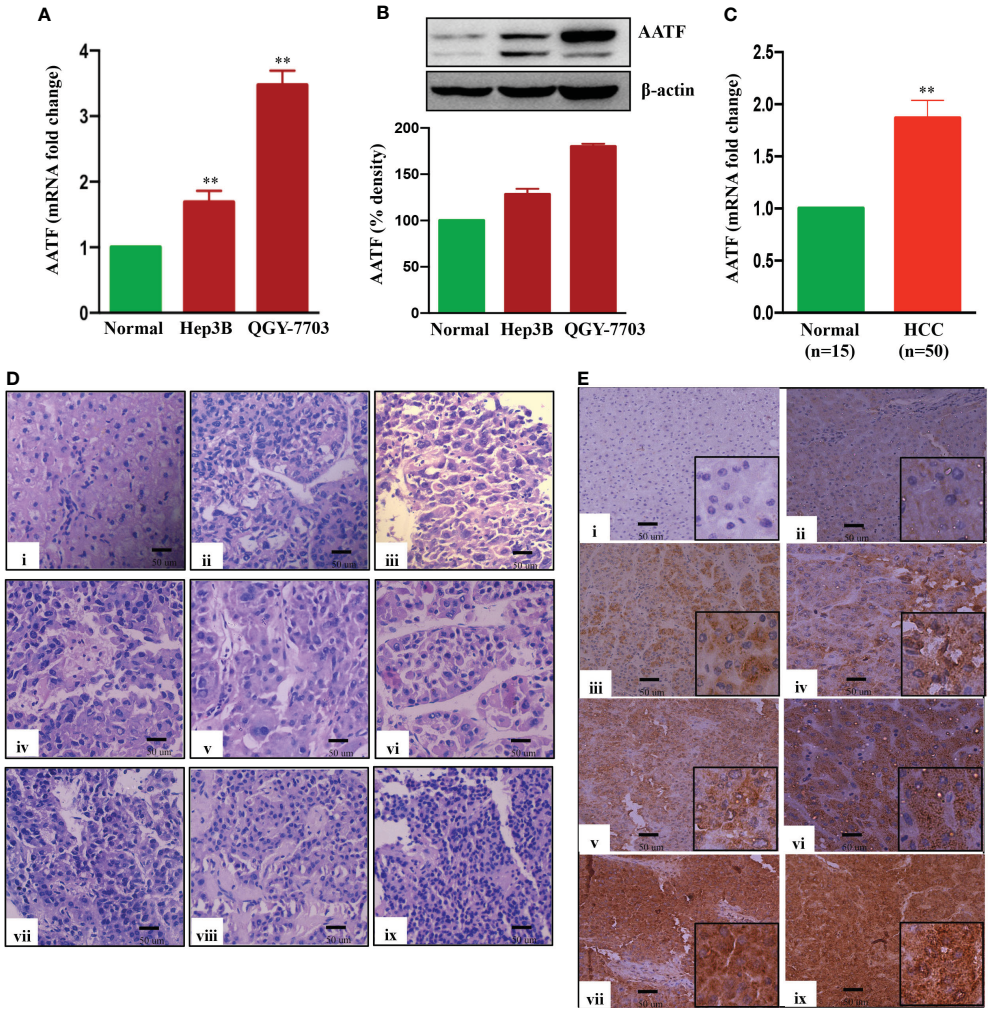


FIGURE 1
Expression of AATF in human HCC cells and HCC tissues. AATF mRNA **(A)** and protein **(B)** expression in human HCC cells. **(C)** AATF mRNA expression in human normal and HCC subjects. **(D)** Representative Hematoxylin and eosin (H&E- 400X)–stained liver sections of human normal and HCC subjects. **(E)** Representative immunohistochemistry images (200X) showing the expression of AATF in formalin-fixed paraffin-embedded human normal liver and HCC tissues. The inset shows images at higher magnification (400X). (i) Normal human liver; (ii) stage I, well differentiated; (iii) stage I, poorly differentiated; (iv) stage II, well differentiated; (v) stage II, poorly differentiated; (vi) stage III, well differentiated; (vii) stage III, poorly differentiated; (viii) stage IV, well differentiated; (ix) stage IV, poorly differentiated. Data are expressed as the mean ± SEM. **p < 0.001 or *p < 0.05 compared to normal.

AATF was significantly reduced in the knockdown clones compared to puromycin-resistant control clones (Figure 2A, Supplementary Figure 3).

Cell proliferation, migration and invasion are critical steps for the endothelial cells to form blood vessels in angiogenesis (36). To determine the effect of AATF on angiogenesis, the influence of conditioned media (CM) of control and AATF knockdown QGY-7703 cells on proliferation, migration, and invasion of human umbilical vein endothelial cells (HUVECs) was analyzed. We hypothesized that AATF knockdown would affect the angiogenic properties of HUVECs and vascular development in chick embryos. Consistent with this hypothesis, the CM of the knockdown cells significantly inhibited the proliferation of HUVECs compared to the control (Figure 2B). Furthermore, the chemotactic motility of endothelial cells was determined by migration assay and matrigel invasion assay. The results showed that CM of knockdown cells inhibited the migration of HUVECs and significantly reduced cell invasion compared to control, providing strong evidence that AATF knockdown affects the motility and matrix degradation capacity of HUVECs, which are critical for angiogenic sprouting (Figures 2C, D).

We further employed the chicken chorioallantoic membrane (CAM) assay, which is a physiological model of embryonic angiogenesis. Similar results were obtained where the CM of AATF knockdown cells showed a remarkable effect on the chicken embryo by significantly decreasing the vascular growth compared to the CM of the control cells (Figure 2E).

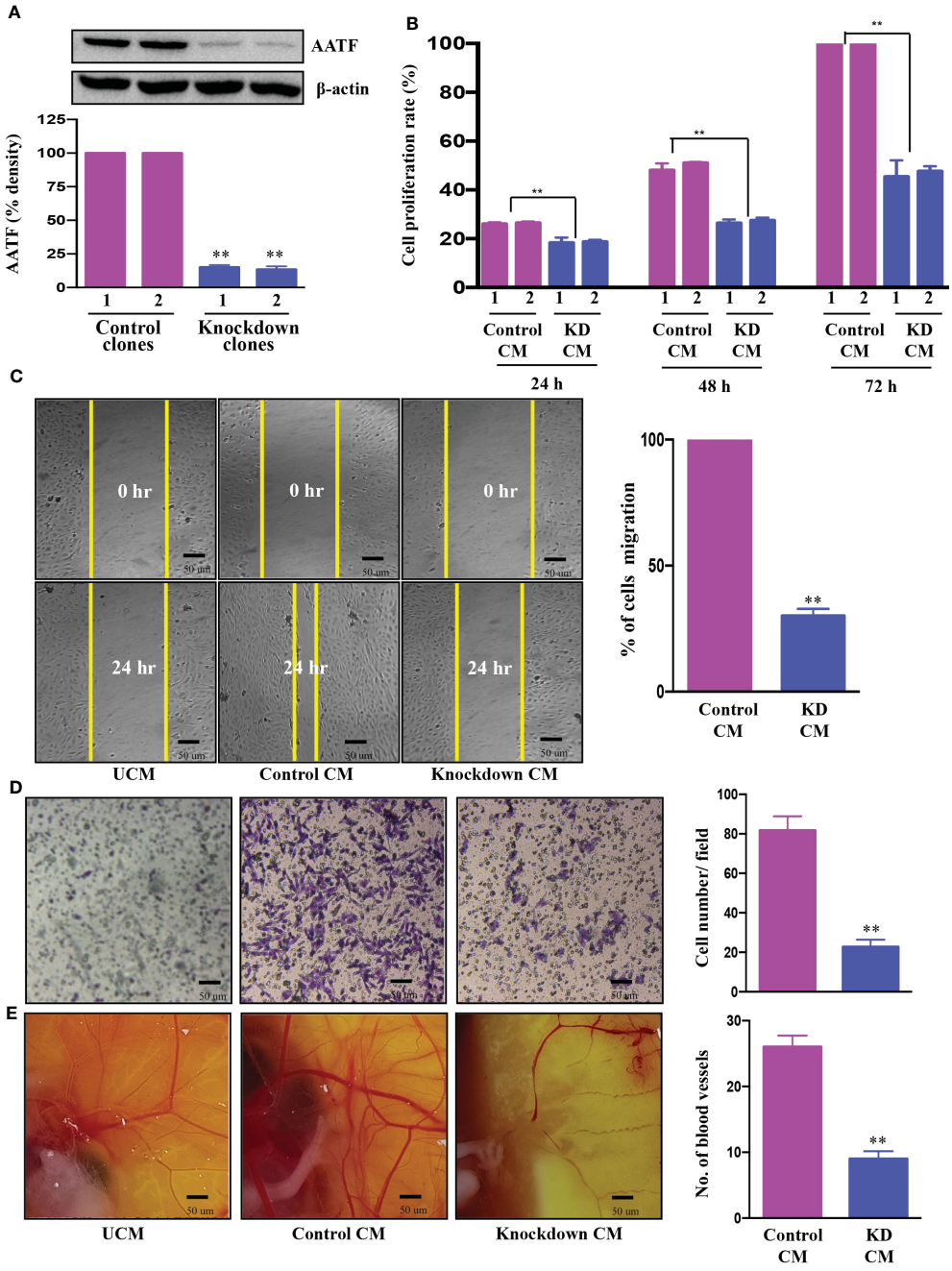


FIGURE 2
Knockdown of AATF inhibits migration, invasion of HUVECs, and vascular growth in chicken embryo chorioallantoic membrane. AATF protein **(A)** expression in control (clone 1 and clone 2) and AATF knockdown (clone 1 and clone 2) QGY- 7703 cells. Effect of conditioned media from control (clone 1 and clone 2) and AATF knockdown (clone 1 and clone 2) QGY-7703 cells on proliferation- represented as cell proliferation rate (%) normalized to 72 h control **(B)**, migration **(C)**, and invasion **(D)** of the human umbilical vein endothelial cells (HUVECs). **(E)** CAM assay performed using the conditioned media from control and AATF knockdown QGY-7703 cells. Representative images are shown. UCM, unconditioned medium, CM, conditioned medium. Data are expressed as the mean ± SEM of three experiments. **p < 0.001 or *p < 0.05 compared to control.

## 3.3 Effect of AATF knockdown on PEDF levels

The proangiogenic and anti-angiogenic genes manifest themselves differently in HCC due to the activation of diverse oncogenic pathways. Our previous study using a human angiogenesis array revealed that PEDF, or SerpinF1, a well-known anti-angiogenic factor, is highly expressed in AATF knockdown cells compared to control cells (32). With this rationale, we investigated the regulatory role of AATF on PEDF levels in control and knockdown QGY-7703 stable cells. The AATF knockdown cells showed upregulated PEDF protein expression compared to controls (Figure 3A). Furthermore, PEDF levels were also measured by ELISA using the CM from control and

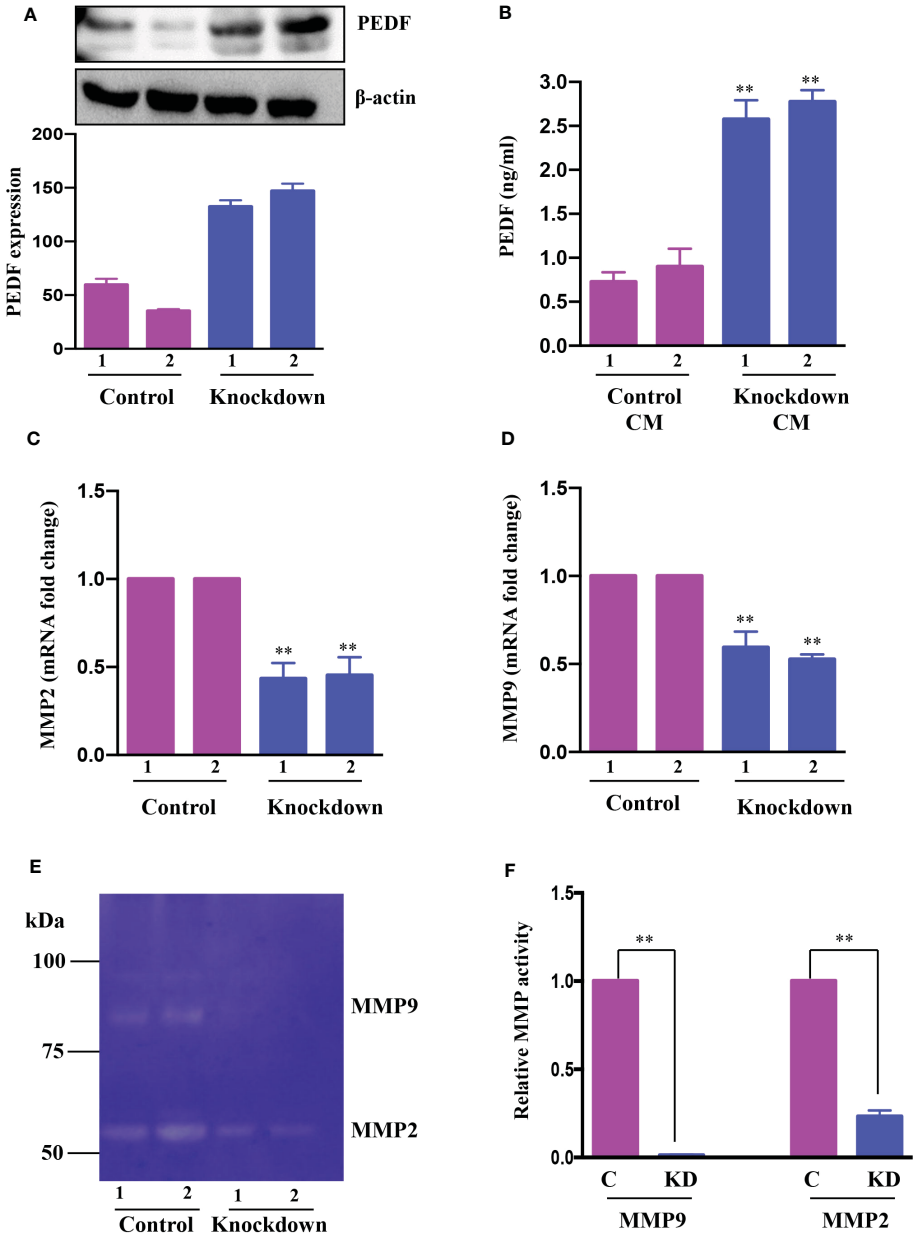


FIGURE 3
AATF knockdown increases PEDF expression. **(A)** The protein expression of PEDF in control (clone 1 and clone 2) and AATF knockdown (clone 1 and clone 2) QGY-7703 cells. The bar plot is the densitometric analysis of PEDF expression normalized to the endogenous control β-actin. **(B)** PEDF levels in conditioned media (CM) from control (clone 1 and clone 2) and AATF knockdown (clone 1 and clone 2) cells as measured by ELISA. The mRNA expression of MMP2 **(C)** and MMP9 **(D)** in control (clone 1 and clone 2) and AATF knockdown (clone 1 and clone 2) QGY-7703 cells. **(E)** MMP2 and MMP9 gelatinolytic activity in the conditioned media of control and AATF knockdown cells was detected by gelatin zymography. **(F)** Quantitative densitometric analysis of MMP2 and MMP9 lysis bands of control and AATF knockdown QGY-7703 cells following zymography. 2 clones of control (control clone #1 and control clone #2) and knockdown (KD clone #1 and KD clone #2) QGY-7703 cells were used for the experiments. Data are expressed as the mean ± SEM of three experiments. **p < 0.001 or *p < 0.05 compared to control.

knockdown cells. Similar results were obtained where the secretion of PEDF was significantly higher in the CM of AATF knockdown cells compared to the control (Figure 3B).

We next explored the mechanism by which PEDF is upregulated in AATF knockdown cells. PEDF, a member of the serpin superfamily, acts as a natural angiogenesis inhibitor and is found to be significantly downregulated in most cancers, including HCC (37). There is an increasing body of evidence for the involvement of matrix metalloproteinases type 2 (MMP2) and type 9 (MMP9) in the degradation of PEDF. Of note, PEDF acts as a substrate for MMP2 and MMP9 (38). Along the same lines, we examined the expression of MMP2 and MMP9 in CM of control and knockdown QGY7703 cells and interestingly found that MMP2 and MMP9 were down regulated in AATF knockdown cells compared to control (Figures 3C, D). Additionally, we also tested the MMP activity by performing gelatin zymography. Consistent with the expression data, there was decreased gelatinolytic activity of MMP2 and MMP9 in knockdown cells compared to control

(Figures 3E, F). Together, these findings suggested that AATF inhibition downregulates MMP2 and MMP9, which prevents PEDF from being degraded in AATF knockdown cells as opposed to control cells.

### 3.4 AATF knockdown exerts anti-angiogenic effect in HCC *via* PEDF

Further investigations were carried out to determine whether PEDF played a key role in the suppression of angiogenesis in AATF knockdown cells. To test this hypothesis, we further validated the effect of conditioned media from control and AATF knockdown QGY-7703 cells on the migration and invasion of HUVECs and vascular formation in CAM in the presence of neutralizing anti-PEDF antibody. A non-specific IgG antibody served as an isotype control. The concentration of anti-PEDF antibody was determined by a dose response experiment on the proliferation of HUVECs with control and AATF knockdown CM, and a concentration of 5 µg/ml was chosen for the experiments. Consistent with the previous experiments, the conditioned media of AATF knockdown cells inhibited the migration (30% vs. 100% of cell migration in the control) and invasion (18 vs. 75 cells per field in the control) of HUVECs, and this inhibition was significantly diminished in the presence of PEDF neutralizing antibody [72% of cell migration (Figures 4A, D) and invasion assay- 46 cells per field (Figures 4B, E)]. Similarly, the decrease in the vascular growth caused by the conditioned media of AATF knockdown cells (7 vs. 23 blood vessels in control) was diminished in the presence of PEDF neutralizing antibody (16 blood vessels) (Figures 4C, F). Taken together, these data provide solid evidence that knockdown of AATF suppresses angiogenesis in HCC *via* PEDF.

### 3.5 Mechanisms involved in AATF-mediated angiogenesis in human HCC

To examine the mechanisms underlying AATF-mediated angiogenesis in human HCC, we sought to explore several downstream signaling effectors that are responsible for endothelial cell survival and vascular permeability, cell proliferation, and migration. To test this hypothesis, HUVECs were treated with CM from control and AATF knockdown cells and examined for Erk1/2, Akt, and FAK phosphorylation by western blot analysis. Our results showed that the activation of the key components of the angiogenesis signaling pathway, including the phosphorylation of Erk1/2 (Figure 5A), Akt (Figure 5B), and FAK (Figure 5C), was decreased in HUVECs treated with CM from knockdown cells compared to control. To corroborate the involvement of PEDF in the angiogenesis signaling pathway, experiments were carried out in the presence of neutralizing anti-PEDF antibody. Consistent with our previous observations, the activation i.e. phosphorylation of Erk1/2, Akt, and FAK, which was decreased by the AATF knockdown, was diminished in the presence of PEDF neutralizing antibody (Figures 5A–C).

## 4 Discussion

The current manuscript describes highly significant and relevant findings in the context of HCC, a highly vascularized tumor in which angiogenesis is critical to its growth, invasion, and metastasis (35). In our experiments and from genomic data mining analysis, AATF was significantly higher as the disease progressed in different stages and grades compared to normal liver tissue samples. While AATF expression is very low or non-existent in normal liver tissues, it gradually increases as the stages and grades of HCC disease progress. Numerous studies have discovered that AATF, a multifunctional and highly conserved protein, contributes significantly to the development of various malignancies (18, 21, 25). We have previously shown the novel regulatory role of AATF in NAFLD-associated HCC (32). This is the first study to elucidate that targeting AATF can be an effective antiangiogenic strategy in the treatment of HCC.

Our findings in NAFLD-associated HCC showed that AATF expression was upregulated, whereas knocking down AATF significantly reduced tumor burden and metastasis in a mouse xenograft model (32). These data led to investigations to understand the role of AATF in the molecular pathogenesis of HCC, and therefore we elucidated the unexplored regulatory role of AATF in tumor angiogenesis, one of the hallmarks that contribute to tumor growth and metastasis. To precisely elucidate the molecular mechanism underlying AATF function in angiogenesis, we focused on knocking down AATF in QGY-7703 human HCC cells. The first finding is that the CM of AATF knockdown cells inhibited the proliferation of human umbilical vein endothelial cells (HUVECs) compared to the control. The data are concordant with the migration and invasion of HUVECs, wherein AATF knockdown caused inhibition compared to control. We also document that the vascular growth in chicken embryos is inhibited with CM of AATF knockdown HCC cells, as assessed by the CAM assay, providing strong experimental evidence that inhibition of AATF suppresses angiogenesis in HCC.

Tumor-induced angiogenesis is typically associated with a complex interplay of multiple factors and pathways, with vascular endothelial growth factor (VEGF) being a key player (39). The process of angiogenesis in HCC is an extremely complex and tightly regulated process characterized by well-balanced interactions between pro- and anti-angiogenic factors. In addition to VEGF, the other key angiogenesis stimulating factors include PEDF, FGF, angiopoietins, and endoglins. On the other hand, endogenous angiogenesis inhibitors include anti-angiogenic peptides, hormone metabolites, and apoptosis modulators (8, 40). Thus, the angiogenic switch involving the proangiogenic factors overexpression as well as anti-angiogenic factors inhibition results in increased tumor vascular burden, which leads to tumor proliferation and progression (41). Perhaps, the strongest evidence to support the role of AATF in angiogenesis came from our previous studies which showed the increase of PEDF or SerpinF1 levels in the AATF knockdown HCC cells compared to control as demonstrated by the human angiogenesis array (32). This is further corroborated in the current study, which confirmed high levels of PEDF, both by

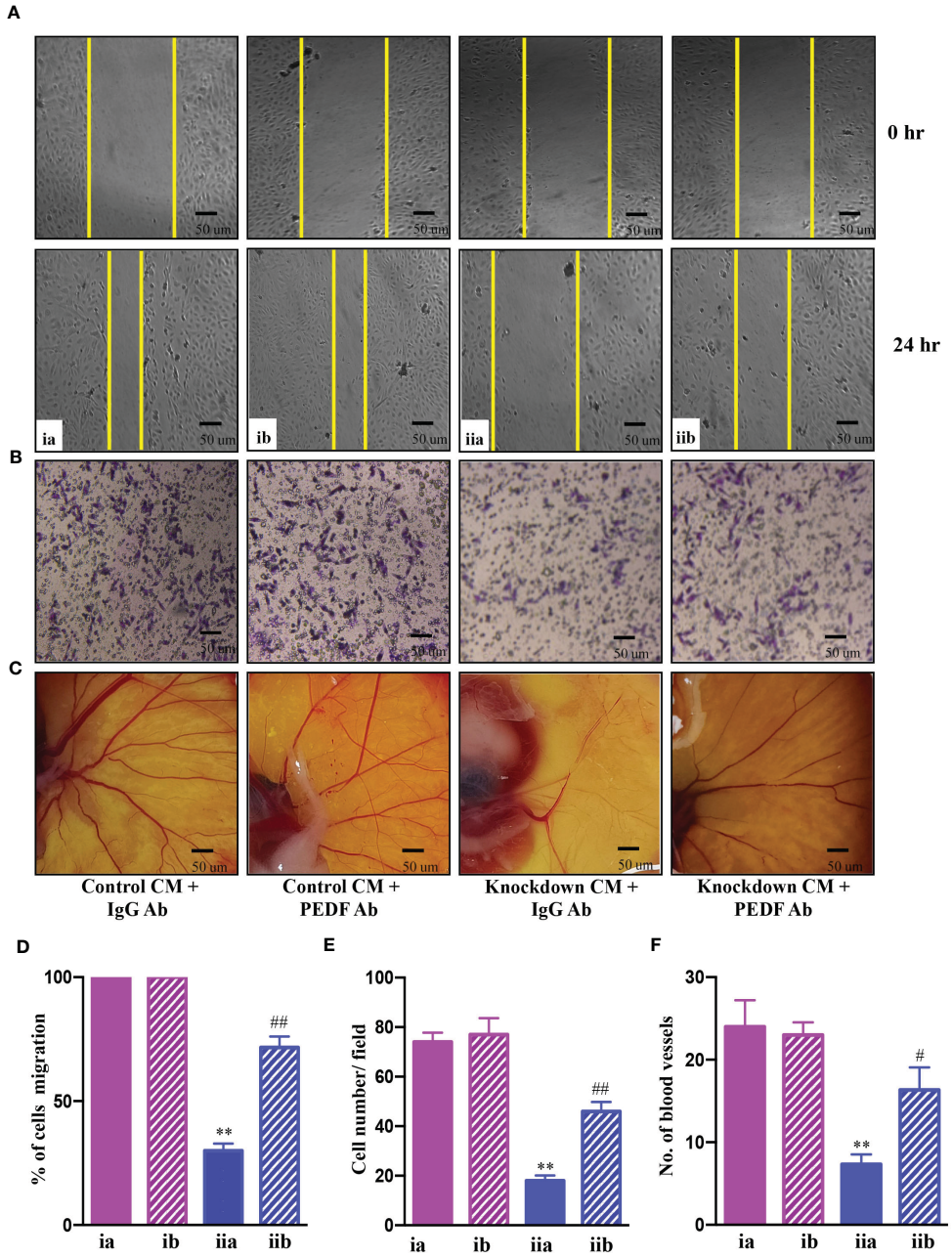


FIGURE 4
AATF knockdown inhibits angiogenesis *via* PEDF. Effect of conditioned media from control and AATF knockdown QGY-7703 cells treated with or without anti-PEDF antibody on migration **(A)** and invasion **(B)** of the human umbilical vein endothelial cells (HUVECs). **(C)** CAM assay performed using the conditioned media from control and AATF knockdown QGY-7703 cells treated with or without anti-PEDF antibody. Representative images are shown. **(D)** Quantification of the gap distance at 0 hr and 24 hr was evaluated using Image J software and expressed as % cells migration. **(E)** Quantitative analysis of HUVECs that passed through the membrane treated with conditioned media as characterized by matrigel invasion assay. **(F)** Quantification of the number of blood vessels was performed using Image J software. CM, conditioned medium; ia, control CM + IgG antibody; ib, control CM + PEDF antibody; iia, knockdown CM + IgG antibody; iib, knockdown CM + PEDF antibody. Data are expressed as the mean ± SEM of three experiments. $^{**}p < 0.001$ or $^{*}p < 0.05$ compared to ia; $^{\#\#}p < 0.001$ or $^{\#}p < 0.05$ compared to iia.

immunoblot analysis and ELISA, in AATF knockdown cells compared to control cells. Similarly, Matsumato K. et al., found lower PEDF serum concentrations in patients with cirrhosis or HCC compared to healthy subjects (37). This provided a strong rationale to further examine the involvement of PEDF in AATF-mediated angiogenesis in HCC.

PEDF, belonging to the serine protease inhibitor (serpin) superfamily, has several roles that frequently work against the pathways that promote the progression of cancer (42). Notably, Dawson and his colleagues for the first time identified the potent anti-angiogenic activity of PEDF in the cornea and vitreous humour of the eye (43), which later paved the way for the exploration of

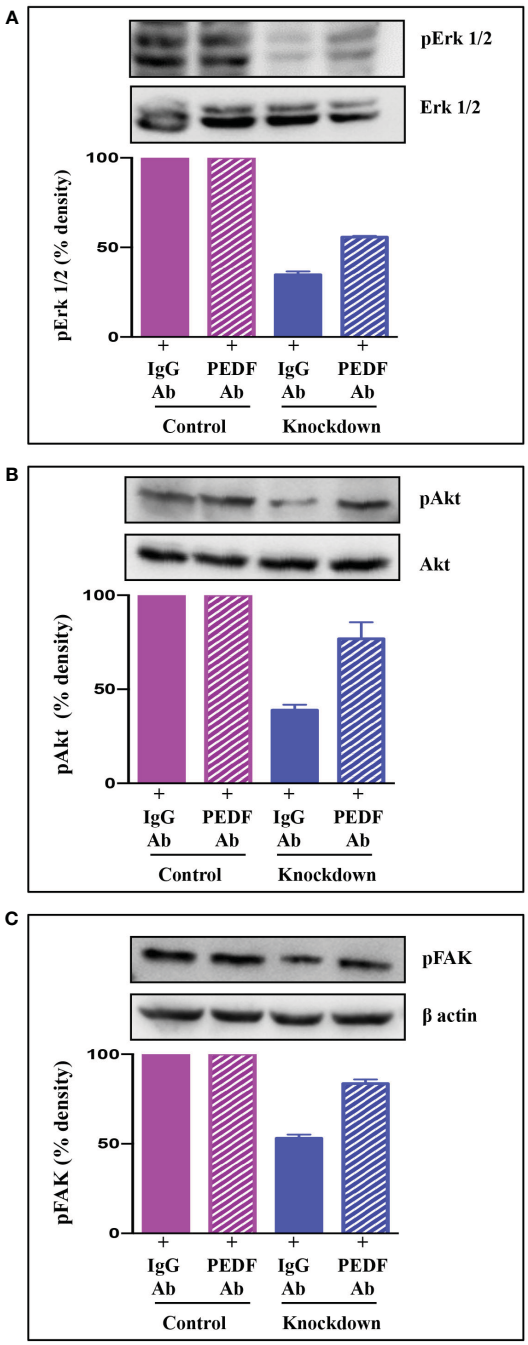


FIGURE 5
Signaling pathway *via* which AATF knockdown inhibits angiogenesis in HCC. Western blots depicting the protein expression of pErk1/2 and Erk1/2 **(A)**, pAkt and Akt **(B)**, and pFAK **(C)** in HUVECs treated with conditioned media from control and AATF knockdown QGY-7703 cells treated with or without anti-PEDF antibody. Bar graphs show the densitometric values calculated after normalization to their respective controls (pErk/Erk, pAkt/Akt and pFAK/β-actin). Data are expressed as the mean ± SEM of three experiments. **p < 0.001 or *p < 0.05 compared to control.

PEDF as an angiogenesis inhibitor in tumors (44). PEDF, on the other hand, is a substrate for extracellular matrix metalloproteinases and has been found to be degraded in several cancers (38, 44). In this regard, our findings revealed a decrease in MMP2 and MMP9 activity in the CM of AATF knockdown cells compared to controls, providing a logical explanation for the presence of PEDF levels in AATF knockdown HCC cells versus controls. These data are in support of the studies carried out by Notari L. et al., which showed MMP-mediated degradation of PEDF leading to increased angiogenesis in the retina (38). In our previous studies, we discovered that human HCC cells have elevated STAT3 levels as well as the AATF-STAT3 nuclear interaction (32). Studies by Zhang et al., have demonstrated that elevated activation of STAT3 is responsible for the upregulation of MMP2 and MMP9 in cancer cells (45). Taken together, it is evident that AATF interacts with STAT3 and upregulates the matrix metalloproteinases, MMP2 and

MMP9, which in turn degrade PEDF. In contrast, inhibiting AATF reduces MMP2 and MMP9 levels, effectively stopping the degradation process, while PEDF remains functionally active. It is interesting to note that, PEDF inhibits angiogenesis either by increasing γ-secretase-mediated cleavage of VEGFR2 or by inhibiting VEGF-induced phosphorylation and activation of VEGFR2 (46). However, in our studies, the activation of Erk1/2, Akt, and FAK, which are the angiogenic mediators, downstream of VEGF signaling, was inhibited in HUVECs treated with CM of knockdown cells. Also, this inhibition was diminished in the presence of the PEDF antibody. These data are thus in line with the mechanism of PEDF antagonizing the action of VEGF-A binding to its receptor, VEGFR2 and thereby preventing the activation and downstream VEGF-A signals (47). From the mechanistic point of view, our current study provides an insight into the mechanisms of AATF inhibition exerting anti-angiogenic effects in human HCC *via* PEDF (Figure 6). This also offers an additional advantage, as PEDF not only blocks angiogenesis but is also involved in anti-tumor and anti-metastatic activities.

This proof-of-concept study supporting the notion that AATF inhibition suppresses angiogenesis holds certain clinical implications. Clinically, liver-specific targeting of AATF by lipid nanoparticle-based delivery of siRNA-AATF or AAV8-mediated siRNA-AATF delivery appears to be an effective antiangiogenic approach. Another approach would be the generation of liver-specific AATF knockout mice that can be used to induce HCC and examine the role of AATF in tumor progression, angiogenesis, and metastasis. Though the FDA-approved angiogenesis inhibitors such as sorafenib, bevacizumab, and ramucirumab possess efficacy, they are known to have adverse effects, and resistance is a major concern (14). There also exists the therapeutic limitation of systemic administration of antiangiogenic compounds restricting their clinical applications (48). Of note, this antiangiogenic gene therapy involving AATF knockdown may be an attractive strategy due to its specificity. Unlike the angiogenic inhibitors/compounds that may inhibit growth factor-induced signal transduction that is required in tumor angiogenesis as well as normal vasculature, resulting in adverse effects. Thus, targeting angiogenesis by AATF inhibition would be a safe antiangiogenic approach. This also warrants future detailed preclinical studies involving AATF inhibition and understanding the molecular mechanisms of AATF-mediated metastasis in HCC. It is of prime importance that current strategies for combating angiogenesis and the potential for combining antiangiogenic therapy with other systemic modalities, like immunotherapy, would help HCC patients have a better prognosis.

In conclusion, the current study adds to the growing body of evidence supporting the key role of angiogenesis in tumor growth and progression. We demonstrated that AATF inhibition suppresses angiogenesis in human HCC *via* PEDF, and AATF

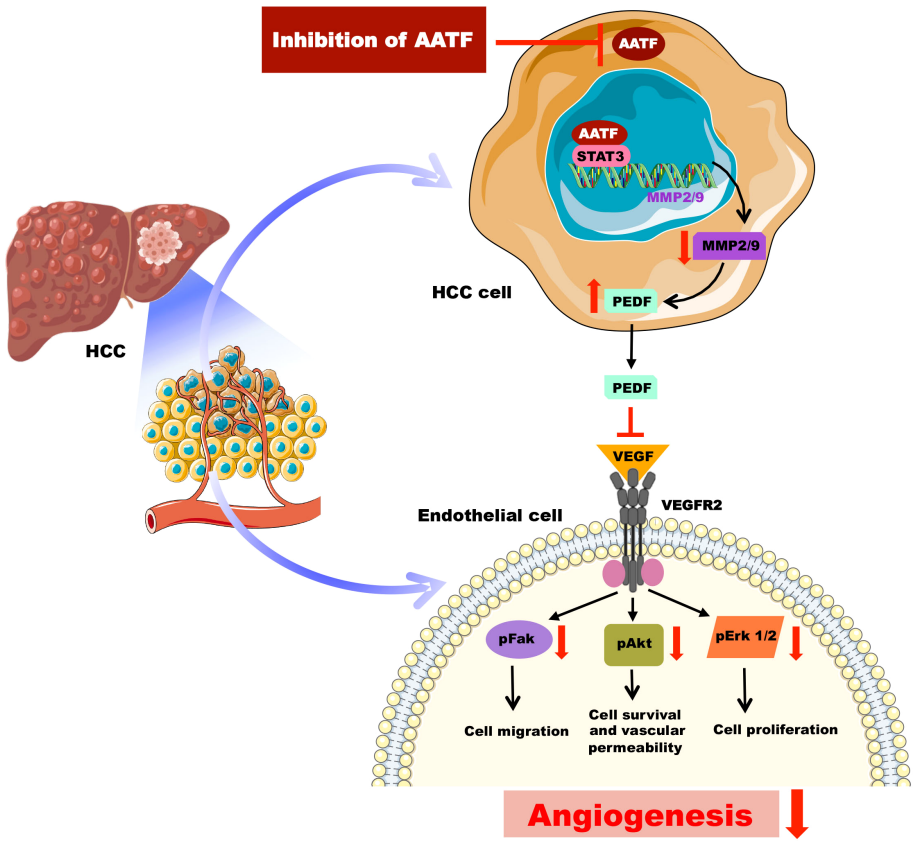


FIGURE 6
Schematic representation of the molecular mechanisms involved in AATF-mediated regulation of angiogenesis in human HCC.

may serve as a promising gene therapy for HCC treatment. The study offers a target for intervention and a direction for investigations to lessen the burden of HCC by targeting angiogenesis, and it provides a basis for future work that can be translated into human trials.

## Data availability statement

The original contributions presented in the study are included in the article/Supplementary Material, Further inquiries can be directed to the corresponding author.

## Ethics statement

The study was approved by the institutional ethics committee at JSS Medical College, JSS AHER, Mysore, Karnataka, India. (JSSMC/IEC/260822/37NCT/2022-23). The patients/participants provided their written informed consent to participate in this study.

## Author contributions

DS designed and performed experiments, analyzed data, and wrote the manuscript; AS performed experiments and analyzed data; SS analyzed the data; AP, SN and PV contributed to the discussion and reviewed the manuscript; PS and SK provided scientific insights and reviewed the manuscript; and DPK conceptualized the project, designed experiments, critically evaluated the results, and wrote the manuscript. All authors contributed to the article and approved the final version of the manuscript submitted.

## Funding

DS' appointment is supported by the Extramural Ad-hoc Grant from the Indian Council of Medical Research (ICMR-Grant No.: 5/3/8/55/2020-ITR) to DPK. This study was supported in whole or in part, by the Extramural Ad-hoc Grant from ICMR and Ramalingaswami Re-entry Fellowship (Grant No.: BT/RLF/Re entry/58/2017) from the Department of Biotechnology to DPK. The authors also acknowledge funding support from the Department of Biotechnology (DBT)- Boost to University Interdisciplinary Life science Departments for Education and Research programme (DBT-BUILDER: BT/INF/22/SP43045/2021).

## Acknowledgments

We gratefully acknowledge Dr. Nalini and her team, Gynecologist, Shree Devi Nursing Home, Mysore, for providing human umbilical cord for the study. Human normal or HCC tissues were obtained from the National Tumor Tissue Repository (NTTR), Tata Memorial Hospital, Mumbai.

## Conflict of interest

Author SK was employed by Omelette Inc.

The remaining authors declare that the research was conducted in the absence of any commercial or financial relationships that could be construed as a potential conflict of interest.

## Publisher's note



## Supplementary material

The Supplementary Material for this article can be found online at: https://www.frontiersin.org/articles/10.3389/fonc.2023.1130380/full#supplementary-material

SUPPLEMENTARY FIGURE 1

**(A)** Quantitation and comparison of the AATF-positive cells in HCC tissues of stage 1, stage 2, stage 3 and stage 4 using Image J software. WD, well differentiated; PD, poorly differentiated HCC tissues. **(B)** Culturing of Human umbilical vein endothelial cells (HUVECs). Images at different magnifications- 10X, 20X and 40X.

SUPPLEMENTARY FIGURE 2

**(A)** Differential expression Analysis of AATF in normal (n=50) and human HCC (n=371) tissues in TCGA microarray data set ($P<1x10^{-12}$). **(B)** Expression of AATF varies across the stages of HCC (normal vs. stage 1: $P<1.62x10^{-12}$; normal vs. stage 2: $P<1.62x10^{-12}$; normal vs. stage 3: $P<1x10^{-12}$; normal vs. stage 4: $P<7.7x10^{-2}$). **(C)** Tumor grades were highly significant (normal vs. grade 1: $P<1.33x10^{-10}$; normal vs. grade 2: $P<1x10^{-12}$; normal vs. grade 3: $P<1x10^{-12}$; normal vs. grade4: $P<6.4x10^{-4}$).

SUPPLEMENTARY FIGURE 3

**(A)** AATF mRNA expression in control (clone 1 and clone 2) and AATF knockdown (clone 1 and clone 2) QGY- 7703 cells. **(B)** Protein concentration (µg/ml) of conditioned media from control and (clone 1 and clone 2) and AATF knockdown (clone 1 and clone 2) QGY- 7703 cells. **(C)** Effect of conditioned media from control (clone 2) and AATF knockdown (clone 2) QGY-7703 cells treated with or without anti-PEDF antibody on migration **(D)** Quantification of the gap distance at 0 hr and 24 hr was evaluated using Image J software and expressed as % cells migration. Data are expressed as the mean ± SEM of three experiments. $^{**}p < 0.001$ or $^{*}p < 0.05$ compared to control.

SUPPLEMENTARY TABLE 1

Demographic and clinicopathological data of HCC patients. M, male; F, female; HCC, hepatocellular carcinoma; TNM, tumor, nodes and metastases; PD, poorly differentiated; MD, moderately differentiated; WD, well differentiated.

SUPPLEMENTARY TABLE 2

List of primers used in qRT-PCR.

# References


1. Rumgay H, Arnold M, Ferlay J, Lesi O, Cabasag CJ, Vignat J, et al. Global burden of primary liver cancer in 2020 and predictions to 2040. *J Hepatol* (2022) 77(6):1598–606. doi: 10.1016/j.jhep.2022.08.021

2. Suresh D, Srinivas AN, Kumar DP. Etiology of hepatocellular carcinoma: special focus on fatty liver disease. *Front Oncol* (2020) 10:601710. doi: 10.3389/fonc.2020.601710

3. Dhar D, Baglieri J, Kisseleva T, Brenner DA. Mechanisms of liver fibrosis and its role in liver cancer. *Exp Biol Med (Maywood).* (2020) 245(2):96–108. doi: 10.1177/1535370219898141

4. Chidambaranathan-Reghupaty S, Fisher PB, Sarkar D. Hepatocellular carcinoma (HCC): epidemiology, etiology, and molecular classification. *Adv Cancer Res* (2021) 149:1–61. doi: 10.1016/bs.acr.2020.10.001

5. Giraud J, Chalopin D, Blanc J-F and Saleh M. Hepatocellular carcinoma immune landscape and the potential of immunotherapies. *Front Immunol* (2021) 12:655697. doi: 10.3389/fimmu.2021.655697

6. Morse MA, Sun W, Kim R, He AR, Abada PB, Mynderse M, et al. The role of angiogenesis in hepatocellular carcinoma. *Clin Cancer Res* (2019) 25(3):912–20. doi: 10.1158/1078-0432.CCR-18-1254

7. Hanahan D. Hallmarks of cancer: new dimensions. *Cancer Discovery* (2022) 12 (1):31–46. doi: 10.1158/2159-8290.CD-21-1059

8. Carmeliet P, Jain RK. Molecular mechanisms and clinical applications of angiogenesis. *Nature* (2011) 473(7347):298–307. doi: 10.1038/nature10144

9. Sampat KR, O'Neil B. Antiangiogenic therapies for advanced hepatocellular carcinoma. *Oncologist* (2013) 18(4):430–8. doi: 10.1634/theoncologist.2012-0388

10. Rivera LB, Bergers G. CANCER. tumor angiogenesis, from foe to friend. *Science* (2015) 349(6249):694–5. doi: 10.1126/science.aad0862

11. Wilhelm SM, Carter C, Tang L, Wilkie D, McNabola A, Rong H, et al. BAY 43-9006 exhibits broad spectrum oral antitumor activity and targets the RAF/MEK/ERK pathway and receptor tyrosine kinases involved in tumor progression and angiogenesis. *Cancer Res* (2004) 64(19):7099–109. doi: 10.1158/0008-5472

12. Zhu AX, Finn RS, Mulcahy M, Gurtler J, Sun W, Schwartz JD, et al. A phase II and biomarker study of ramucirumab, a human monoclonal antibody targeting the VEGF receptor-2, as first-line monotherapy in patients with advanced hepatocellular cancer. *Clin Cancer Res* (2013) 19(23):6614–23. doi: 10.1158/1078-0432

13. Siegel AB, Cohen EI, Ocean A, Lehrer D, Goldenberg A, Knox JJ, et al. Phase II trial evaluating the clinical and biologic effects of bevacizumab in unresectable hepatocellular carcinoma. *J Clin Oncol* (2008) 26(18):2992–8. doi: 10.1200/JCO.2007.15.9947

14. Haibe Y, Kreidieh M, El Hajj H, Khalifeh I, Mukherji D, Temraz S, et al. Resistance mechanisms to anti-angiogenic therapies in cancer. *Front Oncol* (2020) 10:221. doi: 10.3389/fonc.2020.00221

15. Oguntade AS, Al-Amodi F, Alrumayh A, Alobaida M, Bwalya M. Anti-angiogenesis in cancer therapeutics: the magic bullet. *J Egypt Natl Canc Inst* (2021) 33:15. doi: 10.1186/s43046-021-00072-6

16. Kuczynski EA, Yin M, Bar-Zion A, Lee CR, Butz H, Man S, et al. Co-Option of liver vessels and not sprouting angiogenesis drives acquired sorafenib resistance in hepatocellular carcinoma. *J Natl Cancer Inst* (2016) 108(8):djw030. doi: 10.1093/jnci/djw030

17. Abdalla AME, Xiao L, Ullah MW, Yu M, Ouyang C, Yang G. Current challenges of cancer anti-angiogenic therapy and the promise of nanotherapeutics. *Theranostics* (2018) 8(2):533–48. doi: 10.7150/thno.21674

18. Srinivas AN, Suresh D, Mirshahi F, Santhekadur PK, Sanyal AJ, Kumar DP. Emerging roles of AATF: checkpoint signaling and beyond. *J Cell Physiol* (2021) 236 (5):3383–95. doi: 10.1002/jcp.30141

19. Leister P, Burgdorf S, Scheidtmann KH. Apoptosis antagonizing transcription factor AATF is a novel coactivator of nuclear hormone receptors. *Signal Transduction* (2003) 3(1-2):17–25. doi: 10.1002/sita.200300020

20. Bruno T, Desantis A, Bossi G, Di Agostino S, Sorino C, De Nicola F, et al. Che-1 promotes tumor cell survival by sustaining mutant p53 transcription and inhibiting DNA damage response activation. *Cancer Cell* (2010) 18(2):122–34. doi: 10.1016/j.ccr.2010.05.027

21. Di Padova M, Bruno T, De Nicola F, Iezzi S, D'Angelo C, Gallo R, et al. Che-1 arrests human colon carcinoma cell proliferation by displacing HDAC1 from the p21WAF1/CIP1 promoter. *J Biol Chem* (2003) 278(38):36496–504. doi: 10.1074/jbc.M306694200

22. Bruno T, Iezzi S, De Nicola F, Di Padova M, Desantis A, Scarsella M, et al. Che-1 activates XIAP expression in response to DNA damage. *Cell Death Differ* (2008) 15 (3):515–20. doi: 10.1038/sj.cdd.4402284

23. Haanpää M, Reiman M, Nikkilä J, Erkko H, Pylkäs K, Winqvist R. Mutation analysis of the AATF gene in breast cancer families. *BMC Cancer* (2009) 9(1):1–5. doi: 10.1186/1471-2407-9-457

24. Kaul D, Mehrotra A. Functional characterization of AATF transcriptome in human leukemic cells. *Mol Cell Biochem* (2007) 297(1-2):215–20. doi: 10.1007/s11010-006-9317-1

25. Welcker D, Jain M, Khurshid S, Jokić M, Höhne M, Schmitt A, et al. AATF suppresses apoptosis, promotes proliferation and is critical for kras-driven lung cancer. *Oncogene* (2018) 37(11):1503–18. doi: 10.1038/s41388-017-0054-6

26. Jing P, Zou J, Weng K, Peng P. The PI3K/AKT axis modulates AATF activity in wilms' tumor cells. *FEBS Open Bio.* (2018) 8(10):1615–23. doi: 10.1002/2211-5463.12500

27. Liu M, Wang D, Li N. Che-1 gene silencing induces osteosarcoma cell apoptosis by inhibiting mutant p53 expression. *Biochem Biophys Res Commun* (2016) 473 (1):168–73. doi: 10.1016/j.bbrc.2016.03.073

28. Guo Q, Xie J. AATF inhibits aberrant production of amyloid beta peptide 1-42 by interacting directly with par-4. *J Biol Chem* (2004) 279(6):4596–603. doi: 10.1074/jbc.M309811200

29. Ishigaki S, Fonseca SG, Oslowski CM, Jurczyk A, Shearstone JR, Zhu LJ, et al. AATF mediates an antiapoptotic effect of the unfolded protein response through transcriptional regulation of AKT1. *Cell Death Differ* (2010) 17(5):774–86. doi: 10.1038/cdd.2009.175

30. Wang D, Chen TY, Liu FJ. Che-1 attenuates hypoxia/reoxygenation-induced cardiomyocyte apoptosis by upregulation of Nrf2 signaling. *Eur Rev Med Pharmacol Sci* (2018) 22(4):1084–93. doi: 10.26355/eurrev_201802_14395

31. Shimizu D, Kanda M, Sugimoto H, Sueoka S, Takami H, Ezaka K, et al. NRAGE promotes the malignant phenotype of hepatocellular carcinoma. *Oncol Lett* (2016) 11 (3):1847–54. doi: 10.3892/ol.2016.4120

32. Kumar DP, Santhekadur PK, Seneshaw M, Mirshahi F, Uram-Tuculescu C, Sanyal AJ. A regulatory role of apoptosis antagonizing transcription factor in the pathogenesis of nonalcoholic fatty liver disease and hepatocellular carcinoma. *Hepatol* (2019) 69(4):1520–34. doi: 10.1002/hep.30346

33. Nagtegaal ID, Odze RD, Klimstra D, Paradis V, Rugge M, Schirmacher P, et al. WHO classification of tumours editorial board. the 2019 WHO classification of tumours of the digestive system. *Histopathology* (2020) 76(2):182–8. doi: 10.1111/his.13975

34. Park S, Choi S, Cho YA, Sinn DH, Kim JM, Park CK, et al. Evaluation of the American joint committee on cancer (AJCC) 8th edition staging system for hepatocellular carcinoma in 1,008 patients with curative resection. *Cancer Res Treat* (2020) 52(4):1145–52. doi: 10.4143/crt.2020.208

35. Zhu AX, Duda DG, Sahani DV, Jain RK. HCC and angiogenesis: possible targets and future directions. *Nat Rev Clin Oncol* (2011) 8(5):292–301. doi: 10.1038/nrclinonc.2011.30

36. Lamalice L, Le Boeuf F, Huot J. Endothelial cell migration during angiogenesis. *Circ Res* (2007) 100(6):782–94. doi: 10.1161/01.RES.0000259593.07661.1e

37. Matsumoto K, Ishikawa H, Nishimura D, Hamasaki K, Nakao K, Eguchi K. Antiangiogenic property of pigment epithelium-derived factor in hepatocellular carcinoma. *Hepatology* (2004) 40(1):252–9. doi: 10.1002/hep.20259

38. Notari L, Miller A, Martínez A, Amaral J, Ju M, Robinson G, et al. Pigment epithelium-derived factor is a substrate for matrix metalloproteinase type 2 and type 9: implications for downregulation in hypoxia. *Invest Ophthalmol Vis Sci* (2005) 46 (8):2736–47. doi: 10.1167/iovs.04-1489

39. Carmeliet P. VEGF as a key mediator of angiogenesis in cancer. *Oncology* (2005) 69 Suppl 3:4–10. doi: 10.1159/000088478

40. Al-Abd AM, Alamoudi AJ, Abdel-Naim AB, Neamatallah TA, Ashour OM. Anti-angiogenic agents for the treatment of solid tumors: potential pathways, therapy and current strategies - a review. *J Adv Res* (2017) 6):591–605. doi: 10.1016/j.jare.2017.06.006

41. Saman H, Raza SS, Uddin S, Rasul K. Inducing angiogenesis, a key step in cancer vascularization, and treatment approaches. *Cancers (Basel)* (2020) 12(5):1172. doi: 10.3390/cancers12051172

42. Becerra SP, Notario V. The effects of PEDF on cancer biology: mechanisms of action and therapeutic potential. *Nat Rev Cancer.* (2013) 13(4):258–71. doi: 10.1038/nrc3484

43. Dawson DW, Volpert OV, Gillis P, Crawford SE, Xu H, Benedict W, et al. Pigment epithelium-derived factor: a potent inhibitor of angiogenesis. *Science* (1999) 285(5425):245–8. doi: 10.1126/science.285.5425.245

44. Belkacemi L, Zhang SX. Anti-tumor effects of pigment epithelium-derived factor (PEDF): implication for cancer therapy. *A mini-review. J Exp Clin Cancer Res* (2016) 35:4. doi: 10.1186/s13046-015-0278-7

45. Zhang F, Wang Z, Fan Y, Xu Q, Ji W, Tian R, et al. Elevated STAT3 signaling-mediated upregulation of MMP-2/9 confers enhanced invasion ability in multidrug-resistant breast cancer cells. *Int J Mol Sci* (2015) 16(10):24772–90. doi: 10.3390/ijms161024772

46. Cai J, Chen Z, Ruan Q, Han S, Liu L, Qi X, et al. γ-secretase and presenilin mediate cleavage and phosphorylation of vascular endothelial growth factor receptor-1. *J Biol Chem* (2011) 286(49):42514–23. doi: 10.1074/jbc.M111.296590

47. Zhang M, Tombran-Tink J, Yang S, Zhang X, Li X, Barnstable CJ. PEDF is an endogenous inhibitor of VEGF-R2 angiogenesis signaling in endothelial cells. *Exp Eye Res* (2021) 213:108828. doi: 10.1016/j.exer.2021.108828

48. Ribatti D, Annese T, Ruggieri S, Tamma R, Crivellato E. Limitations of anti-angiogenic treatment of tumors. *Transl Oncol* (2019) 12(7):981–6. doi: 10.1016/j.tranon.2019.04.022

frontiers | Frontiers in Oncology

TYPE Original Research
PUBLISHED 22 August 2023
DOI 10.3389/fonc.2023.1227016



OPEN ACCESS

EDITED BY
Sergio Luis Felisbino,
São Paulo State University, Brazil

REVIEWED BY
Jiahui Zhou,
Suzhou Municipal Hospital, China
Kar-Tong Tan,
Harvard University, United States

*CORRESPONDENCE
Stephen Kwok-Wing Tsui
kwtsui@cuhk.edu.hk

RECEIVED 22 May 2023
ACCEPTED 28 July 2023
PUBLISHED 22 August 2023

CITATION
Wang L, Shi L, Liang Y, Ng JK-W, Yin CH, Wang L, Hou J, Wang Y, Fung CS-H, Chiu PK-F, Ng C-F and Tsui SK-W (2023) Dissecting the effects of METTL3 on alternative splicing in prostate cancer. *Front. Oncol.* 13:1227016. doi: 10.3389/fonc.2023.1227016



# Dissecting the effects of METTL3 on alternative splicing in prostate cancer

Lin Wang[1,2], Ling Shi[2], Yonghao Liang[2], Judy Kin-Wing Ng[2], Chan Hoi Yin[2], Lingyi Wang[2], Jinpao Hou[2], Yiwei Wang[2], Cathy Sin-Hang Fung[2], Peter Ka-Fung Chiu[3], Chi-Fai Ng[3] and Stephen Kwok-Wing Tsui[2,4]*

[1]Metabolic Disease Research Center, Zhengzhou Central Hospital Affiliated to Zhengzhou University, Zhengzhou, China, [2]School of Biomedical Sciences, The Chinese University of Hong Kong, Hong Kong, Hong Kong SAR, China, [3]SH Ho Urology Centre, Department of Surgery, The Chinese University of Hong Kong, Hong Kong, Hong Kong SAR, China, [4]Hong Kong Bioinformatics Centre, The Chinese University of Hong Kong, Hong Kong, Hong Kong SAR, China

Although the role of METTL3 has been extensively studied in many cancers, its role in isoform switching in prostate cancer (PCa) has been poorly explored. To investigate its role, we applied standard RNA-sequencing and long-read direct RNA-sequencing from Oxford Nanopore to examine how METTL3 affects alternative splicing (AS) in two PCa cell lines. By dissecting genome-wide METTL3-regulated AS events, we noted that two PCa cell lines (representing two different PCa subtypes, androgen-sensitive or resistant) behave differently in exon skipping and intron retention events following METTL3 depletion, suggesting AS heterogeneity in PCa. Moreover, we revealed that METTL3-regulated AS is dependent on $N^6$-methyladenosine ($m^6A$) and distinct splicing factors. Analysis of the AS landscape also revealed cell type specific AS signatures for some genes (e.g., MKNK2) involved in key functions in PCa tumorigenesis. Finally, we also validated the clinical relevance of MKNK2 AS events in PCa patients and pointed to the possible regulatory mechanism related to $m^6A$ in the exon14a/b region and SRSF1. Overall, we characterize the role of METTL3 in regulating PCa-associated AS programs, expand the role of METTL3 in tumorigenesis, and suggest that MKNK2 AS events may serve as a new potential prognostic biomarker.

KEYWORDS

**METTL3, prostate cancer, RNA splicing, N 6 -methyladenosine, MKNK2, nanopore direct RNA sequencing**

## 1 Introduction

PCa is the second most prevalent malignancy in males and the fifth leading cause of cancer mortality in men worldwide (1). Clinically, relatively indolent PCa (i.e., Gleason grade (GS)≤7) is treated with radical prostatectomy with a favorable prognosis, whereas locally progressed and metastatic PCa is typically treated with androgen deprivation

therapy (ADT) (2). Notably, despite current therapies that improve prognosis, most patients will eventually fail ADT and progress to a deadly condition (androgen insensitive, $AR^-$) known as castration-resistant PCa (CRPC) (3). The molecular mechanisms of PCa progression, particularly CRPC, remain largely undefined.

$m^6A$ modification is ubiquitous in most eukaryotes (4) and plays crucial roles in a variety of bioprocesses, such as DNA damage response (5). Analogous to DNA methylation, the dynamic $m^6A$ is regulated by the methyltransferase complex (writers), demethylases (erasers), and reader proteins (6). Notably, METTL3 catalyzes the $m^6A$ modification process, which can be dramatically reduced by METTL3 deletion (7). Recently, a growing number of studies have revealed the link between imbalanced $m^6A$ levels and cancer progression (6). Experimentally, METTL3 acts synergistically with YTHDF2 to inhibit the expression of SOCS2, encouraging liver cancer (HCC) development and progression (8). In PCa, METTL3 enhances MYC expression thus promoting cell proliferation (9), promotes the invasion through regulating the SHH-GLI1 signaling pathway (10), and modulates the HuR-ITGB1 signaling pathway thus contributing to bone metastasis (11). Despite a few findings in PCa concentrating on specific genes on a small scale, the potential biological consequence of global $m^6A$ abnormalities on a genome-wide scale remains deserved.

Additionally, $m^6A$ alternations not only influence gene expression by changing RNA stability and mRNA export but also regulate AS and 3′-end processing (12). AS is a dynamic process coupled with transcription and involved in many physiological functions as well as disease pathogenesis (13). Evidence has demonstrated that METTL3 deletion can attenuate the inflammatory response induced by lipopolysaccharide by modifying the expression patterns of MyD88 isoforms (14). Moreover, the $m^6A$ reader YTHDC1 can interact with SRSF3 to regulate exon inclusion (15), while FTO regulates the process of SRSF2 binding to the $m^6A$-containing RUNX1T1 transcript and results in exon skipping (16). However, a comprehensive study of the AS landscape governed by METTL3 has not been conducted in PCa.

Recently, the development of long-read sequencing (e.g., direct RNA sequencing of Oxford Nanopore Technologies) provides the possibility to study splicing variants and alternative polyadenylation events (17), which directly obtain the structural information of the entire transcript without the assembling step like standard RNA sequencing (RNA-Seq). Another significant advantage of direct RNA sequencing (DRS) over standard RNA-Seq is the use of long reads to correctly dissect transcript isoforms and simultaneously detect RNA-modified sites (e.g., $m^6A$) (18).

In this study, we combined standard RNA-Seq and long-read DRS of Oxford Nanopore to comprehensively dissect the impact of METTL3 on RNA splicing in the setting of two PCa cell lines with distinct AR sensitivities. We revealed that METTL3 potentially had shared and unique mechanisms affecting alternative splicing in $AR^+$ and $AR^-$ PCa cells. The different effects of METTL3 on exon skipping and intron retention might be related to distinct splicing partners.

# 2 Materials and methods

## 2.1 Cell culture

Normal epithelial prostate cell line (RWPE-1) and PCa cell lines (LNCaP and DU145) were obtained from Prof. Andrew Chan's laboratory in the School of Biomedical Sciences, The Chinese University of Hong Kong. RWPE-1 cells were cultured using the KSFM-1 medium kit (Thermo Fisher, No.17005042) with supplementary bovine pituitary extract (BPE) and human recombinant epidermal growth factor (rEGF). LNCaP cells were maintained in RPMI-1640 medium (Invitrogen) supplemented with 10% FBS and 1% PS, and DU145 cells were cultured in DMEM (Invitrogen) supplemented with 10% FBS and 1% PS. All cells were incubated at 37°C and 5% CO2.

## 2.2 siRNA transfection, RNA extraction, and polyA RNA isolation

The siRNA against METTL3 (Invitrogen, Catalog: #4392422) or control was transfected into LNCaP and DU145 cells using RNAiMAX reagent (Invitrogen). Total RNA was extracted with a Pure-link mini kit (Invitrogen) 48 h after transfection. RNA concentration was measured via a Nanodrop 2000, and RNA integrity (RIN) was detected using an RNA 6000 nanochip (Agilent Technologies) (Requirement: RIN>8.8). PolyA RNA was isolated from 75 μg of total RNA using a Dynabeads™ kit.

## 2.3 Real-time quantitative PCR and western blot

cDNA transcription was performed using a SuperScript III synthesis kit (Invitrogen) and then used for qPCR based on SYBR (Applied Biosystems). Two siRNAs (siM3-1 and siM3-2) targeting METTL3 were designed, and we observed that the knockdown efficiency of siM3-1 was only 50%, which we considered insufficient for further analyses. Therefore, the more effective target-2 (siM3-2) was selected for the following analysis (Figure S1). The sequences of primers and siRNAs used in this study are shown in Supplementary Table S1.

The siRNA-transfected LNCaP and DU145 cells were lysed in RIPA lysis buffer and Western blotting was conducted as previously (9). Then, the intensity of METTL3 (Proteintech, 15073-1-AP) and GAPDH (Santa Cruz, sc-25778) bands was quantified using ImageJ software and GAPDH was used as the housekeeping marker.

## 2.4 RNA-Seq data processing

Paired-end sequencing ($2 \times 150$ bp) of siControl- and siMETTL3-transfected cells was performed on a HiSeq 4000 sequencing platform (Illumina). Clean reads were aligned to the

human hg38 genome (UCSC) using HISAT2 (v2.2.1) software (19). PCA of three replicates was executed, with one outlier in the DU145 siControl group excluded from downstream analysis. Differential gene expression (DEG) analysis was conducted using DESeq2 (20). Gene Ontology (GO) and KEGG enrichment analyses were performed using the clusterProfiler R package (21).

## 2.5 TCGA data analysis

A table containing FPKM values from 551 adjacent normal, and PCa tissue samples was downloaded from the TCGA database (https://portal.gdc.cancer.gov/projects/TCGA-PRAD), wherein we also retrieved the clinical data of 499 primary PCa patients. This FPKM table was used for expression profile analysis of $m^6A$ regulators. The association between METTL3 expression and overall survival and disease-free survival was determined using the GEPIA2 web server (22). The functional enrichment of $m^6A$ regulators was analyzed using Metascape (23) and displayed using Cytoscape software (24).

## 2.6 Nanopore DRS data processing

As previously described, each 1 μg purified polyA RNA was subjected to library preparation following the SQK_RNA002 kit procedure and consequently sequenced on a Nanopore GridION platform for a 48-h runtime (25). Base-calling was performed with Guppy (v4.2.2) to generate passed reads with quality scores ≥7. The alignment of passed reads against human hg38 (UCSC) and transcriptome (GENCODE v32) was implemented via minimap2 (v2.17-r941) (26). Statistics of the passed reads were assessed using NanoStat (v1.4.0) (27). The sequence length distribution of each sample was generated using the wub package (https://github.com/Nanoporetech/wub).

## 2.7 AS analysis of DRS and RNA-Seq data

Splicing analysis of DRS data was performed with the FLAIR (v1.5) pipeline (17). Specifically, BED12 files were converted from primary BAM files and then corrected by annotated GTF files and junction files. Junction files from RNA-Seq data were obtained from the same cell lines, and splice sites (< 3 reads) were filtered out. Then, the corrected files were assembled into high-confidence isoforms with the stringent parameters of at least three supporting reads. Splicing events were determined using the FLAIR diffSplice module based on Fisher's exact test.

Differential AS events of RNA-Seq data were identified using rMATS (v4.1.0) with a strict parameter of cstat=0.05 (28, 29) and filtered with a p-value <0.05. As an indicator of splicing events, the percent spliced in (PSI) index of differential intron retention and exon splicing events refers to the ratio of included reads to total reads (sum of included and excluded reads) (30). The PSI values of differential AS events were assessed using the Wilcoxon rank-sum test, which is used to provide a global overview of inclusion/exclusion levels between the control and knockdown groups. The global difference in PSI distributions was also evaluated by using FDR<0.05, which was supplemented in the Supplementary Figure S8.

The PSI index of MKNK2a/b isoforms in PCa was downloaded from the TCGA SpliceSeq database. The MKNK2_AA_46570 event represents the PSI index of sequencing reads covering between exon 13 (e13) and exon 14a (e14a), indicating the expression of the MKNK2a isoform. While the MKNK2_AT_46567 represents the PSI index of the sequencing reads covering between exon 13 and exon 14b (e14b), producing the MKNK2b isoform. According to the previous reference (31), we set the threshold at the $80^{th}$ percentile, dividing the PCa patients into high PSI and low PSI groups. The survival difference between high and low PSI groups was calculated by using "survival" (3.5) and "survminer" (0.4.9) R software.

## 2.8 Detection of differential $m^6A$ sites

Differential $m^6A$ sites between the siControl and siMETTL3 groups were detected using ELIGOS2 and DRUMMER (32, 33). Both approaches were designed to identify RNA modifications through the comparative analysis of base-calling errors in the Nanopore DRS dataset (34). In our study, ELIGOS2 was utilized to assess the global difference in $m^6A$ modifications, employing strict threshold values of p<0.05 and odd ratio >1.2 (https://gitlab.com/piroonj/eligos2) (32). The criterion of "odd ratio >1.2" indicated at least a 1.2-fold difference between the control and METTL3 knockdown conditions. Therefore, the differential $m^6A$ sites utilized in the further analysis primarily represented the decreased $m^6A$ sites upon METTL3 knockdown. DRUMMER can identify RNA modifications at each site on distinct transcript isoforms by using isoform mode (https://github.com/DepledgeLab/DRUMMER) (33). Therefore, DRUMMER was utilized to detect isoform-specific differences in $m^6A$ levels. All differential $m^6A$ data from ELIGOS2 and DRUMMER were then selected with a p-value <0.05 and the reference "A" site. The 5-kmer motif of differential $m^6A$ sites was generated *via* WebLogo (https://weblogo.berkeley.edu/logo.cgi). The genomic features of $m^6A$ sites were annotated with the ChIPseeker R package (35). The detailed differential $m^6A$ results were included in the Supplementary Tables S3–6.

## 2.9 Motif analysis of spliced genes

The regions of differential intron retention and exon skipping events were extracted for motif analysis using HOMER (http://homer.ucsd.edu/homer/motif/) software. The resulting motifs were visualized using the ggseqlogo R package.

## 2.10 Statistical analysis

Differences in PSI values of differential intron retention and exon skipping events between groups were assessed using the Wilcoxon rank-sum test. The significance of overlaps between m$^6$A sites and DEGs, spliced genes, or junction regions was determined using a hypergeometric test by R software. The significance of candidate genes in qPCR experiments was determined by T-test.

# 3 Results

## 3.1 Increased expression of METTL3 was associated with an aggressive PCa status

Functional enrichment indicated that m$^6$A regulators were more associated with mRNA stability and mRNA processing regulation (Figure 1A). To investigate how m$^6$A regulates mRNA

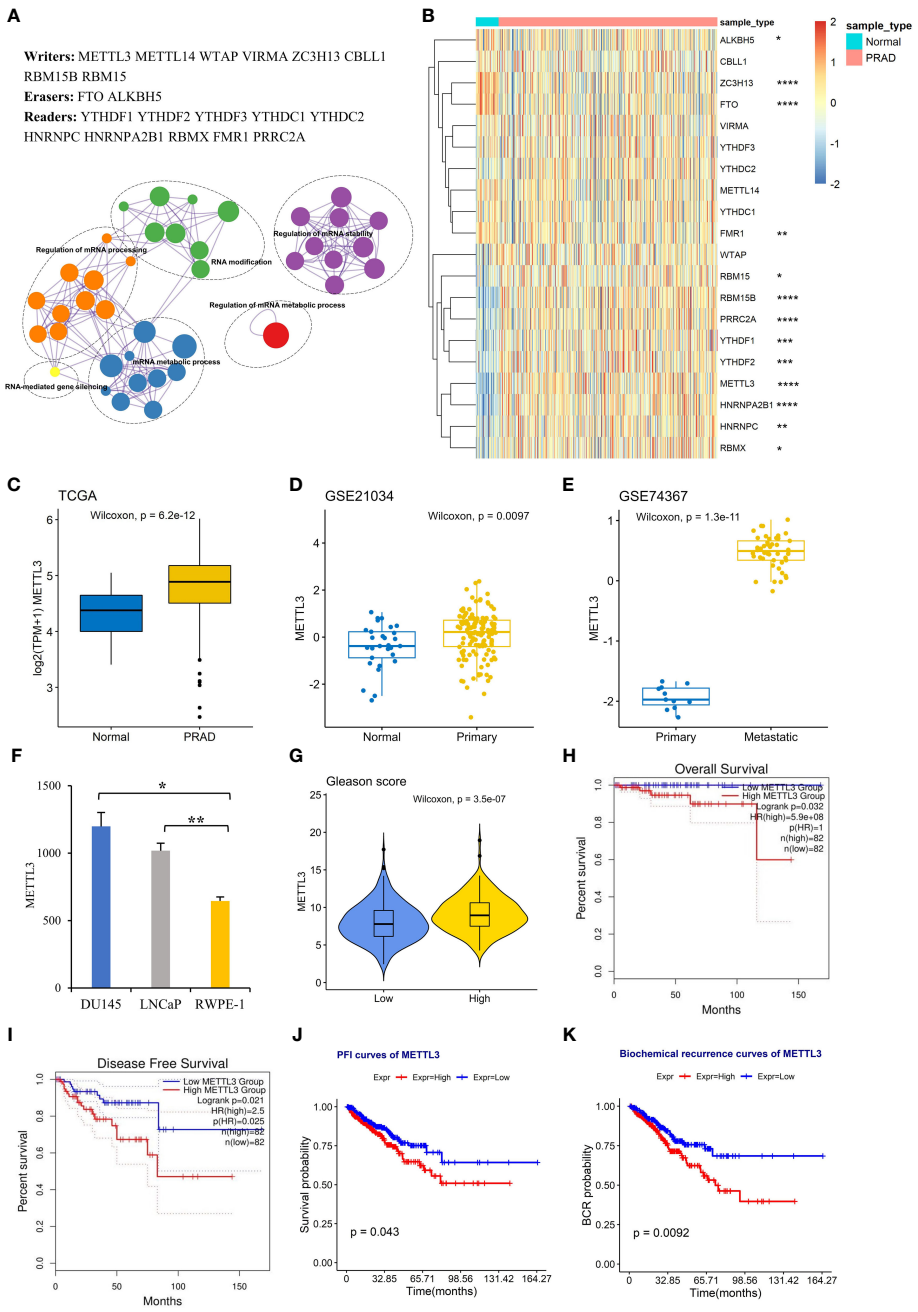


FIGURE 1
High METTL3 expression is associated with an aggressive PCa status. **(A)** Genes and functional ontology related to m$^6$A. **(B)** Heatmap showing the expression profile of 17 m$^6$A regulators in adjacent normal (n=52) and PRAD tissues (n=499). The expression level of METTL3 was analyzed in **(C)** TCGA PRAD dataset, **(D)** GSE21034, **(E)** GSE74367, and **(F)** PCa cell lines (GSE35401). The error bars indicate the variation between the biological replicates in each dataset. **(G)** The difference in METTL3 expression between the low Gleason score (≤7) and high Gleason score (>7) groups. Overall survival **(H)**, disease-free survival **(I)**, progression-free interval **(J)**, and biochemical recurrence **(K)** curves for the high and low METTL3 groups based on the median values. *p<0.05; **p<0.01; ***p <0.001; ****p <0.0001.

processing in PCa, we first conducted an analysis of the expression profiles of m$^6$A regulators by retrieving the FPKM expression data from the TCGA database, comprising adjacent normal (n=52) and prostate adenocarcinoma (n=499). Most m$^6$A "writer" and "reader" proteins were overexpressed in PCa tissues compared to normal tissues (Figure 1B), indicating high m$^6$A levels in PCa.

In particular, we focused on METTL3, the catalytic submit for m$^6$A modifications (7), and its expression patterns in various stages of PCa. We observed that the increase in METTL3 expression between normal and primary groups was statically significant but relatively modest in both TCGA and GSE21034 datasets (Figures 1C, D). However, a more substantial change in METTL3 was evident when comparing the primary and metastatic groups (GSE74367) (Figure 1E), supposing a potential role of METTL3 in PCa metastasis. The overexpression of METTL3 was also observed in PCa cell lines LNCaP (androgen-sensitive, AR$^+$) and DU145 (androgen insensitive, AR$^-$) compared to normal prostate cells (RWPE-1) (Figure 1F, GSE35401) (36). To explore the clinical significance of METTL3 in PCa, we found that the higher METTL3 level was positively associated with a high Gleason score (>7) (Figure 1G). Furthermore, overrepresented METTL3 was linked to aggressive survival stages, including overall survival (OS), disease-free survival (DFS), progression-free interval (PFI), and biochemical recurrence (Figures 1H–K). Collectively, these findings suggested a pro-oncogenic role of METTL3 in PCa progression.

## 3.2 Elucidating functional pathways influenced by METTL3 depletion

To gain further insight into the molecular mechanism by METTL3 in PCa, we performed RNA-Seq in DU145 (AR$^-$) and LNCaP (AR$^+$) cells with METTL3 knockdown. First, the knockdown efficiency of siRNA against METTL3 was assessed in the two PCa cell lines by qPCR and western blotting and shown in Figures 2A, B. In parallel with qPCR and western blotting assessment, the successful knockdown of METTL3 was also confirmed by RNA-Seq data (Figure 2C). Subsequently, we evaluated genes potentially regulated by METTL3 using DESeq2. It was found that 2078 DEGs in DU145 cells between siMETTL3 and siControl groups, of which 1171 genes were upregulated and 907 genes were downregulated (padj <0.05, Figure 2D). In LNCaP cells, we found 1,263 increased genes and 958 decreased genes along with METTL3 knockdown (padj <0.05, Figure 2D). The data revealed that METTL3 depletion has a global impact on gene expression.

We next explored the consistency between LNCaP and DU145 cells in response to METTL3 knockdown. There were 458 genes commonly upregulated, and 224 genes downregulated, respectively (Figures 2E, F). KEGG enrichment of these DEGs indicated that METTL3 was negatively associated with protein processing in endoplasmic reticulum, while favorably connected to various cancer-related pathways, such as HIF-1 signaling, endocrine resistance, FoxO signaling, and proteoglycans (Figures 2G, H). We selected eight known cancer driver genes and PCa-survival genes (37, 38) and then validated the expression change using qPCR. As a result, the expression changes of these eight METTL3-regulated genes showed a consistent trend with RNA-Seq data, demonstrating the accuracy of our RNA-Seq data (Figure 2I). Moreover, these eight genes were identified as having at least one annotated m$^6$A site in public miCLIP data (39, 40) (Figure S2), supposing the potential regulation by m$^6$A. However, more research is required to determine the potential mechanisms involving these genes (e.g., MSI1, NPEPL1).

More interestingly, GSVA analysis also showed that many cancer hallmarks were dysregulated between siControl and siMETTL3 groups, with a noticeable unique pattern in LNCaP (AR$^+$) and DU145 (AR$^-$) cells (Figures S3A, C). For instance, immune (e.g., IFN gamma/alpha response) and metabolism-related (e.g., cholesterol and adipogenesis) signatures were less active in the siMETTL3 group of DU145 cells (Figure S3B). In contrast, metabolism pathways such as cholesterol homeostasis and adipogenesis were more activated in the siMETTL3 LNCaP group (Figure S3D). This may be relevant to cell-specific genomic properties and AR dependence. Previous studies have demonstrated that AR controls critical genes involved in glucose metabolism and lipid metabolism (41). Taken together, the data imply that METTL3 may be engaged in multiple common cancer-related pathways, thus performing pro-oncogenic activities in PCa cells. On the other hand, METTL3 may have partially dissimilar functions in AR$^+$ and AR$^-$ PCa cells, especially in terms of metabolism.

## 3.3 Depletion of METTL3 impacts AS landscape

To gain an insight into the role of METTL3 in AS regulation, we applied direct RNA-sequencing (DRS) performed using the Oxford Nanopore long-read sequencing platform to generate METTL3-dependent AS profiles in LNCaP (AR$^+$) and DU145 (AR$^-$) cells. Overall, 0.6-1.5 million reads were generated for each sample, with an average read length of 1.0 kb and average read quality of 11 (Figure S4; Table S2). Approximately 95% and 99% of the passed reads were aligned to the human genome hg38 and transcriptome (GENCODE v32), respectively (Table S2).

Then, we used FLAIR (17) software to identify the differential AS events upon METTL3 knockdown. Four types of AS events were obtained, including exon skipping (ES), alternative 5'/3'-splice site (A5SS/A3SS), and intron retention (IR). A total of 426 and 172 differential AS events were identified in DU145 and LNCaP cells, respectively (Figure 3A). The predominant AS type in the two cells was the ES type.

The functional enrichment revealed that differential AS events were mainly associated with eukaryotic translation initiation, cellular response to stimuli (e.g., heat, chemical), metabolic pathways, and proliferation hallmarks (MYC targets v1, E2F targets) (Figure 3B). Additionally, transcription factor (TF) analysis showed that differential AS events were highly associated with MYC (Figure 3C), supposing the potential role of MYC in AS regulation.

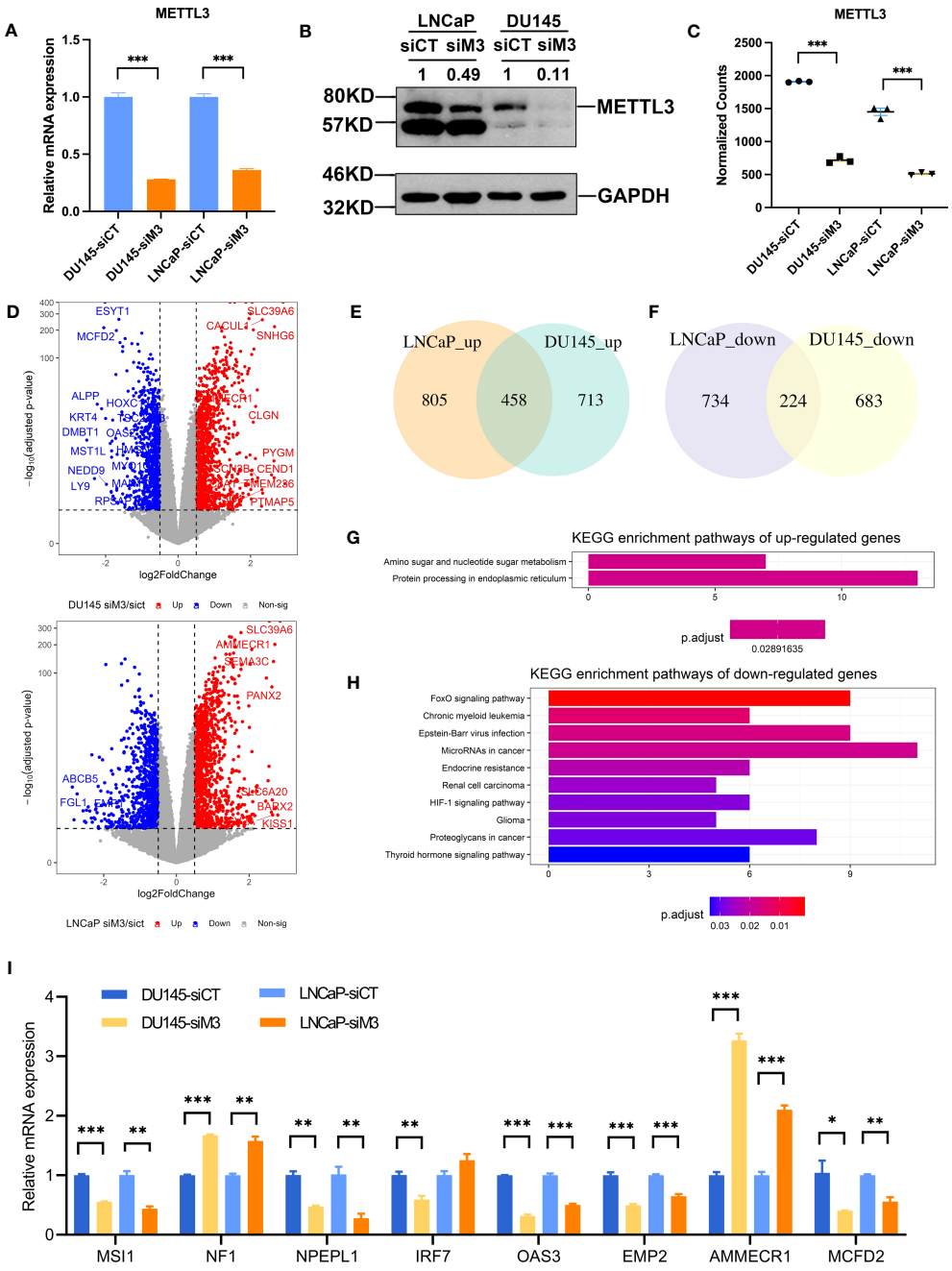


FIGURE 2
Functional annotation of DEGs of the two PCa cell lines. **(A, B)** The relative mRNA and protein level of METTL3 in siControl and siMETTL3 groups of LNCaP and DU145 cells. **(C)** The normalized counts of METTL3 in siControl and siMETTL3 groups of RNA-Seq data. **(D)** Volcano plot of DEGs in the comparison of the siMETTL3 against siControl groups of DU145 and LNCaP cells. The X-axis shows log2fold changes in expression and the Y-axis represents −log10 (adjusted p-value). DEGs with a padj < 0.05 & abs|log2FC| >0.5 were considered significantly differentially expressed. **(E, F)** Venn plot indicated the overlapped genes of upregulated and downregulated DEGs of the two PCa cells. **(G, H)** KEGG functional annotation of overlapped upregulated or downregulated genes. **(I)** The relative mRNA levels of candidate genes in the two cell lines upon METTL3 depletion. siCT, siControl; siM3, siMETTL3; *p<0.05; **p<0.01; ***p<0.001.

## 3.4 METTL3 regulates isoforms switching

As we know that AS is usually coupled with transcriptional processes and thus influences gene expression (42). We found that the functional annotation of METTL3-regulated spliced genes was in line with those discovered in DEGs. However, when intersected AS genes with previously identified DEGs, we noted that only 9-15% of AS genes overlapped (Figure 3D), suggesting that AS dysregulation may have a minor influence on global gene expression but rather functionally tuned transcriptomes (43).

Then, using FLAIR (17), we inspected the isoform-level profiles to explore the functional implications of AS dysregulation on PCa transcriptome. We discovered that, as expected, the majority of differentially expressed isoforms (DEIs) were generated due to

10.3389/fonc.2023.1227016

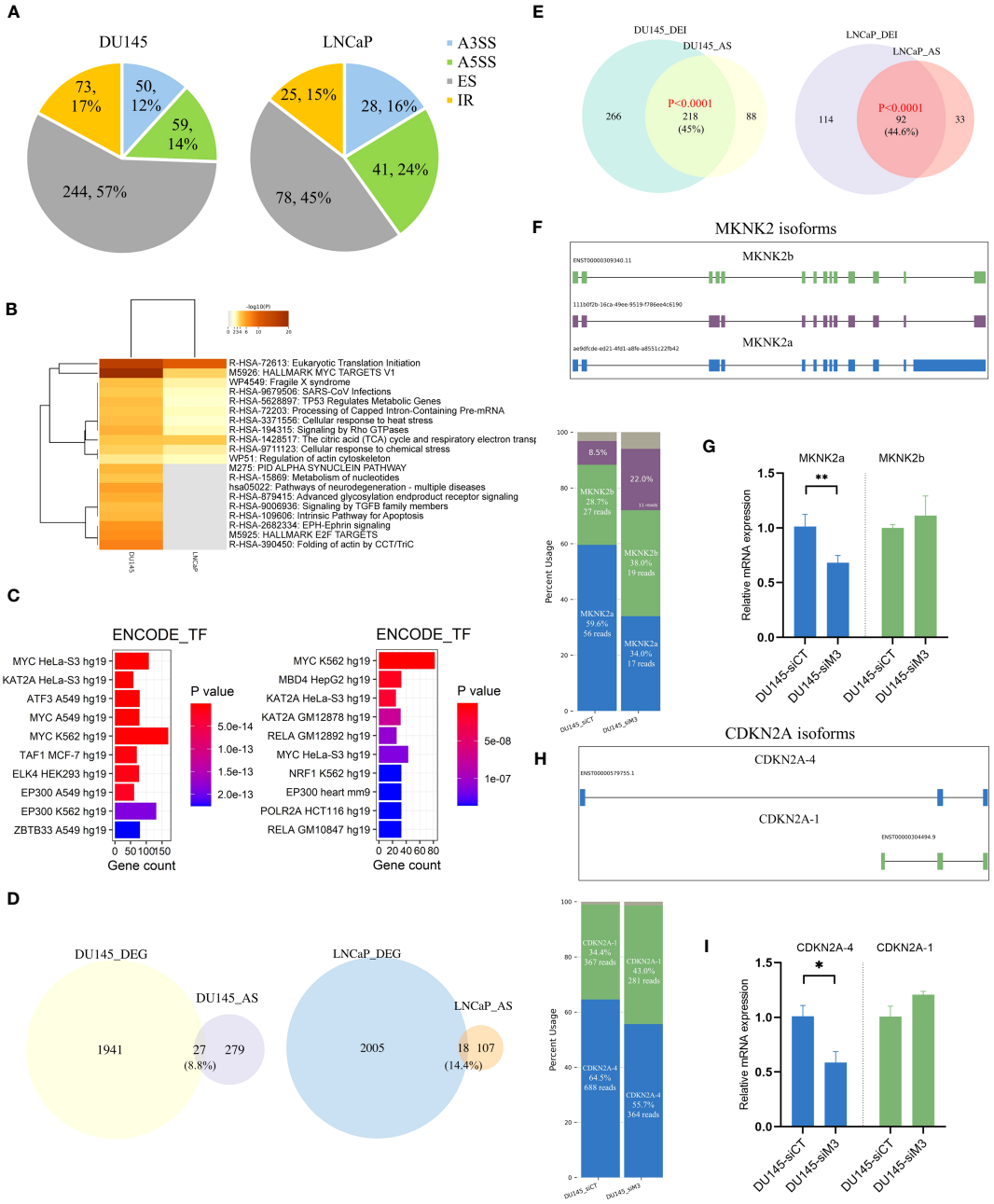


FIGURE 3
The global overview of differential AS events in DU145 and LNCaP cells. **(A)** Pie chart of differential AS events between siControl and siMETTL3 groups of DU145 and LNCaP cells. **(B)** The top 20 functional annotations and **(C)** ENCODE TF terms of AS-associated genes in DU145 (left) and LNCaP (right) cells. **(D)** Venn plot showing the overlapped genes between DEGs and AS-related genes in DU145 and LNCaP cells. **(E)** The intersection between differentially expressed isoforms (DEI) and AS harboring genes. Significance was assessed by a hypergeometric test. **(F, H)** Schematic diagram of isoforms of two known spliced genes (MKNK2 and CDKN2A) in DU145 or LNCaP cells. Stacked bar plots showing the relative proportion and the corresponding read count of each isoform and isoforms were labeled with different colors. **(G, I)** Bar plots displayed the relative mRNA expression of two main isoforms of MKNK2 and CDKN2A genes. siCT, siControl; siM3, siMETTL3. *p<0.05; **p<0.01.

aberrant splicing events (Figure 3E). For example, two known spliced genes (e.g., MKNK2 and CDKN2A) were selected to show distinctive isoforms switching with METTL3 knockdown (Figures 3F–I) (Figure S5-6). Three isoforms of the MKNK2 gene were observed, with a proportionate rise in the shorter transcript ENST00000309340 (MKNK2b) and a comparable reduction in the longer transcript (MKNK2a) upon METTL3 depletion (Figure 3F). We validated the isoform switching of MKNK2 using qPCR and found a similar reduction of MKNK2a with METTL3 knockdown (Figure 3G). Another alternatively spliced gene, CDKN2A, has been found to express two major isoforms, of which the CDKN2A-4 isoform (ENST00000579755) was relatively decreased under the DU145 siMETTL3 condition (Figure 3H) (Figure S5). The qPCR experiment also verified a similar decrease in CDKN2A-4 and a slight rise in the CDKN2A-1 isoform upon METTL3 depletion (Figure 3I). However, more research has to be done to determine

the precise mechanisms of these isoforms and how they relate to PCa development. Nevertheless, our findings suggest that METTL3-induced splicing abnormalities may influence PCa biology in part via isoform switching of key genes.

## 3.5 METTL3 regulates intron retention and exon-skipping events

We previously found that LNCaP ($AR^+$) and DU145 ($AR^-$) cells have different functional enrichments upon METTL3 depletion (Figure S3). Therefore, we further investigated the overlap of AS-related genes in the two PCa cells to see if they also with divergent phenotypes. As a result, there was only limited overlap, indicating cell specificity (Figure S7). This is to be expected, given the transcriptome changes drastically as the disease progresses.

Further, we analyzed the different effects of METTL3 on AS events in DU145 and LNCaP cells and we mainly focused on ES and IR types. In the comparison of siControl versus siMETTL3 of DU145 cells, we observed a preferential increase in upregulated ES (155 up/89 down) and downregulated IR events (11 up/62 down) (Figure 4A). On the other hand, METTL3 knockdown led to the opposite effect in LNCaP cells. That is fewer upregulated ES events (34 up/44 down) and downregulated IR events (15 up/10 down) (Figure 4B). To corroborate this finding, we measured the inclusion levels (PSI values) of differential IR and ES events between siControl and siMETTL3 groups using RNA-Seq data. Consistently, the opposing changes in PSI values of IR and ES events were found in DU145 and LNCaP cells (Figures 4C, D; Figure S8). This indicated an increase in retained introns and skipped exons in the DU145 siMETTL3 group, whereas the LNCaP siMETTL3 group had the opposite tendency. For instance, the transcript (ENST00000392350) of the ORMDL1 gene with exon 2 skipping showed an increased level in the DU145 siMETTL3 group but decreased in the LNCaP siMETTL3 group (Figure 4E; Figure S9). ORMDL1 has been reported to be associated with ceramide biosynthesis and as a regulator of sphingolipid levels implicated in cell proliferation as well as migration (44).

RNA splicing is a complicated process that is coregulated by multiple factors, including splice sites, cis-elements, and splicing factors (SFs) (42). Next, we intended to explore whether the distinct influence on IR and ES in $AR^+$ and $AR^-$ cells is associated with SFs. By analyzing the proteomic data of METTL3 reported by Yue et al. (45), we discovered a substantial overlap between METTL3 pulled-down proteins and known SFs (e.g., SRSF2, U2AF2, KHDRBS3, KHSRP) (P=1.2e-34, hypergeometric test), suggesting a possible interaction between METTL3 and SFs (Figure 4F). Furthermore, motif analysis revealed that SRSF1 (P=1e-13) and KHRBSH1 (P=1e-14) were enriched in differential ES and IR events of DU145 cells, whereas the SRSF2 (P=1e-8) motif was detected in differential ES and IR events for LNCaP cells (Figure 4G), indicating that different mechanisms may be involved in the two PCa cell lines. Taken together, we found that METTL3 depletion resulted in divergent phenotypes for IR and ES events in DU145 and LNCaP cells, and the regulatory effects of METTL3 may be associated with different SF proteins.

## 3.6 Differential $m^6A$ profiles

To understand whether METTL3 modulates RNA splicing through $m^6A$, we first analyzed differential $m^6A$ sites from DRS data using ELIGOS2 software with strict criteria, focusing primarily on decreased $m^6A$ sites (32)(seeing Methods). In DU145 and LNCaP cells, we found 15806 and 16940 potentially decreased $m^6A$ sites, respectively, with 2506 $m^6A$-modified genes shared by the two cell lines (Figure 5A; Tables S3, 4). Moreover, the core residues of the 5-kmer motifs around these $m^6A$ sites were AC (Figure 5B), which was also consistent with prior results (46). Aside from the previously reported major enrichment in the 3'UTR, we observed that identified $m^6A$ sites in PCa cells partially fell into exonic (16.0% or 18.1%) and intronic regions (10.3% or 11%), indicating the potential involvement of $m^6A$ in IR and ES events (Figure 5C). Further, cancer hallmark enrichment of $m^6A$-modified genes revealed a high association with "Myc target V1/V2", "mTORC1 signaling", and several metabolic pathways (Figure 5D). Remarkably, this finding also coincided with previous enrichment by altered genes or AS events.

We next investigated the relationship between decreased $m^6A$ sites and previously identified DEGs or splicing events. As a result, there were 443 (22.5%) and 280 (13.8%) overlapping genes between DEGs and $m^6A$-modified genes in DU145 and LNCaP cells, respectively (P=1.87e-107 and P=2.76e-48, hypergeometric test) (Figure S10A). Additionally, we observed that 182 of 235 (77.4%) spliced genes in DU145 cells and 58 out of 79 (73.4%) genes in LNCaP cells intersected with $m^6A$-modified genes (P=1.08e-158 and P=3.65e-56, hypergeometric test) (Figure S10B). The predicted $m^6A$ levels of three selected examples, namely MYC, TK1, and MTHFD2 genes were presented in Figures 5E–G. Notably, MYC has been previously shown to be regulated by METTL3 in PCa in an $m^6A$-dependent manner (9). In addition, our analysis using the DRUMMER software also revealed intriguing isoform-specific differences in $m^6A$ levels (Tables S5, 6; Figure S11). These data suggest the function of METTL3 in the regulation of gene expression and RNA splicing in PCa cells might be mediated by $m^6A$.

## 3.7 METTL3 modulates MKNK2 isoform expression by SRSF1 and $m^6A$

Based on previous functional enrichment analysis (Figure 3B), we noted that METTL3 was primarily associated with alternative splicing of genes linked to translation initiation. Among these genes, MNK2 (encoded by MKNK2) is the known kinase responsible for phosphorylating eukaryotic translation initiation factor 4E (eIF4E) at serine 209, an essential molecule during the mRNA translation phase (47). Therefore, we further interrogate whether the spliced event of MKNK2 that was validated in PCa cell lines was clinical significance. For MKNK2, two alternative isoforms were analyzed (namely MKNK2a and MKNK2b). The whole mRNA and protein levels of MKNK2 were evaluated in PCa, suggesting its onco-prognosis in PCa (Figures 6A, B). Moreover, we explored the

10.3389/fonc.2023.1227016

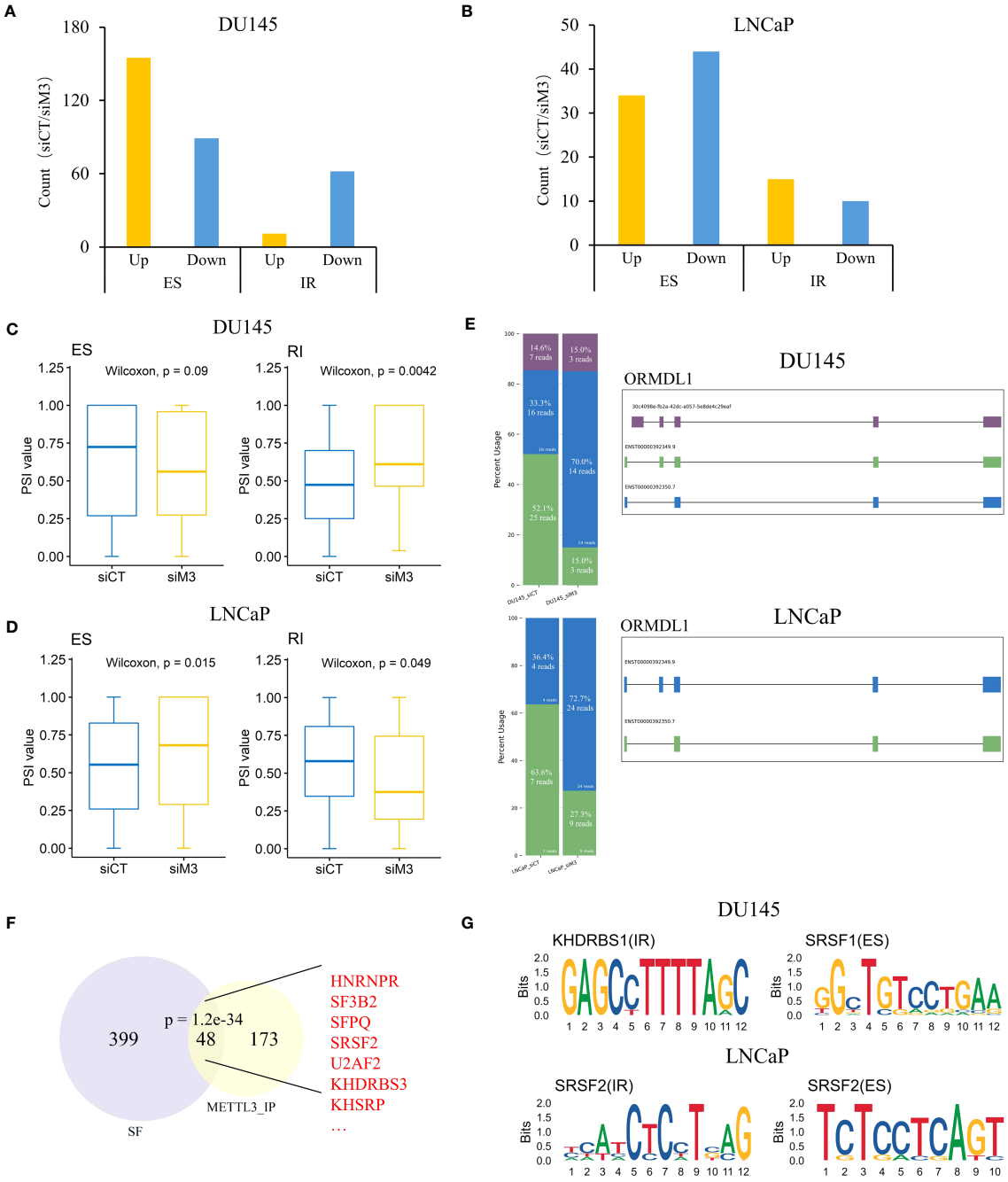


FIGURE 4
Depletion of METTL3 influences intron retention and exon skipping events in DU145 and LNCaP cells. **(A, B)** The bar plot of up and downregulated AS events shows a significant difference between siControl and siMETTL3 groups of DU145 and LNCaP cells. **(C, D)** Box plots showing PSI values of differential IR and ES events in DU145 and LNCaP cells, respectively. **(E)** Schematic diagram of isoforms from ORDML1 gene in DU145 or LNCaP cells. Stacked bar plots showing the relative proportion and the corresponding read count of each isoform and isoforms were labeled with different colors. **(F)** The intersection between METTL3 pulled-down proteins and known SFs. Significance was assessed by a hypergeometric test. Several typical intersecting genes were marked in red. **(G)** Predicted sequence motifs of differential IR and ES events in DU145 and LNCaP cells. siCT, siControl; siM3, siMETTL3; SFs, splicing factors.

relationship between MKNK2a/b isoforms and the prognosis of PCa patients. The data showed that a higher MKNK2a or a lower MKNK2b had a worse prognosis (PFI survival) (Figures 6C, D) and more biochemical recurrences (Figure S12), which indicated MKNK2 isoforms might play roles in PCa progression.

We further validated the relationship between METTL3 and MKNK2a/b isoforms using TCGA Spliceseq datasets. Correlation analysis showed that there was a significant positive/negative correlation between the expression of METTL3 and MKNK2a/b AS events (Figures 6E, F). Consistently, we observed that the AS

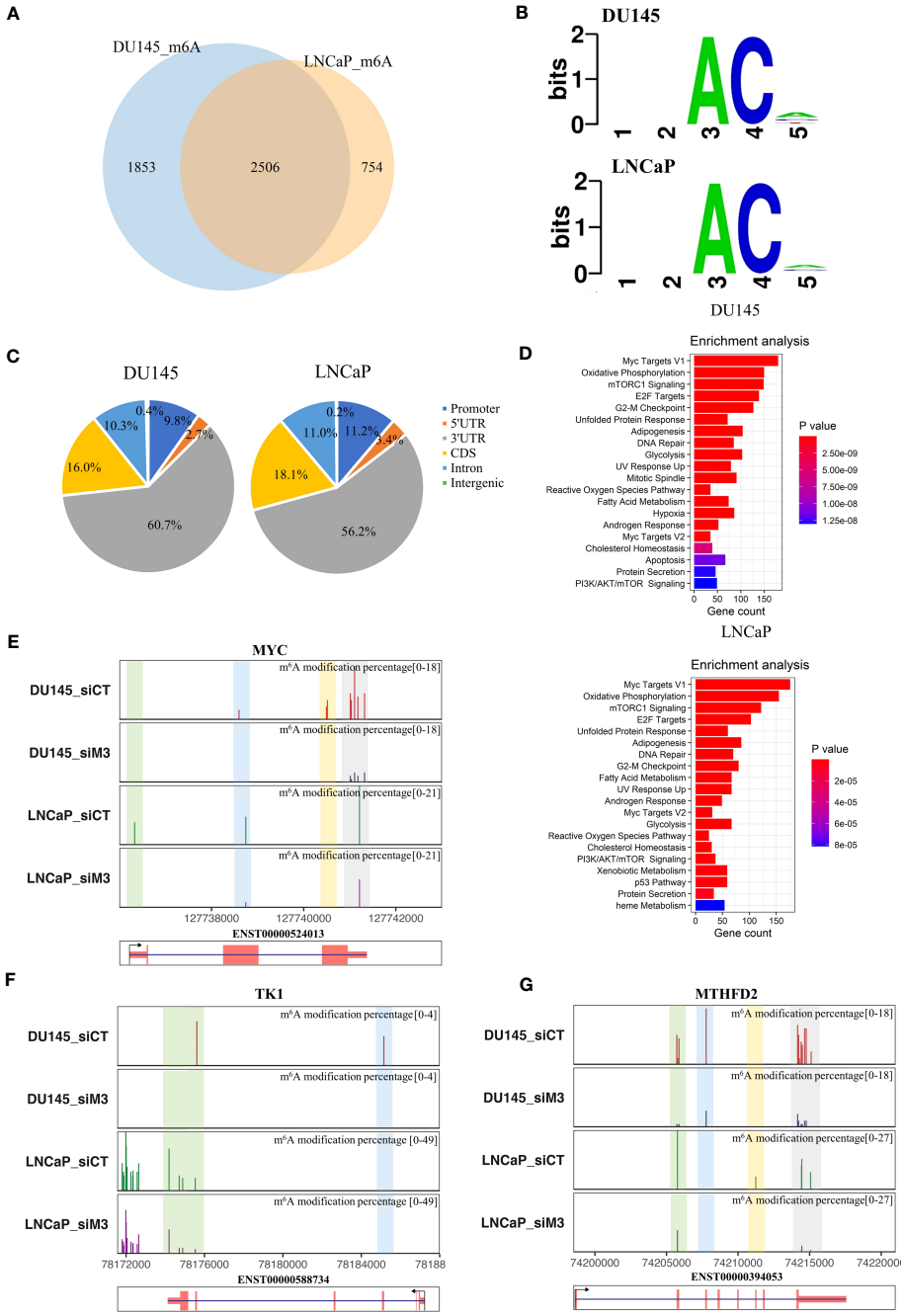


FIGURE 5
Decreased m$^6$A profiles in DU145 and LNCaP cells with METTL3 depletion. **(A)** Venn diagram of the overlapping m$^6$A-modified genes between DU145 and LNCaP cells. **(B)** The 5-kmer motif of differential m$^6$A sites in DU145 and LNCaP cells after METTL3 knockdown. **(C)** The genomic feature distributions of decreased m$^6$A sites in DU145 and LNCaP cells. **(D)** Cancer hallmark enrichments of m$^6$A modified genes in DU145 and LNCaP cells, respectively. Only significant items with a p-value <0.05 are shown in the plot. **(E–G)** Examples of predicted m$^6$A levels in MYC, TK1, and MTHFD2 genes. The top panel represented the proportion of predicted m$^6$A levels in each gene under control (siCT) and METTL3 knockdown (siM3) condition in DU145 and LNCaP cells. Y-axis represents the m$^6$A modification percentage, which is the percent error of specific bases (%ESB) identified by ELIGOS2 software. The bottom panel indicated the longest isoform of each gene.

events for MKNK2a displayed a significantly higher PSI value in METTL3 high patients than in the lower group, while the PSI values were significantly lower for MKNK2b (Figure 6G). These results suggest that METTL3 participated in the splicing process of the MKNK2 gene in PCa patients. Moreover, we also verified that METTL3 depletion (METTL3 inhibitor, STM2457) led to aberrant splicing of MKNK2 using two external datasets (Figure 6H) (48), which was also consistent with our previous findings. Collectively, these data indicated the role of METTL3 in modulating MKNK2 AS events in PCa.

The previous findings indicated that METTL3 regulates the splicing process associated with splicing factors and m$^6$A sites. Our

10.3389/fonc.2023.1227016

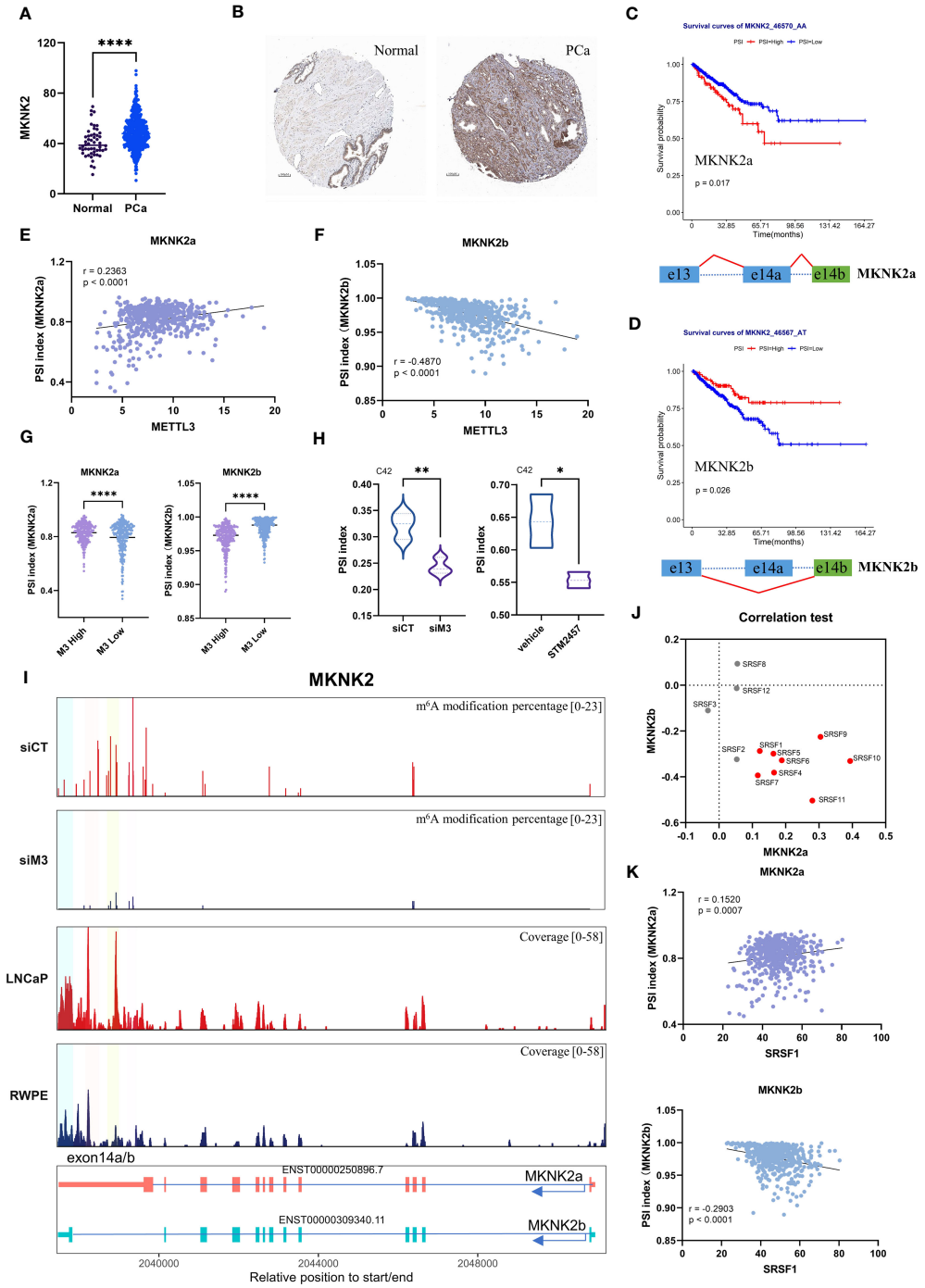


FIGURE 6
The potential mechanism of METTL3 in modulating MKNK2 splicing in PCa. **(A, B)** MKNK2 mRNA and protein levels in normal and PCa tissues. The immunohistochemical results were obtained from the human protein atlas. **(C, D)** Survival analysis showed a significant positive/negative correlation between MKNK2a/b isoforms and progression-free survival (PFI) in PCa patients. Patients were divided into high and low PSI groups based on the 80$^{th}$ percentile. The below represented the splicing pattern indicated by the red line. **(E, F)** The correlation between the PSI index of MKNK2a/b isoforms and METTL3 expression in PCa, respectively. **(G)** The violin plot of PSI index of MKNK2a/b isoforms in METTL3 high and low groups, indicating increased expression of MKNK2a isoforms and decreased expression of MKNK2b isoforms in METTL3 high group. **(H)** The PSI index of the MKNK2 AS event (generating the MKNK2a isoform) in siMETTL3 or STM2457 (METTL3 inhibitor) C42 cells was reduced compared to the control group. **(I)** The top two panels represented the proportion of predicted m$^6$A levels of MKNK2 in control (siCT) and METTTL3 knockdown (siM3) conditions. Y-axis represents the m$^6$A modification percentage, which is the percent error of specific bases (%ESB) identified by ELIGOS2 software. The third and fourth panels represented the read coverage of m$^6$A modification levels on the MKNK2 gene in normal prostate epithelial cells (RWPE-1) and PCa cells (LNCaP) from public sequencing data. Among them, the regions highlighted by four colors are regions with differential m$^6$A modification levels in the exon 14a/b region of MKNK2. The bottom shows the structural features of MKNK2a/b isoforms. **(J)** The correlation between the PSI index of MKNK2a/b isoforms and 1-12 SRSFs expression in PCa, respectively. The red dot represented the significant correlation. **(K)** The correlation between the PSI index of MKNK2a/b isoforms and SRSF1 expression in PCa, respectively. siCT, siControl; siM3, siMETTL3; *p<0.05; **p<0.01; ***p <0.001; ****p<0.0001.

nanopore DRS data showed that after METTL3 knockdown, the m$^6$A modification level in the MKNK2 exon 14a/b region was downregulated (Figure 6I). At the same time, we analyzed the public MeRIP-seq data and found that compared with normal prostate cells (RWPE-1), the exon 14a/b region of the MKNK2 gene in PCa cells has a higher methylation level (Figure 6I). Therefore, we speculate that the m$^6$A modification in the exon 14a/b region of the MKNK2 gene may affect the binding of splicing factors to MKNK2. We next aimed to identify the potential splicing factors targeting MKNK2. Through the correlation test, we found that several SFs were positively correlated with the level of MKNK2a and negatively correlated with the MKNK2b level (Figure 6J). It's known that the splicing process of MKNK2 pre-mRNA is regulated by SRSF1 (49). Here, we found a significant correlation between the expression of SRSF1 and MKNK2a/b isoforms in PCa (Figure 6K). However, RNA-Seq results showed that METTL3 knockdown did not affect the expression level of most SRSFs including SRSF1 (Figure S13). Previous studies indicated that m$^6$A modification near splicing sites may affect the binding of splicing factors to transcripts. Therefore, we speculate that the m$^6$A modification in the exon 14a/b region of the MKNK2 gene may affect the binding of splicing factors such as SRSF1 to MKNK2. The specific regulatory mechanism remains to be studied.

# 4 Discussion

Although mechanisms of METTL3 in many cancers have been well documented, the role of METTL3 in PCa-related AS switch has been poorly explored. Given the inherent differences in each cancer type, a tailored analysis focusing on PCa is still worth exploring and important for drug development. Our study illustrates some findings that are consistent with those in other cancers (e.g., the association between METTL3 and MYC signaling) (50–53), but we did find many PCa-specific findings that differ from other cancer types.

Prior research has found that high METTL3 expression can promote PCa cell proliferation, survival, and invasion *in vitro* and *in vivo* (9, 10, 54–56), however, our understanding of its role in AS regulation is still limited. Thus, we performed RNA-Seq to evaluate the function of METTL3 depletion in PCa. The results showed that METTL3 knockdown resulted in alterations in many cancers and cell proliferation-related genes, such as the FOXO signaling pathway, G2M Checkpoint, E2F Targets, and DNA repair hallmark. This was consistent with results in other cancers. In liver cancer, METTL3 can stabilize FOXO3 mRNA, reducing autophagy and sorafenib resistance (57). Moreover, the METTL3-METTL14 complex participates in DNA repair processing by aggregating at UV-exposed DNA damage sites (5, 58). Moreover, we also verified the expression changes of some genes by qPCR, which showed the same trend with RNA-Seq data and was in line with existing evidence. MSI1 is characterized as an RNA-banding protein (RBP) by repressing the mRNA translation and is associated with cancer stem cell properties of various cancers (59). A recent report has implicated that MSI1 regulated the expression of m$^6$A reader YTHDF1, thus involving glioblastoma cell proliferation and migration (59). Interestingly, a preprinted study by Wei et al. indicated that IGF2BP3, another m$^6$A reader, destabilized the m$^6$A-harboring NF1 mRNA to accelerate triple-negative breast cancer progression, which was also consistent with our data (60). A similar reduction in NPEPL1 protein has been noted in another METTL3 knockdown proteomics dataset in LNCaP cells (39), the detailed mechanism between METTL3 and NPEPL1 in PCa remains unclear and needs to be explored.

We next focused on genome-wide METTL3-regulated AS events in PCa cell lines. Our results revealed that METTL3 primarily regulated the AS switch associated with cell cycle and translation initiation in PCa, and that AS regulation may be associated with MYC signaling. *C. Achour et al.* reported that METTL3 may indirectly regulate AS events through MYC in breast cancer (61). In addition, studies by *Yuan et al.* (9) and *C. Achour et al.* (61) also showed that METTL3 knockdown can suppress MYC protein levels, respectively, which is also common in several other cancers, such as AML, gastric cancer, colorectal cancer, and bladder cancer (50–53). These results suggest that the regulation of carcinogenesis by METTL3 through MYC is a common phenomenon and that METTL3 regulates AS events through a similar mechanism in prostate and breast cancer. In addition, we explored the association of AS alterations with the regulation of gene expression. However, our findings showed that only 9-15% of AS-affected genes overlapped with DEGs, with the majority being related to isoform-switched genes. This suggests that in PCa cells, AS dysregulation may have little effect on global gene expression but functionally tailored transcriptomes instead (43). Interestingly, we found that functional pathways enriched by AS genes (e.g., metabolic pathways, MYC, and E2F target markers) were coordinated with those in METTL3-affected DEGs. These results indicated that METTL3 jointly regulates PCa biological processes through multi-layered gene regulation, and has a broad and complex mechanism of action, which requires further in-depth study of its coordinated mechanism.

Notably, we found that after METTL3 depletion, two PCa cells had different regulatory responses on ES and IR events. Knockdown of METTL3 in AR$^-$ cells (DU145) resulted in more introns being preserved and more exons being skipped, whereas the opposite phenomenon was observed in AR$^+$ cells (LNCaP). It has been shown that m$^6$A promotes exon inclusion or exon exclusion. A breast cancer study showed that depletion of METTL3 causes exons of specific genes to be retained (61). Conversely, another study showed that m$^6$A promotes exon inclusion, and depletion of METTL3 leads to exon skipping (62). The differential effects of m$^6$A on AS appear to be cell- or transcript-specific and depend on specific splicing factors. Studies have shown that m$^6$A reader YTHDC1 binds to m$^6$A sites and recruits the splicing factor SRSF3 to promote exon inclusion (15). A parallel study showed that the accumulation of m$^6$A markers following FTO depletion in mouse preadipocytes promoted the binding of another splicing factor, SRSF2, leading to increased inclusion of target exons (16). Therefore, we also hypothesized that there is heterogeneity in the regulation of AS by METTL3 in AR$^-$ or AR$^+$ cells, depending on the cellular context and specific splicing factors. Exclusion of certain exons has been shown to be controlled by antagonism of the SRSF1/

SRSF2 proteins, with SRSF1 inhibiting exon skipping and SRSF2 activating exon skipping (47). Our results showed that SRSF1 or SRSF2 were enriched in DU145 and LNCaP, respectively. These studies suggest that METTL3 may play different roles in RNA splicing in DU145 and LNCaP cells by interacting with different partners. However, the regulatory network of RNA splicing is complex and dynamic, and the mechanism of METTL3 in the two PCa cell lines requires more studies.

In this study, we took the MKNK2 gene as an example to explore the clinical significance of AS dysregulation in PCa. Our previous results showed that METTL3 mainly regulates alternative splicing of genes related to translation initiation. MNK1/2 are the only known kinases responsible for phosphorylating eukaryotic translation initiation factor 4E (eIF4E) at serine 209, which is a key rate-limiting molecule in the mRNA translation phase (63). Phosphorylation of eIF4E by MNKs proteins enhances its binding to the 5'cap structure of mRNA, thereby enhancing the cap-dependent translation process (64). MNK2/eIF4E signaling pathway is associated with the translation of tumorigenesis-associated mRNAs, contributing to cell proliferation, invasion, and drug resistance (49, 63, 65–69). Our results found that MKNK2 expression was higher in PCa patients than in normal samples. Moreover, splicing variants of MKNK2a were significantly associated with poor PFI in PCa patients and significantly positively correlated with METTL3 expression. These results suggest that METTL3 was also associated with AS of MKNK2 in PCa clinical samples, and the MKNK2a subtype may play a role in promoting cancer progression. At the same time, we also verified that METTL3 knockdown led to abnormal splicing of MKNK2 and reduced expression of MKNK2a isoforms using full-length transcriptome and qPCR. Therefore, METTL3 may affect the translation process of oncogenes by regulating the AS of the translation initiation-related gene MKNK2.

Finally, we explored the possible mechanism of METTL3 in regulating MKNK2 splicing. The variable splicing process of genes is controlled by a variety of regulatory elements, mainly including splicing factors and splicing sites (42). It is known that MKNK2 pre-mRNA is one of the target molecules of the splicing factor SRSF1 (49), which is proven to modulate the MKNK2a-MKNK2b isoforms switch. In our data, a significant correlation was found between the expression of SRSF1 and MKNK2a/b isoforms in PCa, which is consistent with the literature. Furthermore, the binding motif of SRSF1 was significantly enriched in METTL3-regulated splicing events. These results suggest that SRSF1 may be involved in the regulation of MKNK2 alternative splicing by METTL3. However, RNA-Seq results showed that METTL3 knockdown did not affect the expression level of SRSF1. Existing studies have shown that $m^6A$ modification near the cleavage site can affect the binding of cleavage factors to transcripts, thereby changing the way the transcripts are cleaved. Our results also showed that $m^6A$ sites overlap significantly with splice junctions, suggesting that $m^6A$ is involved in the regulation of splice site recognition. Further, the data revealed that the methylation level of the exon14a/b region of the MKNK2 gene in PCa cells was significantly higher than that in normal cells. And after METTL3 knockdown, the predicted methylation level of exon exon14a/b region was significantly reduced. Therefore, the declining $m^6A$ level in MKNK2 caused by METTL3 knockdown potentially reduces the binding of splicing factors. In the future, further experiments are needed to verify the mechanism of METTL3 regulating MKNK2 AS events.

This study has some limitations. First, while offering advantages such as long read lengths and RNA modification analysis, the DRS approach has limitations of higher error rates and more complex bioinformatics analysis. Our results are mainly based on bioinformatic analysis, and further research in experimental cohorts is warranted. It is worth mentioning that our conclusions are supported by other independent datasets and qPCR experiments, demonstrating the validity. Second, we uncovered an intriguing mechanism of METTL3 in $AR^-$ and $AR^+$ PCa cells. However, which factors are functionally related to these responses remains unanswered, which may enhance the understanding of the carcinogenesis process of different PCa stages.

In summary, our study used genome-wide analyses to investigate METTL3-regulated AS events in $AR^+$ and $AR^-$ PCa cell lines via a combination of standard RNA-Seq and long-reads direct RNA-Seq of Nanopore. We revealed both common and phenotypic heterogeneity of different PCa cells regulated by METTL3, which were potentially associated with $m^6A$ modification and SFs. The study identified the clinical relevance of MKNK2 AS events in PCa and explored the potential mechanism of METTL3 in modulating MKNK2 AS events. These findings provide new insights into RNA modifications in PCa and could serve as a favorable molecular basis for novel treatment strategies in androgen-sensitive and androgen-resistant prostate cancer.

## Data availability statement

The datasets presented in this study can be found in online repositories. The names of the repository/repositories and accession number(s) can be found in the article/Supplementary Material.

## Ethics statement

Ethical approval was not required for the studies on humans in accordance with the local legislation and institutional requirements because only commercially available established cell lines were used.

## Author contributions

LW: Study design, Data processing, and Writing-Original draft preparation. LYW, YW, and CF: discussed the data and assisted in the sequencing library preparation. LS, YL, JN and CY: validated the differentially expressed or spliced genes. JH, PC, and CN: Writing-Reviewing and Editing. ST: Supervision, Writing-Reviewing and Editing. All authors contributed to the article and approved the submitted version.

## Funding

This work was made possible by the General Research Fund from Research Grants Council of Hong Kong (Reference numbers:

14175617, 14119219, 14119420, R4012-18F) and Health and Medical Research Fund from Food and Health Bureau of Hong Kong (Reference numbers: 06171016, 07181266).

## Acknowledgments

We thank Professor Andrew Chan's laboratory from the School of Biomedical Sciences, The Chinese University of Hong Kong, for kindly providing PCa cell lines.

## Conflict of interest

The authors declare that the research was conducted in the absence of any commercial or financial relationships that could be construed as a potential conflict of interest.

## Publisher's note



## Supplementary material

The Supplementary Material for this article can be found online at: https://www.frontiersin.org/articles/10.3389/fonc.2023.1227016/full#supplementary-material

## References

1. Sung H, Ferlay J, Siegel RL, Laversanne M, Soerjomataram I, Jemal A, et al. Global cancer statistics 2020: GLOBOCAN estimates of incidence and mortality worldwide for 36 cancers in 185 countries. *CA: Cancer J Clin* (2021) 71(3):209–49. doi: 10.3322/caac.21660

2. Sharifi N, Gulley JL, Dahut WL. Androgen deprivation therapy for prostate cancer. *Jama* (2005) 294(2):238–44. doi: 10.1001/jama.294.2.238

3. Feldman BJ, Feldman D. The development of androgen-independent prostate cancer. *Nat Rev Cancer* (2001) 1(1):34–45. doi: 10.1038/35094009

4. Roundtree IA, Evans ME, Pan T, He C. Dynamic RNA modifications in gene expression regulation. *Cell* (2017) 169(7):1187–200. doi: 10.1016/j.cell.2017.05.045

5. Xiang Y, Laurent B, Hsu C-H, Nachtergaele S, Lu Z, Sheng W, et al. RNA m6A methylation regulates the ultraviolet-induced DNA damage response. *Nature* (2017) 543(7646):573–6. doi: 10.1038/nature21671

6. Chen X-Y, Zhang J, Zhu J-S. The role of m6A RNA methylation in human cancer. *Mol Cancer* (2019) 18(1):1–9. doi: 10.1186/s12943-019-1033-z

7. Geula S, Moshitch-Moshkovitz S, Dominissini D, Mansour AA, Kol N, Salmon-Divon M, et al. m6A mRNA methylation facilitates resolution of naïve pluripotency toward differentiation. *Science* (2015) 347(6225):1002–6. doi: 10.1126/science.1261417

8. Chen M, Wei L, Law CT, Tsang FHC, Shen J, Cheng CLH, et al. RNA N6-methyladenosine methyltransferase-like 3 promotes liver cancer progression through YTHDF2-dependent posttranscriptional silencing of SOCS2. *Hepatology* (2018) 67 (6):2254–70. doi: 10.1002/hep.29683

9. Yuan Y, Du Y, Wang L, Liu X. The M6A methyltransferase METTL3 promotes the development and progression of prostate carcinoma via mediating MYC methylation. *J Cancer* (2020) 11(12):3588. doi: 10.7150/jca.42338

10. Cai J, Yang F, Zhan H, Situ J, Li W, Mao Y, et al. RNA m6A methyltransferase METTL3 promotes the growth of prostate cancer by regulating hedgehog pathway. *OncoTargets Ther* (2019) 12:9143. doi: 10.2147/OTT.S226796

11. Li E, Wei B, Wang X, Kang R. METTL3 enhances cell adhesion through stabilizing integrin β1 mRNA via an m6A-HuR-dependent mechanism in prostatic carcinoma. *Am J Cancer Res* (2020) 10(3):1012.

12. Adhikari S, Xiao W, Zhao Y-L, Yang Y-G. m6A: signaling for mRNA splicing. *RNA Biol* (2016) 13(9):756–9. doi: 10.1080/15476286.2016.1201628

13. Wang Y, Liu J, Huang B, Xu YM, Li J, Huang LF, et al. Mechanism of alternative splicing and its regulation. *Biomed Rep* (2015) 3(2):152–8. doi: 10.3892/br.2014.407

14. Feng Z, Li Q, Meng R, Yi B, Xu Q. METTL 3 regulates alternative splicing of MyD88 upon the lipopolysaccharide-induced inflammatory response in human dental pulp cells. *J Cell Mol Med* (2018) 22(5):2558–68. doi: 10.1111/jcmm.13491

15. Xiao W, Adhikari S, Dahal U, Chen Y-S, Hao Y-J, Sun B-F, et al. Nuclear m6A reader YTHDC1 regulates mRNA splicing. *Mol Cell* (2016) 61(4):507–19. doi: 10.1016/j.molcel.2016.01.012

16. Zhao X, Yang Y, Sun B-F, Shi Y, Yang X, Xiao W, et al. FTO-dependent demethylation of N6-methyladenosine regulates mRNA splicing and is required for adipogenesis. *Cell Res* (2014) 24(12):1403–19. doi: 10.1038/cr.2014.151

17. Tang AD, Soulette CM, van Baren MJ, Hart K, Hrabeta-Robinson E, Wu CJ, et al. Full-length transcript characterization of SF3B1 mutation in chronic lymphocytic leukemia reveals downregulation of retained introns. *Nat Commun* (2020) 11(1):1–12. doi: 10.1038/s41467-020-15171-6

18. Workman RE, Tang AD, Tang PS, Jain M, Tyson JR, Razaghi R, et al. Nanopore native RNA sequencing of a human poly (A) transcriptome. *Nat Methods* (2019) 16 (12):1297–305. doi: 10.1038/s41592-019-0617-2

19. Kim D, Langmead B, Salzberg SL. HISAT: a fast spliced aligner with low memory requirements. *Nat Methods* (2015) 12(4):357–60. doi: 10.1038/nmeth.3317

20. Love MI, Huber W, Anders S. Moderated estimation of fold change and dispersion for RNA-seq data with DESeq2. *Genome Biol* (2014) 15(12):1–21. doi: 10.1186/s13059-014-0550-8

21. Yu G, Wang L-G, Han Y, He Q-Y. clusterProfiler: an R package for comparing biological themes among gene clusters. *Omics: J Integr Biol* (2012) 16(5):284–7. doi: 10.1089/omi.2011.0118

22. Tang Z, Kang B, Li C, Chen T, Zhang Z. GEPIA2: an enhanced web server for large-scale expression profiling and interactive analysis. *Nucleic Acids Res* (2019) 47 (W1):W556–W60. doi: 10.1093/nar/gkz430

23. Zhou Y, Zhou B, Pache L, Chang M, Khodabakhshi AH, Tanaseichuk O, et al. Metascape provides a biologist-oriented resource for the analysis of systems-level datasets. *Nat Commun* (2019) 10(1):1523. doi: 10.1038/s41467-019-09234-6

24. Shannon P, Markiel A, Ozier O, Baliga NS, Wang JT, Ramage D, et al. Cytoscape: a software environment for integrated models of biomolecular interaction networks. *Genome Res* (2003) 13(11):2498–504. doi: 10.1101/gr.1239303

25. Garalde DR, Snell EA, Jachimowicz D, Sipos B, Lloyd JH, Bruce M, et al. Highly parallel direct RNA sequencing on an array of nanopores. *Nat Methods* (2018) 15 (3):201–6. doi: 10.1038/nmeth.4577

26. Li H. Minimap2: pairwise alignment for nucleotide sequences. *Bioinformatics* (2018) 34(18):3094–100. doi: 10.1093/bioinformatics/bty191

27. De Coster W, D'hert S, Schultz DT, Cruts M, Van Broeckhoven C. NanoPack: visualizing and processing long-read sequencing data. *Bioinformatics* (2018) 34 (15):2666–9. doi: 10.1093/bioinformatics/bty149

28. Shen S, Park JW, Z-x Lu, Lin L, Henry MD, Wu YN, et al. rMATS: robust and flexible detection of differential alternative splicing from replicate RNA-Seq data. *Proc Natl Acad Sci* (2014) 111(51):E5593–E601. doi: 10.1073/pnas.1419161111

29. Jiang M, Zhang S, Yin H, Zhuo Z, Meng G. A comprehensive benchmarking of differential splicing tools for RNA-se q analysis at the event level. *Briefings Bioinf* (2023) 24(3):bbad121. doi: 10.1093/bib/bbad121

30. Katz Y, Wang ET, Airoldi EM, Burge CB. Analysis and design of RNA sequencing experiments for identifying isoform regulation. *Nat Methods* (2010) 7 (12):1009–15. doi: 10.1038/nmeth.1528

31. Zhang B, Yang L, Wang X, Fu D. Identification of survival-related alternative splicing signatures in acute myeloid leukemia. *Bioscience Rep* (2021) 41(7): BSR20204037. doi: 10.1042/BSR20204037

32. Jenjaroenpun P, Wongsurawat T, Wadley TD, Wassenaar TM, Liu J, Dai Q, et al. Decoding the epitranscriptional landscape from native RNA sequences. *Nucleic Acids Res* (2021) 49(2):e7–e. doi: 10.1093/nar/gkaa620

33. Abebe JS, Price AM, Hayer KE, Mohr I, Weitzman MD, Wilson AC, et al. DRUMMER—rapid detection of RNA modifications through comparative nanopore sequencing. *Bioinformatics* (2022) 38(11):3113–5. doi: 10.1093/bioinformatics/btac274

34. Hong A, Kim D, Kim VN, Chang H. Analyzing viral epitranscriptomes using nanopore direct RNA sequencing. *J Microbiol* (2022) 60(9):867–76. doi: 10.1007/s12275-022-2324-4

35. Yu G, Wang L-G, He Q-Y. ChIPseeker: an R/Bioconductor package for ChIP peak annotation, comparison and visualization. *Bioinformatics* (2015) 31(14):2382–3. doi: 10.1093/bioinformatics/btv145

36. Lee BH, Taylor MG, Robinet P, Smith JD, Schweitzer J, Sehayek E, et al. Dysregulation of cholesterol homeostasis in human prostate cancer through loss of ABCA1Loss of ABCA1 promotes prostate cancer. *Cancer Res* (2013) 73(3):1211–8. doi: 10.1158/0008-5472.CAN-12-3128

37. Zhang B, Zhang Z, Hu H, Dong J-T. Novel gene signatures predictive of patient recurrence-free survival and castration resistance in prostate cancer. *Cancers* (2021) 13(4):917. doi: 10.3390/cancers13040917

38. Yarmishyn AA, Yang Y-P, Lu K-H, Chen Y-C, Chien Y, Chou S-J, et al. Musashi-1 promotes cancer stem cell properties of glioblastoma cells via upregulation of YTHDF1. *Cancer Cell Int* (2020) 20(1):1–15. doi: 10.1186/s12935-020-01696-9

39. Cotter KA, Gallon J, Uebersax N, Rubin P, Meyer KD, Piscuoglio S, et al. Mapping of m6A and its regulatory targets in prostate cancer reveals a METTL3-low induction of therapy resistance. *Mol Cancer Res* (2021) 19(8):1398–411. doi: 10.1158/1541-7786.MCR-21-0014

40. Zheng Y, Nie P, Peng D, He Z, Liu M, Xie Y, et al. m6AVar: a database of functional variants involved in m6A modification. *Nucleic Acids Res* (2018) 46(D1):D139–D45. doi: 10.1093/nar/gkx895

41. Massie CE, Lynch A, Ramos-Montoya A, Boren J, Stark R, Fazli L, et al. The androgen receptor fuels prostate cancer by regulating central metabolism and biosynthesis. *EMBO J* (2011) 30(13):2719–33. doi: 10.1038/emboj.2011.158

42. Naftelberg S, Schor IE, Ast G, Kornblihtt AR. Regulation of alternative splicing through coupling with transcription and chromatin structure. *Annu Rev Biochem* (2015) 84:165–98. doi: 10.1146/annurev-biochem-060614-034242

43. Zhang D, Hu Q, Liu X, Ji Y, Chao H-P, Liu Y, et al. Intron retention is a hallmark and spliceosome represents a therapeutic vulnerability in aggressive prostate cancer. *Nat Commun* (2020) 11(1):1–19. doi: 10.1038/s41467-020-15815-7

44. Zhu T, Chen Y, Min S, Li F, Tian Y. Expression patterns and prognostic values of ORMDL1 in different cancers. *BioMed Res Int* (2020) 2020. doi: 10.1155/2020/5178397

45. Yue Y, Liu J, Cui X, Cao J, Luo G, Zhang Z, et al. VIRMA mediates preferential m6A mRNA methylation in 3′ UTR and near stop codon and associates with alternative polyadenylation. *Cell Discovery* (2018) 4(1):1–17. doi: 10.1038/s41421-018-0019-0

46. Dominissini D, Moshitch-Moshkovitz S, Schwartz S, Salmon-Divon M, Ungar L, Osenberg S, et al. Topology of the human and mouse m6A RNA methylomes revealed by m6A-seq. *Nature* (2012) 485(7397):201–6. doi: 10.1038/nature11112

47. Pandit S, Zhou Y, Shiue L, Coutinho-Mansfield G, Li H, Qiu J, et al. Genome-wide analysis reveals SR protein cooperation and competition in regulated splicing. *Mol Cell* (2013) 50(2):223–35. doi: 10.1016/j.molcel.2013.03.001

48. Haigh DB, Woodcock CL, Lothion-Roy J, Harris AE, Metzler VM, Persson JL, et al. The METTL3 RNA methyltransferase regulates transcriptional networks in prostate cancer. *Cancers* (2022) 14(20):5148. doi: 10.3390/cancers14205148

49. Liu H, Gong Z, Li K, Zhang Q, Xu Z, Xu Y. SRPK1/2 and PP1α exert opposite functions by modulating SRSF1-guided MKNK2 alternative splicing in colon adenocarcinoma. *J Exp Clin Cancer Res* (2021) 40(1):75. doi: 10.1186/s13046-021-01877-y

50. Su R, Dong L, Li C, Nachtergaele S, Wunderlich M, Qing Y, et al. R-2HG exhibits anti-tumor activity by targeting FTO/m6A/MYC/CEBPA signaling. *Cell* (2018) 172(1-2):90–105.e23. doi: 10.1016/j.cell.2017.11.031

51. Yang D-D, Chen Z-H, Yu K, Lu J-H, Wu Q-N, Wang Y, et al. METTL3 promotes the progression of gastric cancer via targeting the MYC pathway. *Front Oncol* (2020) 10:115. doi: 10.3389/fonc.2020.00115

52. Xiang S, Liang X, Yin S, Liu J, Xiang Z. N6-methyladenosine methyltransferase METTL3 promotes colorectal cancer cell proliferation through enhancing MYC expression. *Am J Trans Res* (2020) 12(5):1789.

53. Cheng M, Sheng L, Gao Q, Xiong Q, Zhang H, Wu M, et al. The m6A methyltransferase METTL3 promotes bladder cancer progression via AFF4/NF-κB/MYC signaling network. *Oncogene* (2019) 38(19):3667–80. doi: 10.1038/s41388-019-0683-z

54. Chen Y, Pan C, Wang X, Xu D, Ma Y, Hu J, et al. Silencing of METTL3 effectively hinders invasion and metastasis of prostate cancer cells. *Theranostics* (2021) 11(16):7640. doi: 10.7150/thno.61178

55. Li J, Xie H, Ying Y, Chen H, Yan H, He L, et al. YTHDF2 mediates the mRNA degradation of the tumor suppressors to induce AKT phosphorylation in N6-methyladenosine-dependent way in prostate cancer. *Mol Cancer* (2020) 19(1):1–18. doi: 10.1186/s12943-020-01267-6

56. Lothion-Roy J, Haigh DB, Harris AE, Metzler VM, Alsaleem M, Toss MS, et al. Clinical and molecular significance of the RNA m6A methyltransferase complex in prostate cancer. *Front Genet* (2023) 13. doi: 10.3389/fgene.2022.1096071

57. Lin Z, Niu Y, Wan A, Chen D, Liang H, Chen X, et al. RNA m6A methylation regulates sorafenib resistance in liver cancer through FOXO3-mediated autophagy. *EMBO J* (2020) 39(12):e103181. doi: 10.15252/embj.2019103181

58. Yu D, Horton JR, Yang J, Hajian T, Vedadi M, Sagum CA, et al. Human MettL3-MettL14 RNA adenine methyltransferase complex is active on double-stranded DNA containing lesions. *Nucleic Acids Res* (2021) 49(20):11629–42. doi: 10.1093/nar/gkab460

59. Yarmishyn AA, Yang Y-P, Lu K-H, Chen Y-C, Chien Y, Chou S-J, et al. Musashi-1 promotes cancer stem cell properties of glioblastoma cells via upregulation of YTHDF1. *Cancer Cell Int* (2020) 20(1):597. doi: 10.1186/s12935-020-01696-9

60. Ding Q, Zhang X, Shi L, Sun H, Wang Z-W, Xu F, et al. IGF2BP3 Mediates the mRNA Degradation of NF1 to Promote Triple-Negative Breast Cancer Progress via an m6A-Dependent Manner. *Res Square* (2022). doi: 10.21203/rs.3.rs-1752002/v1

61. Achour C, Bhattarai DP, Groza P, Román Á-C, Aguilo F. METTL3 regulates breast cancer-associated alternative splicing switches. *Oncogene* (2023) 42(12):911–25. doi: 10.1038/s41388-023-02602-z

62. Xu K, Yang Y, Feng G-H, Sun B-F, Chen J-Q, Li Y-F, et al. Mettl3-mediated m6A regulates spermaTogonial differentiation and meiosis initiation. *Cell Res* (2017) 27(9):1100–14. doi: 10.1038/cr.2017.100

63. Furic L, Rong L, Larsson O, Koumakpayi IH, Yoshida K, Brueschke A, et al. eIF4E phosphorylation promotes tumorigenesis and is associated with prostate cancer progression. *Proc Natl Acad Sci* (2010) 107(32):14134–9. doi: 10.1073/pnas.1005320107

64. Yang X, Zhong W, Cao R. Phosphorylation of the mRNA cap-binding protein eIF4E and cancer. *Cell Signalling* (2020) 73:109689. doi: 10.1016/j.cellsig.2020.109689

65. Ueda T, Sasaki M, Elia AJ, Chio II, Hamada K, Fukunaga R, et al. Combined deficiency for MAP kinase-interacting kinase 1 and 2 (Mnk1 and Mnk2) delays tumor development. *Proc Natl Acad Sci USA* (2010) 107(32):13984–90. doi: 10.1073/pnas.1008136107

66. Prabhu SA, Moussa O, Gonçalves C, LaPierre JH, Chou H, Huang F, et al. Inhibition of the MNK1/2-eIF4E axis augments palbociclib-mediated antitumor activity in melanoma and breast cancer. *Mol Cancer Ther* (2023) 22(2):192–204. doi: 10.1158/1535-7163.MCT-22-0092

67. Prabhu SA, Moussa O, Miller WH Jr., Del Rincón SV. The MNK1/2-eIF4E axis as a potential therapeutic target in melanoma. *Int J Mol Sci* (2020) 21(11):4055. doi: 10.3390/ijms21114055

68. Wang J, Da C, Su Y, Song R, Bai Z. MKNK2 enhances chemoresistance of ovarian cancer by suppressing autophagy via miR-125b. *Biochem Biophys Res Commun* (2021) 556:31–8. doi: 10.1016/j.bbrc.2021.02.084

69. Xie J, Shen K, Jones AT, Yang J, Tee AR, Shen MH, et al. Reciprocal signaling between mTORC1 and MNK2 controls cell growth and oncogenesis. *Cell Mol Life Sci* (2021) 78(1):249–70. doi: 10.1007/s00018-020-03491-1

frontiers | Frontiers in Oncology

TYPE Original Research
PUBLISHED 22 August 2023
DOI 10.3389/fonc.2023.1151687



OPEN ACCESS

EDITED BY
Shihori Tanabe,
National Institute of Health Sciences (NIHS), Japan

REVIEWED BY
Kelong Fan,
Chinese Academy of Sciences (CAS), China
Tatsuo Shimura,
Maki Hospital, Japan

*CORRESPONDENCE
Ming Wang
wangming1882@hotmail.com
Bo Ni
nibo9465@163.com

†These authors have contributed equally to this work

RECEIVED 26 January 2023
ACCEPTED 04 August 2023
PUBLISHED 22 August 2023

CITATION
Zhuang C, Li X, Yang L, Ma X, Shen Y, Huang C, Pan T, Cui J, Ni B and Wang M (2023) Overexpressed transferrin receptor implied poor prognosis and relapse in gastrointestinal stromal tumors. *Front. Oncol.* 13:1151687. doi: 10.3389/fonc.2023.1151687



# Overexpressed transferrin receptor implied poor prognosis and relapse in gastrointestinal stromal tumors

Chun Zhuang†, Xiaoqi Li†, Linxi Yang, Xinli Ma, Yanying Shen, Chen Huang, Tao Pan, Jianzhi Cui, Bo Ni* and Ming Wang*

Department of Gastrointestinal Surgery, Renji Hospital, Shanghai Jiao Tong University School of Medicine, Shanghai, China

Ferroptosis, as a novel-induced programmed cell death, plays critical roles in the pathogenesis of cancers. However, the promising biomarkers of ferroptosis in gastrointestinal stromal tumor (GIST) remain to be elucidated. Herein, the expression of ferroptosis-related genes was analyzed in GIST. Among the 64 ferroptosis-related genes, transferrin receptor (TFRC) expression presented a remarkable upregulation in high-risk patients through Gene Expression Omnibus (GEO) dataset analysis, as well as its significant change after imatinib was treated. Kyoto Encyclopedia of Genes and Genomes (KEGG) pathway enrichment analysis of TFRC-relevant genes revealed that TFRC expression was closely associated with cell growth pathways and metabolism-related pathways. Furthermore, patients at high risk of recurrence were more likely to exhibit high TFRC expression by immunohistochemistry. Additionally, high TFRC expression indicated an undesirable state of patient relapse, which could serve as a powerful significant independent predictor of recurrence-free survival (RFS). In summary, we systematically summarize the expression characteristics and clinical relevance of TFRC and show that TFRC can be used as a prognostic factor, which can be considered a potential therapeutic target in GIST.

KEYWORDS

**gastrointestinal stromal tumor (GIST), ferroptosis, TFRC, tumor biomarkers, prognosis**

## Introduction

Gastrointestinal stromal tumor (GIST) is a class of mesenchymal neoplasms of the digestive tract, and most of them possess an activated mutation of KIT or platelet-derived growth factor receptor alpha (PDGFRA) (1). People over 50 years have a high incidence of suffering from GIST, and an increasing incidence of GIST occurs among younger people (2). Until now, surgical resection remains the primary therapeutic regimen for GIST. Although imatinib mesylate was approved for first-line treatment and yields significant

improvement in survival for unresectable and metastasized GIST patients since 2002, the majority of them would suffer disease progression after treatment for 2–3 years (2). There are no alternative treatments available to treat them. Hence, it is urgently required to develop novel biomarkers and molecule targets against GIST.

Ferroptosis, as a novel-induced programmed cell death, is characterized by the accumulation of intracellular iron and lipid reactive oxygen species (ROS) (3). Recently, extensive studies were reported on cancer initiation, progression, or drug sensitivity, which showed great promise in cancer treatment (4, 5). For example, erastin, a ferroptosis inducer, showed a significant synergistic effect on the effect of antitumor therapy when combined with cisplatin (6).

In addition, emerging evidence suggested that aberrant expression of ferroptosis-related genes was closely related to clinical characteristics. SLC7A11, a core target-regulating ferroptosis, is frequently overexpressed in most tumors, such as colon adenocarcinoma (COAD), lung adenocarcinoma (LUAD), and esophageal cancer (ESCA), which would affect lymphatic metastasis, the infiltration of immune cells, etc. (7). Additionally, SLC3A2, VDAC2, and SLC7A11 expression increased continuously with the TNM stage, and FTH1 and LPLCAT3 expression increased continuously with pathological grade in pan-cancer (8). However, the expression pattern of ferroptosis-related genes and the association between them and clinical relevance remain largely unknown in GIST.

In this study, data mining of ferroptosis-related genes using the Gene Expression Omnibus (GEO) dataset confirmed that transferrin receptor (TFRC) expression was aberrant in high-risk patients and would be affected by imatinib mesylate treatment. We then investigated the enriched signaling pathways by TFRC driving. Next, we validated its expression and evaluated its clinical relevance, as well as the prognostic value in the collected GIST patient cohorts.

# Materials and methods

## Data mining

All original data were downloaded from GEO (https://www.ncbi.nlm.nih.gov/geo/) databases. Gene set enrichment analysis (GSEA) was performed to investigate the differences in signaling pathways involved by TFRC, with the gene set "c2.cp.kegg.v6.2.symbols.gmt" as the reference.

## Patient characteristics and ethics

In total, 587 samples containing detailed clinical prognostic information of pathologic diagnosis of GIST were obtained from pathology files, which were treated in the Department of General Surgery, Ren Ji Hospital, School of Medicine, Shanghai Jiao Tong University. Informed consent forms were signed by all patients. The clinical information including age at diagnosis, gender, modified National Institutes of Health (NIH) criteria, tumor size, mitotic figures, recurrence, and overall survival (OS) state is summarized in Table 1. Preoperative imaging data and surgery records were confirmed to ensure that the included patients had resected localized GISTs. Patients with unresectable or metastatic GISTs or other malignant tumors were excluded. Tissue microarray (TMA) was made using the 587 formalin-fixed paraffin-embedded tumor biopsies. All samples were collected under institutional review board approval. The study was approved by the Research Ethics Committee of Ren Ji Hospital and carried out in accordance with ethical standards as formulated in the Declaration of Helsinki, with ethical approval number 2018-029.

## Immunohistochemistry

The protocol for immunohistochemistry (IHC) was performed according to a previous description (9). The prepared TMA sections were dewaxed with xylene and hydrated with alcohol. Sodium citrate was used for antigen retrieval, and hydrogen peroxide was used to block endogenous peroxidase. Bovine serum albumin (BSA) was used to block non-specific sites. All sections were incubated with an appropriate primary antibody and secondary antibody. The primary antibody used was TFRC (Proteintech, Rosemont, IL, USA; 10084-2-AP, 1:400). TFRC expression was classified semi-quantitatively, which was independently scored by two pathologists blinded to clinical outcomes, and differences were resolved by mutual agreement, as previously described (10, 11). Briefly, the score of

TABLE 1 Patients' characteristics.

| Clinicopathological factors | | n (%) |
|---|---|---|
| **Age** | ≤61 | 298 (50.77) |
| | >61 | 289 (49.23) |
| **Gender** | Male | 294 (50.09) |
| | Female | 293 (49.91) |
| **Modified NIH criteria** | Low risk | 254 (43.27) |
| | Intermediate risk | 95 (16.18) |
| | High risk | 238 (40.55) |
| **Tumor size** | ≤2 cm | 51 (8.69) |
| | 2–5 cm | 247 (42.08) |
| | 5–10 cm | 212 (36.11) |
| | >10 cm | 77 (13.12) |
| **Mitotic figures** | ≤5 | 442 (75.30) |
| | 5–10 | 75 (12.78) |
| | >10 | 70 (11.92) |
| Recurrence | No | 513 (87.39) |
| | Yes | 74 (12.61) |
| **Overall survival state** | Alive | 556 (94.72) |
| | Dead | 31 (5.28) |

NIH, National Institutes of Health.

TFRC expression was assigned semi-quantitative terms, namely, "–", "+", "++", or "+++": "–" = "none" (no staining), "+" = "weak staining", "++" = "moderate staining", or "+++" = "strong staining" (Figure 1A). "++" and "+++" were considered as higher expression, and the others were considered as lower expression.

## Statistical analyses

Data are shown as means ± SD. GraphPad Prism 5 software was used to calculate cumulative survival time by the Kaplan–Meier method *via* the log-rank test or Cox regression analysis, as shown by the Kaplan–Meier (KM) curve. Fisher's exact test and chi-square test were used for comparison between groups through SPSS 20.0 (Chicago, IL, USA). Correlation between markers was obtained using Spearman's correlation method. All tests were two-sided except as indicated, and $p < 0.05$ was considered statistically significant.

# Results

## Identification of TFRC as a key upregulated ferroptosis gene in GISTs

Ferroptosis, as a novel-induced programmed cell death, has been widely researched in cancers. Hence, 64 genes assigned to ferroptosis pathways in the MSigDB database were gathered (Supplementary Table 1). To determine the potential dysregulated ferroptosis association in GIST, two independent GEO datasets (GSE31802 and GSE136755) containing high- and low-risk patients were utilized. As shown in Figures 2A, B, many ferroptosis-associated genes were significantly up- or downregulated in high-risk compared to low-risk patients. In addition, only GCLC and TFRC with obvious upregulation were obtained by the overlapping analysis of these two gene sets (Supplementary Figures 1A, B). A gradient increased expression pattern of GCLC and TFRC was demonstrated with the increase in risk level (Supplementary Figures 1C, D). As known to us, imatinib mesylate (IM) has been used as a major adjuvant treatment for advanced GIST patients (12). Here, we were more interested in determining potentially dysregulated ferroptosis association in GISTs with IM treatment. As shown in Figure 2C, multiple genes displayed significant up- or downregulation in patients after IM treatment compared to that before IM treatment analyzed in GSE15966. Finally, TFRC was selected for further research *via* overlapping analysis of these three gene sets (Figure 2D).

## Exploration of the potential molecular pathways associated with TFRC in GIST

To further study the signaling pathways involved in TFRC in GIST, we conducted GSEA in the GEO dataset. Through the cutoff values of p-value < 0.05 and false discovery rate (FDR) < 0.25, we determined that high TFRC expression was positively correlated to the P53 signaling pathway, DNA replication, Pentose phosphate pathway, Mismatch repair, Pyrimidine metabolism, etc., in

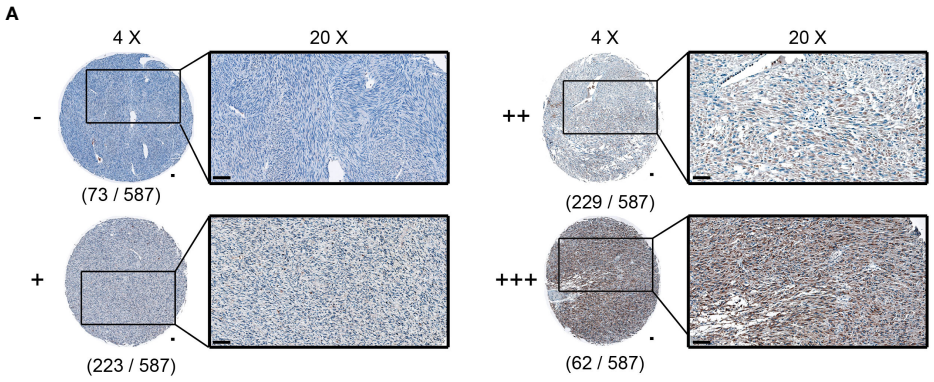


B

IHC scores for TFRC expression in 587 GIST patients

| Modified NIH criteria | Score | | | | Total |
|---|---|---|---|---|---|
| | TFRC low expression | | TFRC high expression | | |
| | - | + | ++ | +++ | |
| Low risk | 27 | 113 | 85 | 29 | 254 |
| Intermediate risk | 16 | 40 | 34 | 5 | 95 |
| High risk | 30 | 70 | 110 | 28 | 238 |
| Total | 73 | 223 | 229 | 62 | 587 |

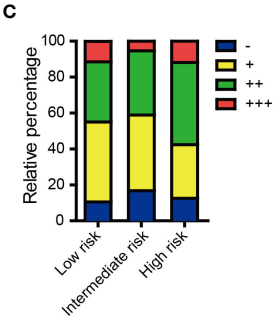


FIGURE 1
IHC scores of TFRC expression in 587 GIST patients. **(A)** Representative IHC score for TFRC expression in GIST tissues (original magnification: ×4 and ×20, round panel and orthogonal panel, respectively; scale bars, 100 μm). **(B)** IHC score distribution of TFRC in 587 cases. **(C)** Statistical analysis of the IHC score distribution in patients with different degrees of risk. IHC, immunohistochemistry; GIST, gastrointestinal stromal tumor.

10.3389/fonc.2023.1151687

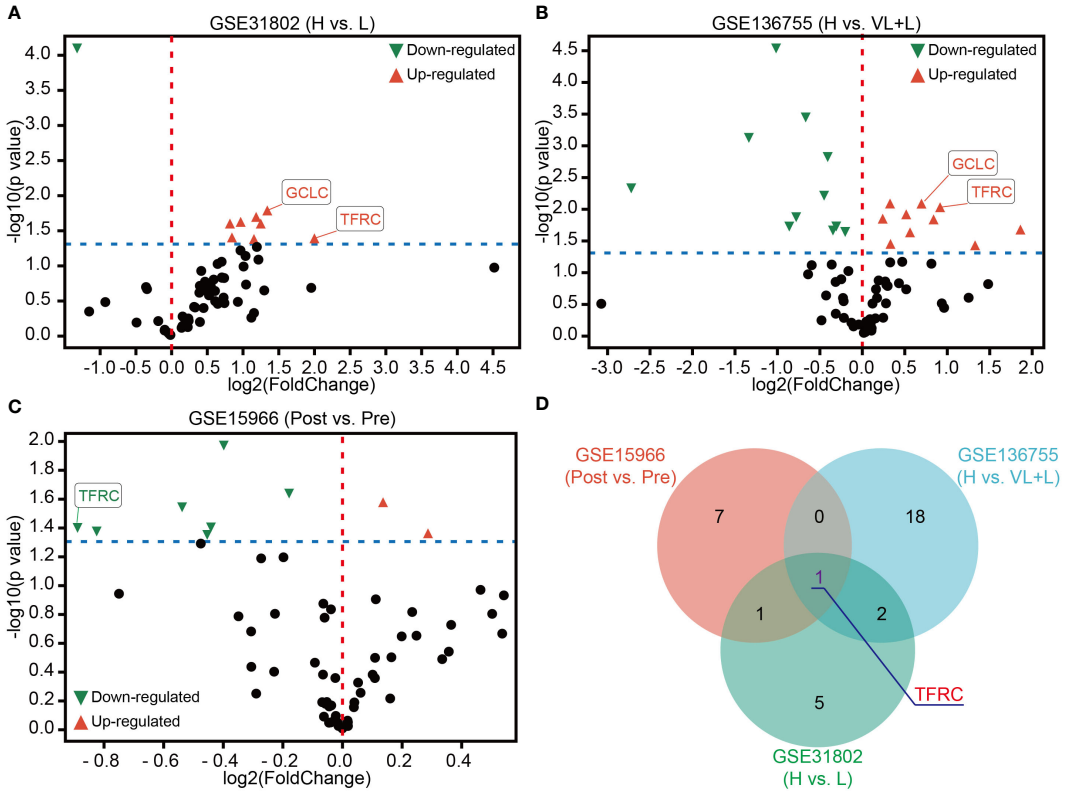


FIGURE 2
Identification of TFRC as a key ferroptosis association in GIST. **(A, B)** Volcano plots of differentially expressed ferroptosis-associated genes in GSE31802 and GSE136755 between high- and low- or very low-risk patients. **(C)** Volcano plots of differential expression of ferroptosis-associated genes before and after treatment with IM in GSE15966. **(D)** Venn diagram showing that TFRC was the common dysregulated gene of ferroptosis association in GSE31802, GSE136755, and GSE15966. p-Value < 0.05. Green, downregulated genes; red, upregulated genes. IM, imatinib mesylate.

GSE136755 (Figure 3A), and Glycolysis gluconeogenesis, Purine metabolism, Pyrimidine metabolism, Oxidative phosphorylation, Pyruvate metabolism, etc., in GSE15966 pre-IM treatment (Figure 3B). These data displayed that TFRC was mainly involved in metabolism-related signaling pathways to exert an oncogenic role in GIST. Additionally, we further analyzed the potential signaling pathways involved in TFRC with IM treatment in GIST. First, we found there were remarkable interactions between IM treatment with cell growth pathways (such as Nucleotide excision repair, Base excision repair, DNA replication, Mismatch repair, and Cell Cycle) and metabolism-related pathways (Oxidative phosphorylation, Pyrimidine metabolism, Purine metabolism, and Glycolysis gluconeogenesis) (Figure 3C). Meanwhile, there were remarkable interactions of TFRC with the mTOR signaling pathway, Nucleotide excision repair, and cell cycle in GSE15966 post-IM treatment (Figure 3D). Overall, TFRC plays an important role in GIST progression, as well as in the process of IM treatment.

## Analysis of TFRC expression and its association with clinical characteristics in GIST

To evaluate TFRC expression levels, IHC was performed in a set of TMAs containing 587 GIST samples. According to the staining score of TFRC, GIST patients were clustered into high and low TFRC expression subpopulations. As shown in Figure 2A, 291 cases were divided into a high group (scores of "++" and "+++") and others into a low group (scores of "–" and "+"; Figure 1A). Consistent with the analyzed results by the GEO dataset, remarkably more patients possessed higher TFRC expression in high-risk subpopulations (Figures 1B, C).

## Prognostic significance of TFRC in GIST

Subsequently, the prognostic value of TFRC in GISTs was confirmed. As depicted in Table 2, clinical association analyses revealed that in addition to a positive correlation with modified NIH criteria, upregulation of TFRC expression was also associated with most relapsed patients. Moreover, Kaplan–Meier analyses showed that TFRC negatively correlates with OS and recurrence-free survival (RFS) in GIST patients (Figure 4A). Next, Cox proportional hazards models were applied to analyze the relationship between TFRC expression and patient outcomes. Univariate analyses showed that TFRC expression, NIH risk degree, mitotic figures, and tumor size were significantly correlated with OS (Table 3) and RFS (Table 4). However, multivariate analyses showed that TFRC expression was merely an independent prognostic predictor for RFS (Figure 4B). These

10.3389/fonc.2023.1151687

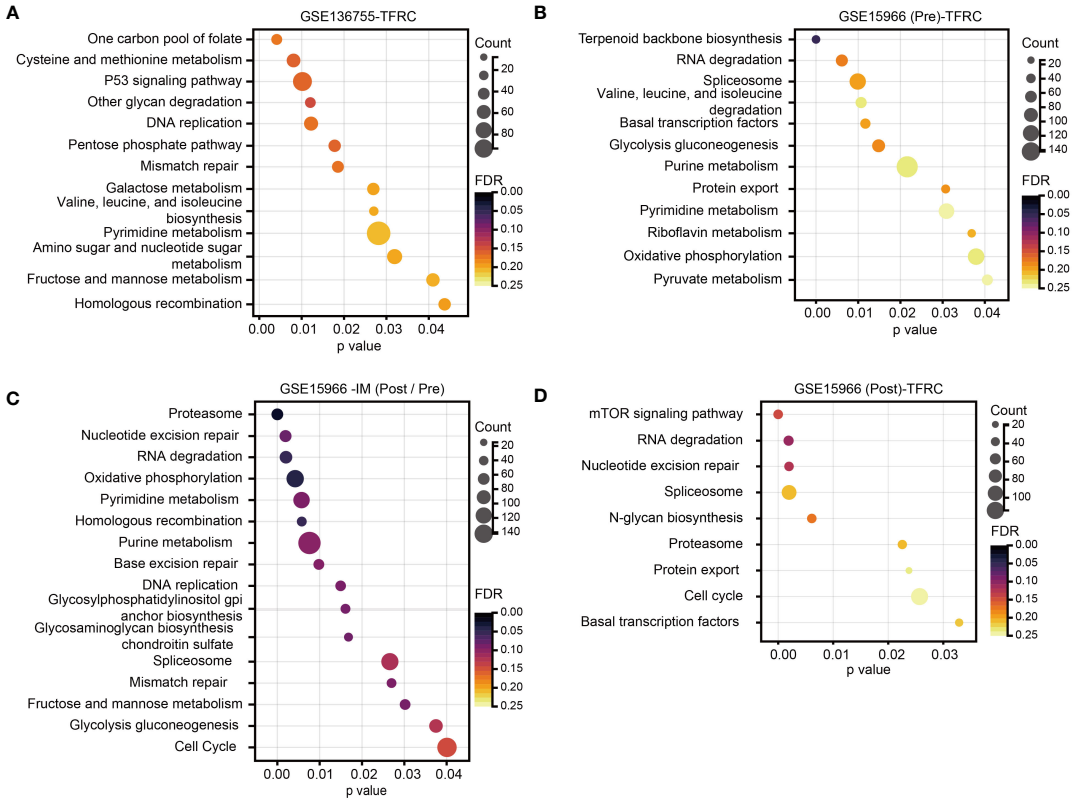


FIGURE 3
Analysis of TFRC-involved signaling pathways in GIST. **(A, B)** GSEA for the signaling pathways involved in the high TFRC expression subpopulation of GSE136755, as well as the high TFRC expression subpopulation GSE15966 pre-IM treatment. **(C)** GSEA for the signaling pathways involved in IM treatment in GSE15966. **(D)** GSEA for the signaling pathways of TFRC participants after IM treatment in GSE15966. p-Value < 0.05, FDR < 0.25. GIST, gastrointestinal stromal tumor; GSEA, gene set enrichment analysis; IM, imatinib mesylate; FDR, false discovery rate.

findings indicate that TFRC might be a key ferroptosis gene, which is commonly upregulated and associated with relapse in high-risk GISTs.

## The sensitivity and specificity of TFRC for RFS in GISTs

To further confirm the prognostic accuracy of TFRC in GIST, logistic regression was conducted to compare the sensitivity and specificity of TFRC for RFS. Multiple models were constructed, including TFRC as a single clinicopathological feature, combinations of clinicopathological features, and TFRC combined with clinicopathological features Figure 5. A receiver operating characteristic (ROC) curve comparison demonstrated that the area under the curve (AUC) for TFRC combined with other clinicopathological features was higher than that for any other single or combined factor (AUC = 0.831, $p < 0.001$). These results indicated that TFRC combined with other clinicopathological features had greater sensitivity and specificity and was a stronger RFS predictor than any single risk factor or their combination.

# Discussion

Ferroptosis, a newly defined form of programmed cell death, is characterized by iron overload, lipid ROS accumulation, and lipid peroxidation. Extensive studies in cancers have shown the intimate association between ferroptosis with cancer initiation and progression. For example, SLC7A11, a core target-regulating ferroptosis, is overexpressed and is correlated with worse survival in non-small cell lung cancer (NSCLC) (13) and pancreatic ductal adenocarcinoma (PDAC) (14) patients, which is classified as a suppressor of ferroptosis. However, few studies about the primary mechanisms and signal pathways relevant to ferroptosis have been performed, as well as their potential roles in GIST. Therefore, our study aimed to reveal the clinical significance of ferroptosis-related genes in GIST.

TABLE 2 Correlations between TFRC expression and clinicopathological features in GISTs.

| Clinicopathological feature | | Expression of TFRC | | p-Value ($\chi^2$ test) |
|---|---|---|---|---|
| | | Low (n = 296, 50.43%) | High (n = 291, 49.57%) | |
| **Age** | ≤61 | 139 | 159 | 0.063 |
| | >61 | 157 | 132 | |
| **Gender** | Male | 146 | 148 | 0.710 |
| | Female | 150 | 143 | |
| **Modified NIH criteria** | Low risk | 140 | 114 | **0.003** |
| | Intermediate risk | 56 | 39 | |
| | High risk | 100 | 138 | |
| **Tumor size** | ≤2 cm | 28 | 23 | 0.311 |
| | 2–5 cm | 131 | 116 | |
| | 5–10 cm | 105 | 107 | |
| | >10 cm | 32 | 45 | |
| **Mitotic figures** | ≤5 | 234 | 208 | 0.085 |
| | 5–10 | 34 | 41 | |
| | >10 | 28 | 42 | |
| Recurrence | Yes | 23 | 51 | **<0.001** |
| | No | 273 | 240 | |

GIST, gastrointestinal stromal tumor; NIH, National Institutes of Health. P-values < 0.05 are indicated using bold font

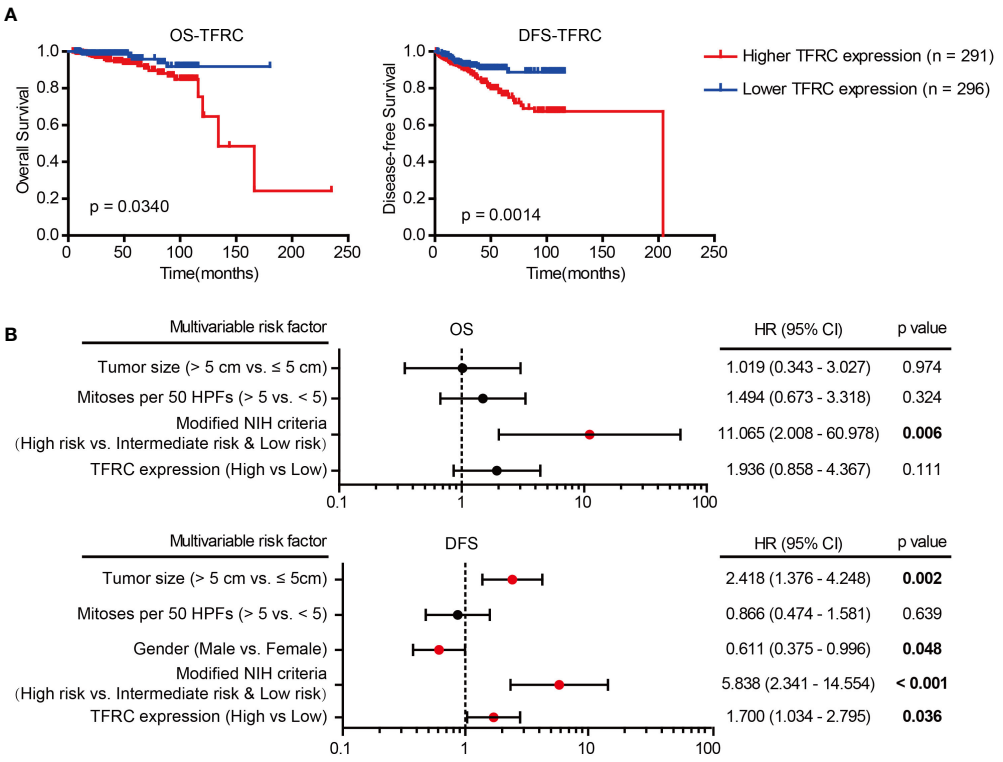


FIGURE 4
Prognostic significance of TFRC. **(A)** Kaplan–Meier analyses of overall survival (OS; p = 0.0340) and relapse-free survival (RFS; p = 0.0014) of GIST patients in correlation with high or low TFRC expression. **(B)** Multivariate Cox regression analysis of OS and RFS performed in GIST patients. GIST, gastrointestinal stromal tumor; OS, overall survival; RFS, recurrence-free survival.

10.3389/fonc.2023.1151687

TABLE 3 Univariate analyses of prognostic parameters for OS in GISTs.

| Prognostic parameter | Univariate analysis | | |
|---|---|---|---|
| | HR | 95% CI | p-Value |
| **Expression of TFRC (high *vs.* low)** | 2.352 | 1.042–5.307 | **0.039** |
| **Age (>61 *vs.* ≤ 61)** | 0.514 | 0.242–1.090 | 0.083 |
| **Gender (male *vs.* female)** | 0.753 | 0.368–1.540 | 0.437 |
| **Modified NIH criteria (high risk *vs.* intermediate risk and low risk)** | 15.314 | 3.626–64.680 | **<0.001** |
| **Tumor size (>5 cm *vs.* ≤ 5 cm)** | 3.826 | 1.448–10.111 | **0.007** |
| **Mitotic figures (>5 *vs.* ≤ 5)** | 4.034 | 1.899–8.567 | **<0.001** |
| **Recurrence (yes *vs.* no)** | 2,305.866 | 0.787–6,751,922.497 | 0.057 |

OS, overall survival; GIST, gastrointestinal stromal tumor; NIH, National Institutes of Health. P-values < 0.05 are indicated using bold font

First, data mining using GEO datasets displayed that overexpressed TFRC exists in high-risk patients. However, the clinical relevance of TFRC expression and its prognostic value for GIST patients remain unclear. Here, we found that increased TFRC expression was closely related to tumor relapse and poor prognosis, which suggested that TFRC has a role in carcinogenesis. However, its detailed function and underlying mechanism in GIST remain unclear and warrant further studies.

TFRC, also known as CD71, is one of the most important receptor-mediated controls during the iron intake process in generic cells *via* binding with iron–transferrin complex to facilitate iron into cells. Meanwhile, TFRC has been verified to be abnormally expressed in various cancers (15). Dramatically increased TFRC expression was associated with a worse prognosis in epithelial ovarian cancer, which would accelerate the progression *via* upregulation of AXIN2 expression (16). CD71-positive cells enriched by HPV-E6 protein promoted cancer aggressiveness in cervical cancer cells (17). In hepatocellular carcinoma (HCC), O-GlcNAcylation can increase ferroptosis sensitivity *via* transcriptional elevation of TFRC to increase the iron concentration in cells (18). In general, inducing ferroptosis in tumor cells can effectively inhibit tumor growth (19). Moreover, TFRC was categorized into ferroptosis drivers by summarizing ferroptosis regulators by Kyoto Encyclopedia of Genes and Genomes (KEGG) pathway enrichment and selecting genes using the FerrDb database, PubMed, and Google Scholar (8). Hence, more in-depth studies need to be conducted to verify the role of TFRC on ferroptosis in GIST. Although TFRC is an important iron uptake receptor in cancer cells, its functions and mechanisms in ferroptosis and tumor progression remain unclear. Therefore, TFRC may not mediate GIST progression by regulating ferroptosis, and other pathways may be involved, such as the metabolism-related pathway shown in Figure 3, which suggests that TFRC is tissue and tumor type. Several studies in gastric cancer (GC) have shown that the expression of TFRC is reversely correlated with a poor prognosis in primary GC (20). Xiaojing Cheng et al. (21) conducted experiments both *in vitro* and *in vivo*, revealing that TFRC-negative cells exhibit properties of tumor-initiating cells and possess immune escape features. Further investigation into the effects of TFRC on GIST cells could offer potential therapeutic strategies for patients with GIST.

Moreover, data mining also revealed that decreased expression of TFRC occurred after treatment with imatinib, which indicates its relationship with drug sensitivity. In addition, clinical sample analysis revealed a positive correlation between TFRC expression and patient relapse. Survival analysis was indicative that patients

TABLE 4 Univariate analyses of prognostic parameters for DFS in GISTs.

| Prognostic parameter | Univariate analysis | | |
|---|---|---|---|
| | HR | 95% CI | p-Value |
| **Expression of TFRC (high *vs.* low)** | 2.192 | 1.337–3.593 | **0.002** |
| **Age (>61 *vs.* ≤ 61)** | 0.731 | 0.461–1.160 | 0.184 |
| **Gender (male *vs.* female)** | 0.511 | 0.315–0.829 | **0.007** |
| **Modified NIH criteria (high risk *vs.* intermediate risk and low risk)** | 10.208 | 5.080–20.512 | **<0.001** |
| **Tumor size (>5 cm *vs.* ≤ 5 cm)** | 2.785 | 1.650–4.701 | **<0.001** |
| **Mitotic figures (>5 *vs.* ≤ 5)** | 6.061 | 3.737–9.832 | **<0.001** |

P-values < 0.05 are indicated using bold font.

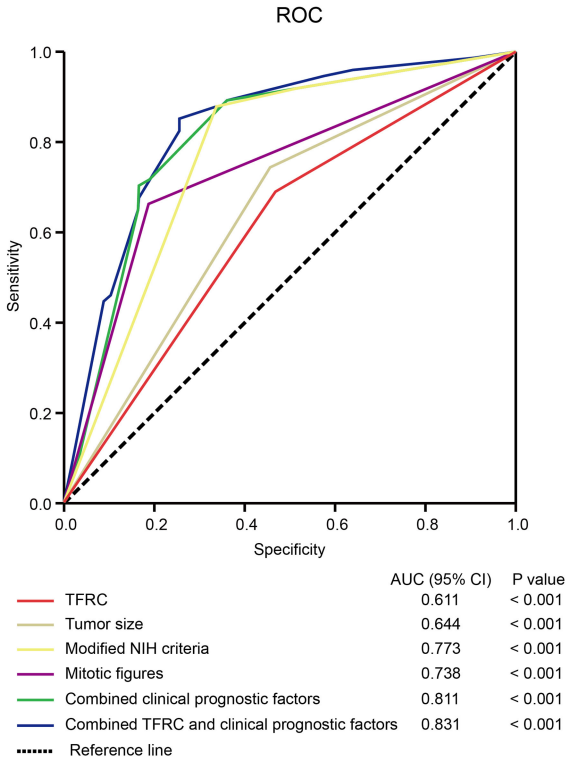


FIGURE 5
The sensitivity and specificity of TFRC for DFS. The ROC curve compares the prognostic accuracy of TFRC with clinicopathological features in all 587 GIST patients by logistic regression. ROC, receiver operating characteristic; AUC, area under the curve. Combined clinical prognostic factors include modified NIH criteria, tumor size, and mitotic figures. DFS, disease-free survival; GIST, gastrointestinal stromal tumor; NIH, National Institutes of Health. Note. DFS, disease-free survival; GIST, gastrointestinal stromal tumor; NIH, National Institutes of Health.

with high TFRC expression possessed more undesirable disease-free survival (DFS) outcomes than those with low TFRC expression. These data are consistent with the analyzed results in previous reports of other cancers, which further supported the pivotal role in cancer progression. Previous research has revealed that the $CD71^{+}$ subpopulation of cervical cancer cells exhibited enhanced resistance to irradiation and suppression of CD71-inhibited sensitized cells to irradiation treatment (17). Furthermore, more frequently upregulated TFRC expressions occur in some drug-resistant human cancer cells (22), therefore requiring more in-depth studies to clarify the role of TFRC in the sensitivity and resistance of cancer cells to imatinib in GIST therapy. Targeting TFRC using compounds such as curcumin (one of the most successful chemo-preventive compounds) to intervene with the progression of cancers seems feasible (23). Moreover, increasing the concentrations of TFRC-targeted superparamagnetic iron oxides in tumor tissues *via* magnetic fields could inhibit tumor progression, which is a promising cancer treatment (24, 25). However, whether TFRC can be an effective target for GIST treatment needs more theoretical support.

In summary, our study found that the expression of TFRC was significantly upregulated in high-risk GIST and resulted in a higher relapse rate. Meanwhile, decreased expression of TFRC caused by imatinib treatment occurred. Therefore, developing new treatments targeting TFRC would be a potential therapeutic approach in GIST, as well as its combination with imatinib.

## Data availability statement

The original contributions presented in the study are included in the article/Supplementary Material. Further inquiries can be directed to the corresponding authors.

## Ethics statement

The studies involving humans were approved by Shanghai Jiaotong University School of Medicine, Renji Hospital Ethics Committee. The studies were conducted in accordance with the local legislation and institutional requirements. The participants provided their written informed consent to participate in this study.

## Author contributions

MW provided the whole study design. BN supervised the experiment conduction. CZ and XL carried out the experiments and organized the manuscript. LY finished the bioinformatics analysis. XM and YS collaborated to collect the specimens and record clinical information. CH, TP, and JC were responsible for statistical analysis. MW and BN offered critical reviews. All authors contributed to the article and approved the submitted version.

## Conflict of interest

The authors declare that the research was conducted in the absence of any commercial or financial relationships that could be construed as a potential conflict of interest.

## Publisher's note



## Supplementary material

The Supplementary Material for this article can be found online at: https://www.frontiersin.org/articles/10.3389/fonc.2023.1151687/full#supplementary-material

SUPPLEMENTARY FIGURE 1
Aberrantly expression of ferroptosis-associated genes in GIST. (A) Venn diagram showed the overlap of significantly down-regulated ferroptosis-associated genes in GSE31802 and GSE136755. (B) Venn diagram showed the overlap of significantly up-regulated ferroptosis-associated genes in GSE31802 and GSE136755. (C) Expression analysis of GCLC in different risk degree patients (p = 0.0041). (D) Expression analysis of TFRC in different risk degree patients (p = 0.0041). H: High risk, Inter: Intermediate risk, L: Low risk, VL: Very low risk.

## References

1. Bello DM, Dematteo RP, Ariyan CE. The GIST of targeted therapy for Malignant melanoma. *Ann Surg Oncol* (2014) 21:2059–67. doi: 10.1245/s10434-013-3373-z

2. Kelly CM, Gutierrez Sainz L, Chi P. The management of metastatic GIST: current standard and investigational therapeutics. *J Hematol Oncol* (2021) 14:2. doi: 10.1186/s13045-020-01026-6

3. Li J, Cao F, Yin HL, Huang ZJ, Lin ZT, Mao N, et al. Ferroptosis: past, present and future. *Cell death & disease* (2020) 11:88. doi: 10.1038/s41419-020-2298-2

4. Su Y, Zhao B, Zhou L, Zhang Z, Shen Y, Lv H, et al. Ferroptosis, a novel pharmacological mechanism of anti-cancer drugs. *Cancer Lett* (2020) 483:127–36. doi: 10.1016/j.canlet.2020.02.015

5. Wang Y, Wei Z, Pan K, Li J, Chen Q. The function and mechanism of ferroptosis in cancer. *Apoptosis: an Int J programmed Cell Death* (2020) 25:786–98. doi: 10.1007/s10495-020-01638-w

6. Guo J, Xu B, Han Q, Zhou H, Xia Y, Gong C, et al. Ferroptosis: A novel anti-tumor action for cisplatin. *Cancer Res Treat* (2018) 50:445–60. doi: 10.4143/crt.2016.572

7. Cheng X, Wang Y, Liu L, Lv C, Liu C, Xu J. SLC7A11, a potential therapeutic target through induced ferroptosis in colon adenocarcinoma. *Front Mol Biosci* (2022) 9:889688. doi: 10.3389/fmolb.2022.889688

8. Tang B, Yan R, Zhu J, Cheng S, Kong C, Chen W, et al. Integrative analysis of the molecular mechanisms, immunological features and immunotherapy response of ferroptosis regulators across 33 cancer types. *Int J Biol Sci* (2022) 18:180–98. doi: 10.7150/ijbs.64654

9. Xu C, Tian G, Jiang C, Xue H, Kuerbanjiang M, Sun L, et al. NPTX2 promotes colorectal cancer growth and liver metastasis by the activation of the canonical Wnt/β-catenin pathway *via* FZD6. *Cell death & disease* (2019) 10:217. doi: 10.1038/s41419-019-1467-7

10. Tian GA, Zhu CC, Zhang XX, Zhu L, Yang XM, Jiang SH, et al. CCBE1 promotes GIST development through enhancing angiogenesis and mediating resistance to imatinib. *Sci Rep* (2016) 6:31071. doi: 10.1038/srep31071

11. Taube JM, Anders RA, Young GD, Xu H, Sharma R, McMiller TL, et al. Colocalization of inflammatory response with B7-h1 expression in human melanocytic lesions supports an adaptive resistance mechanism of immune escape. *Sci Trans Med* (2012) 4:127ra137. doi: 10.1126/scitranslmed.3003689

12. Joensuu H, Eriksson M, Sundby Hall K, Reichardt A, Hartmann JT, Pink D, et al. Adjuvant imatinib for high-risk GI stromal tumor: analysis of a randomized trial. *J Clin Oncol* (2016) 34:244–50. doi: 10.1200/jco.2015.62.9170

13. Ji X, Qian J, Rahman SMJ, Siska PJ, Zou Y, Harris BK, et al. xCT (SLC7A11)-mediated metabolic reprogramming promotes non-small cell lung cancer progression. *Oncogene* (2018) 37:5007–19. doi: 10.1038/s41388-018-0307-z

14. Lo M, Ling V, Wang YZ, Gout PW. The xc- cystine/glutamate antiporter: a mediator of pancreatic cancer growth with a role in drug resistance. *Br J Cancer* (2008) 99:464–72. doi: 10.1038/sj.bjc.6604485

15. Shen Y, Li X, Dong D, Zhang B, Xue Y, Shang P. Transferrin receptor 1 in cancer: a new sight for cancer therapy. *Am J Cancer Res* (2018) 8:916–31.

16. Huang Y, Huang J, Huang Y, Gan L, Long L, Pu A, et al. TFRC promotes epithelial ovarian cancer cell proliferation and metastasis *via* up-regulation of AXIN2 expression. *Am J Cancer Res* (2020) 10:131–47.

17. Leung TH, Tang HW, Siu MK, Chan DW, Chan KK, Cheung AN, et al. CD71(+) population enriched by HPV-E6 protein promotes cancer aggressiveness and radioresistance in cervical cancer cells. *Mol Cancer research: MCR* (2019) 17:1867–80. doi: 10.1158/1541-7786.Mcr-19-0068

18. Zhu G, Murshed A, Li H, Ma J, Zhen N, Ding M, et al. O-GlcNAcylation enhances sensitivity to RSL3-induced ferroptosis *via* the YAP/TFRC pathway in liver cancer. *Cell Death Discovery* (2021) 7:83. doi: 10.1038/s41420-021-00468-2

19. Mou Y, Wang J, Wu J, He D, Zhang C, Duan C, et al. Ferroptosis, a new form of cell death: opportunities and challenges in cancer. *J Hematol Oncol* (2019) 12:34. doi: 10.1186/s13045-019-0720-y

20. Ohkuma M, Haraguchi N, Ishii H, Mimori K, Tanaka F, Kim HM, et al. Absence of CD71 transferrin receptor characterizes human gastric adenosquamous carcinoma stem cells. *Ann Surg Oncol* (2012) 19:1357–64. doi: 10.1245/s10434-011-1739-7

21. Cheng X, Fan K, Wang L, Ying X, Sanders AJ, Guo T, et al. TfR1 binding with H-ferritin nanocarrier achieves prognostic diagnosis and enhances the therapeutic efficacy in clinical gastric cancer. *Cell Death Dis* (2020) 11:92. doi: 10.1038/s41419-020-2272-z

22. Kazan HH, Urfali-Mamatoglu C, Gunduz U. Iron metabolism and drug resistance in cancer. *Biometals: an Int J role metal ions biology biochemistry Med* (2017) 30:629–41. doi: 10.1007/s10534-017-0037-7

23. Yang C, Ma X, Wang Z, Zeng X, Hu Z, Ye Z, et al. Curcumin induces apoptosis and protective autophagy in castration-resistant prostate cancer cells through iron chelation. *Drug design Dev Ther* (2017) 11:431–9. doi: 10.2147/dddt.S126964

24. Aldahoun MA, Jaafar MS, Al-Akhras MH, Bououdina M. Enhanced nanocurcumin toxicity against (PC3) tumor and microbial by using magnetic field in *vitro*. *Artificial cells, nanomedicine, and biotechnology* (2017) 45:843–53. doi: 10.1080/21691401.2016.1178137

25. Liu Z, Zhan X, Yang M, Yang Q, Xu X, Lan F, et al. A magnetic-dependent protein corona of tailor-made superparamagnetic iron oxides alters their biological behaviors. *Nanoscale* (2016) 8:7544–55. doi: 10.1039/c5nr08447d

frontiers | Frontiers in Oncology

TYPE Mini Review
PUBLISHED 16 October 2023
DOI 10.3389/fonc.2023.1285661



OPEN ACCESS

EDITED BY
Shanye Yin,
Albert Einstein College of Medicine,
United States

REVIEWED BY
Ruichen Ye,
Stony Brook University, United States
Yan Sun,
Albert Einstein College of Medicine,
United States
Wei Ke,
The State University of New Jersey,
United States

*CORRESPONDENCE
Kohichi Takada
ktakada@sapmed.ac.jp

RECEIVED 30 August 2023
ACCEPTED 03 October 2023
PUBLISHED 16 October 2023

CITATION
Nakamura H, Arihara Y and Takada K (2023) Targeting STEAP1 as an anticancer strategy. *Front. Oncol.* 13:1285661.
doi: 10.3389/fonc.2023.1285661



# Targeting STEAP1 as an anticancer strategy

Hajime Nakamura, Yohei Arihara and Kohichi Takada*

Department of Medical Oncology, Sapporo Medical University School of Medicine, Sapporo, Japan

Although the six-transmembrane epithelial antigen of prostate 1 (STEAP1) was first identified in advanced prostate cancer, its overexpression is recognized in multiple types of cancer and associated with a poor prognosis. STEAP1 is now drawing attention as a promising therapeutic target because of its tumor specificity and membrane-bound localization. The clinical efficacy of an antibody-drug conjugate targeting STEAP1 in metastatic, castration-resistant, prostate cancer was demonstrated in a phase 1 trial. Furthermore, growing evidence suggests that STEAP1 is an attractive target for immunotherapies such as chimeric antigen receptor-T cell therapy. In this review, we summarize the oncogenic functions of STEAP1 by cancer type. This review also provides new insights into the development of new anticancer strategies targeting STEAP1.

KEYWORDS

**STEAP1, antibody therapy, CAR-T therapy, cancer vaccine, anticancer strategies**

## 1 Introduction

Cancer is still a major burden of disease worldwide despite the development of new therapeutic strategies. An estimated 19.3 million new cases and almost 10 million deaths have reportedly occurred due to cancer in 2020 (1). Further efforts are needed to prolong the survival time of patients with cancer, especially at the advanced stages.

The six-transmembrane epithelial antigen of prostate 1 (STEAP1), first identified in advanced prostate cancer, is a cell surface protein that functions as a transporter (2). STEAP1 is reportedly overexpressed in a subset of human cancers (3, 4). The Gene Expression Profiling Interactive Analysis (GEPIA) web server, which contains 9,736 tumors and 8,587 normal samples from the Cancer Genome Atlas (TCGA) and Genotype-Tissue Expression (GTEx) projects, also revealed high expression of STEAP1 in multiple cancer tissues compared to normal tissues (Figure S1) (5). Thus, considering its cell surface location and cancer specificity, STEAP1 is regarded as a promising therapeutic target in cancer. DSPT3068S, an antibody-drug conjugate (ADC) -targeting STEAP1, has been investigated in a phase I trial for patients with metastatic castration-resistant prostate cancer (6). Furthermore, a recent study demonstrated the development of a chimeric antigen receptor (CAR) against STEAP1, which showed remarkable efficacy against prostate cancer cells both *in vitro* and *in vivo* (7). Thus, STEAP1 is rapidly gaining attention for the development of novel treatment strategies of cancer.

In this review, we initially focus on the molecular mechanisms and functions of STEAP1 by cancer type and subsequently present several potential therapeutic strategies targeting STEAP1 based on previous pre-clinical and clinical reports.

## 2 Molecular mechanisms and functions of STEAP1

The STEAP family contains four members, named STEAP1–4, all of which have in common a six transmembrane domain with the COOH- and N-terminals located in the cytosol (8). STEAP1 was the first member of the STEAP family to be identified and has been widely studied as a gene related to cancer progression. STEAP1 was previously predicted not to promote iron and cooper reduction or uptake mainly due to the lack of the N-terminal NADPH-binding F420H2:NADP+ oxidoreductase domain unlike other STEAP members. However, a recent study revealed that STEAP1 exhibits cellular ferric reductase activity by fusing to the intracellular NADPH-binding domain of STEAP4. These findings can ultimately contribute to the development of STEAP1 targeted therapy (9). In contrast, the pathological functions of STEAP1 in cancer still need further investigation. In this section, we discuss the molecular mechanisms and functions of STEAP1 in a cancer-type-dependent manner.

### 2.1 Prostate cancer

STEAP1 was first identified as a prostate-specific-cell surface-antigen that is highly expressed in human prostate cancer (2). STEAP1 is reportedly expressed in more than 80% of the cases of metastatic castration-resistant prostate cancer with bone or lymph node involvement and its expression is elevated in all stages of the disease (10). A high level of STEAP1 expression was positively associated with Gleason scores, which is the most reliable histological grading for prostate cancer, and poor prognoses, suggesting that STEAP1 is involved in tumor initiation and progression (11, 12). Knockdown of *STEAP1* induces apoptosis and inhibits proliferation in prostate cancer cells (13). Further, monoclonal antibodies against STEAP1 were found to inhibit intercellular communication *in vitro* and suppress proliferation of tumor xenografts in a xenograft model of prostate cancer (14).

In terms of diagnosis, immunohistochemical analysis of prostate cancer specimens with a range of Gleason scores revealed that STEAP1 could be a suitable candidate to distinguish patients with cancer from patients without tumor (15). Furthermore, a recent study revealed that STEAP1-positive extracellular vesicle levels in plasma are significantly associated with prostate cancer diagnoses (16). The current standard diagnostic methods are prostate-specific antigen (PSA) screening and tissue biopsy, which have a high false-positive rate and are invasive, respectively (17, 18). Therefore, STEAP1 extracellular vesicles can be used for screening to improve the clinical management of prostate cancer.

Prostate cancer is thus the most investigated type of cancer with respect to STEAP1-targeted therapy. However, the underlying mechanisms of proliferation and invasiveness triggered by STEAP1 are still controversial, and little is known about the underlying pathways related to STEAP1 in prostate cancer compared to other types of cancer. Further efforts are warranted to clarify the STEAP1-related pathway to develop STEAP1-targeted treatment strategies in prostate cancer.

### 2.2 Colorectal cancer

We have previously reported that STEAP1 is overexpressed in colorectal cancer (CRC) cells compared with the normal counterparts (19). Knockdown of *STEAP1* evoked intrinsic apoptosis in several CRC cell lines. We also measured intracellular ROS using flow cytometry to assess whether the knockdown of *STEAP1* stimulated ROS generation in CRC cell lines. Contrary to the results mentioned above, an increased generation of intracellular ROS was observed in CRC cell lines such as DLD-1 and SW480. *N*-Acetyl-cysteine, a ROS scavenger, suppressed the increase in ROS production and the intrinsic apoptosis evoked by *STEAP1* silencing. We also found that the expression of several nuclear factor-erythroid 2-related factor 2 (NRF2)-mediated antioxidant molecules, including heme oxygenase 1 (HMOX1), NAD(P)H quinone dehydrogenase 1 (NQO1), and thioredoxin reductase 1 (TXNRD1), was significantly down regulated by *STEAP1* silencing. Under normal circumstances, kelch-like ECH-associated protein 1 (KEAP1) binds to NRF2 and retains it in the cytoplasm. However, NRF2 dissociates from KEAP1 and translocates to the nucleus to activate downstream antioxidant enzymes (20, 21). Immunocytochemical analysis revealed that the nuclear translocation of NRF2 was inhibited by *STEAP1* silencing in DLD-1 cells. A significantly positive relationship between STEAP1 and NRF2 was also detected by performing Pearson's correlation coefficient analysis on publicly accessible gene expression profiling data. These findings suggest that the STEAP1-NRF2 axis may be beneficial as a novel strategy to combat CRC (Figure 1).

### 2.3 Hepatocellular carcinoma

We had also previously investigated the biological mechanisms of STEAP1 in hepatocellular carcinoma (HCC). Similar to CRC, STEAP1 is overexpressed in HCC and associated with poor prognoses. The knockdown of *STEAP1* triggered G1 arrest, leading to the inhibition of cell proliferation in HCC. The results of bioinformatic analysis indicated that c-Myc, which is known to contribute to the pathogenesis of a broad range of human cancers, lies downstream of STEAP1, and the pathway promotes cell proliferation and cell-cycle progression in HCC. A recent study revealed that *STEAP1* silencing leads to increased phosphorylation of c-Myc in prostate cancer cells (22). Although there might be several types of STEAP1 pathways related to c-Myc, the underlying mechanisms still needs further investigation. In addition, intracellular ROS levels were also increased by STEAP1 inhibition, similar to CRC. However, we found no relationship between STEAP1 and NRF2 in HCC. Previous reports had demonstrated that c-Myc generates ROS in liver cancer cells, which is inconsistent with our findings (23, 24). These results

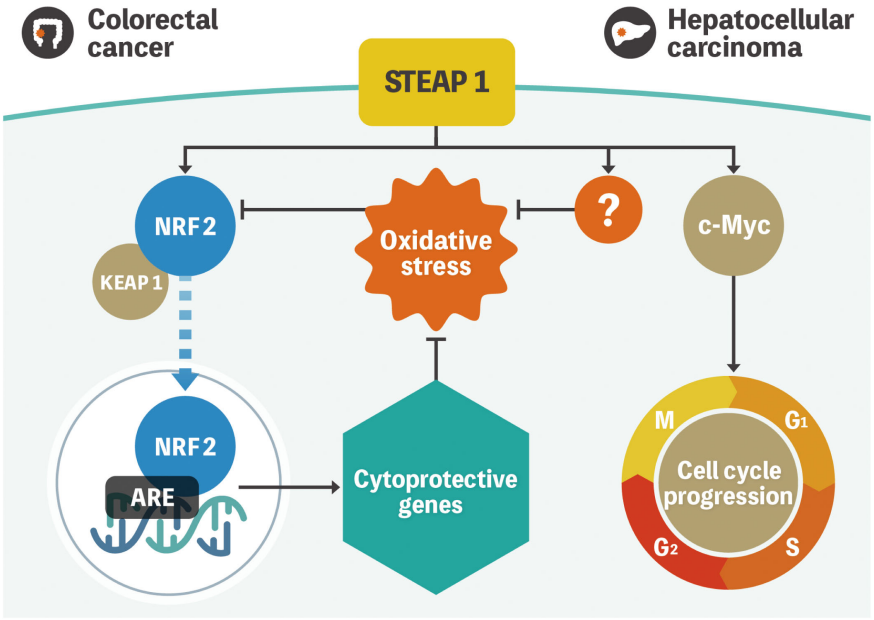


FIGURE 1
Model representation of STEAP1-mediated gene regulation in colorectal cancer and hepatocellular carcinoma. NRF2 is located in the cytoplasm and is regulated by KEAP1 under normal conditions. Oxidative stress triggers NRF2 dissociation from KEAP1 and subsequent translocation to the nucleus to activate multiple cytoprotective genes. STEAP1 seems to play a role in the activation of the pathway in colorectal cancer. Conversely, STEAP1 modulates ROS levels, although the role of the STEAP1-NRF2 axis is uncertain in hepatocellular carcinoma. In addition, STEAP1 promotes cell cycle progression by regulating the expression of c-Myc. STEAP1, the six-transmembrane epithelial antigen of prostate 1; NRF2, nuclear factor-erythroid 2-related factor 2; KEAP1, kelch-like ECH-associated protein 1; ROS, reactive oxygen species.

suggest the existence of an NRF2- or c-Myc- independent ROS-related pathway in the regulation of STEAP1-mediated cell proliferation (Figure 1) (25).

## 2.4 Gastric cancer

Zhang et al. reported that STEAP1 was overexpressed and associated with poor prognoses in gastric cancer. Up-regulation of *STEAP1* increased cell proliferation, migration, and invasion via the AKT/FOXO1 pathway and caused epithelial–mesenchymal transition (EMT); these effects decreased after *STEAP1* silencing (26). Furthermore, Wu et al. revealed that STEAP1 is translationally induced during peritoneal metastasis and can drive both tumorigenesis and chemoresistance to docetaxel (27). These studies concluded that STEAP1 can be a potent candidate for targeted therapy.

## 2.5 Lung cancer

Several groups have reported that *STEAP1* is significantly upregulated in lung cancer compared to the normal cells and is associated with poor prognoses (28, 29). Gene Ontology (GO) and Kyoto Encyclopedia of Genes and Genomes (KEGG) analyses also revealed that *STEAP1* upregulation potentially regulates tumor progression via homologous recombination, p53 signaling, cell cycle, DNA replication, and apoptosis (24). Furthermore, knockdown of *STEAP1* using siRNA reduced endothelial cell migration and tube formation, which implicated STEAP1 as a novel vascular target in lung cancer (30). Importantly, STEAP1 regulates EMT via the Janus kinase 2 (JAK2)/signal transducer and activator of transcription 3 (STAT3) signaling pathway that is often detected in various tumors and involved in oncogenesis (31). Collectively, STEAP1 appears to be a promising biomarker and therapeutic target in lung cancer.

## 2.6 Ewing's sarcoma

Ewing's sarcoma (EWS) is the second most common bone cancer in children. Despite recent advances in the multimodal treatment for EWS, the 5-year survival rate is less than 30% in patients with metastases (32). STEAP1 has emerged as a target for EWS therapy. In EWS cells, overexpressed *STEAP1*, whose expression is induced by the EWS::FLI fusion gene binding to the *STEAP1* promoter lesion as a transcription factor, confers enhanced proliferative and invasive properties on the cells. STEAP1 induces the production of intracellular reactive oxygen species (ROS), followed by STAT1 activation (Figure S2) (33). In contrast, high membranous STEAP1 expression was correlated with improved overall survival (OS) in patients with EWS, which could be attributed to a correlation with sensitivity to chemotherapeutic agents such as doxorubicin and etoposide (34). Although these observations are valuable, they complicate decision-making while considering therapeutic interventions.

In addition to EWS::FLI1, NKX2.2 is a positive regulator of STEAP1 expression (35). Initially, the transcriptional repressive roles of NKX2.2 were recognized as being necessary and sufficient for the oncogenic properties of EWS (36). However, Markey et al. showed that NKX2.2 binds to two sites of the *STEAP1* promoter lesion, leading to increased STEAP1 expression. Moreover, by interacting with EWS::FLI1 at sites proximal to the EWS::FLI1 sites, NKX2.2 works as a co-regulator of STEAP1 expression (Figure S2). Thus, the elucidation of master transcriptional regulators of STEAP1 can help identify potential therapeutic targets of EWS.

## 2.7 Breast cancer

As mentioned earlier, STEAP1 confers oncogenic properties such as enhanced proliferation and metastatic potential and its high expression is a poor prognostic maker in a subset of cancers (37). In contrast, STEAP1 exerts tumor suppressive effects on breast cancer cells. *STEAP1* expression is downregulated in breast cancer tissues compared to normal cells, and low STEAP1 expression is associated with poor prognoses in patients with breast cancer (38). This can be attributed to EMT suppression by STEAP1 through *CDH1* upregulation and the downregulation of EMT-related genes in breast cancer cells. Researchers have also used bioinformatics analyses to demonstrate that low STEAP1 expression is related to poor prognoses (39). Therefore, interventions to inhibit STEAP1 can be useful as antimetastatic drugs for breast cancer.

# 3 Development of novel therapies by targeting STEAP1

STEAP1 is rapidly gaining attention as a novel therapeutic target because of its location on the cell surface and specificity to cancer versus normal cells. Of note, the functions of STEAP1 depend on the type of cancer. In this section, we discuss the development of STEAP1-targeting novel therapies.

## 3.1 Antibody therapy

DSTP3086S, a STEAP1-targeting ADC, has shown acceptable safety and potential benefit for patients with STEAP1-expressing, metastatic, castration-resistant, prostate cancer in a phase I trial (6). Eleven out of 77 patients treated with DSTP3086S once every 3 weeks met the response criteria of PSA reduction of ≥50%, while 26 out of 46 patients with evaluable disease at the baseline presented clinical response (two partial response; 24 stable disease). However, 69 out of 77 participants experienced an adverse event, with grade 3/4 noted in 24 participants, whereas no treatment-related deaths were observed in the study.

Bispecific T-cell engagers (BiTEs) are recombinant proteins made up of two single-chain variable fragments from two different antibodies, one targeting a tumor-specific antigen and the other targeting the effector T cell. Although these proteins have demonstrated dramatic therapeutic effects in patients with hematologic malignancies, they have not been investigated extensively for solid cancers (40, 41). Lin et al. demonstrated the efficacy of BC261, a rehumanized STEAP1-IgG, which is bispecific for STEAP1 and CD3 (42). BC261 reportedly showed significant elevation of T-cell infiltration and tumor ablation in EWS-family tumors and prostate cancer cell lines, confirmed by preclinical studies.

## 3.2 Chimeric antigen receptor -T cell therapy

CAR-T cell therapy is now one of the cutting-edge therapies for cancer. To date, six CAR-T therapies have been approved by the Food and Drug Administration (FDA) for the treatment of hematological malignancies such as lymphomas, some forms of leukemia, and multiple myeloma (43). In contrast to the results observed with hematologic malignancies, those from clinical trials of CAR-T cells targeting solid tumors were disappointing (44). However, Qi et al. recently reported the remarkable antitumor efficacy of anti-Claudin18.2 CAR-T for patients with gastric cancer, suggesting the potential benefit of CAR-T cell therapy for solid tumors (45).

Considering the principles of CAR-T cell therapy, the most important aspect is identifying the tumor-specific antigen to be detected by the CAR, which should be highly expressed on the cell surface of the target but not on healthy human tissues. In this context, STEAP1 could be an attractive target as it is expressed in many cancer types, and high normal tissue expression of STEAP1 is only documented in the prostate, which is not a vital organ (Figure 2).

Although STEAP1 CAR-T has not yet been applied in the clinical trial setting, it showed promising anti-tumor activity in prostate cancer with CAR-T cell expansion and infiltration into the tumor microenvironment both *in vivo* and *in vitro* (7). In this preclinical study, the authors tested the second-generation anti-STEAP1 CAR with the 4-1BB co-stimulatory domain. The CAR-T product showed high transduction efficiency and polyfunctionality that were reported to be associated with clinical outcomes in anti-CD19 CARs (46). Furthermore, Bhatia et al. reported that STEAP1 CAR-T cells demonstrated reactivity in low antigen density, antitumor activity across metastatic prostate cancer models, and safety in a human STEAP1 knock-in mouse model (10). These preclinical results warrant further development of STEAP1 CAR-T for clinical trials.

## 3.3 Other immunotherapies

T cells expressing an engineered T cell receptor (TCR-T cells) have recently drawn attention as a novel immunotherapy for cancer, especially for solid tumors (47). Schirmer et al. successfully isolated a STEAP1$^{130/}$HLA-A*02:01-peptide-restricted TCR. EWS cell growth was suppressed when treated with respective TCR tg CD8+ T cells compared to non-specific CD8+ T cells both *in vivo* and *in vitro* (48). A subsequent report from the group also revealed the local tumor control effect of TCR tg CD4+ T cells

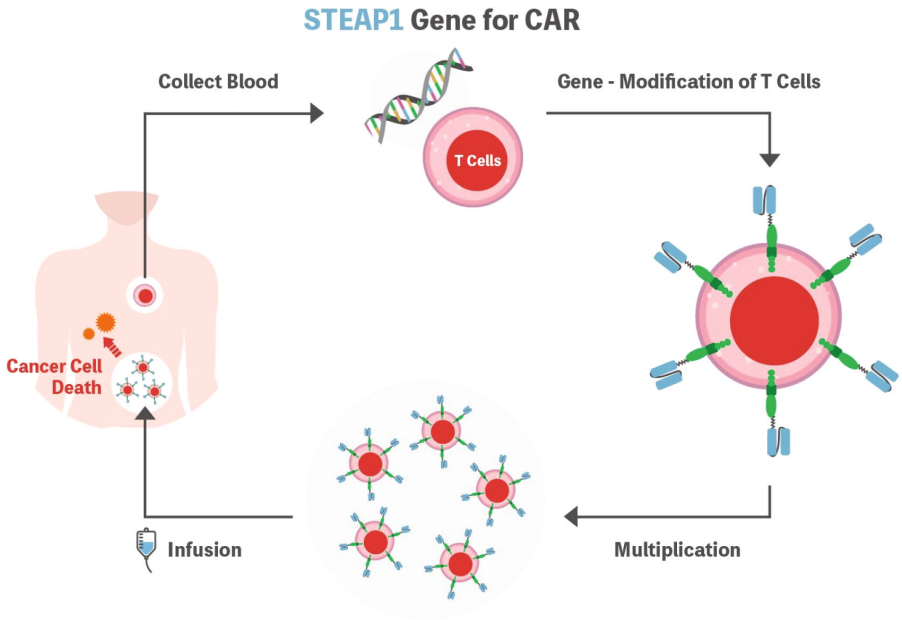


FIGURE 2
Schematic representation of the STEAP1 CAR-T cell. T cells are isolated from the patient's blood and genetically modified to express CAR. Subsequently, cells are expanded ex vivo and then infused into the patient's body to fight cancer cells. STEAP1 could be an attractive target as it is expressed in many cancer types. STEAP1, the six-transmembrane epithelial antigen of prostate 1; CAR, chimeric antigen receptor.

*in vivo* (49). Thus, STEAP1-specific TCRs could be useful for STEAP1-expressing tumors.

Furthermore, due to its specific overexpression in cancer tissues but not in normal tissues, STEAP1 is considered an attractive target for several immunotherapies, including cancer vaccines. Cancer vaccines for STEAP1 have been developed because several epitopes of STEAP1 are recognized by cytotoxic T lymphocytes (CTLs) and successfully evoke the activation of CTLs (50). Although some of these STEAP1-targeted vaccines were well tolerated and successfully evoked immunogenicity, these preclinical observations have yet to translate into clinical success (51, 52).

## 4 Discussion

STEAP1 has been recently investigated in a variety of tumor tissues in addition to prostate cancer. As mentioned in section 2, STEAP1 has an oncogenic role in multiple types of tumors such as prostate cancer, CRC, HCC, gastric cancer, and lung cancer. Conversely, a tumor-suppressive function has also been reported in some types of tumors such as EWS and breast cancer. These inconsistent results suggest multiple roles of STEAP1 in a cancer-dependent manner, which need to be investigated further. Based on our findings and reports from other groups, ROS could be one of the possible factors giving rise to this inconsistency. We previously reported that *STEAP1* silencing contributed to increased ROS levels, which resulted in cell apoptosis in CRC and HCC (19, 25). In contrast, *STEAP1* knockdown decreased ROS levels and *STEAP1* upregulation induced ROS production in EWS (33). In CRC, we hypothesized that the contribution of NRF2 to ROS manipulation was related to STEAP1. In EWS, STAT1 is reported to be a key regulator of ROS production induced by STEAP1. Collectively, it is assumed that multiple pathways exist between STEAP1 and ROS in a cancer-type specific manner. Furthermore, ROS has a dual role in cancer cell pathophysiology. At low to moderate levels, ROS act as signal transducers demonstrating the oncogenic properties in cancer cells. In contrast, excessive levels of ROS cause damage to cancer cells, leading to cell death. Therefore, evaluating the cell's responsiveness to ROS depending on cancer types may also be crucial to assess the relationship between STEAP1 and ROS.

As discussed in section 3, STEAP1 is an ideal target of cancer treatment because it is located on the cell surface and is specifically expressed in various types of cancer. In this review, we mentioned different types of STEAP1 targeted therapy, including antibody therapy, CAR-T therapy, TCR-T therapy, and cancer vaccines. The results of these therapies are promising, and the diagnostic roles of STEAP1 such as in liquid biopsy in prostate cancer have also been reported recently (16). Although most of the research related to STEAP1 was conducted in prostate cancer, we believe that STEAP1 could also be an ideal target in other types of malignant tumors as growing evidence has revealed the overexpression of STEAP1 in cancerous cells compared to the normal counterpart. However, therapeutic or diagnostic strategies targeting STEAP1 have not been applied in clinical settings. Thus, large clinical trials are warranted in addition to further investigation of the role of STEAP1 at the molecular level.

## 5 Conclusion

In this review, we summarized the oncogenic functions of STEAP1 and several potential therapeutic strategies targeting STEAP1. Growing evidence has revealed that STEAP1 is an ideal target for cancer therapy. Further efforts are warranted to apply STEAP1 targeted therapy in a clinical setting.

## Author contributions

HN: Writing – original draft, Writing – review & editing. YA: Writing – original draft, Writing – review & editing. KT: Writing – original draft, Writing – review & editing.

## Funding

The author(s) declare financial support was received for the research, authorship, and/or publication of this article. This work was supported in part by the Japan Society for the Promotion of Science (grants C/19K08397, C/16K07178 to KT).

## Conflict of interest

KT received lecture fee from Daiichi Sankyo.

The remaining authors declare that the research was conducted in the absence of any commercial or financial relationships that could be constructed as a potential conflict of interest.

## Publisher's note



## Supplementary material

The Supplementary Material for this article can be found online at: https://www.frontiersin.org/articles/10.3389/fonc.2023.1285661/full#supplementary-material

## References

1. Sung H, Ferlay J, Siegel RL, Laversanne M, Soerjomataram I, Jemal A, et al. Global cancer statistics 2020: GLOBOCAN estimates of incidence and mortality worldwide for 36 cancers in 185 countries. *CA Cancer J Clin* (2021) 71:209–49. doi: 10.3322/caac.21660

2. Hubert RS, Vivanco I, Chen E, Rastegar S, Leong K, Mitchell SC, et al. STEAP: a prostate-specific cell-surface antigen highly expressed in human prostate tumors. *Proc Natl Acad Sci U.S.A.* (1999) 96:14523–8. doi: 10.1073/pnas.96.25.14523

3. Moreaux J, Kassambara A, Hose D, Klein B. STEAP1 is overexpressed in cancers: a promising therapeutic target. *Biochem Biophys Res Commun* (2012) 429:148–55. doi: 10.1016/j.bbrc.2012.10.123

4. Barroca-Ferreira J, Pais JP, Santos MM, Goncalves AM, Gomes IM, Sousa I, et al. Targeting STEAP1 protein in human cancer: current trends and future challenges. *Curr Cancer Drug Targets* (2018) 18:222–30. doi: 10.2174/1568009617666170427103732

5. Tang Z, Li C, Kang B, Gao G, Li C, Zhang Z. GEPIA: a web server for cancer and normal gene expression profiling and interactive analyses. *Nucleic Acids Res* (2017) 45: W98–W102. doi: 10.1093/nar/gkx247

6. Danila DC, Szmulewitz RZ, Vaishampayan U, Higano CS, Baron AD, Gilbert HN, et al. Phase I study of DSTP3086S, an antibody-drug conjugate targeting six-transmembrane epithelial antigen of prostate 1, in metastatic castration-resistant prostate cancer. *J Clin Oncol* (2019) 37:3518–27. doi: 10.1200/JCO.19.00646

7. Jin Y, Lorvik KB, Jin Y, Beck C, Sike A, Persiconi I, et al. Development of STEAP1 targeting chimeric antigen receptor for adoptive cell therapy against cancer. *Mol Ther Oncolytics* (2022) 26:189–206. doi: 10.1016/j.omto.2022.06.007

8. Gomes IM, Maia CJ, Santos CR. STEAP proteins: from structure to applications in cancer therapy. *Mol Cancer Res* (2012) 10:573–87. doi: 10.1158/1541-7786.MCR-11-0281

9. Oosterheert W, Gros P. Cryo-electron microscopy structure and potential enzymatic function of human six-transmembrane epithelial antigen of the prostate 1 (STEAP1). *J Biol Chem* (2020) 295:9502–12. doi: 10.1074/jbc.RA120.013690

10. Bhatia V, Kamat NV, Pariva TE, Wu LT, Tsao A, Sasaki K, et al. Targeting advanced prostate cancer with STEAP1 chimeric antigen receptor T cell and tumor-localized IL-12 immunotherapy. *Nat Commun* (2023) 14:2041. doi: 10.1038/s41467-023-37874-2

11. Gomes IM, Arinto P, Lopes C, Santos CR, Maia CJ. STEAP1 is overexpressed in prostate cancer and prostatic intraepithelial neoplasia lesions, and it is positively associated with Gleason score. *Urol Oncol* (2014) 32:53.e23–9. doi: 10.1016/j.urolonc.2013.08.028

12. Ihlaseh-Catalano SM, Drigo SA, de Jesus CM, Domingues MA, Trindade Filho JC, de Camargo JL, et al. STEAP1 protein overexpression is an independent marker for biochemical recurrence in prostate carcinoma. *Histopathology* (2013) 63:678–85. doi: 10.1111/his.12226

13. Gomes IM, Rocha SM, Gaspar C, Alvelos MI, Santos CR, Socorro S, et al. Knockdown of STEAP1 inhibits cell growth and induces apoptosis in LNCaP prostate cancer cells counteracting the effect of androgens. *Med Oncol* (2018) 35:40. doi: 10.1007/s12032-018-1100-0

14. Challita-Eid PM, Morrison K, Etessami S, An Z, Morrison KJ, Perez-Villar JJ, et al. Monoclonal antibodies to six-transmembrane epithelial antigen of the prostate-1 inhibit intercellular communication in *vitro* and growth of human tumor xenografts in vivo. *Cancer Res* (2007) 67:5798–805. doi: 10.1158/0008-5472.CAN-06-3849

15. Burnell SEA, Spencer-Harty S, Howarth S, Bodger O, Kynaston H, Morgan C, et al. Utilisation of the STEAP protein family in a diagnostic setting may provide a more comprehensive prognosis of prostate cancer. *PloS One* (2019) 14:e0220456. doi: 10.1371/journal.pone.0220456

16. Khanna K, Salmond N, Lynn KS, Leong HS, Williams KC. Clinical significance of STEAP1 extracellular vesicles in prostate cancer. *Prostate Cancer Prostatic Dis* (2021) 24:802–11. doi: 10.1038/s41391-021-00319-2

17. Pinsky PF, Parnes H. Screening for prostate cancer. *N Engl J Med* (2023) 388:1405–14. doi: 10.1056/NEJMcp2209151

18. Quinlan MR, Bolton D, Casey RG. The management of rectal bleeding following transrectal prostate biopsy: a review of the current literature. *Can Urol Assoc J* (2018) 12:E146–53. doi: 10.5489/cuaj.4660

19. Nakamura H, Takada K, Arihara Y, Hayasaka N, Murase K, Iyama S, et al. Six-transmembrane epithelial antigen of the prostate 1 protects against increased oxidative stress via a nuclear erythroid 2-related factor pathway in colorectal cancer. *Cancer Gene Ther* (2019) 26:313–22. doi: 10.1038/s41417-018-0056-8

20. Motohashi H, Yamamoto M. Nrf2-Keap1 defines a physiologically important stress response mechanism. *Trends Mol Med* (2004) 10:549–57. doi: 10.1016/j.molmed.2004.09.003

21. Kansanen E, Kuosmanen SM, Leinonen H, Levonen AL. The Keap1-Nrf2 pathway: mechanisms of activation and dysregulation in cancer. *Redox Biol* (2013) 1:45–9. doi: 10.1016/j.redox.2012.10.001

22. Rocha SM, Nascimento D, Coelho RS, Cardoso AM, Passarinha LA, Socorro S, et al. STEAP1 knockdown decreases the sensitivity of prostate cancer cells to paclitaxel, docetaxel and cabazitaxel. *Int J Mol Sci* (2023) 24:6643. doi: 10.3390/ijms24076643

23. Dolezal JM, Wang H, Kulkarni S, Jackson L, Lu J, Ranganathan S, et al. Sequential adaptive changes in a c-Myc-driven model of hepatocellular carcinoma. *J Biol Chem* (2017) 292:10068–86. doi: 10.1074/jbc.M117.782052

24. Zheng K, Cubero FJ, Nevzorova YA. c-MYC-making liver sick: role of c-MYC in hepatic cell function, homeostasis and disease. *Genes (Basel)* (2017) 8:123. doi: 10.3390/genes8040123

25. Iijima K, Nakamura H, Takada K, Hayasaka N, Kubo T, Umeyama Y, et al. Six-transmembrane epithelial antigen of the prostate 1 accelerates cell proliferation by targeting c-Myc in liver cancer cells. *Oncol Lett* (2021) 22:546. doi: 10.3892/ol.2021.12807

26. Zhang Z, Hou WB, Zhang C, Tan YE, Zhang DD, An W, et al. A research of STEAP1 regulated gastric cancer cell proliferation, migration and invasion *in vitro* and in *vivo*s. *J Cell Mol Med* (2020) 24:14217–30. doi: 10.1111/jcmm.16038

27. Wu YY, Jiang JN, Fang XD, Ji FJ. STEAP1 regulates tumorigenesis and chemoresistance during peritoneal metastasis of gastric cancer. *Front Physiol* (2018) 9:1132. doi: 10.3389/fphys.2018.01132

28. Guo Q, Ke XX, Liu Z, Gao WL, Fang SX, Chen C, et al. Evaluation of the prognostic value of STEAP1 in lung adenocarcinoma and insights into its potential molecular pathways via bioinformatic analysis. *Front Genet* (2020) 11:242. doi: 10.3389/fgene.2020.00242

29. Liu T, Niu X, Li Y, Xu Z, Chen J, Xu G. Expression and prognostic analyses of the significance of STEAP1 and STEAP2 in lung cancer. *World J Surg Oncol* (2022) 20:96. doi: 10.1186/s12957-022-02566-6

30. Zhuang X, Herbert JM, Lodhia P, Bradford J, Turner AM, Newby PM, et al. Identification of novel vascular targets in lung cancer. *Br J Cancer* (2015) 112:485–94. doi: 10.1038/bjc.2014.626

31. Huo SF, Shang WL, Yu M, Ren XP, Wen HX, Chai CY, et al. STEAP1 facilitates metastasis and epithelial-mesenchymal transition of lung adenocarcinoma via the JAK2/STAT3 signaling pathway. *Biosci Rep* (2020) 40:BSR20193169. doi: 10.1042/BSR20193169

32. Riggi N, Suvà ML, Stamenkovic I. Ewing's sarcoma. *N Engl J Med* (2021) 384:154–64. doi: 10.1056/NEJMra2028910

33. Grunewald TG, Diebold I, Esposito I, Plehm S, Hauer K, Thiel U, et al. STEAP1 is associated with the invasive and oxidative stress phenotype of Ewing tumors. *Mol Cancer Res* (2012) 10:52–65. doi: 10.1158/1541-7786.MCR-11-0524

34. Grunewald TGP, Ranft A, Esposito I, da Silva-Buttkus P, Aichler M, Baumhoer D, et al. High STEAP1 expression is associated with improved outcome of Ewing's sarcoma patients. *Ann Oncol* (2012) 23:2185–90. doi: 10.1093/annonc/mdr605

35. Markey FB, Romero B, Parashar V, Batish M. Identification of a new transcriptional co-regulator of STEAP1 in ewing's sarcoma. *Cells* (2021) 10:1300. doi: 10.3390/cells10061300

36. Owen LA, Kowalewski AA, Lessnick SL. EWS/FLI mediates transcriptional repression via NKX2.2 during oncogenic transformation in Ewing's sarcoma. *PloS One* (2008) 3:e1965. doi: 10.1371/journal.pone.0001965

37. Zhao C, Xiong K, Ji Z, Liu F, Li X. The prognostic value and immunological role of STEAP1 in pan-cancer: A result of data-based analysis. *Oxid Med Cell Longev* (2022) 2022:8297011. doi: 10.1155/2022/8297011

38. Xie J, Yang Y, Sun J, Jiao Z, Zhang H, Chen J. STEAP1 inhibits breast cancer metastasis and is associated with epithelial-mesenchymal transition procession. *Clin Breast Cancer* (2019) 19:e195–207. doi: 10.1016/j.clbc.2018.08.010

39. Wu HT, Chen WJ, Xu Y, Shen JX, Chen WT, Liu J. The tumor suppressive roles and prognostic values of STEAP family members in breast cancer. *BioMed Res Int* (2020) 2020:9578484. doi: 10.1155/2020/9578484

40. Slaney CY, Wang P, Darcy PK, Kershaw MH. CARs versus biTEs: A comparison between T cell-redirection strategies for cancer treatment. *Cancer Discovery* (2018) 8:924–34. doi: 10.1158/2159-8290.CD-18-0297

41. Goebeler ME, Bargou RC. T cell-engaging therapies - BiTEs and beyond. *Nat Rev Clin Oncol* (2020) 17:418–34. doi: 10.1038/s41571-020-0347-5

42. Lin TY, Park JA, Long A, Guo HF, Cheung NV. Novel potent anti-STEAP1 bispecific antibody to redirect T cells for cancer immunotherapy. *J Immunother Cancer* (2021) 9:e003114. doi: 10.1136/jitc-2021-003114

43. Zhang X, Zhu L, Zhang H, Chen S, Xiao Y. CAR-T cell therapy in hematological Malignancies: current opportunities and challenges. *Front Immunol* (2022) 13:927153. doi: 10.3389/fimmu.2022.927153

44. Marofi F, Motavalli R, Safonov VA, Thangavelu L, Yumashev AV, Alexander M, et al. CAR T cells in solid tumors: challenges and opportunities. *Stem Cell Res Ther* (2021) 12:81. doi: 10.1186/s13287-020-02128-1

45. Qi C, Gong J, Li J, Liu D, Qin Y, Ge S, et al. Claudin18.2-specific CAR T cells in gastrointestinal cancers: phase 1 trial interim results. *Nat Med* (2022) 28:1189–98. doi: 10.1038/s41591-022-01800-8

46. Rossi J, Paczkowski P, Shen YW, Morse K, Flynn B, Kaiser A, et al. Preinfusion polyfunctional anti-CD19 chimeric antigen receptor T cells are associated with clinical outcomes in NHL. *Blood* (2018) 132:804–14. doi: 10.1182/blood-2018-01-828343

47. Baulu E, Gardet C, Chuvin N, Depil S. TCR-engineered T cell therapy in solid tumors: state of the art and perspectives. *Sci Adv* (2023) 9:eadf3700. doi: 10.1126/sciadv.adf3700

48. Schirmer D, Grünewald TG, Klar R, Schmidt O, Wohlleber D, Rubío RA, et al. Transgenic antigen-specific, HLA-A*02:01-allo-restricted cytotoxic T cells recognize tumor-associated target antigen STEAP1 with high specificity. *Oncoimmunology* (2016) 5:e1175795. doi: 10.1080/2162402X.2016.1175795

49. Schober SJ, Thiede M, Gassmann H, Prexler C, Xue B, Schirmer D, et al. MHC class I-restricted TCR-transgenic CD4+ T cells against STEAP1 mediate local tumor control of ewing sarcoma in vivo. *Cells* (2020) 9:1581. doi: 10.3390/cells9071581

50. Alves PM, Faure O, Graff-Dubois S, Cornet S, Bolonakis I, Gross DA, et al. STEAP, a prostate tumor antigen, is a target of human CD8+ T cells. *Cancer Immunol Immunother* (2006) 55:1515–23. doi: 10.1007/s00262-006-0165-3

51. Kübler H, Scheel B, Gnad-Vogt U, Miller K, Schultze-Seemann W, Vom Dorp F, et al. Self-adjuvanted mRNA vaccination in advanced prostate cancer patients: a first-in-man phase I/IIa study. *J Immunother Cancer* (2015) 3:26. doi: 10.1186/s40425-015-0068-y

52. Guo L, Xie H, Zhang Z, Wang Z, Peng S, Niu Y, et al. Fusion protein vaccine based on ag85B and STEAP1 induces a protective immune response against prostate cancer. *Vaccines (Basel)* (2021) 9:786. doi: 10.3390/vaccines9070786

frontiers | Frontiers in Oncology

TYPE Mini Review
PUBLISHED 21 December 2023
DOI 10.3389/fonc.2023.1333812



OPEN ACCESS

EDITED BY
Shihori Tanabe,
National Institute of Health Sciences (NIHS), Japan

REVIEWED BY
Prajish Iyer,
City of Hope National Medical Center, United States

*CORRESPONDENCE
Wenjun Deng
wdeng@mgh.harvard.edu
Xinyi Zhang
zhangxinyi80@163.com
Shanye Yin
shanye.yin@einsteinmed.edu

†These authors have contributed equally to this work

RECEIVED 07 November 2023
ACCEPTED 06 December 2023
PUBLISHED 21 December 2023

CITATION
Ye R, Wang A, Bu B, Luo P, Deng W, Zhang X and Yin S (2023) Viral oncogenes, viruses, and cancer: a third-generation sequencing perspective on viral integration into the human genome.
*Front. Oncol.* 13:1333812.
doi: 10.3389/fonc.2023.1333812



# Viral oncogenes, viruses, and cancer: a third-generation sequencing perspective on viral integration into the human genome

Ruichen Ye[1,2,3†], Angelina Wang[4†], Brady Bu[5†], Pengxiang Luo[6], Wenjun Deng[7*], Xinyi Zhang[8*] and Shanye Yin[1,2*]

[1]Department of Pathology, Albert Einstein College of Medicine, Bronx, NY, United States, [2]Einstein Pathology Single-cell & Bioinformatics Laboratory, Bronx, NY, United States, [3]Stony Brook University, Stony Brook, NY, United States, [4]Tufts Friedman School of Nutrition, Boston, MA, United States, [5]Horace Mann School, Bronx, NY, United States, [6]Tongji Medical College, Huazhong University of Science and Technology, Wuhan, China, [7]Clinical Proteomics Research Center, Massachusetts General Hospital, Harvard Medical School, Boston, MA, United States, [8]Department of Respiratory Diseases, The Second Affiliated Hospital of Nanchang University, Nanchang, China

The link between viruses and cancer has intrigued scientists for decades. Certain viruses have been shown to be vital in the development of various cancers by integrating viral DNA into the host genome and activating viral oncogenes. These viruses include the Human Papillomavirus (HPV), Hepatitis B and C Viruses (HBV and HCV), Epstein-Barr Virus (EBV), and Human T-Cell Leukemia Virus (HTLV-1), which are all linked to the development of a myriad of human cancers. Third-generation sequencing technologies have revolutionized our ability to study viral integration events at unprecedented resolution in recent years. They offer long sequencing capabilities along with the ability to map viral integration sites, assess host gene expression, and track clonal evolution in cancer cells. Recently, researchers have been exploring the application of Oxford Nanopore Technologies (ONT) nanopore sequencing and Pacific BioSciences (PacBio) single-molecule real-time (SMRT) sequencing in cancer research. As viral integration is crucial to the development of cancer via viruses, third-generation sequencing would provide a novel approach to studying the relationship interlinking viral oncogenes, viruses, and cancer. This review article explores the molecular mechanisms underlying viral oncogenesis, the role of viruses in cancer development, and the impact of third-generation sequencing on our understanding of viral integration into the human genome.

KEYWORDS

**viral integration, cancer sequencing, third generation sequencing, nanopore, PacBio**

# 1 Introduction

Cancer is a complex and multifaceted disease with genetic alterations playing a central role in its initiation and progression. It is comprised of genetically diverse heterogeneous groups of diseases that are constantly evolving, stretching across populations and individuals (1–6). Throughout the years, several studies, such as the PCAWG Project (7), have investigated these variations or mutations in cancer cells to see the relationship between the genetic changes and their role in cancer (1, 8, 9). Although somatic mutations have traditionally been the focus of cancer genetics, viral infections also contribute significantly to the global cancer burden (10–12). 15.4% of all cancers are attributable to infections and 9.9% are linked to viruses, according to the World Health Organization (WHO). After Helicobacter pylori, the four most prominent infection-related causes of cancer are HPV, HBV, hepatitis C, and EBV. These viruses are widely known to the general population and, with their rising infection rates, are to be a significant matter to raise up. Viruses are part of a multistep pathway of oncogenesis and contribute to the development of cancer (8, 12). Characteristics that can be attributed to the development of cancer through human viruses include the presence and persistence of viral DNA in tumors, growth-promoting activity of viral genes in model systems, malignant phenotype dependence on viral oncogene expression, and epidemiological evidence that viral infection can be a major risk of cancer development (11). Recently, there have been efforts made by the worldwide scientific community to specifically analyze comprehensive genomes and whole transcriptomes from tissue samples from cancer patients. The PCAWG Project, for example, collected whole genome sequencing data from 2,658 cancers in 38 tumor types, most likely from third-generation sequencing, a new and uprising technique being used to sequence genomes (8, 11, 13–15). This review aims to provide an overview of viral oncogenes, their role in cancer, and the recent advancements in third-generation sequencing that have enhanced our ability to study viral integration into the human genome.

# 2 Viral oncogenes and their role in cancer

Viral oncogenes are genes carried by certain viruses that can promote cellular transformation and lead to the development of cancer. These genes are often homologous to cellular proto-oncogenes, but their regulation and expression are altered in infected cells. In these infected cells, normal cell growth control mechanisms are disrupted, and they display uncontrolled proliferation. Tissue-specific functions cease and ultimately lead to the development of cancer. 15-20% of all human cancers have been caused via infection by oncogenic viruses (12). Key viral oncogenes include E6 and E7 from human papillomavirus (HPV), E1A and E1B from adenovirus, and Tax from human T-cell leukemia virus (HTLV-1). These oncogenes disrupt normal cellular processes, such as cell cycle regulation, apoptosis, and DNA repair, leading to uncontrolled cell growth and eventual tumor formation.

## 2.1 Viruses implicated in human cancer

Several viruses have been linked to the development of various cancers. Notable examples include:

### 2.1.1 Human papillomavirus

HPV is a DNA virus associated with cervical, anal, and oropharyngeal cancers. More than half of all malignancies related to infection around the world are caused by HPV, with an incidence of approximately 5% among all cancers worldwide (16–18). HPV16 and HPV18, with less frequency, are involved in a subset of head and neck cancers (HNCs) which are called oropharyngeal squamous cell carcinomas (OPSCCs) (19, 20). The fraction of OPSCCs arising from HPV infection has been around 20%. Integration of HPV DNA into the host genome disrupts tumor suppressor genes and promotes oncogene expression. HPV carries two critical oncogenes: E6 and E7. E6 promotes the degradation of the tumor suppressor protein p53, and E7 disrupts the function of the retinoblastoma protein (pRb), leading to uncontrolled cell division (17, 21, 22). Specifically, hrHPV E6 binds to p53 and promotes its degradation, triggering uncontrolled cell proliferation through cell cycle checkpoint evasion. HPV+ cancer cells have been shown to retain unaltered p53 and pRb genes, which is unlike most human tumors containing mutations in these tumor suppressor genes. Understanding the molecular mechanisms of these oncogenes is crucial for developing targeted therapies against HPV-associated cancers.

### 2.1.2 Hepatitis B and C viruses

Viral hepatitis stemming from the hepatitis B and C viruses is primarily associated with severe health complications, including liver cirrhosis, hepatocellular carcinoma, hepatic fibrosis, and steatosis. Both are considered to be a major healthcare problem and are blood-borne viruses that primarily infect the liver. Hepatitis B is a life-threatening liver disease caused by the highly contagious viral pathogen called hepatitis B virus (HBV) (23–25), which is an enveloped virus belonging to Hepadnavirida. Hepatitis C virus (HCV) is a positive-stranded RNA virus that causes severe liver disorders and is related to Togaviridae or Flaviviridae. It is a small spherical enveloped virion with an icosahedral capsid (26–28). Chronic hepatitis B and C viral infections can result in hepatocellular carcinoma (HCC) through mechanisms involving viral integration and chronic inflammation. Integration of viral DNA into the host genome can cause genomic instability and chronic inflammation, promoting the progression of liver cancer. Studying these viral integration sites and their impact on host genes is essential for identifying potential therapeutic targets. It is crucial to implement preventative strategies and therapies to eradicate chronic infection of HCV and suppress viral replication for HBV (26, 27).

### 2.1.3 Epstein-Barr virus

Epstein-Barr Virus, a member of the herpesvirus family, is associated with several cancers including nasopharyngeal carcinoma, Burkitt's lymphoma, and gastric carcinoma. EBV infects B cells and epithelial cells, maintaining itself in a latent

state in B cells for the lifetime of the host (29–32). The association of EBV with various human cancers has been well-documented. The virus encodes several genes that promote cell growth and inhibit apoptosis, such as LMP1 and EBNA2. LMP1 acts as a constitutively active receptor, activating several signaling pathways leading to cell proliferation and survival. EBNA2, on the other hand, controls the expression of genes promoting B cell growth (33–35). While integration of the EBV genome into the host chromosome isn't common, the expression of its viral oncogenes and their interaction with cellular pathways plays a pivotal role in the development of EBV-associated cancers (36–40).

### 2.1.4 Human T-cell leukemia virus

HTLV-1 is a retrovirus known to cause adult T-cell leukemia/lymphoma (ATL). This virus integrates its DNA into the host genome, leading to the clonal expansion of infected cells (41). HTLV-1 is a key viral oncogene encoding for Tax protein, which can activate a variety of cellular pathways leading to cell proliferation. While the precise factors contributing to the varied outcomes of HTLV-1 infection remain incompletely elucidated, mounting evidence indicates that a intricate interplay between the virus and the host, along with the host's immune response to HTLV-1, likely govern the emergence of HTLV-1-associated diseases (42–44). By disrupting cell cycle regulation and DNA repair mechanisms, Tax promotes genetic instability and the survival of damaged cells, paving the way for leukemogenesis. In some cases, HTLV-1-associated adult T cell leukemia/lymphoma can present with unique clinical manifestations, such as granulomatous pneumocystis jiroveci pneumonia and hypercalcemia.

## 2.2 Viral integration into the human genome

The contribution of viruses to carcinogenesis has been a topic of profound significance in the realm of cancer biology. Central to this paradigm is the mechanism through which viruses integrate their DNA into the human genome (45–47). Such integration events play a pivotal role in the life cycle of oncogenic viruses, often precipitating a cascade of cellular disruptions that culminate in tumorigenesis. Timely identification of these human-infecting viruses is crucial for understanding their role in carcinogenesis and for implementing appropriate interventions (48). Recent advancements have enabled rapid identification of such viruses, providing a more comprehensive understanding of their implications in human health.

### 2.2.1 Mechanisms of viral integration

Viral integration into the host genome is not a random event. Research has shown that integration sites often cluster with fragile sites in the genome, which may have implications for the activation of proto-oncogenes. It is orchestrated through a repertoire of intricate mechanisms, including non-homologous end joining (NHEJ) and microhomology-mediated end joining (MMEJ). The precise loci of these integration events can significantly differ across instances, determining the severity of genetic disruption and subsequent activation of oncogenes. Delving into the specific mechanisms employed by different viruses helps elucidate their unique contributions to cancer.

### 2.2.2 Consequences of viral integration

Once viruses find their way into the human genome, their repercussions on cellular machinery are multifaceted: The integration of the viral genome into the host can be seen as a double-edged sword, with both benefits and detriments for both parties. Activation of Cellular Oncogenes: Viral DNA, when integrated, can strategically position viral enhancers or promoters in proximity to cellular proto-oncogenes. This can lead to the aberrant activation of genes like MYC in the case of HPV-associated cervical cancers, accelerating the journey to tumorigenesis. Disruption of Regulatory Elements and Pathways: Beyond the activation of proto-oncogenes, viral integration can also disrupt host genes, alter regulatory elements, or introduce novel oncogenes. Such disruptions can skew gene expression, compromise cellular function, and enhance cellular growth or survival tendencies. Inactivation of Tumor Suppressor Genes: Notably, viruses also have the ability to incapacitate tumor suppressor genes, such as TP53 and PTEN. The loss of these sentinels of cellular regulation paves the way for uncontrolled growth and genomic instability.

### 2.2.3 Viral-induced genomic instability and clonal evolution

The integration of viral DNA into the host genome can lead to genomic instability, fostering an environment ripe for mutations. Certain viruses can directly induce DNA damage through their replication processes, leading to genomic instability. Viruses may interfere with host DNA repair mechanisms, compromising genome stability. This interference can result in the accumulation of DNA mutations, which are critical for clonal evolution. As these mutations accumulate, as the immune system exerts selective pressure on viral variants, certain cell clones with conferred growth advantages may begin to dominate the tumor landscape. Over time, the tumor evolves, becoming a heterogeneous entity teeming with sub-clones, each potentially harboring distinct viral integration patterns. In the context of antiviral therapy, viral-induced genomic instability can contribute to the emergence of drug-resistant viral strains. Understanding the dynamics of clonal evolution is essential for designing effective therapeutic strategies. Developing strategies to interfere with viral integration or eliminate integrated viral genomes could be a promising approach to reduce viral-induced genomic instability and its associated pathologies.

# 3 Third-generation sequencing technologies and viral integration

The genomic landscape of cancer has been revolutionized by advancements in sequencing technologies (13, 49). A significant facet of this change has been brought about by third-generation sequencing technologies, which illuminate the dynamics of viral

integration into the human genome (50–52). Long-read sequencing allowed the sequencing of chimeric reads, incorporating both viral DNA and the host genome fragments on either side (53). This aids in detecting multiple clonal integration events and uncovering key features of viral integration in the cancer genome. The promise of these technologies lies in their capability to offer extended read lengths, real-time sequencing, and unprecedented resolution, all of which are pivotal in studying the intricate relationships between viral oncogenes, viruses, and cancer (54–57).

## 3.1 Pacific biosciences sequencing

PacBio sequencing has emerged as a pioneering technology in genomics, particularly for its unique capabilities in generating long reads. This groundbreaking approach enables researchers to delve deeper into the complexities of genomes, transcriptomes, and epigenomes, unlocking a wealth of biological information that was previously challenging to access. One of the standout features of PacBio sequencing is the ability to produce exceptionally long reads, often spanning thousands to tens of thousands of base pairs. This stands in stark contrast to short-read sequencing technologies, allowing for the detection of structural variants, complex genomic rearrangements, and complete characterization of repetitive regions that were previously elusive. Such extended read lengths are especially advantageous in the context of viral-related tumors, as they facilitate the precise mapping of viral integration sites within the human genome, offering a deeper understanding of the molecular events underpinning tumorigenesis. Moreover, PacBio sequencing excels in deciphering the epigenetic landscape through the analysis of DNA modifications, offering insights into the role of DNA methylation and histone modifications in viral-related tumors (58, 59). These capabilities make PacBio sequencing an invaluable tool for unraveling the intricacies of viral oncogenesis and hold significant promise for the development of advanced diagnostic and therapeutic strategies in the field of cancer research.

## 3.2 Nanopore sequencing

Another formidable player in the third-generation sequencing realm is nanopore sequencing, which involves the passage of DNA or RNA molecules through nanometer-sized pores, enabling real-time monitoring of nucleotide sequences (60–63). Its advantages include long-read capabilities, portability, and the potential for direct RNA sequencing. Beyond the capability to provide long reads, nanopore sequencing is distinctive due to its real-time, single-molecule sequencing of DNA strands. For studies central to viral integration, this technology holds promise by allowing direct observation of the integration process. Such insights grant researchers the capability to identify structural variants that have arisen due to viral integration, providing a more comprehensive understanding of the process. Nanopore sequencing has been instrumental in characterizing the integration patterns of the HPV genome into host DNA, providing insights into the molecular events driving cervical cancer (52, 64–66). Importantly, the study showed that within the same sample, separate integration events often clustered closely, with partial overlap at different breakpoints (52, 65).

## 3.3 Implications on epigenetics and functional genomics

Third-generation sequencing technologies, when juxtaposed with functional genomics methodologies like RNA-seq and chromatin immunoprecipitation sequencing (ChIP-seq), forge a powerful toolset. In the context of investigating CpG methylation in novel and existing transposable element (TE) insertions, both Oxford Nanopore Technologies and PacBio long-read sequencing techniques offer valuable capabilities (60, 67, 68). These sequencing platforms enable the analysis of CpG methylation patterns within TE insertions in a comprehensive and detailed manner. Specifically, researchers can employ ONT and PacBio long-read sequencing to capture long sequences and comprehensively cover TE insertions, many of which can be extensive and complex. Moreover, these long sequencing technologies can resolve methylation patterns and allow for precise mapping of CpG methylation, providing important insights into the epigenetic alterations associated with tumorigenesis and other biological processes (69, 70). This combination enables researchers to probe deeper, investigating the ramifications of viral integration on host gene expression, epigenetic shifts, and chromatin configurations. It is this intersection of technologies that holds the potential to unravel the mechanisms steering viral oncogenesis. Moreover, as sequencing technologies evolve, so do the methods for virus detection. Current and emerging molecular and immunological methods are expanding the toolkit for researchers, allowing for more comprehensive and accurate identification of viruses in various samples.

## 3.4 Analysis of HPV integration

Recent progress in sequencing technology has led to the capability of producing exceptionally long reads, averaging around 100 kb. This advancement includes the generation of high-throughput, full-length mRNA or cDNA reads and the construction of genomic contigs exceeding 100 Mb. However, this technological leap presents a challenge: existing alignment programs are either incapable or inefficient in handling such extensive data, highlighting the urgent need for new, more capable alignment algorithms. The field of bioinformatics has been evolving rapidly to meet these demands, with significant strides made in the development of alignment methods for long sequencing reads. These methods are particularly adept at chimeric sequence-aware alignment, crucial for identifying reads that align with both human and viral reference genomes – a key process in understanding pathogen-host interactions and disease mechanisms.

One standout tool in this domain is Minimap2 (71), a versatile alignment program designed to map DNA or long mRNA sequences against extensive reference databases. Alongside Minimap2, other notable aligners have emerged, including desalt

(72), which is tailored for aligning long DNA or mRNA sequences. Additionally, tools originally developed for short reads are being adapted and enhanced for the unique challenges posed by error-prone long reads. This includes TAGET (73) and a newly adapted mode of the STAR aligner (73). These improvements reflect the ongoing evolution of bioinformatics tools, ensuring they remain at the forefront of managing and interpreting the burgeoning data from next-generation sequencing technologies.

## 4 Discussion

Viral-induced genomic instability and clonal evolution represent an intricate and multifaceted aspect of viral infections. Understanding the mechanisms and consequences of this phenomenon is essential for the development of effective therapeutic strategies. As our knowledge continues to expand, further research is needed to unveil new insights into this complex relationship and its potential implications for human health. Ultimately, deciphering the interplay between viruses and host genomes will be critical in advancing our ability to prevent and treat viral-associated diseases.

Third-generation sequencing technologies have ushered in a new era in the study of viral-related tumors, offering unprecedented insights into the molecular intricacies of viral oncogenesis. The intricate interplay between viruses, oncogenes, and human cancers remains a vital research frontier, with oncogenic viruses playing an undeniable role in global cancer epidemiology. Our understanding of this dynamic has been immensely enriched by third-generation sequencing technologies, which have cast light on the hitherto elusive mechanisms underlying viral integration into the human genome.

The advent of third generation sequencing has revolutionized our capacity to pinpoint viral integration sites with exceptional resolution, enabling a deeper comprehension of their implications on functional genomics. As the genomic landscape of cancer continually evolves, these technologies provide a dynamic lens, capturing shifts in viral integration sites over time and documenting tumor progression and heterogeneity. The ability to map viral integration sites, study epigenetic modifications, and track clonal evolution provides a multifaceted view of these complex diseases. The practical implications are vast, from innovative diagnostic markers to personalized treatment strategies and the exploration of novel therapeutic targets.

However, the significance of these insights extends beyond the domain of academic research. The translational potential of understanding viral oncogenesis is vast. Recognizing unique viral integration patterns can provide innovative diagnostic markers, heralding early detection and improved patient outcomes. The meticulous mapping of the relationship between viral integration and cellular response can pave the way for novel therapeutic strategies. The insights gained from third-generation sequencing in viral-related tumors hold significant potential for clinical applications. Here are some practical implications: 1) Innovative Diagnostic Markers: Third-generation sequencing can identify unique patterns of viral integration and epigenetic alterations in viral-related tumors. These patterns can serve as innovative diagnostic markers, allowing for the early detection and stratification of cancer subtypes. 2) Personalized Treatment Strategies: Understanding the clonal evolution and heterogeneity of viral-related tumors through third-generation sequencing helps in tailoring personalized treatment approaches. This can lead to more effective therapies and improved patient outcomes. 3) Exploring Novel Therapeutic Targets: The precise characterization of viral oncogenes and their interactions with the host genome can uncover novel therapeutic targets. Inhibiting viral-specific factors can be a promising avenue for targeted cancer therapies.4) Monitoring Treatment Response: Third-generation sequencing can be used to monitor the response of viral-related tumors to treatments over time. This real-time monitoring can guide adjustments in therapeutic strategies and help predict the course of the disease.

As we move forward, addressing the challenges of data analysis, integration with other omics data, validation in clinical settings, and cost considerations will be essential (74, 75). It is also important to integrate these findings with other functional and clinical data. This holistic approach will be essential in realizing the full potential of these insights, from bench to bedside. While third-generation sequencing has brought about remarkable advancements in the study of viral-related tumors, several challenges and future directions warrant attention. 1) Data Analysis and Interpretation: Managing the large volumes of data generated by third-generation sequencing is a considerable challenge. The development of robust bioinformatics tools and analytical pipelines is crucial to extract meaningful insights. 2) Integration with Other Omics Data: A holistic understanding of viral-related tumors often requires the integration of genomic, transcriptomic, proteomic, and epigenomic data. Future research should focus on methods for seamless integration of these multidimensional datasets. 3) Validation in Clinical Settings: To translate the findings from third-generation sequencing into clinical practice, rigorous validation studies are essential. These studies should assess the diagnostic and prognostic utility of the identified markers and therapeutic targets. 4) Cost and Accessibility: While third-generation sequencing technologies have advanced, their cost and accessibility remain barriers to widespread adoption. Efforts to reduce costs and improve accessibility will be instrumental in realizing the full potential of these technologies in clinical settings.

## Author contributions

RY: Conceptualization, Investigation, Writing – original draft, Writing – review & editing. AW: Data curation, Writing – original draft, Writing – review & editing. BB: Investigation, Writing – original draft, Writing – review & editing. PL: Data curation, Writing – review & editing. WD: Conceptualization, Data curation, Formal analysis, Investigation, Methodology, Resources, Software, Supervision, Writing – original draft, Writing – review & editing. XZ: Funding acquisition, Investigation, Methodology, Resources, Supervision, Writing – original draft, Writing – review & editing. SY: Conceptualization, Data curation, Formal analysis, Funding acquisition, Investigation, Resources, Supervision, Writing – original draft, Writing – review & editing, Methodology, Project administration, Software, Validation, Visualization.

## Acknowledgments

This work was in part supported by NIH R21 CA267527-01 (SY) and the Feldstein Medical Foundation grant (SY), Domestic Cooperation Project of the Science and Technology Department of Jiangxi province No. 20212BDH81021 (XZ), Project of the Science and Technology Department of Jiangxi province No.20203BBGL73148 (XZ) and Project of Health Commission of Jiangxi Province No.202210038 (XZ).

## Conflict of interest

WD and SY hold equity in Yihui Bio, Inc.

The remaining authors declare that the research was conducted in the absence of any commercial or financial relationships that could be constructed as a potential conflict of interest.

The author(s) declared that they were an editorial board member of Frontiers, at the time of submission. This had no impact on the peer review process and the final decision.

## Publisher's note



## References

1. Li YL, Roberts ND, Wala JA, Shapira O, Schumacher SE, Kumar K, et al. Patterns of somatic structural variation in human cancer genomes. *Nature* (2020) 578:112. doi: 10.1038/s41586-019-1913-9

2. Sakamoto Y, Sereewattanawoot S, Suzuki A. A new era of long-read sequencing for cancer genomics. *J Hum Genet* (2020) 65:3–10. doi: 10.1038/s10038-019-0658-5

3. Feuk L, Carson AR, Scherer SW. Structural variation in the human genome. *Nat Rev Genet* (2006) 7:85–97. doi: 10.1038/nrg1767

4. Tuzun E, Sharp AJ, Bailey JA, Kaul R, Morrison VA, Pertz LM, et al. Fine-scale structural variation of the human genome. *Nat Genet* (2005) 37:727–32. doi: 10.1038/ng1562

5. Lin YL, Gokcumen O. Fine-scale characterization of genomic structural variation in the human genome reveals adaptive and biomedically relevant hotspots. *Genome Biol Evol* (2019) 11:1136–51. doi: 10.1093/gbe/evz058

6. Yadav S, Hu CL, Nathanson KL, Weitzel JN, Goldgar DE, Kraft P, et al. Germline pathogenic variants in cancer predisposition genes among women with invasive lobular carcinoma of the breast. *J Clin Oncol* (2021) 39:3918. doi: 10.1200/JCO.21.00640

7. Giunta S. Decoding human cancer with whole genome sequencing: a review of PCAWG Project studies published in February 2020. *Cancer Metastasis Rev* (2021) 40:909–24. doi: 10.1007/s10555-021-09969-z

8. Shendure J, Balasubramanian S, Church GM, Gilbert W, Rogers J, Schloss JA, et al. DNA sequencing at 40: past, present and future. *Nature* (2017) 550:345–53. doi: 10.1038/nature24286

9. Manier S, Park J, Capelletti M, Bustoros M, Freeman SS, Ha G, et al. Whole-exome sequencing of cell-free DNA and circulating tumor cells in multiple myeloma. *Nat Commun 9* (2018). doi: 10.1038/s41467-018-04001-5

10. Lawrence MS, Stojanov P, Polak P, Kryukov GV, Cibulskis K, Sivachenko A, et al. Mutational heterogeneity in cancer and the search for new cancer-associated genes. *Nature* (2013) 499:214–8. doi: 10.1038/nature12213

11. Zapatka M, Borozan I, Brewer DS, Iskar M, Grundhoff A, Alawi M, et al. The landscape of viral associations in human cancers. *Nat Genet* (2020) 52:320–30. doi: 10.1038/s41588-019-0558-9

12. Krump NA, You J. Molecular mechanisms of viral oncogenesis in humans. *Nat Rev Microbiol* (2018) 16:684–98. doi: 10.1038/s41579-018-0064-6

13. van Dijk EL, Jaszczyszyn Y, Naquin D, Thermes C. The third revolution in sequencing technology. *Trends Genet* (2018) 34:666–81. doi: 10.1016/j.tig.2018.05.008

14. Wang KC, Chang HY. Epigenomics technologies and applications. *Circ Res* (2018) 122:1191–9. doi: 10.1161/CIRCRESAHA.118.310998

15. Flaherty P, Natsoulis G, Muralidharan O, Winters M, Buenrostro J, Bell J, et al. Ultrasensitive detection of rare mutations using next-generation targeted resequencing. *Nucleic Acids Res 40* (2012). doi: 10.1093/nar/gkr861

16. de Villiers EM, Fauquet C, Broker TR, Bernard HU, zur Hausen HU. Classification of papillomaviruses. *Virology* (2004) 324:17–27. doi: 10.1016/j.virol.2004.03.033

17. zur Hausen H. Papillomaviruses and cancer: From basic studies to clinical application. *Nat Rev Cancer* (2002) 2:342–50. doi: 10.1038/nrc798

18. Gillison ML, D'Souza G, Westra W, Sugar E, Xiao WH, Begum S, et al. Distinct risk factor profiles for human papillomavirus type 16-positive and human papillomavirus type 16-negative head and neck cancers. *Jnci-Journal Natl Cancer Institute* (2008) 100:407–20. doi: 10.1093/jnci/djn025

19. Wakeham K, Kavanagh K, Cuschieri K, Millan D, Pollock KG, Bell S, et al. HPV status and favourable outcome in vulvar squamous cancer. *Int J Cancer* (2017) 140:1134–46. doi: 10.1002/ijc.30523

20. Tuna M, Amos CI. Next generation sequencing and its applications in HPV-associated cancers. *Oncotarget* (2017) 8:8877–89. doi: 10.18632/oncotarget.12830

21. Shen CL, Liu YZ, Shi S, Zhang RY, Zhang T, Xu Q, et al. Long-distance interaction of the integrated HPV fragment with MYC gene and 8q24.22 region upregulating the allele-specific MYC expression in HeLa cells. *Int J Cancer* (2017) 141:540–8. doi: 10.1002/ijc.30763

22. Mirabello L, Yeager M, Yu K, Clifford GM, Xiao YZ, Zhu B, et al. HPV16 E7 genetic conservation is critical to carcinogenesis. *Cell* (2017) 170:1164–74. doi: 10.1016/j.cell.2017.08.001

23. Bouchard MJ, Navas-Martin S, Hepatitis B. and C virus hepatocarcinogenesis: lessons learned and future challenges. *Cancer Lett* (2011) 305:123–43. doi: 10.1016/j.canlet.2010.11.014

24. Guidotti LG, Chisari FV. Immunobiology and pathogenesis of viral hepatitis. *Annu Rev Pathol* (2006) 1:23–61. doi: 10.1146/annurev.pathol.1.110304.100230

25. Chisari FV. Hepatitis B virus transgenic mice: models of viral immunobiology and pathogenesis. *Curr Top Microbiol Immunol* (1996) 206:149–73. doi: 10.1007/978-3-642-85208-4_9

26. Das A, Rivera-Serrano EE, Yin X, Walker CM, Feng Z, Lemon SM. Cell entry and release of quasi-enveloped human hepatitis viruses. *Nat Rev Microbiol* (2023) 21:573–89. doi: 10.1038/s41579-023-00889-z

27. Biswas A, Datta S. Editorial: Origin and evolution of hepatitis viruses, volume II. *Front Microbiol* (2023) 14:1241705. doi: 10.3389/fmicb.2023.1241705

28. Anzola M. Hepatocellular carcinoma: role of hepatitis B and hepatitis C viruses proteins in hepatocarcinogenesis. *J Viral Hepat* (2004) 11:383–93. doi: 10.1111/j.1365-2893.2004.00521.x

29. Heawchaiyaphum C, Ekalaksananan T, Patarapadungkit N, Vatanasapt P, Pientong C. Association of human papillomavirus and epstein-barr virus infection with tonsil cancer in Northeastern Thailand. *Asian Pac J Cancer Prev* (2022) 23:781–7. doi: 10.31557/APJCP.2022.23.3.781

30. Mashaly M, Ghorab D, Hegazy M, Abdelkhalek M, Gaballah K, Elzehery R. Association between epstein-barr virus gene polymorphism and breast cancer risk among Egyptian females. *Asian Pac J Cancer Prev* (2022) 23:641–50. doi: 10.31557/APJCP.2022.23.2.641

31. Tavakoli A, Monavari SH, Solaymani Mohammadi F, Kiani SJ, Armat S, Farahmand M. Association between Epstein-Barr virus infection and gastric cancer: a systematic review and meta-analysis. *BMC Cancer* (2020) 20:493. doi: 10.1186/s12885-020-07013-x

32. Wu SS, Chen B, Fleming CW, Shah AA, Griffith CC, Domb C, et al. Nasopharyngeal cancer: Incidence and prognosis of human papillomavirus and Epstein-Barr virus association at a single North American institution. *Head Neck* (2022) 44:851–61. doi: 10.1002/hed.26976

33. Arias-Calvachi C, Blanco R, Calaf GM, Aguayo F. Epstein-barr virus association with breast cancer: evidence and perspectives. *Biol (Basel)* (2022) 11. doi: 10.3390/biology11060799

34. Carvalho M, de Melo YLF. Association between human papillomavirus and epstein-barr virus infections and cancer of the uterine cervix. *Crit Rev Oncog* (2019) 24:379–83. doi: 10.1615/CritRevOncog.2019031545

35. Gupta I, Al Farsi H, Jabeen A, Skenderi F, Al-Thawadi H, AlAhmad YM, et al. High-risk human papillomaviruses and epstein-barr virus in colorectal cancer and their association with clinicopathological status. *Pathogens* (2020) 9. doi: 10.3390/pathogens9060452

36. Rodriguez H, Zenklusen JC, Staudt LM, Doroshow JH, Lowy DR. The next horizon in precision oncology: Proteogenomics to inform cancer diagnosis and treatment. *Cell* (2021) 184:1661–70. doi: 10.1016/j.cell.2021.02.055

37. Hou YM, Dong J, Liu MY, Yu S. Expression of Epstein-Barr virus-induced gene 3 in cervical cancer: Association with clinicopathological parameters and prognosis. *Oncol Lett* (2016) 11:330–4. doi: 10.3892/ol.2015.3849

38. Patel PD, Alghareeb R, Hussain A, Maheshwari MV, Khalid N. The association of epstein-barr virus with cancer. *Cureus* (2022) 14:e26314. doi: 10.7759/cureus.26314

39. Santos E, Silva M, Canedo NHS, Gaui MFD, Britto A, Silva W, et al. Epstein-Barr virus in gastric cancer and association with 30 bp del-latent membrane protein 1 polymorphism. *Rev Assoc Med Bras (1992)* (2023) 69:e20221571. doi: 10.1590/1806-9282.20221571

40. Zhang WT, Zhu GL, Xu WQ, Zhang W, Wang HZ, Wang YB, et al. Association of PD-1/PD-L1 expression and Epstein–Barr virus infection in patients with invasive breast cancer. *Diagn Pathol* (2022) 17:61. doi: 10.1186/s13000-022-01234-3

41. Miura M, Naito T, Saito M. Current perspectives in human T-cell leukemia virus type 1 infection and its associated diseases. *Front Med (Lausanne)* (2022) 9:867478. doi: 10.3389/fmed.2022.867478

42. Ghobadi MZ, Afsaneh E, Emamzadeh R, Soroush M. Potential miRNA-gene interactions determining progression of various ATLL cancer subtypes after infection by HTLV-1 oncovirus. *BMC Med Genomics* (2023) 16:62. doi: 10.1186/s12920-023-01492-0

43. Valcarcel B, Enriquez-Vera D, De-la-Cruz-Ku G, Chambergo-Michilot D, Calderon-Huaycochea H, Malpica L. Epidemiological features and outcomes of HTLV-1 carriers diagnosed with cancer: A retrospective cohort study in an endemic country. *JCO Glob Oncol* (2023) 9:e2200369. doi: 10.1200/GO.22.00369

44. Zarei Ghobadi M, Afsaneh E, Emamzadeh R. Gene biomarkers and classifiers for various subtypes of HTLV-1-caused ATLL cancer identified by a combination of differential gene co–expression and support vector machine algorithms. *Med Microbiol Immunol* (2023) 212:263–70. doi: 10.1007/s00430-023-00767-8

45. Gao G, Wang JT, Kasperbauer JL, Tombers NM, Teng F, Gou HL, et al. Whole genome sequencing reveals complexity in both HPV sequences present and HPV integrations in HPV-positive oropharyngeal squamous cell carcinomas. *BMC Cancer 19* (2019). doi: 10.1186/s12885-019-5536-1

46. Koneva LA, Zhang YX, Virani S, Hall PB, McHugh JB, Chepeha DB, et al. HPV integration in HNSCC correlates with survival outcomes, immune response signatures, and candidate drivers. *Mol Cancer Res* (2018) 16:90–102. doi: 10.1158/1541-7786.MCR-17-0153

47. Ibragimova M, Tsyganov M, Shpileva O, Churuksaeva O, Bychkov V, Kolomiets L, et al. HPV status and its genomic integration affect survival of patients with cervical cancer. *Neoplasma* (2018) 65:441–8. doi: 10.4149/neo_2018_170414N277

48. Kumar S, Razzaq SK, Vo AD, Gautam M, Li H. Identifying fusion transcripts using next generation sequencing. *Wiley Interdiscip Reviews-Rna* (2016) 7:811–23. doi: 10.1002/wrna.1382

49. Sedlazeck FJ, Lee H, Darby CA, Schatz MC. Piercing the dark matter: bioinformatics of long-range sequencing and mapping. *Nat Rev Genet* (2018) 19:329–46. doi: 10.1038/s41576-018-0003-4

50. Lee JY, Cutts RJ, White I, Augustin Y, Garcia-Murillas I, Fenwick K, et al. Next generation sequencing assay for detection of circulating HPV DNA (cHPV-DNA) in patients undergoing radical (Chemo)Radiotherapy in anal squamous cell carcinoma (ASCC). *Front Oncol* (2020) 10. doi: 10.3389/fonc.2020.00505

51. Mühr LSA, Lagheden C, Eklund C, Lei JY, Nordqvist-Kleppe S, Sparén P, et al. Sequencing detects human papillomavirus in some apparently HPV-negative invasive cervical cancers. *J Gen Virol* (2020) 101:265–70. doi: 10.1099/jgv.0.001374

52. Zhou L, Qiu Q, Zhou Q, Li J, Yu M, Li K, et al. Long-read sequencing unveils high-resolution HPV integration and its oncogenic progression in cervical cancer. *Nat Commun* (2022) 13:2563. doi: 10.1038/s41467-022-30190-1

53. Mitchell K, Brito JJ, Mandric I, Wu QZ, Knyazev S, Chang S, et al. Benchmarking of computational error-correction methods for next-generation sequencing data. *Genome Biol 21* (2020). doi: 10.1186/s13059-020-01988-3

54. Pareek CS, Smoczynski R, Tretyn A. Sequencing technologies and genome sequencing. *J Appl Genet* (2011) 52:413–35. doi: 10.1007/s13353-011-0057-x

55. Mardis ER. The impact of next-generation sequencing technology on genetics. *Trends Genet* (2008) 24:133–41. doi: 10.1016/j.tig.2007.12.007

56. Branton D, Deamer DW, Marziali A, Bayley H, Benner SA, Butler T, et al. The potential and challenges of nanopore sequencing. *Nat Biotechnol* (2008) 26:1146–53. doi: 10.1038/nbt.1495

57. Chan WS, Chan TL, Au CH, Leung CP, To MY, Ng MK, et al. An economical Nanopore sequencing assay for human papillomavirus (HPV) genotyping. *Diagn Pathol* (2020) 15. doi: 10.1186/s13000-020-00964-6

58. Sarkar A, Gasperi W, Begley U, Nevins S, Huber SM, Dedon PC, et al. Detecting the epitranscriptome. *Wiley Interdiscip Reviews-Rna* (2021) 12. doi: 10.1002/wrna.1663

59. Li YY. Modern epigenetics methods in biological research. *Methods* (2021) 187:104–13. doi: 10.1016/j.ymeth.2020.06.022

60. Wang Y, Zheng DL, Tan QL, Wang MX, Gu LQ. Nanopore-based detection of circulating microRNAs in lung cancer patients. *Nat Nanotechnology* (2011) 6:668–74. doi: 10.1038/nnano.2011.147

61. Gu LQ, Wanunu M, Wang MX, McReynolds L, Wang Y. Detection of miRNAs with a nanopore single-molecule counter. *Expert Rev Mol Diagnostics* (2012) 12:573–84. doi: 10.1586/erm.12.58

62. Wylie TN, Wylie KM, Herter BN, Storchl GA. Enhanced virome sequencing using targeted sequence capture. *Genome Res* (2015) 25:1910–20. doi: 10.1101/gr.191049.115

63. Chandrani P, Kulkarni V, Iyer P, Upadhyay P, Chaubal R, Das P, et al. NGS-based approach to determine the presence of HPV and their sites of integration in human cancer genome. *Br J Cancer* (2015) 112:1958–65. doi: 10.1038/bjc.2015.121

64. Li X, Wei X, Liu X, Wang N, Xu F, Liu X, et al. The analysis of HPV integration sites based on nanopore sequencing and the profiling changes along the course of photodynamic therapy. *BMC Cancer* (2023) 23:1052. doi: 10.1186/s12885-023-11538-2

65. Yang WJ, Liu Y, Dong RY, Liu J, Lang JD, Yang JL, et al. Accurate detection of HPV integration sites in cervical cancer samples using the nanopore minION sequencer without error correction. *Front Genet* (2020) 11. doi: 10.3389/fgene.2020.00660

66. Muhr LSA, Lagheden C, Lei JY, Eklund C, Kleppe SN, Sparén P, et al. Deep sequencing detects human papillomavirus (HPV) in cervical cancers negative for HPV by PCR. *Br J Cancer* (2020) 123:1790–5. doi: 10.1038/s41416-020-01111-0

67. Flusberg BA, Webster DR, Lee JH, Travers KJ, Olivares EC, Clark TA, et al. Direct detection of DNA methylation during single-molecule, real-time sequencing. *Nat Methods* (2010) 7:461–U72. doi: 10.1038/nmeth.1459

68. Wallace EVB, Stoddart D, Heron AJ, Mikhailova E, Maglia G, Donohoe TJ, et al. Identification of epigenetic DNA modifications with a protein nanopore. *Chem Commun* (2010) 46:8195–7. doi: 10.1039/c0cc02864a

69. Nebbioso A, Tambaro FP, Dell'Aversana C, Altucci L. Cancer epigenetics: Moving forward. *PloS Genet 14* (2018). doi: 10.1371/journal.pgen.1007362

70. Rivera CM, Ren B. Mapping human epigenomes. *Cell* (2013) 155:39–55. doi: 10.1016/j.cell.2013.09.011

71. Li H. Minimap2: pairwise alignment for nucleotide sequences. *Bioinformatics* (2018) 34:3094–100. doi: 10.1093/bioinformatics/bty191

72. Liu B, Liu Y, Li J, Guo H, Zang T, Wang Y. deSALT: fast and accurate long transcriptomic read alignment with de Bruijn graph-based index. *Genome Biol* (2019) 20:274. doi: 10.1186/s13059-019-1895-9

73. Xia Y, Jin Z, Zhang C, Ouyang L, Dong Y, Li J, et al. TAGET: a toolkit for analyzing full-length transcripts from long-read sequencing. *Nat Commun* (2023) 14:5935. doi: 10.1038/s41467-023-41649-0

74. Olivier M, Asmis R, Hawkins GA, Howard TD, Cox LA. The need for multi-omics biomarker signatures in precision medicine. *Int J Mol Sci 20* (2019). doi: 10.3390/ijms20194781

75. Nagahashi M, Shimada Y, Ichikawa H, Kameyama H, Takabe K, Okuda S, et al. Next generation sequencing-based gene panel tests for the management of solid tumors. *Cancer Sci* (2019) 110:6–15. doi: 10.1111/cas.13837

frontiers | Frontiers in Oncology

TYPE Review
PUBLISHED 04 January 2024
DOI 10.3389/fonc.2023.1324819



OPEN ACCESS

EDITED BY
Guangchuang Yu,
Southern Medical University, China

REVIEWED BY
Huaichao Luo,
Sichuan Cancer Hospital, China
Mehdi Montazer,
Mashhad University of Medical Sciences, Iran

*CORRESPONDENCE
Xiaolong Cheng
chengxl@sxmu.edu.cn
Ting Yan
enntei@hotmail.com

RECEIVED 20 October 2023
ACCEPTED 01 December 2023
PUBLISHED 04 January 2024

CITATION
Wang L, Liu H, Liu Y, Guo S, Yan Z, Chen G, Wu Q, Xu S, Zhou Q, Liu L, Peng M, Cheng X and Yan T (2024) Potential markers of cancer stem-like cells in ESCC: a review of the current knowledge.
*Front. Oncol.* 13:1324819.
doi: 10.3389/fonc.2023.1324819



# Potential markers of cancer stem-like cells in ESCC: a review of the current knowledge

Lu Wang[1,2], Huijuan Liu[1,2], Yiqian Liu[1,2], Shixing Guo[3], Zhenpeng Yan[1,2], Guohui Chen[1,2], Qinglu Wu[1,2], Songrui Xu[1,2], Qichao Zhou[1,2], Lili Liu[1,2], Meilan Peng[1,2], Xiaolong Cheng[1,2]* and Ting Yan[1,2]*

[1]Translational Medicine Research Center, Shanxi Medical University, Taiyuan, Shanxi, China, [2]Key Laboratory of Cellular Physiology of the Ministry of Education, Department of Pathology, Shanxi Medical University, Taiyuan, Shanxi, China, [3]Clinical Laboratory Medicine Centre, Shenzhen Hospital, Southern Medical University, Shenzhen, China

In patients with esophageal squamous cell carcinoma (ESCC), the incidence and mortality rate of ESCC in our country are also higher than those in the rest of the world. Despite advances in the treatment department method, patient survival rates have not obviously improved, which often leads to treatment obstruction and cancer repeat. ESCC has special cells called cancer stem-like cells (CSLCs) with self-renewal and differentiation ability, which reflect the development process and prognosis of cancer. In this review, we evaluated CSLCs, which are identified from the expression of cell surface markers in ESCC. By inciting EMTs to participate in tumor migration and invasion, stem cells promote tumor redifferentiation. Some factors can inhibit the migration and invasion of ESCC via the EMT-related pathway. We here summarize the research progress on the surface markers of CSLCs, EMT pathway, and the microenvironment in the process of tumor growth. Thus, these data may be more valuable for clinical applications.

KEYWORDS

**esophageal squamous cell carcinoma, cancer stem-like cells, EMT, surface markers, microenvironment**

## Introduction

In the past year, esophageal cancer (EC) has increased by 572,000 new cases and 509,000 deaths globally. It ranks seventh in occurrence in all kinds of cancers, which means one of 20 cancer deaths was due to EC (1). Tumor mass is a heterogeneous hierarchy. Most of the cells could no longer differentiate. Only a small set of them has the capacity of self-renewal and could differentiate into malignant cancer cells (2). This small

group of cells is called CSLCs, or tumor-initiating cells (TICs). Theories of CSLCs believe that the poor effect of cancer therapies, which showed relapse and metastasis of cancer cells, might be because of the therapeutic resistance of CSLCs (3, 4). For example, in breast cancer cells, studies show that miR-155 enhances stemness, decitabine (DCA) resistance, and CSLC properties by targeting TSPAN5, which causes TNBC to have an unfortunate forecast (5). Studies by Li et al. showed that single-cell RNA sequencing in hepatocellular carcinoma has produced an abundance of information to validate a panel of cells with cancer stem-like cells' properties (6). In cancer treatment, only the differentiated cells could make a response. However, the surviving CSLCs may differentiate into new cancer cells. CSLCs are thought to be seed cells in the process of tumor formation, control of the occurrence, and metastasis through complex signal transduction (7). In light of this feature, it should be better to target the CSLCs in cancer treatments. The targeted molecules specific to CSLCs became a hot topic in cancer research.

Up to now, a good deal of studies have shown the existence of CSLCs in ESCC, and their functions involve proliferation and tumor growth and even indicate poor prognosis. In this review, that is the reason why we explain recent advances in identification markers of CSLCs and the link between CSLCs and EMT and the immune cell microenvironment. There is a need to create new therapies for CSLCs in ESCC.

## Materials and methods

We followed the PRISMA 2020 rules and applied for our review (8). The articles were carefully reviewed using literature resources such as PubMed service of the US National Library of Medicine and Geen Medical. Search algorithms such as "ESCC", "EMT", "cancer stem-like cells", "marker", "cancer", "tumor", and "pathway" were used in searches. In this review, references to retrieved articles were also filtered for additional data. It is important to note that the studies described in this article did not use any data (Supplementary Figure S1).

## Overview of CSLC marker in ESCC

Studies suggest that focusing on CSLC marker-based treatments might act as a more powerful procedure to take out these recalcitrant cells (9). These markers and some signaling pathways may also serve as targets for the elimination of CSLCs (10). First, Mardani et al. showed that co-articulation of CSLC markers CD133/CXCR4 might have a poor prognosis in osteosarcoma. Meanwhile, CD133/SALL4 has a critical relationship among SALL4 and BMP signal target genes, including SIZN1, VENTX, and DIDO1. It assumes a significant role in tumorigenesis in ESCC (11). Next, for CSLC therapy, SN-38 is a nanocarrier for topoisomerase inhibitors; CD133 is a theoretical CSLC marker; CD133-NPS-SN-38 represses growth development and can dispose CD133-positive cells, which is a potential CSLC-designated treatment (12). Therefore, the exploration of more ESCC-CSLC markers on the surface can provide a basis for the recognizable proof of CSLCs and targeted therapy of CSLCs (Figure 1, green).

Similar to other kinds of solid tumors, several cell surface molecules have been recognized as markers of ESCC-CSLCs. Wang and Yang exhibited that ALDH1-expressing cells are highly invasive metastases in ESCC (13, 14). ALDH1 is accounted for as a marker of normal and malignant stem cells in several lineages. Nuclear expression of ALDH1 is related to lymph hub metastasis and low endurance in ESCC (13–15). Based on this research, the expression of ALDH1 was associated with a poor prognosis in 577 cases of breast cancer (16). CD44 has been utilized as a cell surface marker for stemness, has CD133. It was also confirmed as the CSLC marker in ESCC cell lines (17) that could be utilized to efficiently enrich TICs (17). One study showed cells with $CD44^{High}/CD24^{Low}$, which is a recognized marker for CSLCs in breast cancer (18), have

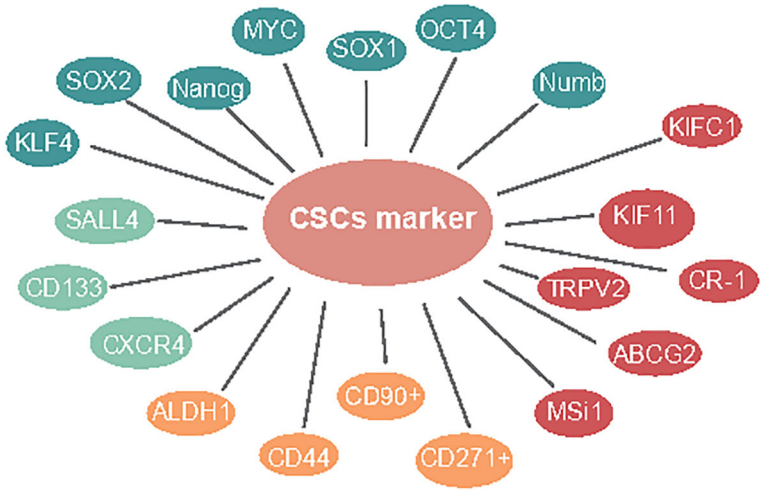


FIGURE 1
Markers in ESCC CSLCs.

been confirmed to possess CSLC properties (19). Additionally, CD90+ cells show an improved capacity for self-renewal, differentiation, and resistance to chemotherapy (20). $CD271^+$ malignant growth cells showed higher sphericity and state-framing limits, high articulation of immature microorganism-related qualities, and protection from chemotherapy (21) (Figure 1, yellow).

CSLC surface markers are important for targeted therapy in ESCC. Similarly, we also believe that regulating genes associated with stem cell markers is important. The inhibition of TRPV2 by low concentrations of Tranilast is more cytotoxic in CSLCs than in the non-CSLC population, indicating that Tranilast could be utilized as a novel targeted therapeutic agent against ESCC-CSLCs (22). ABCG2 (23) and Msi1 (24) overexpression cells were found to represent CSLCs with special harmful potential in ESCC and could regulate the proliferation, apoptosis, sphere formation, and migration ability in spheroid cells (25). Cripto-1-positive ESCC cells were higher stemness-related genes, self-renewal, tumorigenesis, boosting tumor cell migration, invasion, and angiogenesis (26). Moreover, it has been reported that KIFC1 (27) and kinesin family 11 (KIF11) (28) were overexpressed and required for sphere formation in ESCC cells. Interestingly, in cells with Ras-like expression without CAAX1 (RIT1) exogenously overexpressing, the stemness genes, for example, ALDH1, ABCG2, OCT4, CD44, and CXCR4, were significantly downregulated (29) (Figure 1, red).

The green illustrates CD133, CXCR4, and SALL4 presented in a one-paragraph overview in CSLC marker in ESCC. The yellow illustrates ALDH1, CD44, $CD90^+$, and $CD271^+$ presented in a two-paragraph overview of CSLC markers in ESCC. The red illustrates TRPV2, ABCG2, MSi1, CR-1, KIFC1, and KIF11 presented in a three-paragraph overview of CSLC markers in ESCC. The blue illustrates OCT4, SOX1, MYC, Nanog, KLF4, SOX2, and Numb, presented in a four-paragraph overview of CSLC markers in ESCC.

The organic action of CSLCs is controlled by pluripotent record factors like SOX2, MYC, KLF4, OCT4, and Nanog (30). Moreover, studies have shown that pluripotent stem cells could be produced straightforwardly from the fibroblast culture with certain factors, such as Oct3/4, c-MYC, and Sox2 (31). The immature microorganism marker Nanog regulates stem cell differentiation, proliferation, and asymmetric division (32). Du et al. demonstrated the overexpression of Nanog and that a mix of Nanog siRNA with cisplatin showed further improved chemosensitivity in ESCC (33). While SALL4 is obviously increased in cell spheres, which is deemed as an enrichment of CSC-like cells (34), SOX1, a tumor-suppressor gene, was shown to be underexpressed combined with SALL4 overexpression in ESCC and showed a critical role in the inhibition of aggressiveness, indicating the therapeutic potential of the molecule against ESCC-CSLCs (35). Furthermore, the downregulation of the Numb inhibited cell proliferation and expression of CSLC markers (36) (Figure 1, blue).

## EMT pathway and tumor microenvironment in ESCC-CSLC targeting

In addition to marker identifications, studies started to focus on exploring CSC features, such as the tumorigenesis, metastasis, and therapeutic resistance role of CSLCs in ESCC. However, when the tumor metastases, the primary tumor needs to invade the blood vessels, and the distant metastasis needs to activate EMT to dedifferentiate so that the cancer cells can spread and move (37) so that the cancer stem-like cells can migrate and move (38). In addition, cancer-associated EMT results in more migratory cells capable of forming new tumor tissue, indicating increased stemness (38, 39). In that way, whether EMT triggers tumor progression by stimulating CSLC's potential. One study identified that Twist1 is an important transcription factor that upregulates the expression of Oct4 protein and Sox2 protein (40, 41). Knocking down USP4 resulted in a decrease in OCT4 and SOX2 proteins (42). Evolving evidence suggests that CTAs induce EMT and CSLC generation (43). In addition, silencing SRPX2 inhibited cell proliferation and EMT via the Wnt/β-catenin pathway, increasing sensitivity toward cisplatin for ESCC cells (44). Therefore, this article means to sum up the progress of EMT regulatory mechanisms, aiming to elucidate the potential role of EMT in CSLC-targeted therapy and tumor resistance research.

## EMT-associated pathway in CSLCs

EMT-related signaling pathways are involved in the survival, self-renewal, and differentiation of ESCC-CSLCs. These signaling pathways form a network of interlaced signaling media that regulate the growth of CSLCs. The investigation of small-molecule inhibitors of this signal pathway is a functioning area of cancer drug advancement (45). It has been found that the abnormal activation of Notch, NF-κB, and Wnt signaling pathways can result in the proliferation, differentiation, and self-renewal of CSLCs. It is suggested that Notch can induce the growth of CSLCs and maintain the stem cells, which is an effective measure to treat tumors and reverse the drug resistance of tumor chemotherapy. Therefore, the following describes how signaling pathways are regulated.

## TGF-β signaling pathway in ESCC (ESCC)

TGF-β signaling plays a protumor role by promoting EMT, migration, and invasion (46). Relevant studies have shown that knockdown TIP30 can result in EMT via the TGF-B pathway, improving the invasive ability and advancing growth metastasis in *in vivo* and *in vitro* (47). Additionally, MLL2 (48), EGFR (49), and LncRNA SPRY4-IT1 (50) were found to directly promote EMT through the TGF-β pathway in ESCC, which may participate EMT for patients with ESCC through the different mechanisms (51). Meanwhile, UHRF2 and miR-655 were recognized to suppress EMT by the TGF-β pathway (52, 53). Based on research, Tian et al. found that miR-130a-3p suppressed TGF-β-promoted EMT progression in a SMAD4-dependent manner in ESCC (54). Moreover, the PTEN/PI3K/Akt signaling pathway is the major regulator that promotes EMT progress in ESCC. Hence, these should be considered in the strategies against EMT (55–57) (Figure 2).

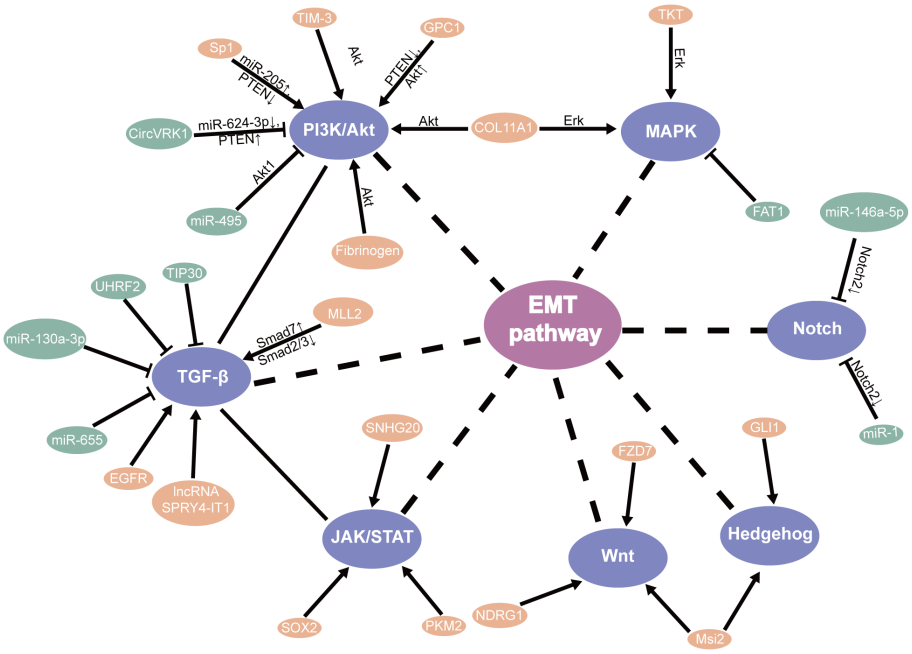


FIGURE 2
EMT-related signaling pathways in ESCC CSLCs.

## PI3K/AKT signaling pathway in ESCC and association with its targeting CSLCs

The PI3K/AKT Signaling pathway has been demonstrated to be essential to the regulator of CSLCs by EMT (30). AKT is a vital individual from the PI3K/AKT signal pathway, which has been shown to promote the progression of multiple cancers, especially in the self-renewal of CSLCs (58).

Recent studies showed that B7H4 (59), TNC (60), and LETM1 (61) were further confirmed to induce CSLC character through the PI3K/AKT pathway. Additionally, miR-664a attenuates stem-cell-associated phenotype and ESCC cell malignancy, in part due to the inactivation of the Akt/GSK-3β/β-catenin pathway through Pitx2 (62). Li et al. also showed that PTEN was also involved in the PI3K/Akt/ABCG2 pathway and regulated the CSLC population of ESCC (63). Further studies have shown that stem cell properties of drug resistance, tumor initiation, an increase of glycolysis, and oxidative phosphorylation are dependent on the Hsp27-AKT-HK2 pathway in ESCC (64). Nevertheless, it upholds the significance of the IGF2-PI3K/AKT-miR-377-CD133 axis in maintaining the malignant growth of CSLCs (65). Interestingly, CD133 has been found downstream of PI3K/AKT/miR-377 to mediate the functions of CSLCs (65). Simultaneously, the PI3K-AKT signaling pathway can upregulate c-MYC, which will promote stemness in ESCC (66) (Figure 3).

In addition, the PI3K/mTOR signal pathway plays a significant part in cell proliferation and survival. Studies have shown that miR-

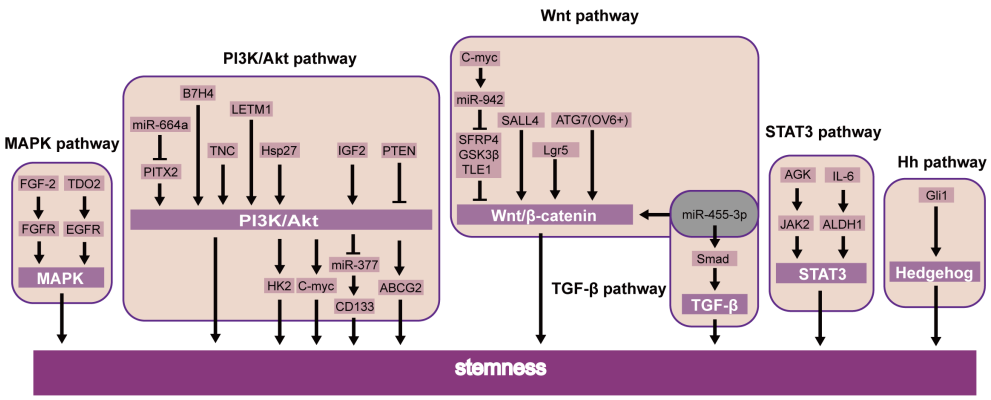


FIGURE 3
Activated and inhibitor pathways in ESCC CSLCs.

495 suppresses proliferation, migration, and invasion in ESCC cells by AKT1 (67). It has been reported and demonstrated that circVRK1 suppressed EMT progression and radioresistance. The possible worth of circVRK1 on ESCC was proposed by miR-624-3p/PTEN and the PI3K/AKT signal pathway (68). Conversely, knockdown of TIM-3 suppressed EMT through the Akt/GSK-3β/Snail pathway in ESCC (69). It was likewise recommended that fibrinogen promoted EMT via the p-AKT/p-mTOR pathway to increase cell motility (70). One study showed that silencing Rab3D inhibited the proliferation by the PI3K/Akt pathway in ESCC (71). Furthermore, Glypican-1 (GPC1), via the regulation of the PTEN/Akt/β-catenin signaling pathways, and Sp1/miR-205 via the PTEN/PI3K/Akt pathway (72) directly enhances EMT in ESCC (73). These discoveries suggested that they might be a new therapeutic target and prognostic biomarker for ESCC through the PI3k/Akt pathway (Figure 2).

## JAK-STAT signaling pathway in ESCC (ESCC) and association with its targeting CSLCs

Moreover, transcription factors likewise prompt the self-renewal of CSLCs via the JAK-STAT signaling pathway. STAT3 is essential for self-renewal in embryonic stem cells (74). Current studies have focused on its role in oncogenesis. In breast cancer, STAT3 induces cell proliferation and maintains CSLC stemness (75). Similarly, the same effect was demonstrated by another group by means of the AGK/JAK2/STAT3 axis. Patients with ESCC had a more limited general endurance and a more terrible sickness-free endurance (76). Interestingly, STAT3β inhibited chemoresistance and stemness through STAT3α (77), which requires further clinical investigations (Figure 3).

The impact of other transcription factors' expression was induced/reduced by cell migration, invasion, and EMT by the JAK-STAT pathway. Gao et al. also concluded that it was associated with SOX2-incited Slug-interceded EMT (78). Moreover, PKM2 promoted the progress of EMT which induced TGF-β1 via phosphorylation STAT3 (79). Furthermore, SNHG20 affects EMT by ATM/JAK/PD-L1 pathway in ESCC (80) (Figure 2).

## MAPK signaling pathway in ESCC and association with its targeting CSLCs

The MAPK pathway responds to multiple input signals as growth factors (75). Research has demonstrated that the MAPK signaling pathway is a valid target for cancer treatment. For example, the best progress has been made in drug targets by the RAS-RAF-MEK-ERK axis (81). Furthermore, some findings indicate that the FGF-2/FGFR (19) and TDO2/EGFR (82) axes were essential factors regulating CSLCs via the MAPK pathway in ESCC. These transcription factors could be potential targets for ESCC through MAPK stemness (Figure 3).

In addition, other factors were shown to modulate the EMT through the MAPK signaling pathway. Our early research suggested inhibition of FAT1 promotes the progression of EMT, which induces the MAPK/ERK pathway in ESCC (83). Meanwhile, relevant research showed that triptolide suppresses cell proliferation, invasion, and migration through the MAPK/ERK pathway in ESCC (84). For example, TKT has been identified as a critical determinant that promotes cell invasion by mediating the EMT process, leading to esophageal cancer (85). Knockdown of COL11A1 inhibited migration and invasion capabilities by EMT (86) (Figure 3).

## Wnt, Hh, and Notch signaling pathways in ESCC and their association with their targeting CSLCs

The Wnt pathway may directly regulate the self-renewal of CSLCs (46). MiR-455-3p can promote chemoresistance and tumorigenesis in ESCC cells through the Wnt/β-catenin pathway and the TGF-β/Smad pathway (87). Taken together, SALL4 (34), Lgr5 (88), and ATG7 (89) can also regulate CSLC proliferation by the Wnt/β-catenin pathway in ESCC. c-Myc combined the miR-942 promoter and suppressed sFRP4, GSK3β, and TLE1, which regulated the Wnt/β-catenin pathway (90). A similar study of CSLCs of patients with esophageal cancer also showed the Hedgehog pathway, a key signaling for stemness maintenance of ESCC cells, played a role in the self-renewal of ESCC-CSLCs based on overexpression of glioma-associated oncogene homolog1 (Gli1) (91). The current study found that the Wnt inhibitor IWP-2 can target the Wnt pathway. Therefore, by inhibiting the Wnt signaling pathway, it can inhibit the growth of CSLC and achieve the goal of treating cancer (92). The above experimental results suggest that these factors may be used as new prognostic biomarkers or therapeutic targets in ESCC (Figure 3).

Aberrant Notch signaling promotes self-renewal and the transfer of mammary stem cells (93). Stearoyl-coa desaturase-1 (SCD1) has been found to be important in the survival of CSLCs. SCD1 inhibitors can significantly reduce the Notch signaling pathway, which further damages CSLC and increases the sensitivity of tumors. Therefore, SCD1 may be a new target in colorectal cancer (94). The Hedgehog pathway assumes a significant part in cancer through EMT (95). Strikingly, increased levels of N-myc-downregulated NDRG1 activated the Wnt pathway and EMT, which decreased the expression of TLE2 and increased β-catenin in ESCC (93). Cao et al. also concluded that FZD7 promoted the progress of EMT through the Wnt/β-catenin pathway in ESCC (96). Additionally, the presence of Msi2 promotes ESCC cell proliferation, between Hedgehog (Hh) and Wnt/β-catenin by EMT pathways (97). Furthermore, the EMT regulator SIP1 is positively regulated by the Hh signal sensor GLI1 (95). On the other hand, Notch2 as the target gene for miR-146a-5p and miR-1 (98) inhibits EMT in ESCC (50). In particular, knockdown of NHE leads to EMT by inhibiting the Notch3 pathway in ESCC (99) (Figure 2).

## The microenvironment associated with EMT in CSLCs

In addition to pathway and transcription factors, EMT-related microenvironments are also noteworthy. CSLCs were regarded as super stem cells and out of control (100). In the tumor microenvironment, inflammatory cells and molecules influence almost every process. Research showed that FBXW7-ZEB2 regulates the drug resistance and migration of tumor cells (101). Chronic tumor-associated inflammation is a marker that stimulates the progression of metastasis in cancer (5). The tumor microenvironment is also essential in EMT. Ionizing radiation is known to induce the self-renewal of CSLCs and promote tumor progression by activating EMT (102). Hypoxia induces EMT, in which only the cancer stem-like cells induce invasion and metastasis (103). CSLC exosomes transported by miR-19b-3p promote cell proliferation and active EMT (104). ALDH1-positive tumors are associated with aggressive tumor growth through EMT and IL-6 increases (105). The cancer microenvironment assumes a significant part in prompting EMTs and keeping up with CSLCs. These studies reveal interactions between different types of cells in the tumor microenvironment and their impact on promoting EMT and enhancing the self-renewal of CSLC. Therefore, there is a bidirectional relationship among tumor microenvironment, EMT, and CSLC, which affect each other and promote the development of tumors and the formation of drug resistance (Figure 4).

# Discussion

CSLCs are believed to be the main cause of the development of most solid tumors and the major factor in drug resistance. Targeting cancer patients with stem cells is promising for the future. Therefore, effective molecular targets for CSLCs must be carefully selected, and the mechanism of the targeted therapy for CSLCs must be thoroughly revealed. This paper reviews the characteristics and identification of CSLCs and discusses the potential targeted therapies for CSLCs. The identification of specific early diagnosis and prognostic CSLC markers in ESCC gives a strategy for the classification of diseases. In order to improve the outcomes of ESCC treatment, new targeted CSLC therapies are also needed. The above provides insights into how ESCC CSLCs initiate cancer and treat resistance and metastasis. At present, drug development for cell signaling has become a new type of chemotherapy. It is worth considering that, despite the focus on key signaling pathways and their potential as a potential treatment strategy, the trial failure rate remains high. Many drugs may work, but they may have different effects for patients at different times. This highlights the importance of precision treatment. The different roles of CSLCs in ESCC emphasize the importance of their related genes as therapeutic targets.

Advances in translational medicine have enabled us to better understand the role and outcomes of cancer therapies. In particular, the introduction of the CSC concept and the link between EMT and

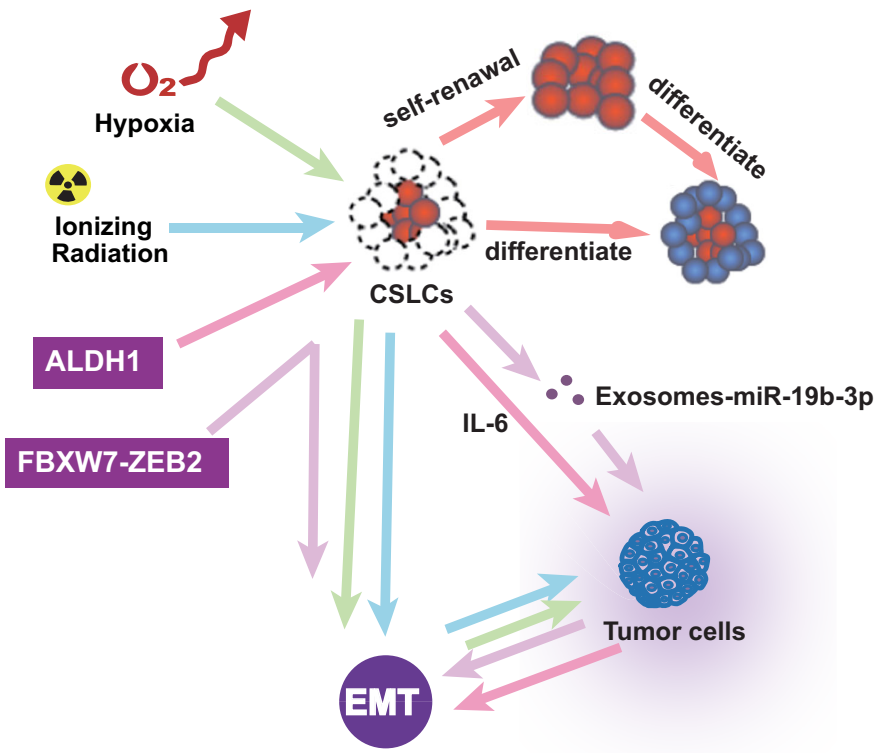


FIGURE 4
The microenvironment associated with EMT in ESCC CSLCs.

CSC provide us with new insights into solving ESCC problems. In addition, EMT may be the main pathway for ESCC cells to obtain the CSC phenotype, which makes it a powerful new target for ESCC treatment. That makes these pathways attractive targets for cancer treatment. Therefore, further study is needed on the association between EMT and CSC in order to use the EMT-CSC link to improve treatment practices.

However, there are still many obstacles to the complete elimination of stem cells. First, stem cells have not yet been accurately identified. Second, some of the current ESCC-CSC studies are in bulk cell research. Due to the limitations of research methods, it is difficult to study the function of related genes in SP. Cell experiments and other *in vitro* experiments cannot fully reflect the changes in the human body. In the context of precision medicine, patients derived from ESCC organoids can serve as a reliable model system for studying tumor evolution and treatment response. Therefore, the development of new methods is very important. Third, in light of the fact that CSLCs additionally share some pathways with normal cells, not all controllers that cause CSLCs are appropriate as focuses for disease treatment. Fourth, we need to pay more attention to the role of natural products targeting CSLCs in research. For example, curcumin cannot only clear cancer cells but also target tumor cells (106). Fifth, related signaling molecules have emerged as potential stem cell therapies. Therefore, multitarget inhibitors will be one of the fundamental techniques to conquer the drug resistance of CSLCs (106). Sixth, CSLC therapy targets the activation or inhibition of stem cells to promote or prevent CSLCs from entering the cell cycle, which is also a problem worth considering (107). Finally, the treatment of cancer with CSLCs as the target is very promising, which is a hot topic at present and needs to be further explored.

## Author contributions

LW: Investigation, Writing – original draft. HL: Data curation, Supervision, Writing – review & editing. YL: Methodology, Supervision, Writing – review & editing. SG: Investigation, Writing – review & editing. ZY: Methodology, Conceptualization, Data curation, Writing – review & editing. GC: Formal analysis, Writing – review & editing. QW: Formal analysis, Writing – review & editing. SX: Formal analysis, Writing – review & editing. QZ: Writing – review & editing, Investigation, Software. LL: Methodology, Writing – review & editing. MP: Methodology, Writing – review & editing. XC: Writing – review & editing, Methodology, Formal analysis, Validation. TY: Conceptualization, Funding acquisition, Writing – review & editing.

## Funding

The author(s) declare financial support was received for the research, authorship, and/or publication of this article. This work was supported by funding from the Research Program of Shanxi Province (20210302123292), the Central Guidance on Local Science and Technology Development Fund of Shanxi Province (YDZJSX2021A018), the Shenzhen Project of Science and Technology (JCYJ20190813094203600), and the innovative project of graduate education in Shanxi province (2022Y366).

## Conflict of interest

The authors declare that the research was conducted in the absence of any commercial or financial relationships that could be construed as a potential conflict of interest.

## Publisher's note



## Supplementary material

The Supplementary Material for this article can be found online at: https://www.frontiersin.org/articles/10.3389/fonc.2023.1324819/full#supplementary-material

## References

1. Bray F, Ferlay J, Soerjomataram I, Siegel RL, Torre LA, Jemal A. Global cancer statistics 2018: GLOBOCAN estimates of incidence and mortality worldwide for 36 cancers in 185 countries. *CA Cancer J Clin* (2018) 68(6):394–424. doi: 10.3322/caac.21492

2. Shackleton M, Quintana E, Fearon ER, Morrison SJ. Heterogeneity in cancer: cancer stem-like cells versus clonal evolution. *Cell* (2009) 138(5):822–9. doi: 10.1016/j.cell.2009.08.017

3. Yang L, Shi P, Zhao G, Xu J, Peng W, Zhang J, et al. Targeting cancer stem cell pathways for cancer therapy. *Signal Transduct Target Ther* (2020) 5(1):8. doi: 10.1038/s41392-020-0110-5

4. Huang T, Song X, Xu D, Tiek D, Goenka A, Wu B, et al. Stem cell programs in cancer initiation, progression, and therapy resistance. *Theranostics* (2020) 10(19):8721–43. doi: 10.7150/thno.41648

5. Yang LW, Wu XJ, Liang Y, Ye GQ, Che YC, Wu XZ, et al. miR-155 increases stemness and decitabine resistance in triple-negative breast cancer cells by inhibiting TSPAN5. *Mol Carcinog* (2020) 59(4):447–61. doi: 10.1002/mc.23167

6. Li XY, Shen Y, Zhang L, Guo X, Wu J. Understanding initiation and progression of hepatocellular carcinoma through single cell sequencing. *Biochim Biophys Acta Rev Cancer* (2022) 1877(3):188720. doi: 10.1016/j.bbcan.2022.188720

7. Clarke MF, Dick JE, Dirks PB, Eaves CJ, Jamieson CH, Jones DL, et al. Cancer stem-like cells–perspectives on current status and future directions: AACR Workshop on cancer stem-like cells. *Cancer Res* (2006) 66(19):9339–44. doi: 10.1158/0008-5472.Can-06-3126

8. Page MJ, McKenzie JE, Bossuyt PM, Boutron I, Hoffmann TC, Mulrow CD, et al. The PRISMA 2020 statement: an updated guideline for reporting systematic reviews. *Bmj* (2021) 372:n71. doi: 10.1136/bmj.n71

9. Wang JH, Huang ST, Zhang L, Liu ZG, Liang RX, Jiang SW, et al. Combined prognostic value of the cancer stem cell markers CD47 and CD133 in ESCC. *Cancer Med* (2019) 8(3):1315–25. doi: 10.1002/cam4.1894

10. Wang D, Plukker JTM, Coppes RP. Cancer stem-like cells with increased metastatic potential as a therapeutic target for esophageal cancer. *Semin Cancer Biol* (2017) 44:60–6. doi: 10.1016/j.semcancer.2017.03.010

11. Assarnia S, Ardalan Khales S, Forghanifard MM. Correlation between SALL4 stemness marker and bone morphogenetic protein signaling genes in ESCC. *J Biochem Mol Toxicol* (2019) 33(3):e22262. doi: 10.1002/jbt.22262

12. Ning ST, Lee SY, Wei MF, Peng CL, Lin SY, Tsai MH, et al. Targeting colorectal cancer stem-like cells with anti-CD133 antibody-conjugated SN-38 nanoparticles. *ACS Appl Mater Interfaces* (2016) 8(28):17793–804. doi: 10.1021/acsami.6b04403

13. Wang Y, Zhe H, Gao P, Zhang N, Li G, Qin J. Cancer stem cell marker ALDH1 expression is associated with lymph node metastasis and poor survival in ESCC: a study from high incidence area of northern China. *Dis Esophagus* (2012) 25(6):560–5. doi: 10.1111/j.1442-2050.2011.01279.x

14. Yang L, Ren Y, Yu X, Qian F, Bian BS, Xiao HL, et al. ALDH1A1 defines invasive cancer stem-like cells and predicts poor prognosis in patients with ESCC. *Mod Pathol* (2014) 27(5):775–83. doi: 10.1038/modpathol.2013.189

15. Ji Y, Li X, Li Y, Zhong Y, Cao J, Xu R, et al. Aldehyde dehydrogenase-1 expression predicts unfavorable outcomes in patients with ESCC. *Anticancer Res* (2016) 36(1):343–9.

16. Ginestier C, Hur MH, Charafe-Jauffret E, Monville F, Dutcher J, Brown M, et al. ALDH1 is a marker of normal and Malignant human mammary stem cells and a predictor of poor clinical outcome. *Cell Stem Cell* (2007) 1(5):555–67. doi: 10.1016/j.stem.2007.08.014

17. Rassouli FB, Matin MM, Bahrami AR, Ghaffarzadegan K, Cheshomi H, Lari S, et al. Evaluating stem and cancerous biomarkers in CD15+CD44+ KYSE30 cells. *Tumour Biol* (2013) 34(5):2909–20. doi: 10.1007/s13277-013-0853-5

18. de Beça FF, Caetano P, Gerhard R, Alvarenga CA, Gomes M, Paredes J, et al. Cancer stem-like cells markers CD44, CD24 and ALDH1 in breast cancer special histological types. *J Clin Pathol* (2013) 66(3):187–91. doi: 10.1136/jclinpath-2012-201169

19. Maehara O, Suda G, Natsuizaka M, Ohnishi S, Komatsu Y, Sato F, et al. Fibroblast growth factor-2-mediated FGFR/Erk signaling supports maintenance of cancer stem-like cells in ESCC. *Carcinogenesis* (2017) 38(11):1073–83. doi: 10.1093/carcin/bgx095

20. Tang KH, Dai YD, Tong M, Chan YP, Kwan PS, Fu L, et al. A CD90(+) tumor-initiating cell population with an aggressive signature and metastatic capacity in esophageal cancer. *Cancer Res* (2013) 73(7):2322–32. doi: 10.1158/0008-5472.Can-12-2991

21. Li S, Yue D, Chen X, Wang L, Li J, Ping Y, et al. Epigenetic regulation of CD271, a potential cancer stem cell marker associated with chemoresistance and metastatic capacity. *Oncol Rep* (2015) 33(1):425–32. doi: 10.3892/or.2014.3569

22. Shiozaki A, Kudou M, Ichikawa D, Fujiwara H, Shimizu H, Ishimoto T, et al. Esophageal cancer stem-like cells are suppressed by tranilast, a TRPV2 channel inhibitor. *J Gastroenterol* (2018) 53(2):197–207. doi: 10.1007/s00535-017-1338-x

23. Hang D, Dong HC, Ning T, Dong B, Hou DL, Xu WG. Prognostic value of the stem cell markers CD133 and ABCG2 expression in ESCC. *Dis Esophagus* (2012) 25 (7):638–44. doi: 10.1111/j.1442-2050.2011.01298.x

24. Moghbeli M, Forghanifard MM, Aarabi A, Mansourian A, Abbaszadegan MR. Clinicopathological sex- related relevance of musashi1 mRNA expression in ESCC patients. *Pathol Oncol Res* (2014) 20(2):427–33. doi: 10.1007/s12253-013-9712-3

25. Qin G, Lian J, Yue D, Chen X, Nan S, Qi Y, et al. Musashi1, a potential prognostic marker in ESCC. *Oncol Rep* (2017) 38(3):1724–32. doi: 10.3892/or.2017.5809

26. Zhang Y, Jin X, Wang Z, Zhang X, Liu S, Liu G. Downregulation of SNHG1 suppresses cell proliferation and invasion by regulating Notch signaling pathway in esophageal squamous cell cancer. *Cancer biomark* (2017) 21(1):89–96. doi: 10.3233/cbm-170286

27. Imai T, Oue N, Yamamoto Y, Asai R, Uraoka N, Sentani K, et al. Overexpression of KIFC1 and its association with spheroid formation in ESCC. *Pathol Res Pract* (2017) 213(11):1388–93. doi: 10.1016/j.prp.2017.09.009

28. Imai T, Oue N, Sentani K, Sakamoto N, Uraoka N, Egi H, et al. KIF11 is required for spheroid formation by oesophageal and colorectal cancer cells. *Anticancer Res* (2017) 37(1):47–55. doi: 10.21873/anticanres.11287

29. Feng YF, Lei YY, Lu JB, Xi SY, Zhang Y, Huang QT, et al. RIT1 suppresses ESCC growth and metastasis and predicts good prognosis. *Cell Death Dis* (2018) 9(11):1085. doi: 10.1038/s41419-018-0979-x

30. Forghanifard MM, Azaraz S, Ardalan Khales S, Morshedi Rad D, Abbaszadegan MR. MAML1 promotes ESCC aggressiveness through upregulation of EMT marker TWIST1. *Mol Biol Rep* (2020) 47(4):2659–68. doi: 10.1007/s11033-020-05356-z

31. Yamasaki S, Taguchi Y, Shimamoto A, Mukasa H, Tahara H, Okamoto T. Generation of human induced pluripotent stem (Ips) cells in serum- and feeder-free defined culture and TGF-B1 regulation of pluripotency. *PloS One* (2014) 9(1):e87151. doi: 10.1371/journal.pone.0087151

32. Derynck R, Weinberg RA. EMT and cancer: more than meets the eye. *Dev Cell* (2019) 49(3):313–6. doi: 10.1016/j.devcel.2019.04.026

33. Du Y, Shi L, Wang T, Liu Z, Wang Z. Nanog siRNA plus Cisplatin may enhance the sensitivity of chemotherapy in esophageal cancer. *J Cancer Res Clin Oncol* (2012) 138(10):1759–67. doi: 10.1007/s00432-012-1253-8

34. He J, Zhou M, Chen X, Yue D, Yang L, Qin G, et al. Inhibition of SALL4 reduces tumorigenicity involving epithelial-mesenchymal transition via Wnt/β-catenin pathway in ESCC. *J Exp Clin Cancer Res* (,(2016) 35(1):98. doi: 10.1186/s13046-016-0378-z

35. Rad A, Esmaeili Dizghandi S, Abbaszadegan MR, Taghechian N, Najafi M, Forghanifard MM. SOX1 is correlated to stemness state regulator SALL4 through progression and invasiveness of ESCC. *Gene* (2016) 594(2):171–5. doi: 10.1016/j.gene.2016.08.045

36. Liu Z, Luo C, Yang W, Wang K, Hu C, Zou J, et al. Increased Numb protein expression predicts poor clinical outcomes in ESCC patients. *Cancer Biol Ther* (2018) 19(1):34–41. doi: 10.1080/15384047.2016.1276131

37. Thiery JP, Acloque H, Huang RY, Nieto MA. Epithelial-mesenchymal transitions in development and disease. *Cell* (2009) 139(5):871–90. doi: 10.1016/j.cell.2009.11.007

38. Brabletz T, Jung A, Spaderna S, Hlubek F, Kirchner T. Opinion: migrating cancer stem-like cells - an integrated concept of Malignant tumour progression. *Nat Rev Cancer* (2005) 5(9):744–9. doi: 10.1038/nrc1694

39. Lüönd F, Sugiyama N, Bill R, Bornes L, Hager C, Tang F, et al. Distinct contributions of partial and full EMT to breast cancer Malignancy. *Dev Cell* (2021) 56(23):3203–3221.e3211. doi: 10.1016/j.devcel.2021.11.006

40. Maia AM, da Silva JH, Mencalha AL, Caffarena ER, Abdelhay E. Computational modeling of the bHLH domain of the transcription factor TWIST1 and R118C, S144R and K145E mutants. *BMC Bioinf* (2012) 13:184. doi: 10.1186/1471-2105-13-184

41. Zhu QQ, Ma C, Wang Q, Song Y, Lv T. The role of TWIST1 in epithelial-mesenchymal transition and cancers. *Tumour Biol* (2016) 37(1):185–97. doi: 10.1007/s13277-015-4450-7

42. Li F, Hu Q, He T, Xu J, Yi Y, Xie S, et al. The deubiquitinase USP4 stabilizes twist1 protein to promote lung cancer cell stemness. *Cancers (Basel)* (2020) 12(6):1582. doi: 10.3390/cancers12061582

43. Salmaninejad A, Zamani MR, Pourvahedi M, Golchehre Z, Hosseini Bereshneh A, Rezaei N. Cancer/testis antigens: expression, regulation, tumor invasion, and use in immunotherapy of cancers. *Immunol Invest* (2016) 45(7):619–40. doi: 10.1080/08820139.2016.1197241

44. He F, Wang H, Li Y, Liu W, Gao X, Chen D, et al. SRPX2 knockdown inhibits cell proliferation and metastasis and promotes chemosensitivity in ESCC. *BioMed Pharmacother* (2019) 109:671–8. doi: 10.1016/j.biopha.2018.10.042

45. Wang Q, Chen X, Hay N. Akt as a target for cancer therapy: more is not always better (lessons from studies in mice). *Br J Cancer* (2017) 117(2):159–63. doi: 10.1038/bjc.2017.153

46. Tripathi V, Shin JH, Stuelten CH, Zhang YE. TGF-β-induced alternative splicing of TAK1 promotes EMT and drug resistance. *Oncogene* (2019) 38(17):3185–200. doi: 10.1038/s41388-018-0655-8

47. Shapira KE, Hirschhorn T, Barzilay L, Smorodinsky NI, Henis YI, Ehrlich M. Dab2 inhibits the cholesterol-dependent activation of JNK by TGF-β. *Mol Biol Cell* (2014) 25(10):1620–8. doi: 10.1091/mbc.E13-09-0537

48. Abudureheman A, Ainiwaer J, Hou Z, Niyaz M, Turghun A, Hasim A, et al. High MLL2 expression predicts poor prognosis and promotes tumor progression by inducing EMT in ESCC. *J Cancer Res Clin Oncol* (2018) 144(6):1025–35. doi: 10.1007/s00432-018-2625-5

49. Sato F, Kubota Y, Natsuizaka M, Maehara O, Hatanaka Y, Marukawa K, et al. EGFR inhibitors prevent induction of cancer stem-like cells in ESCC by suppressing epithelial-mesenchymal transition. *Cancer Biol Ther* (2015) 16(6):933–40. doi: 10.1080/15384047.2015.1040959

50. Wang C, Zhang W, Zhang L, Chen X, Liu F, Zhang J, et al. miR-146a-5p mediates epithelial-mesenchymal transition of oESCC via targeting Notch2. *Br J Cancer* (2016) 115(12):1548–54. doi: 10.1038/bjc.2016.367

51. Pang L, Li Q, Wei C, Zou H, Li S, Cao W, et al. TGF-β1/Smad signaling pathway regulates epithelial-to-mesenchymal transition in ESCC: in *vitro* and clinical analyses of cell lines and nomadic Kazakh patients from northwest Xinjiang, China. *PloS One* (2014) 9(12):e112300. doi: 10.1371/journal.pone.0112300

52. Harazono Y, Muramatsu T, Endo H, Uzawa N, Kawano T, Harada K, et al. miR-655 Is an EMT-suppressive microRNA targeting ZEB1 and TGFBR2. *PloS One* (2013) 8 (5):e62757. doi: 10.1371/journal.pone.0062757

53. Iguchi T, Ueda M, Masuda T, Nambara S, Kidogami S, Komatsu H, et al. Identification of UHRF2 as a negative regulator of epithelial-mesenchymal transition and its clinical significance in ESCC. *Oncology* (2018) 95(3):179–87. doi: 10.1159/000488860

54. Tian X, Fei Q, Du M, Zhu H, Ye J, Qian L, et al. miR-130a-3p regulated TGF-β1-induced epithelial-mesenchymal transition depends on SMAD4 in EC-1 cells. *Cancer Med* (2019) 8(3):1197–208. doi: 10.1002/cam4.1981

55. Bai X, Li YY, Zhang HY, Wang F, He HL, Yao JC, et al. Role of matrix metalloproteinase-9 in transforming growth factor-β1-induced epithelial-mesenchymal transition in ESCC. *Onco Targets Ther* (2017) 10:2837–47. doi: 10.2147/ott.S134813

56. Zhang HY, Wang ZQ, Li YY, Wang F, Zeng QR, Gao Y, et al. Transforming growth factor-β1-induced epithelial-mesenchymal transition in human ESCC via the PTEN/PI3K signaling pathway. *Oncol Rep* (2014) 32(5):2134–42. doi: 10.3892/or.2014.3453

57. Xuan X, Zeng Q, Li Y, Gao Y, Wang F, Zhang H, et al. Akt-mediated transforming growth factor-β1-induced epithelial-mesenchymal transition in cultured human esophageal squamous cancer cells. *Cancer Gene Ther* (2014) 21 (6):238–45. doi: 10.1038/cgt.2014.23

58. Knowles MA, Platt FM, Ross RL, Hurst CD. Phosphatidylinositol 3-kinase (PI3K) pathway activation in bladder cancer. *Cancer Metastasis Rev* (2009) 28(3-4):305–16. doi: 10.1007/s10555-009-9198-3

59. Piao L, Yang Z, Jin J, Ni W, Qi W, Xuan Y. B7H4 is associated with stemness and cancer progression in ESCC. *Hum Pathol* (2018) 80:152–62. doi: 10.1016/j.humpath.2018.05.021

60. Yang Z, Zhang C, Feng Y, Qi W, Cui Y, Xuan Y. Tenascin-C is involved in promotion of cancer stemness via the Akt/HIF1α axis in ESCC. *Exp Mol Pathol* (2019) 109:104239. doi: 10.1016/j.yexmp.2019.03.007

61. Yang Z, Ni W, Cui C, Qi W, Piao L, Xuan Y. Identification of LETM1 as a marker of cancer stem-like cells and predictor of poor prognosis in ESCC. *Hum Pathol* (2018) 81:148–56. doi: 10.1016/j.humpath.2018.07.001

62. Zhang JX, Chen ZH, Xu Y, Chen JW, Weng HW, Yun M, et al. Downregulation of microRNA-644a promotes ESCC aggressiveness and stem cell-like phenotype via dysregulation of PITX2. *Clin Cancer Res* (2017) 23(1):298–310. doi: 10.1158/1078-0432.Ccr-16-0414

63. Li H, Gao Q, Guo L, Lu SH. The PTEN/PI3K/Akt pathway regulates stem-like cells in primary esophageal carcinoma cells. *Cancer Biol Ther* (2011) 11(11):950–8. doi: 10.4161/cbt.11.11.15531

64. Liu CC, Chou KT, Hsu JW, Lin JH, Hsu TW, Yen DH, et al. High metabolic rate and stem cell characteristics of esophageal cancer stem-like cells depend on the Hsp27-AKT-HK2 pathway. *Int J Cancer* (2019) 145(8):2144–56. doi: 10.1002/ijc.32301

65. Xu WW, Li B, Zhao JF, Yang JG, Li JQ, Tsao SW, et al. IGF2 induces CD133 expression in esophageal cancer cells to promote cancer stemness. *Cancer Lett* (2018) 425:88–100. doi: 10.1016/j.canlet.2018.03.039

66. Zhang HF, Wu C, Alshareef A, Gupta N, Zhao Q, Xu XE, et al. The PI3K/AKT/c-MYC axis promotes the acquisition of cancer stem-like features in ESCC. *Stem Cells* (2016) 34(8):2040–51. doi: 10.1002/stem.2395

67. Mao Y, Li L, Liu J, Wang L, Zhou Y. MiR-495 inhibits ESCC progression by targeting Akt1. *Oncotarget* (2016) 7(32):51223–36. doi: 10.18632/oncotarget.9981

68. Jiang Q, Crews LA, Holm F, Jamieson CHM. RNA editing-dependent epitranscriptome diversity in cancer stem-like cells. *Nat Rev Cancer* (2017) 17 (6):381–92. doi: 10.1038/nrc.2017.23

69. Shan B, Man H, Liu J, Wang L, Zhu T, Ma M, et al. TIM-3 promotes the metastasis of ESCC by targeting epithelial-mesenchymal transition via the Akt/GSK-3β/Snail signaling pathway. *Oncol Rep* (2016) 36(3):1551–61. doi: 10.3892/or.2016.4938

70. Zhang F, Wang Y, Sun P, Wang ZQ, Wang DS, Zhang DS, et al. Fibrinogen promotes Malignant biological tumor behavior involving epithelial-mesenchymal transition via the p-AKT/p-mTOR pathway in ESCC. *J Cancer Res Clin Oncol* (2017) 143(12):2413–24. doi: 10.1007/s00432-017-2493-4

71. Zhang J, Kong R, Sun L. Silencing of Rab3D suppresses the proliferation and invasion of ESCC cells. *BioMed Pharmacother* (2017) 91:402–7. doi: 10.1016/j.biopha.2017.04.010

72. Pan F, Mao H, Bu F, Tong X, Li J, Zhang S, et al. Sp1-mediated transcriptional activation of miR-205 promotes radioresistance in ESCC. *Oncotarget* (2017) 8(4):5735–52. doi: 10.18632/oncotarget.13902

73. Li J, Chen Y, Zhan C, Zhu J, Weng S, Dong L, et al. Glypican-1 promotes tumorigenesis by regulating the PTEN/akt/β-catenin signaling pathway in ESCC. *Dig Dis Sci* (2019) 64(6):1493–502. doi: 10.1007/s10620-019-5461-9

74. Matsuda T, Nakamura T, Nakao K, Arai T, Katsuki M, Heike T, et al. STAT3 activation is sufficient to maintain an undifferentiated state of mouse embryonic stem cells. *EMBO J* (1999) 18(15):4261–9. doi: 10.1093/emboj/18.15.4261

75. Kim EK, Choi EJ. Pathological roles of MAPK signaling pathways in human diseases. *Biochim Biophys Acta* (2010) 1802(4):396–405. doi: 10.1016/j.bbadis.2009.12.009

76. Chen X, Ying Z, Lin X, Lin H, Wu J, Li M, et al. Acylglycerol kinase augments JAK2/STAT3 signaling in esophageal squamous cells. *J Clin Invest* (2013) 123(6):2576–89. doi: 10.1172/jci68143

77. Zhang HF, Chen Y, Wu C, Wu ZY, Tweardy DJ, Alshareef A, et al. The opposing function of STAT3 as an oncoprotein and tumor suppressor is dictated by the expression status of STAT3β in ESCC. *Clin Cancer Res* (2016) 22(3):691–703. doi: 10.1158/1078-0432.Ccr-15-1253

78. Gao H, Teng C, Huang W, Peng J, Wang C. SOX2 promotes the epithelial to mesenchymal transition of esophageal squamous cells by modulating slug expression through the activation of STAT3/HIF-α Signaling. *Int J Mol Sci* (2015) 16(9):21643–57. doi: 10.3390/ijms160921643

79. Ma R, Liu Q, Zheng S, Liu T, Tan D, Lu X. PKM2-regulated STAT3 promotes ESCC progression via TGF-β1-induced EMT. *J Cell Biochem* (2019) 120(7):11539–50. doi: 10.1002/jcb.28434

80. Zhang C, Jiang F, Su C, Xie P, Xu L. Upregulation of long noncoding RNA SNHG20 promotes cell growth and metastasis in ESCC via modulating ATM-JAK-PD-L1 pathway. *J Cell Biochem* (2019) 120(7):11642–50. doi: 10.1002/jcb.28444

81. Stylianou S, Clarke RB, Brennan K. Aberrant activation of notch signaling in human breast cancer. *Cancer Res* (2006) 66(3):1517–25. doi: 10.1158/0008-5472.Can-05-3054

82. Pham QT, Oue N, Sekino Y, Yamamoto Y, Shigematsu Y, Sakamoto N, et al. TDO2 Overexpression Is Associated with Cancer stem-like cells and Poor Prognosis in ESCC. *Oncology* (2018) 95(5):297–308. doi: 10.1159/000490725

83. Hu X, Zhai Y, Kong P, Cui H, Yan T, Yang J, et al. FAT1 prevents epithelial mesenchymal transition (EMT) via MAPK/ERK signaling pathway in esophageal squamous cell cancer. *Cancer Lett* (2017) 397:83–93. doi: 10.1016/j.canlet.2017.03.033

84. Yanchun M, Yi W, Lu W, Yu Q, Jian Y, Pengzhou K, et al. Triptolide prevents proliferation and migration of Esophageal Squamous Cell Cancer via MAPK/ERK signaling pathway. *Eur J Pharmacol* (2019) 851:43–51. doi: 10.1016/j.ejphar.2019.02.030

85. Chao YK, Peng TL, Chuang WY, Yeh CJ, Li YL, Lu YC, et al. Transketolase serves a poor prognosticator in esophageal cancer by promoting cell invasion via epithelial-mesenchymal transition. *J Cancer* (2016) 7(13):1804–11. doi: 10.7150/jca.15467

86. Zhang B, Zhang C, Yang X, Chen Y, Zhang H, Liu J, et al. Cytoplasmic collagen XIαI as a prognostic biomarker in ESCC. *Cancer Biol Ther* (2018) 19(5):364–72. doi: 10.1080/15384047.2018.1423915

87. Liu A, Zhu J, Wu G, Cao L, Tan Z, Zhang S, et al. Antagonizing miR-455-3p inhibits chemoresistance and aggressiveness in ESCC. *Mol Cancer* (2017) 16(1):106. doi: 10.1186/s12943-017-0669-9

88. Lv Z, Yu JJ, Zhang WJ, Xiong L, Wang F, Li LF, et al. Expression and functional regulation of stemness gene Lgr5 in ESCC. *Oncotarget* (2017) 8(16):26492–504. doi: 10.18632/oncotarget.15624

89. Wang C, Yan FH, Zhang JJ, Huang H, Cui QS, Dong W, et al. OV6(+) cancer stem-like cells drive ESCC progression through ATG7-dependent β-catenin stabilization. *Cancer Lett* (2017) 391:100–13. doi: 10.1016/j.canlet.2017.01.026

90. Ge C, Wu S, Wang W, Liu Z, Zhang J, Wang Z, et al. miR-942 promotes cancer stem cell-like traits in ESCC through activation of Wnt/β-catenin signalling pathway. *Oncotarget* (2015) 6(13):10964–77. doi: 10.18632/oncotarget.3696

91. Yang Z, Cui Y, Ni W, Kim S, Xuan Y. Gli1, a potential regulator of esophageal cancer stem cell, is identified as an independent adverse prognostic factor in ESCC. *J Cancer Res Clin Oncol* (2017) 143(2):243–54. doi: 10.1007/s00432-016-2273-6

92. Osthus RC, Shim H, Kim S, Li Q, Reddy R, Mukherjee M, et al. Deregulation of glucose transporter 1 and glycolytic gene expression by c-Myc. *J Biol Chem* (2000) 275 (29):21797–800. doi: 10.1074/jbc.C000023200

93. Ai R, Sun Y, Guo Z, Wei W, Zhou L, Liu F, et al. NDRG1 overexpression promotes the progression of ESCC through modulating Wnt signaling pathway. *Cancer Biol Ther* (2016) 17(9):943–54. doi: 10.1080/15384047.2016.1210734

94. Huang R, Wang G, Song Y, Tang Q, You Q, Liu Z, et al. Colorectal cancer stem cell and chemoresistant colorectal cancer cell phenotypes and increased sensitivity to Notch pathway inhibitor. *Mol Med Rep* (2015) 12(2):2417–24. doi: 10.3892/mmr.2015.3694

95. Isohata N, Aoyagi K, Mabuchi T, Daiko H, Fukaya M, Ohta H, et al. Hedgehog and epithelial-mesenchymal transition signaling in normal and Malignant epithelial cells of the esophagus. *Int J Cancer* (2009) 125(5):1212–21. doi: 10.1002/ijc.24400

96. Li P, Liu X, Dong ZM, Ling ZQ. Epigenetic silencing of HIC1 promotes epithelial-mesenchymal transition and drives progression in ESCC. *Oncotarget* (2015) 6(35):38151–65. doi: 10.18632/oncotarget.5832

97. Li Z, Jin H, Mao G, Wu L, Guo Q. Msi2 plays a carcinogenic role in ESCC via regulation of the Wnt/β-catenin and Hedgehog signaling pathways. *Exp Cell Res* (2017) 361(1):170–7. doi: 10.1016/j.yexcr.2017.10.016

98. Liu W, Li M, Chen X, Zhu S, Shi H, Zhang D, et al. MicroRNA-1 suppresses proliferation, migration and invasion by targeting Notch2 in ESCC. *Sci Rep* (2018) 8 (1):5183. doi: 10.1038/s41598-018-23421-3

99. Ariyoshi Y, Shiozaki A, Ichikawa D, Shimizu H, Kosuga T, Konishi H, et al. Na +/H+ exchanger 1 has tumor suppressive activity and prognostic value in ESCC. *Oncotarget* (2017) 8(2):2209–23. doi: 10.18632/oncotarget.13645

100. Reya T, Morrison SJ, Clarke MF, Weissman IL. Stem cells, cancer, and cancer stem-like cells. *Nature* (2001) 414(6859):105–11. doi: 10.1038/35102167

101. Li N, Babaei-Jadidi R, Lorenzi F, Spencer-Dene B, Clarke P, Domingo E, et al. An FBXW7-ZEB2 axis links EMT and tumour microenvironment to promote colorectal cancer stem-like cells and chemoresistance. *Oncogenesis* (2019) 8(3):13. doi: 10.1038/s41389-019-0125-3

102. Lee SY, Jeong EK, Ju MK, Jeon HM, Kim MY, Kim CH, et al. Induction of metastasis, cancer stem cell phenotype, and oncogenic metabolism in cancer cells by ionizing radiation. *Mol Cancer* (2017) 16(1):10. doi: 10.1186/s12943-016-0577-4

103. Salnikov AV, Liu L, Platen M, Gladkich J, Salnikova O, Ryschich E, et al. Hypoxia induces EMT in low and highly aggressive pancreatic tumor cells but only cells with cancer stem cell characteristics acquire pronounced migratory potential. *PloS One* (2012) 7(9):e46391. doi: 10.1371/journal.pone.0046391

104. Wang L, Yang G, Zhao D, Wang J, Bai Y, Peng Q, et al. CD103-positive CSC exosome promotes EMT of clear cell renal cell carcinoma: role of remote MiR-19b-3p. *Mol Cancer* (2019) 18(1):86. doi: 10.1186/s12943-019-0997-z

105. Chen MF, Chen PT, Lu MS, Chen WC. Role of ALDH1 in the prognosis of esophageal cancer and its relationship with tumor microenvironment. *Mol Carcinog* (2018) 57(1):78–88. doi: 10.1002/mc.22733

106. Almanaa TN, Geusz ME, Jamasbi RJ. Effects of curcumin on stem-like cells in human esophageal squamous carcinoma cell lines. *BMC Complement Altern Med* (2012) 12:195. doi: 10.1186/1472-6882-12-195

107. Takeishi S, Nakayama KI. To wake up cancer stem-like cells, or to let them sleep, that is the question. *Cancer Sci* (2016) 107(7):875–81. doi: 10.1111/cas.12958

frontiers | Frontiers in Oncology

TYPE Case Report
PUBLISHED 18 January 2024
DOI 10.3389/fonc.2023.1268260



OPEN ACCESS

EDITED BY
Shanye Yin,
Albert Einstein College of Medicine,
United States

REVIEWED BY
Wei Ke,
Rutgers, The State University of New Jersey,
United States
Wenjun Deng,
Massachusetts General Hospital and Harvard
Medical School, United States
Yunjia Song,
Johns Hopkins University, United States, in
collaboration with reviewer WD

*CORRESPONDENCE
Wei Hu
huweikeyan@163.com
Jian-Guo Zhou
jianguo.zhou@yahoo.com

RECEIVED 27 July 2023
ACCEPTED 22 December 2023
PUBLISHED 18 January 2024

CITATION
Xu J, He B, Wang Y, Wu M, Lu Y, Su Z, Liu S, Yin F, Zhou J-G and Hu W (2024) Positive response to trastuzumab deruxtecan in a patient with HER2-mutant NSCLC after multiple lines therapy, including T-DM1: a case report. *Front. Oncol.* 13:1268260. doi: 10.3389/fonc.2023.1268260



# Positive response to trastuzumab deruxtecan in a patient with HER2-mutant NSCLC after multiple lines therapy, including T-DM1: a case report

Junzhu Xu, Bo He, Yunan Wang, Mengjia Wu, Yanyi Lu, Zixuan Su, Shujun Liu, Fengmin Yin, Jian-Guo Zhou* and Wei Hu*

Department of Oncology, The Second Affiliated Hospital of Zunyi Medical University, Zunyi, Guizhou, China

Human epidermal growth factor 2 (*HER2*) mutations are uncommon in non-small cell lung cancer (NSCLC), and the lack of established, effective, targeted drugs has resulted in a persistently poor prognosis. Herein, we report the case of a non-smoking, 58-year-old man diagnosed with lung adenocarcinoma (cT3N0M1c, stage IVB) harboring a *HER2* mutation (Y772_A775dupYVMA) and PD-L1 (-). The patient's Eastern Cooperative Oncology Group performance status (PS) score was assessed as 1. He commenced first-line treatment with chemotherapy, followed by immuno-chemotherapy, and with disease progression, he received HER2-targeted therapy and chemotherapy with an anti-angiogenic agent. However, HER2-targeted therapy, including pan-HER tyrosine kinase inhibitors (afatinib, pyrotinib, and pozitinib) and antibody–drug conjugate (T-DM1), produced only stable disease (SD) as the best response. After the previously described treatment, primary tumor recurrence and multiple brain metastases were observed. Despite the patient's compromised overall physical condition with a PS score of 3-4, he was administered T-DXd in addition to whole-brain radiotherapy (WBRT). Remarkably, both intracranial metastases and primary lesions were significantly reduced, he achieved a partial response (PR), and his PS score increased from 3-4 to 1. He was then treated with T-DXd for almost 9 months until the disease again progressed, and he did not discontinue the drug despite the occurrence of myelosuppression during this period. This is a critical case as it exerted an effective response to T-DXd despite multiple lines therapy, including T-DM1. Simultaneously, despite the occurrence of myelosuppression in the patient during T-DXd, it was controlled after aggressive treatment.

KEYWORDS

**HER2 mutation, non-small cell lung cancer, chemotherapy, target-therapy, T-DXd, ADCS**

## Background

Lung cancer is the most common cause of cancer-related death worldwide (1). Non-small cell lung cancer (NSCLC) is the predominant type of lung cancer, accounting for 85% of all cases. However, human epidermal growth factor 2 (HER2, erbB-2/neu) mutations occur in only 2–4% of NSCLC patients, more commonly in women, never-smokers, and adenocarcinoma (2). HER2 is a member of the ErbB receptor tyrosine kinase family, and its mutations in NSCLC are predominantly an in-frame insertion of exon 20 into the tyrosine kinase structural domain, including Y772_A775dupYVMA, G778_P780dup, and G776delinsVC (G776delinsLC) (3, 4), which is associated with poor overall survival (OS) of only 18–21 months (5). Although HER2 can be regarded as a therapeutic target, the efficacy of targeted therapy in HER2-mutant NSCLC has been disputed. Therefore, the standard first-line treatment remains a reference for advanced "driverless" NSCLC. Antibody-drug conjugates (ADCs) are novel antitumor agents that combine the high specificity of antibody targeting with potent cytotoxic drugs (6). For cancer patients with HER2 mutation or amplification, particularly breast and gastric cancer, numerous clinical trials have demonstrated the promise of ADCs as an effective treatment strategy. Nevertheless, research into potentially effective treatments for advanced NSCLC with HER2 mutations is still ongoing.

Herein, we present a patient with an overall survival (OS) of 46.5 months who underwent chemotherapy, immune checkpoint inhibitors (ICIs), anti-angiogenesis agents (bevacizumab and anlotinib), pan-HER tyrosine kinase inhibitors (afatinib, pyrotinib, and poziotinib), and ADCs (ado-trastuzumab emtansine [T-DM1], trastuzumab deruxtecan [T-DXd]), and attempt to provide new evidence for effective treatment of patients with HER2-mutant cancer (Figure 1-I).

## Case presentation

A 58-year-old male never-smoker was found to have an occupying lesion in the right hilar lung on chest computed tomography (CT) during a medical examination on 12.05.2019 (Figure 1-IIa). A biopsy was performed, and pathology revealed adenocarcinoma. The patient had diabetes, but it was under control. He then completed a systemic evaluation, which revealed pericardial and sacrococcygeal metastases. Next-generation sequencing identified a HER2 mutation (p.Y772_A775dupYVMA) and a *BRCA2* germline mutation with PD-L1 (-) and microsatellite stability. He was ultimately diagnosed with advanced-stage lung adenocarcinoma (cT3N0M1c [pericardial and sacral metastases], stage IVB) with an Eastern Cooperative Oncology Group performance status (ECOG PS) of 1. The pericardial effusion was drained, and the patient was administered one cycle of cisplatin. Subsequently, he underwent six cycles of first-line chemotherapy (pemetrexed plus cisplatin plus bevacizumab) and four cycles of maintenance therapy. A partial response (PR) was achieved at each efficacy evaluation, and progression-free survival (PFS) from first-line treatment was 11.3 months. In May 2020, with progressive disease (PD), the subject received a second-line immuno-chemotherapy regimen (paclitaxel albumin plus pembrolizumab plus bevacizumab) and was deemed to have achieved PR after two cycles. However, he discontinued paclitaxel albumin owing to unbearable bone pain. Strikingly, after two cycles, new frontal lobe and lung metastases were observed (Figure 1-IIb). Based on the HER2 mutation, he then received four anti-HER2 therapies, including ADCs (afatinib, T-DM1, pyrotinib, and poziotinib) for each relapse at recurrence (Figures 1-IIc, d). During this period, the patient underwent stereotactic radiotherapy (45 Gy/3 Gy/15 fractions) for significant enlargement of the intracranial metastasis (Figure 1-IId). Subsequently, a chest CT revealed an increase in bilateral pulmonary nodules. He was treated with anlotinib plus paclitaxel albumin for six cycles. After the second cycle, CT revealed a reduction in the size of the nodules in both lungs, with some lesions exhibiting cavity formation (Figure 1-IIe).

On 16/05/2022, significantly enlarged primary foci and multiple brain metastases were observed (Figure 1-IIf). The patient subsequently underwent whole-brain radiotherapy (36 Gy/2 Gy/18 f). Despite the previous treatment with T-DM1 and its poor efficacy, he chose to try T-DXd (400mg q3w) with a poor PS of 3-4. Interestingly, the patient responded to T-DXd even after heavy treatment and achieved PR (Figure 1-IIg), showing a significant improvement in PS (1–2). He was treated with T-DXd for almost 9 months before his disease progressed again, and he experienced neutropenia of grade 4 caused by T-DXd, which improved after supportive care. The patient died on 30.03.2023, having achieved an OS of 46.5 months.

## Discussion and conclusion

HER2 mutations are uncommon in advanced-stage NSCLC with poor prognosis, and the current standard treatment still refers to the National Comprehensive Cancer Network (NCCN) (7) recommended driverless NSCLC using platinum-pemetrexed plus bevacizumab or pembrolizumab. Also, a European EUHER2 cohort reported that in first-line treatment, PFS was 6 months and 4.8 months for chemotherapy and HER2-targeted therapy, respectively (8). In our case, we chose pemetrexed plus cisplatin plus bevacizumab as first-line treatment, and the patient was evaluated as PR during treatment with a PFS of 11.3 months. Additionally, the KEYNOTE-189 trial reported significant improvements in PFS and OS in chemotherapy-naive patients with non-squamous

**Abbreviations:** ADCs, antibody-drug conjugates; CT, computed tomography; DoR, duration of response; ECOG PS, Eastern Cooperative Oncology Group performance status; I+C+A, immune checkpoint inhibitors + chemotherapy + angiogenesis inhibitors; ICI, immune checkpoint inhibitor; IMRT, intensity-modulated radiotherapy; MRI, magnetic resonance imaging; NGS, next-generation sequencing; NSCLC, non-small cell lung cancer; NCCN, National Comprehensive Cancer Network; PD, progressive disease; PR, partial response; RECIST, Response Evaluation Criteria In Solid Tumors; SD, stable disease; T-DM1, ado-trastuzumab emtansine; T-DXd, trastuzumab deruxtecan.

10.3389/fonc.2023.1268260

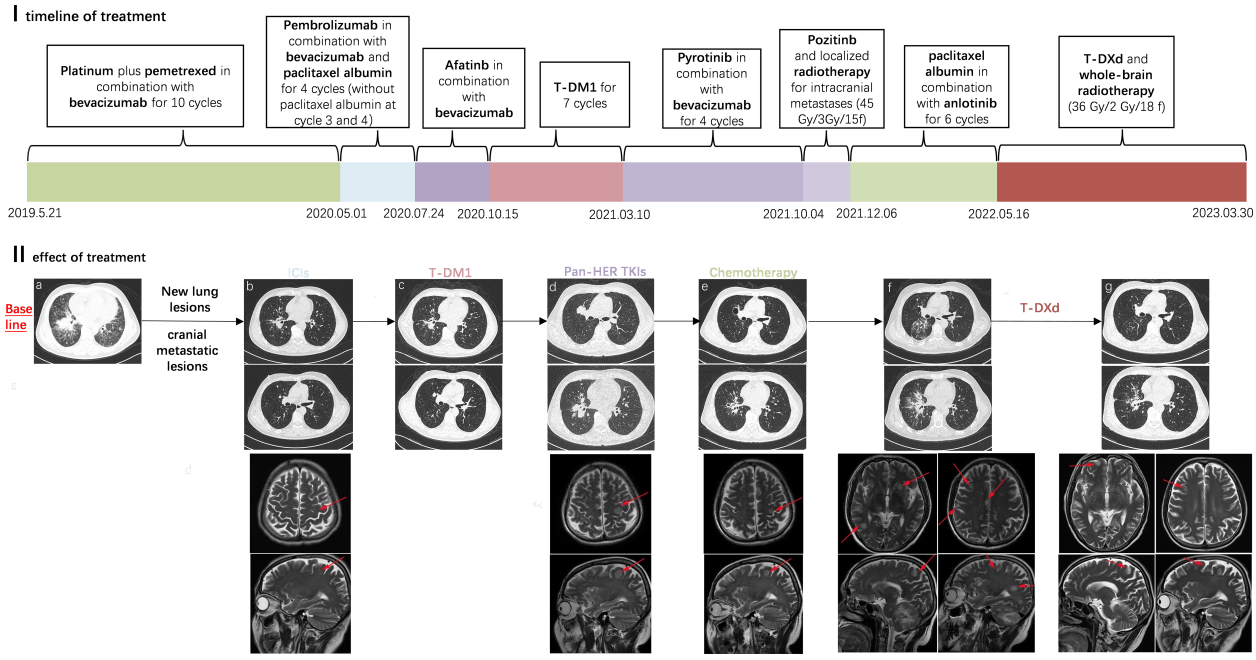


FIGURE 1
I (x-coordinate is the time, the unit is months): timeline diagram of the case receiving multiple lines of treatment; the PFS during this treatment period is expressed in length. II: Efficacy of treatment as demonstrated by chest CT and cranial MRI; **(a)** Primary lesions in the lungs **(b)** After treatment with ICIs, new lesions in the lungs and cranial metastatic lesions were observed **(c)** During treatment with T-DM1 **(d)** Disease progression after multiple lines pan-HER TKI therapy **(e)** Significant reduction in lung and brain lesions during treatment with re-challenge chemotherapy combination **(f)** Disease progression and multiple metastases in the brain **(g)** Radiotherapy was given for the cranial metastases, and subsequently in treatment with T-Dxd.

NSCLC, regardless of their PD-L1 expression status, using immuno-combination therapy (9). In this study, our patient received second-line albumin paclitaxel, bevacizumab, and pembrolizumab, and unfortunately, his PFS was only 2.8 months, similar to that reported in the IMMUNOTARGET retrospective study of HER2-mutant NSCLC receiving immunotherapy (10). Notably, although PR was achieved at the first evaluation, disease progression occurred after the last two cycles without albumin-paclitaxel due to bone pain. Whether disease progression is related to the discontinuation of chemotherapy or the ineffectiveness of immunotherapy remains inconclusive. However, in the first two lines of treatment, we noticed that this patient appeared to have a better response to chemotherapy. In addition, it was confirmed that afatinib and pirotinib had similar mPFS and produced responses in patients with HER2-mutant NSCLC with or without prior treatment (11–13). Also, the ZENITH20-2 trial demonstrated that poziotinib had antitumor activity in previously treated patients with HER2 exon 20 insertion NSCLC. This patient was treated with multiple pan-HER TKIs (afatinib, pyrotinib, and pozitinib) and ADC (T-DM1) based on the *HER2* mutation, but neither reached an objective response. For T-DM1, the duration of response (DoR) in our case was similar to the lung cancer cohort in the phase 2 basket study (14). Our multiple treatment attempts have failed at this point. According to the ALTER0303 trial, the mPFS of the anlotinib group in advanced NSCLC beyond third-line treatment was 5.4 months; thus, we chose conventional treatment plus anlotinib (15). Every efficacy evaluation showed PR, with a PFS of 5.7 months. In this case, we chose multiple lines therapy including chemotherapy, immunotherapy, pan-HER TKIs, and ADC, and despite the chemotherapy used in front-line and back-line, which both achieved PR and contributed to delayed progression, the disease still inevitably progressed.

With the previous multiple lines treatment having failed, the DESTINY series of studies (Table 1), which reported the positive efficacy of third-generation ADC (T-DXd) in HER2-altered breast and gastric cancer, has given us a new direction for treatment options (16, 17). T-DXd is a novel *HER2*-targeted ADC that consists of trastuzumab and a topoisomerase I inhibitor. Subsequently, in Destiny-Lung01 by Li et al., previously treated HER2-mutant NSCLC patients receiving T-DXd (6.4 mg/kg) had an mPFS of 8.2 months and a median overall survival of 17.8 months, while the most common drug-related adverse event of grade 3 or higher was neutropenia, and drug-related interstitial lung disease occurred in 26% of patients (18). The pivotal findings from the Destiny-Lung02 study for T-DXd dose exploration significantly contributed to the subsequent FDA approval of T-DXd on 11/08/2022 for adults with HER2-mutant NSCLC who have experienced disease progression following systemic platinum-based therapy (19). Our patient received T-DXd in failure of T-DM1 treatment and a poor PS score (3-4) and maintained PFS for almost 9 months. The best response was assessed as PR, and the ECOG PS score improved to 1-2, which is

TABLE 1 Several trials and cases of ADC.

| Study/case report | Sample size | Population | Best response | PFS (m) | ORR n (%) | Duration of response(m) |
|---|---|---|---|---|---|---|
| Ph II, DESTINY-Gastric01study (NCT03329690) | 119 | Progression on and after ≥ 2 prior regimens | CR (1) | 5.6 | 61/119 (51.3) | 12.5 |
| Ph Il, DESTINY-Breast01study (NCTO3248492) | 184 | Previously treated with T-DM1 | CR (11) | 16.4 | 112/184 (60.9) | 14.8 |
| Ph II, DESTINY-Lung01study (NCTO3505710) | 91(cohort 2) | Previously not treated with HER2-targeted therapies (except for pan-HER TKIs); ECOG PS of 0 to 1 | CR (11) | 8.2 | 50/91(50) | 10.6 |
| Ph II, DESTINY-Lung02study (NCT04644237) | 52(cohort of 5.4mg/kg) | Previously not treated with T-DM1, ECOG PS of 0 to 1 | CR (1) | / | 27/52(53.8) | / |
| Case report | / | Progression after 5 lines of chemotherapy, ECOG PS of 3 | PR | / | / | 6(Ongoing, ECOG PS of 1) |

similar to a case that reported an objective response and ECOG PS score improvement following treatment with T-DXd in poor PS (20). However, both Destiny-Lung01 and Destiny-Lung02 excluded patients with a PS score >2 or who had previously received T-DM1. Prior to this, only the 'DESTINY-Breast' clinical trial series reported a significant delay in disease progression with T-DXd in HER2-positive breast cancer patients who had previously received T-DM1 (17, 21). Our case suggests that the efficacy and safety of T-DXd were maintained in patients with advanced NSCLC who had previously received multiple lines therapy, despite the failure of T-DM1, and with poor PS scores. Although at that time we chose to administer T-DXd at a dose of 6.4 mg/kg according to Destiny-lung01, the recent Destiny-lung02 clinical trial demonstrated the efficacy of low-dose T-DXd in treating HER2-mutant NSCLC with a lower incidence of grade 3 or higher adverse events than the high-dose group (22). In addition, we caution clinicians about the four-degree myelosuppression caused by T-DXd. Based on the limitations of individual cases, the efficacy and safety of T-DXd in this group of patients still require further clinical case accumulation for validation.

This patient had both HER2 and *BRCA2* germline mutations. Our therapeutic work has focused on standard treatment for driverless advanced NSCLC in addition to treatment for the HER2 gene mutation. Notably, the patient achieved a positive response with T-DXd after T-DM1 resistance demonstrated promising survival benefits. The efficacy of T-DXd on T-DM1-resistant HER2-positive cancer cells has been suggested to be related to the elevated expression of ABCC2 (MPR2) and ABCG2 (BCRP) (23). Furthermore, for lung cancer patients with BRCA germline mutations, BRCA inhibitors in combination with chemotherapeutic agents are emerging as a viable option. Taofeek et al. reported the efficacy and safety of veliparib compared to conventional platinum-based chemotherapeutic agents for the treatment of SCLC (24, 25). Lynnette et al. revealed a significant anti-tumor effect when combining olaparib and icotinib (26). Based on the above positive results of combination therapy with BRCA inhibitors in the treatment of lung cancer, more extensive research is required to ascertain whether combining ADCs with BRCA inhibitors could offer a novel and potential treatment approach for patients with concurrent HER2 and BRCA germline mutations.

In conclusion, we have reported a case with the HER2 mutation in an NSCLC patient who tried various treatments after progressing on standard therapy and achieved an OS of 46.5 months. This case is a reminder to clinicians that such patients could still benefit from T-DXd despite having poor PS scores after multiple lines therapy, including T-DM1, which still needs to be confirmed by more data and prospective clinical trials.

## Data availability statement

The data are not available for public access due to patient privacy concerns but are available from the corresponding author upon reasonable request.

## Ethics statement

This study complied with the tenets of the Declaration of Helsinki. It was conducted following formal approval by the Ethics Committee of the Second Affiliated Hospital of Zunyi Medical University (YXLL(KY-R)-2021-012). Written informed consent was obtained from the patient for the publication of any identifiable images or data contained herein.

## Author contributions

JX: Writing – original draft. BH: Writing – review & editing. YW: Writing – review & editing. MW: Writing – review & editing.

YL: Writing – review & editing. ZS: Writing – review & editing. SL: Writing – review & editing. FY: Writing – review & editing. JZ: Funding acquisition, Writing – review & editing. WH: Funding acquisition, Writing – review & editing.

## Funding

The author(s) declare financial support was received for the research, authorship, and/or publication of this article. This research was funded by the Science and Technology Department of Guizhou Province, grant no.: ZK (2021)-452, China, the Zunyi Medical University School-level Education Reform, grant no.: XJJG2021-45, the National Natural Science Foundation of China (Grant No. 82060475), and the Natural Science Foundation of Guizhou Province (Grant No. ZK2022-YB632).

## Conflict of interest

The authors declare that the research was conducted in the absence of any commercial or financial relationships that could be construed as a potential conflict of interest.

## Publisher's note



## References

1. Sung H, Ferlay J, Siegel RL, Laversanne M, Soerjomataram I, Jemal A, et al. Global cancer statistics 2020: GLOBOCAN estimates of incidence and mortality worldwide for 36 cancers in 185 countries. *CA Cancer J Clin* (2021) 71(3):209–49. doi: 10.3322/caac.21660

2. Takeda M, Sakai K, Hayashi H, Tanaka K, Tanizaki J, Takahama T, et al. Clinical characteristics of non-small cell lung cancer harboring mutations in exon 20 of EGFR or HER2. *Oncotarget* (2018) 9(30):21132–40. doi: 10.18632/oncotarget.24958

3. Hyman DM, Piha-Paul SA, Won H, Rodon J, Saura C, Shapiro GI, et al. HER kinase inhibition in patients with HER2- and HER3-mutant cancers. *Nature* (2018) 554 (7691):189–94. doi: 10.1038/nature25475

4. Wei XW, Gao X, Zhang XC, Yang JJ, Chen ZH, Wu YL, et al. Mutational landscape and characteristics of ERBB2 in non-small cell lung cancer. *Thorac Cancer* (2020) 11(6):1512–21. doi: 10.1111/1759-7714.13419

5. Wang Y, Jiang T, Qin Z, Jiang J, Wang Q, Yang S, et al. HER2 exon 20 insertions in non-small-cell lung cancer are sensitive to the irreversible pan-HER receptor tyrosine kinase inhibitor pyrotinib. *Ann Oncol* (2019) 30(3):447–55. doi: 10.1093/annonc/mdy542

6. Li BT, Michelini F, Misale S, Cocco E, Baldino L, Cai Y, et al. HER2-mediated internalization of cytotoxic agents in ERBB2 amplified or mutant lung cancers. *Cancer Discovery* (2020) 10(5):674–87. doi: 10.1158/2159-8290.CD-20-0215

7. Ettinger DS, Wood DE, Aisner DL, Akerley W, Bauman JR, Bharat A, et al. NCCN guidelines® Insights: non-small cell lung cancer, version 2.2023. *J Natl Compr Cancer Network JNCCN* (2023) 21(4):340–50. doi: 10.6004/jnccn.2023.0020

8. Mazières J, Barlesi F, Filleron T, Besse B, Monnet I, Beau-Faller M, et al. Lung cancer patients with HER2 mutations treated with chemotherapy and HER2-targeted drugs: results from the European EUHER2 cohort. *Ann Oncol* (2016) 27(2):281–6. doi: 10.1093/annonc/mdv573

9. Gandhi L, Rodríguez-Abreu D, Gadgeel S, Esteban E, Felip E, De Angelis F, et al. Pembrolizumab plus chemotherapy in metastatic non-small-cell lung cancer. *N Engl J Med* (2018) 378(22):2078–92. doi: 10.1056/NEJMoa1801005

10. Mazieres J, Drilon A, Lusque A, Mhanna L, Cortot AB, Mezquita L, et al. Immune checkpoint inhibitors for patients with advanced lung cancer and oncogenic driver alterations: results from the IMMUNOTARGET registry. *Ann Oncol* (2019) 30 (8):1321–8. doi: 10.1093/annonc/mdz167

11. Fan Y, Chen J, Zhou C, Wang H, Shu Y, Zhang J, et al. Afatinib in patients with advanced non-small cell lung cancer harboring HER2 mutations, previously treated with chemotherapy: A phase II trial. *Lung Cancer* (2020) 147:209–13. doi: 10.1016/j.lungcan.2020.07.017

12. Zhou C, Li X, Wang Q, Gao G, Zhang Y, Chen J, et al. Pyrotinib in HER2-mutant advanced lung adenocarcinoma after platinum-based chemotherapy: A multicenter, open-label, single-arm, phase II study. *J Clin Oncol* (2020) 38(24):2753–61. doi: 10.1200/JCO.20.00297

13. Yang G, Xu H, Hu J, Liu R, Hu P, Yang Y, et al. Specific HER2 exon 20 gly776 deletion-insertions in non-small cell lung cancer: structural analysis and sensitivity to HER2-targeted tyrosine kinase inhibitors. *Front Pharmacol* (2022) 13:806737. doi: 10.3389/fphar.2022.806737

14. Li BT, Shen R, Buonocore D, Olah ZT, Ni A, Ginsberg MS, et al. Ado-trastuzumab emtansine for patients with HER2-mutant lung cancers: results from a phase II basket trial. *J Clin Oncol* (2018) 36(24):2532–7. doi: 10.1200/JCO.2018.77.9777

15. Han B, Li K, Wang Q, Zhang L, Shi J, Wang Z, et al. Effect of anlotinib as a third-line or further treatment on overall survival of patients with advanced non-small cell lung cancer: the ALTER 0303 phase 3 randomized clinical trial. *JAMA Oncol* (2018) 4 (11):1569–75. doi: 10.1001/jamaoncol.2018.3039

16. Shitara K, Bang YJ, Iwasa S, Sugimoto N, Ryu MH, Sakai D, et al. Trastuzumab deruxtecan in previously treated HER2-positive gastric cancer. *N Engl J Med* (2020) 382 (25):2419–30. doi: 10.1056/NEJMoa2004413

17. Modi S, Saura C, Yamashita T, Park YH, Kim SB, Tamura K, et al. Trastuzumab deruxtecan in previously treated HER2-positive breast cancer. *N Engl J Med* (2020) 382 (7):610–21. doi: 10.1056/NEJMoa1914510

18. Li B, Smit EF, Goto Y, Nakagawa K, Udagawa H, Mazières J, et al. Trastuzumab Deruxtecan in HER2-Mutant Non-Small-Cell Lung Cancer. *N Engl J Med* (2021) 386:241–51. doi: 10.1056/NEJMoa2112431

19. FDA gives nod to T-DXd for HER2-mutant NSCLC. *Cancer Discov* (2022) 12 (10):2224. doi: 10.1158/2159-8290.CD-NB2022-0053

20. Kato Y, Kato Y, Minegishi Y, Suzuki T, Nakamichi S, Matsumoto M, et al. Efficacy with trastuzumab deruxtecan for non-small-cell lung cancer harboring HER2 exon 20 insertion mutation in a patient with a poor performance status: A case report. *Onco Targets Ther* (2021) 14:5315–9. doi: 10.2147/OTT.S341290

21. André F, Hee Park Y, Kim SB, Takano T, Im SA, Borges G, et al. Trastuzumab deruxtecan versus treatment of physician's choice in patients with HER2-positive metastatic breast cancer (DESTINY-Breast02): a randomised, open-label, multicentre, phase 3 trial. *Lancet (London England)* (2023) 401(10390):1773–85. doi: 10.1016/S0140-6736(23)00725-0

22. Goto K, Goto Y, Kubo T, Ninomiya K, Kim SW, Planchard D, et al. Trastuzumab deruxtecan in patients with HER2-mutant metastatic non-small-cell lung cancer: primary results from the randomized, phase II DESTINY-lung02 trial. *J Clin Oncol: Official J Am Soc Clin Oncol* (2023) 41(31):4852–63. doi: 10.1200/JCO.23.01361

23. Drago JZ, Modi S, Chandarlapaty S. Unlocking the potential of antibody-drug conjugates for cancer therapy, Nature reviews. *Clin Oncol* (2021) 18(6):327–44. doi: 10.1038/s41571-021-00470-8

24. Owonikoko TK, Dahlberg SE, Khan SA, Gerber DE, Dowell J, Moss RA, et al. A phase 1 safety study of veliparib combined with cisplatin and etoposide in extensive stage small cell lung cancer: A trial of the ECOG-ACRIN Cancer Research Group (E2511). *Lung Cancer* (2015) 89(1):66–70. doi: 10.1016/j.lungcan.2015.04.015

25. Atrafi F, Groen HJM, Byers LA, Garralda E, Lolkema MP, Sangha RS, et al. A phase I dose-escalation study of veliparib combined with carboplatin and etoposide in patients with extensive-stage small cell lung cancer and other solid tumors. *Clin Cancer Res* (2019) 25(2):496–505. doi: 10.1158/1078-0432.CCR-18-2014

26. Marcar L, Bardhan K, Gheorghiu L, Dinkelborg P, Pfäffle H, Liu Q, et al. Acquired resistance of EGFR-mutated lung cancer to tyrosine kinase inhibitor treatment promotes PARP inhibitor sensitivity. *Cell Rep* (2019) 27(12):3422–3432.e4. doi: 10.1016/j.celrep.2019.05.058

frontiers | Frontiers in Oncology

TYPE Systematic Review
PUBLISHED 28 October 2024
DOI 10.3389/fonc.2024.1424100



OPEN ACCESS

EDITED BY
Yinghao Wu,
Albert Einstein College of Medicine,
United States

REVIEWED BY
Banzhan Ruan,
Hainan Medical University, China
Sungchan Gwark,
Ewha Womans University Seoul Hospital,
Republic of Korea

*CORRESPONDENCE
Ye Tao
ty2100519792@163.com

†These authors have contributed equally to this work

RECEIVED 27 April 2024
ACCEPTED 09 October 2024
PUBLISHED 28 October 2024

CITATION
Yang X, Tu J, Zang X, Huang X and Tao Y (2024) A bibliometric and visualization analysis of entosis research from 2007 to 2024.
*Front. Oncol.* 14:1424100.
doi: 10.3389/fonc.2024.1424100



# A bibliometric and visualization analysis of entosis research from 2007 to 2024

Xinyu Yang†, Jiatao Tu†, Xinyi Zang†, Xuan Huang and Ye Tao*

Department of Gastroenterology, The First Affiliated Hospital of Zhejiang Chinese Medical University (Zhejiang Provincial Hospital of Traditional Chinese Medicine), Hangzhou, China

**Objective:** In 2007, entosis was proposed as a form of programmed cell death, distinct from apoptosis. This process involves a living cell (internalized cell) actively invading a neighboring live cell of the same type (host cell), forming a cell-in-cell structure. Recently, entosis has been increasingly associated with cancer, leading to significant advancements in research. Despite this progress, a comprehensive and unbiased review of the current state of entosis research is lacking. This study aims to evaluate the developments in the field of entosis over the past decade and highlight emerging research trends.

**Materials and methods:** We performed a literature search for studies published since the introduction of the entosis concept, using the Web of Science Core Collection database. The bibliometric analysis was conducted using VOSviewer, CiteSpace, Microsoft Excel, and the Bibliometrix R package.

**Results:** A total of 196 articles from 39 countries and 346 institutions were included. Between 2007 and 2024, research on entosis has seen rapid growth, with most publications originating from China and the United States. The United States also leads in total citations, with Memorial Sloan Kettering Cancer Center emerging as the top research institution. Sun Qiang is the most prolific author in this field, while Overholtzer M has the highest number of citations. *Current Molecular Medicine* has published the most articles related to entosis. Frequently occurring keywords include "entosis," "cannibalism," "autophagy," and "apoptosis." In recent years, keywords such as "phagocytosis," "drug resistance," and "human cancers" have surged, indicating a growing focus on understanding the role of entosis in tumor progression and exploring its potential as a therapeutic target for cancer treatment.

**Conclusions:** This study provides the first bibliometric analysis of entosis, detailing its evolution over the last decade. It highlights critical areas of interest, including the development of inhibitors targeting entosis and their potential clinical applications. This research aims to guide future investigations and serve as a valuable resource for scholars exploring entosis in cancer biology.

KEYWORDS

**entosis, cell-in-cell, VOSviewer, CiteSpace, R package "bibliometrix"**

# 1 Introduction

Entosis, proposed in 2007, refers to a form of programmed cell death distinct from apoptosis (1). This process involves a living cell (internalized cell) actively penetrating a neighboring live cell (host cell) of the same type, resulting in the formation of a cell-in-cell (CIC) structure. Several outcomes are possible for the cells involved in entosis. The most common fate for the internalized cell is death, mediated by the lysosomal pathway of the host cell. However, a small fraction of internalized cells can survive within the host, be re-released, and, in some cases, even undergo division and proliferation (2).

Initial studies on entosis suggested that it primarily results in cell death, which may provide anticancer benefits. For example, Overholtzer et al. (2007) found that entosis restricts the abnormal proliferation of tumor cells grown in soft agar, supporting its potential role in tumor inhibition (3). Additionally, the inhibition of entotic cell death through autophagy protein knockdown increases the transformed growth of cells with high rates of entosis, suggesting that entosis may reduce such growth, at least partially, by inducing cell death (4).

As research has progressed, however, the focus has shifted toward the idea that entosis may promote tumor cell proliferation and metastasis. Entosis induces aneuploidy, a known driver of tumor development. During entosis, the internalized cell can disrupt the host cell's division by interfering with the cleavage furrow, often leading to cytokinesis failure (5, 6). This failure can result in binucleated cells with significant aneuploidy, contributing to the formation of melanoma lesions (7). Consistently, host cells can recover nutrients from digested entotic cells, a process known as nutrient scavenging, which helps support cell proliferation and survival under starvation conditions (8). With the growing understanding of entosis as a promoter of tumor progression, the development of entosis inhibitors has emerged as a promising area of research. For instance, a study published in *Cell Death & Disease* demonstrated that, in the absence of glucose, the inhibition of PEPCK-M with iPEPCK-2 promotes entosis, while overexpression of PEPCK-M inhibits it (9). Furthermore, recent studies have identified $Ca^{2+}$ chelators and inhibitors of SEPTIN, Orai1, and MLCK as suppressors of entosis (10). The future discovery and development of additional entosis inhibitors hold great promise for their application in clinical anticancer treatments, potentially leading to advanced therapeutic approaches.

Entosis, one of the emerging modes of cell death, has garnered increasing attention from researchers in the field of cancer biology. The growing number of studies on entosis reflects a rapidly expanding interest in understanding its role, placing a significant demand on researchers to stay updated on the latest findings, track current research hotspots, and anticipate future developments in the field. Bibliometric analysis, a quantitative analytical method, employs mathematical and statistical tools to systematically examine the literature of a specific research domain. This method helps construct a knowledge network within a field, enabling researchers to identify key areas of study and the boundaries of academic discourse. The objectivity and rigor of bibliometric analysis have made it a widely used tool across numerous disciplines, allowing scholars to quickly understand prevailing trends in their respective fields (11, 12). Bibliometric analysis can more accurately assist researchers in the field of entosis to understand the latest scientific discoveries, identify research hotspots, and predict the future development of the field.

However, no bibliometric studies have yet been conducted on entosis. To address this gap, our study searched the Web of Science Core Collection for literature related to cellular entosis published from January 1, 2007, to February 15, 2024. Using tools such as CiteSpace, VOSviewer, and R (version 4.2.2), we performed a comprehensive bibliometric analysis and visualized the results. Our aim was to summarize the current state of entosis research, assess emerging trends, and predict future research directions in the field (13–15).

# 2 Materials and methods

## 2.1 Literature source and retrieval strategy

Data were retrieved from the Web of Science Core Collection on a single day, February 15, 2024, using the search formula TS = (entosis). The search covered literature published from January 1, 2007, to February 15, 2024. Out of the 237 articles initially identified, 41 were excluded, including meeting abstracts, editorial content, corrections, correspondences, retractions, and conference papers. Ultimately, 196 articles were selected for analysis and exported under the categories "Full Record and Cited References" and "Plain Text." To ensure comprehensive examination, the exported files were renamed as "download_*.txt" to enable processing in CiteSpace. The retrieval and analysis process is illustrated in Figure 1.

## 2.2 Data analysis and visualization

To ensure the accuracy and consistency of the literature data, we utilized the "DEAN" data-cleaning process proposed by Pan Wei et al. for pre-processing and screening the data (16). Following this, we analyzed and visualized the literature using four software programs: Microsoft Excel 2021, CiteSpace, VOSviewer, and R (version 4.3.1). CiteSpace, developed by Chao-Mei Chen, is the most widely used tool for bibliometric analysis, and version 6.1.6 was used in this study for institutional collaboration analysis, journal cluster analysis, co-citation clustering and bursts, keyword timelines, and keyword bursts (17). VOSviewer, created by Nees Jan van Eck and colleagues, focuses on analyzing bibliometric knowledge graphs (18), and version 1.6.20 were used to visualize and analyze countries, journals, cited authors, co-cited authors, high-impact papers, and keywords. Additionally, the Bibliometrix R package (version 4.1.4) (https://www.bibliometrix.org) was used to display publication output by country (19), illustrate international collaboration, and present thematic trend analyses and a three-field plot. We also visualized the annual output of the top five institutions, journals, and the top 10 authors. Microsoft Excel 2021 was used to examine annual publication trends and conduct curve fitting.

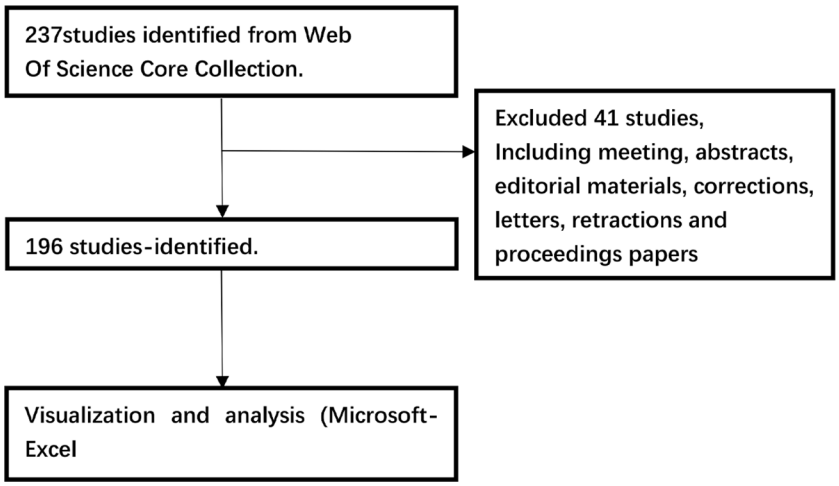


FIGURE 1
The flow chart depicting bibliometric analysis.

# 3 Results

## 3.1 Annual quantitative distribution of publications

The annual publication of scholarly articles reflects the advancements in research within this domain. Our search strategy included all articles published since the definition of entosis was proposed, yielding a total of 237 English publications. After excluding publication types such as conference abstracts, book reviews, letters, and retracted articles, we conducted a comprehensive review of 196 papers, comprising 138 research articles and 58 reviews. Between 2007 and 2010, the number of publications was limited, indicating a period of stagnation in research, as illustrated in Figure 2A. However, following 2011, there has been a consistent increase in research literature in this field, with a peak in published articles observed from 2020 to 2023. This signifies a recent surge in recognition of entosis research among scholars. It is evident that entosis holds significant potential for clinical applications, particularly in anticancer therapy, and the trend in this research area is expected to continue expanding.

## 3.2 Analysis of countries and institutions

Since the introduction of the entosis definition, publications have emerged from 39 different countries and regions, as well as 346 organizations. As depicted in the geographical network map in Figure 2D, the top 10 countries were primarily located in Asia, Europe, and North America.

Table 1 shows that China (71 publications, 36.22%) and the United States (61 publications, 31.12%) together accounted for 67.34% of the total global publications, significantly distancing themselves from the third-ranked country. The U.S. publications garnered the highest overall citation frequency (6,024), followed by the UK (3,230), France (2,808), and Italy (2,558). Figure 2C illustrates the frequency of international academic collaboration, with the size of each node representing the number of publications from that country. Collaborative research efforts among various nations were strong, with dynamic partnerships notably between the U.S., China, and the UK. Furthermore, Italy and the UK showed a strong partnership. However, China's multi-country publication research constituted only a small fraction of its domestic research output (see Figure 2B), indicating a limited degree of close academic collaboration with other countries and continents in this research area. By incorporating these advanced analytical tools, we provide a comprehensive review of entosis-related research, establishing a solid foundation for assessing the current state of the field and its future potential.

Using CiteSpace software, we visualized and analyzed the 346 institutions involved in this research (Figure 3A). The ranking of publications is presented in Table 1, which highlights the top 10 institutions contributing to this field. The leading research institution is Memorial Sloan Kettering Cancer Center, with 24 publications, accounting for 12.24% of the total output. Notably, the list of institutions also includes several Chinese research entities. The diagram in Figure 3A shows the network of interinstitutional collaboration. As shown, Memorial Sloan Kettering Cancer Center actively collaborates with The Babraham Institute, while Capital Medical University maintains close ties with the Chinese People's Liberation Army General Hospital. Moreover, partnerships among institutions are predominantly confined to their respective countries, reflecting a lack of dynamic academic cooperation across various nations. Figure 3B indicates a steady upward trend in the annual publication output of the top five institutions in recent years.

## 3.3 Journals and co-cited journals

The journals and co-cited journals within this research domain were visualized and analyzed using VOSviewer. A total of 119 journals were included in this analysis. Figure 3D displays the top

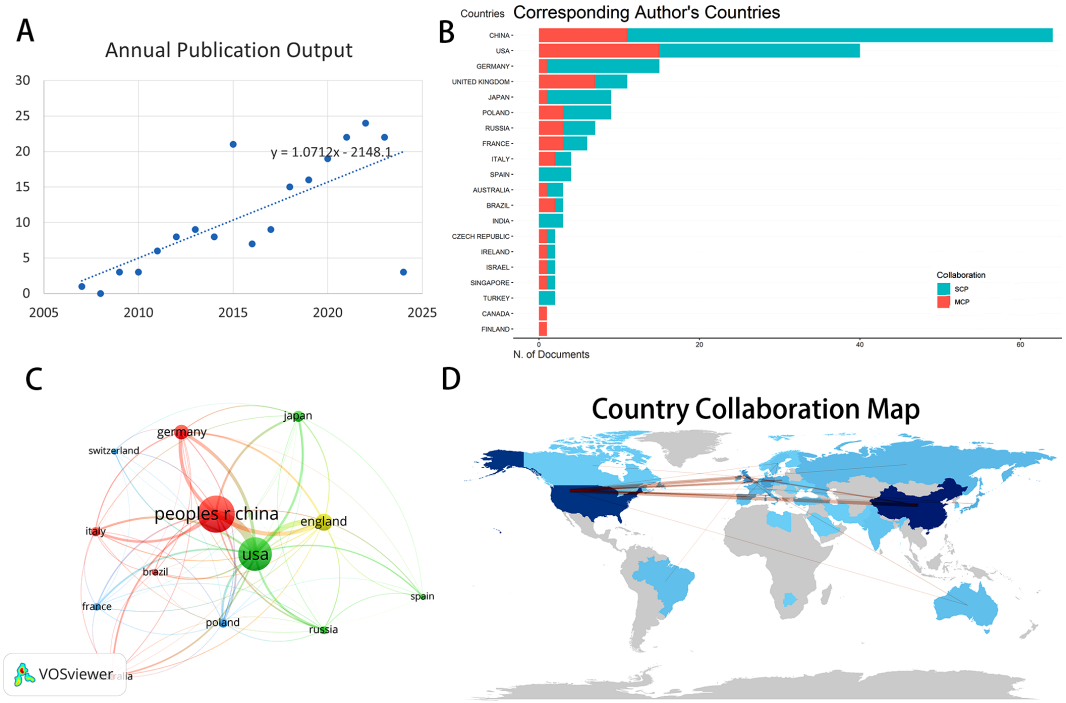


FIGURE 2
**(A)** Annual outputs of publications regarding Entosis field. **(B)** TOP 20 corresponding author's countries that produced the largest number of literature. **(C)** The overlay visualization map of country co-authorship analysis conducted by VOSviewer. **(D)** The geographical network map of Entosis. SCP, Single Country Publications; MCP, Multiple Country Publications.

10 journals based on the number of publications, with a minimum threshold of 4 publications; the size of the nodes corresponds to the volume of publications for each journal. Figure 4A presents the network layout of journals cited together, including those with a minimum of 20 citations. This figure shows that the 119 journals cited together are represented in the overall strength of the links. Leading the list of journals in terms of overall link strength are *Cell* (total link strength = 38,061), *Nature* (total link strength = 35,478), *Cell Death & Differentiation* (total link strength = 26,500), *Proceedings of the National Academy of Sciences USA* (total link strength = 22,200), and *Journal of Biological Chemistry* (total link strength = 19,828). There has been a consistent increase in the publication numbers of the leading five journals in this field of study in recent years, as illustrated in Figure 4B.

Table 2 numbers the top 10 most prolific and co-cited journals included in this study. *Molecular Medicine*, with an impact factor (IF) of 2.50 in 2024, emerged as the leading publisher with nine publications. Additionally, there were nine articles published in *Cell and Developmental Biology* (IF = 5.50, 2024), eight in *Cell Death & Disease* (IF = 9.00, 2024), and four in *Cell Research* (IF = 44.1, 2024). Notably, 7 out of the top 10 journals classified under JCR Region I contained relevant articles.

TABLE 1 Top 10 nations and institutes for Entosis research.

| Rank | Country | Citation | Articles | Institution | Year | Count (%) |
|---|---|---|---|---|---|---|
| 1 | China | 1886 | 71(36.22%) | Memorial Sloan Kettering Cancer Center | 2011 | 24(12.24%) |
| 2 | USA | 6024 | 61(31.12%) | Capital Medical University | 2014 | 19(9.69%) |
| 3 | England | 3230 | 23(11.73%) | Chinese People's Liberation Army General. | 2013 | 18(9.18%) |
| 4 | Germany | 506 | 18(9.18%) | Cornell University | 2011 | 16(8.16%) |
| 5 | Japan | 316 | 12(6.12%) | Weill Cornell Medicine | 2011 | 15(7.65%) |
| 6 | Italy | 2558 | 9(4.59%) | Southern Medical University- China | 2009 | 12(6.12%) |
| 7 | Poland | 72 | 9(4.59%) | Chinese Academy of Sciences | 2009 | 12(6.12%) |
| 8 | Russia | 48 | 8(4.08%)) | Biotechnology and Biological Sciences Res | 2013 | 10(5.10%) |
| 9 | France | 2808 | 7(3.57%) | South China University of Technology | 2009 | 9(4.59%) |
| 10 | Australia | 2515 | 6(3.06%) | Babraham Institute | 2014 | 9(4.59%) |

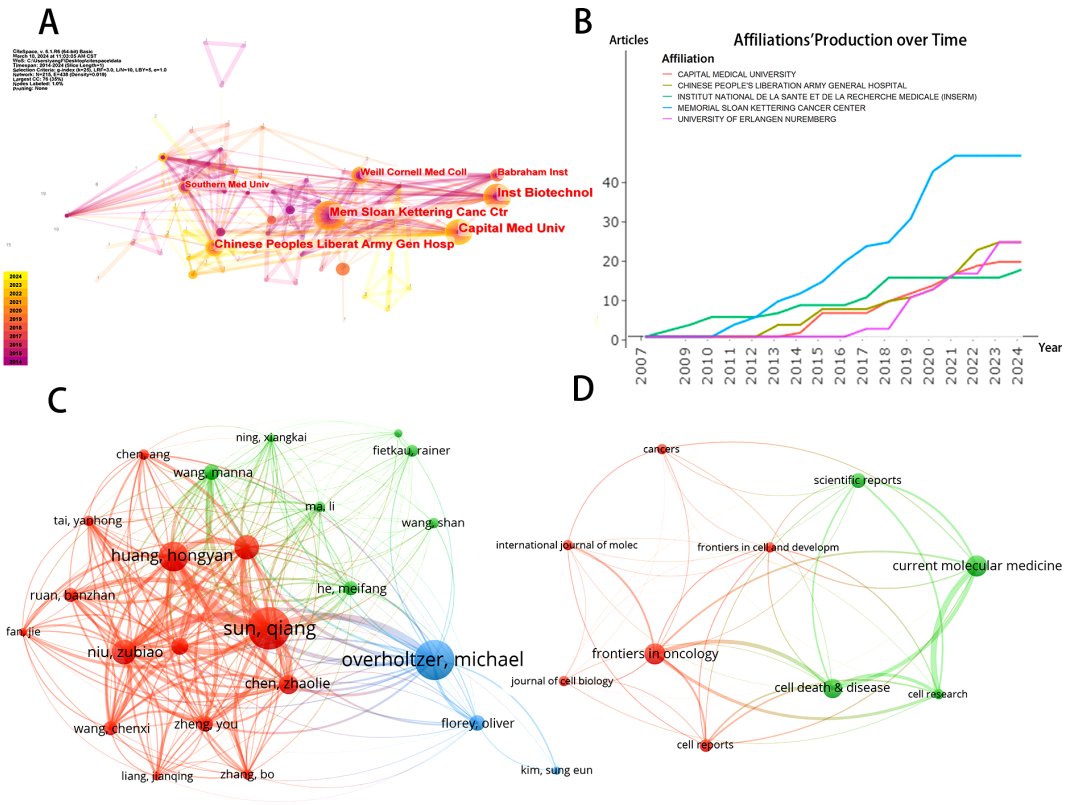


FIGURE 3
**(A)** The visualization of institutions' cooperation networks based on CiteSpace. **(B)** Top 5 institutions' production over time. **(C)** Map of authors' cooperative relationship. **(D)** Visualization of journals on the research of entosis based on VOSviewer.

The journal biplot overlay provides a visual representation of the distribution of journals, the evolution of citation trajectories, and the shift in research focus across various research areas. In each subplot of Figure 4C, the left side displays the citing journal groups, while the right side illustrates the cited journal groups. As shown in Figure 4C, most citations in the curve are concentrated in the yellow citation link area, with the thickest citation link identified using the Z-score function of CiteSpace. The results indicate that the citing journals clustered around entosis primarily encompass molecular biology and immunology, whereas the cited journals cluster predominantly within the fields of molecular biology and genetics. These findings suggest that current research on entosis is mainly focused on molecular biology and immunology.

## 3.4 Authors and co-cited authors

A total of 1,055 authors have contributed to entosis research. As presented in Table 3, the top 10 authors contributed 140 publications, accounting for approximately 71% of all publications in this domain. Sun, Qiang emerged as the leading author with 24 research publications, followed by Overholtzer, M with 23 papers, and Huang, Hongyan with 17 papers. Figure 5B illustrates the yearly contributions of the leading 10 authors from 2007 to 2024. Overholtzer, M has been active in the field since the introduction of the concept of entosis, while Wang, Xiaoning and Florey, Oliver began their major research contributions after 2009 and 2011, respectively. As depicted in Figure 3C, VOSviewer illustrates the connections among authors, highlighting that those from the same countries or regions often collaborate more frequently and exhibit stronger connections. However, collaboration among authors from different countries remains inadequate.

## 3.5 Co-citation analysis

The co-citation analysis evaluates the relevance of scholarly articles based on their co-citation frequency. Using VOSviewer, we examined 48 authors who each have at least 20 citations. As illustrated in Figure 5A, notable collaborations include those between Qiang Sun and Manna Wang, as well as between Overholtzer, M and Fais, S. Table 3 lists these authors, showing that Overholtzer, M is the most cited author (240 citations), followed closely by Sun, Q (187 citations) and Florey, O (129 citations). Notably, four authors in total have surpassed the 100-citation mark.

## 3.6 Highly valuable papers

To assess the impact of key papers on entosis studies, we analyzed citation counts from various regions. In total, over 150

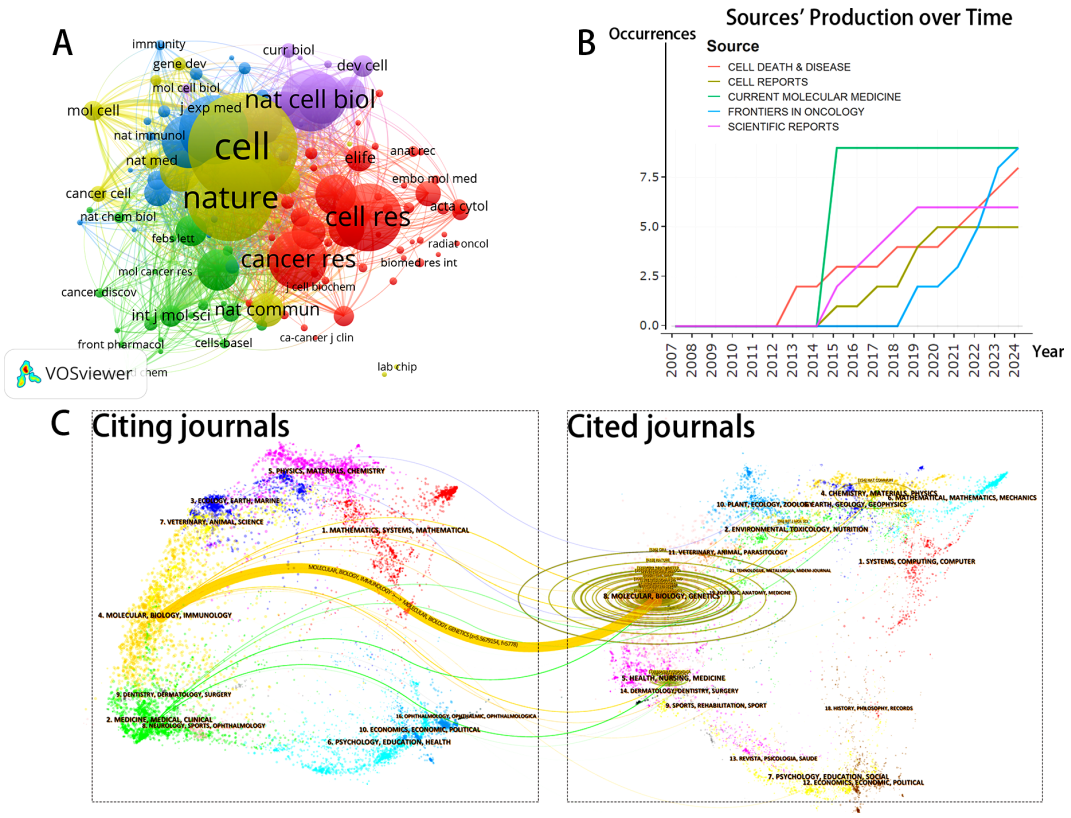


FIGURE 4
**(A)** Network map of journals that were co-cited in more than 20 citations. **(B)** Top 5 journals' publication over time. **(C)** The dual-map overlay of journals related to Entosis.

papers in this area received more than five citations (Figure 6A). The paper titled "Classification of Cell Death: The 2009 Recommendations of the Committee on Nomenclature of Cell Death" has garnered an impressive 2,314 citations. This study details the NCCD's 2009 recommendations regarding cell death terminology, including terms like "entosis," "mitotic catastrophe," "necrosis," "necroptosis," and "pyroptosis." (20). It emphasizes that "entosis is a default pathway that becomes apparent only when other catabolic processes are inhibited."

The second most cited article, "A Non-Apoptotic Cell Death Process, Entosis, That Occurs by Cell-in-Cell Invasion," has received 499 citations. This paper introduces the concept of "entosis" and provides evidence of its role in the CIC cytological features commonly observed in human cancers (3). The third most

TABLE 2 Top 10 journals and co-cited journals for studies Entosis.

| Ranks | Journals | Count | IF | Q | Co-Cited Journals | Co-Citation | IF | Q |
|---|---|---|---|---|---|---|---|---|
| 1 | *Current Molecular Medicine* | 9 | 2.5 | Q3 | *Cell* | 537 | 64.5 | Q1 |
| 2 | *Frontiers in Cell and Developmental Biology* | 9 | 5.5 | Q1 | *Nature* | 418 | 64.8 | Q1 |
| 3 | *Cell Death and Disease* | 8 | 9 | Q1 | *Cell Death Differ* | 328 | 12.4 | Q1 |
| 4 | *Scientific Reports* | 6 | 4.6 | Q2 | *Cell Res* | 322 | 44.1 | Q1 |
| 5 | *Cell Reports* | 5 | 8.8 | Q1 | *P Natl Acad Sci USA* | 296 | 11.1 | Q1 |
| 6 | *Cell Research* | 4 | 44.1 | Q1 | *Nat Cell Biol* | 292 | 21.3 | Q1 |
| 7 | *Frontiers in Cell and Developmental Biology* | 4 | 5.5 | Q1 | *Cancer Res* | 278 | 11.2 | Q1 |
| 8 | *International Journal of Molecular Sciences* | 4 | 5.6 | Q1 | *J Biol Chem* | 249 | 4.8 | Q2 |
| 9 | *Cancers* | 4 | 5.2 | Q2 | *J Cell Biol* | 235 | 7.8 | Q1 |
| 10 | *Journal of Cell Biology* | 4 | 7.8 | Q1 | *Nat Rev Mol Cell Bio* | 200 | 112.7 | Q1 |

TABLE 3 Top 10 authors and co-cited authors on Entosis.

| Rank | Authors | Counts | Co-Cited Authors | Citations | Total Link Strength |
|---|---|---|---|---|---|
| 1 | Sun, Qiang | 24 | Overholtzer, M | 240 | 22186 |
| 2 | Overholtzer, M | 23 | Sun, Qiang | 187 | 17261 |
| 3 | Huang, Hongyan | 17 | Florey, O | 129 | 12227 |
| 4 | Niu, Zubiao | 14 | Fais, S | 112 | 10369 |
| 5 | Wang, Xiaoning | 14 | Galluzzi, L | 99 | 9371 |
| 6 | Chen, ZhaoLie | 11 | Wang, S | 90 | 8695 |
| 7 | Gao, Lihua | 10 | Kroemer, G | 90 | 7401 |
| 8 | Zheng, You | 9 | Lugini, L | 71 | 6767 |
| 9 | Wang, Manna | 9 | Durgan, J | 546 | 612 |
| 10 | Florey, O | 9 | Hamann, Jc | 539 | 6066 |

cited article, "Autophagy Machinery Mediates Macroendocytic Processing and Entotic Cell Death by Targeting Single Membranes," has been cited 332 times and discusses how autophagy proteins can target single-membrane vacuoles in cells even in the absence of pathogenic organisms (4).

VOSviewer identifies three primary groups (Figure 6B) with extensive interconnections among the references, highlighting the intricate relationships in this research area. Table 4 presents the 10 most frequently cited sources in entosis research, with "Overholtzer M, 2007, Cell, v131, p966" standing out as the second most frequently cited reference, accumulating 169 citations.

Additionally, references that have been widely cited by scholars in a specific field over time are referred to as references with citation bursts. These citations serve as important indicators, highlighting sources that have generated significant scholarly interest within a particular area over a specific period. Using CiteSpace, we identified

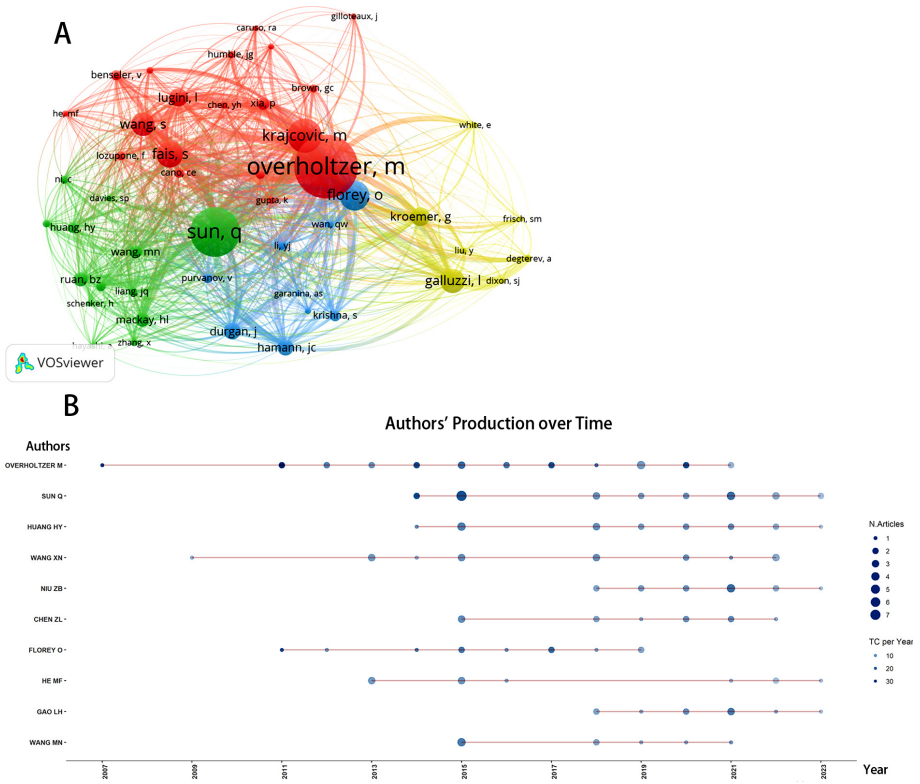


FIGURE 5
**(A)** Network visualization diagram of the co-cited authors regarding Entosis. **(B)** Top 10 authors' production over time. TC, total citation.

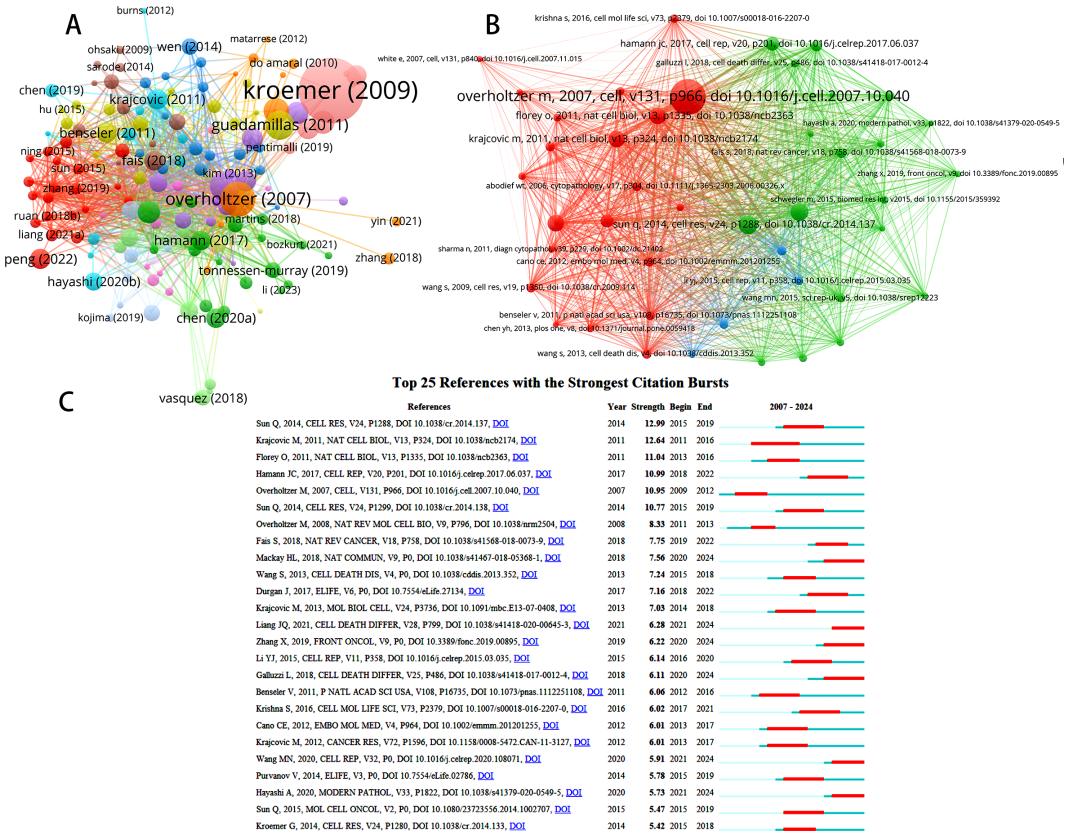


FIGURE 6
**(A)** Network map of citation analysis of documents with more than 5 citations. **(B)** Network map of co-citation analysis of references. **(C)** Top 25 references with strongest citation bursts of publications regarding Entosis.

TABLE 4 Top 10 co-cited references for Entosis research.

| Ranks | Cited Reference | Citations | Total Link Strength |
|---|---|---|---|
| 1 | Overholtzer M, 2007, *Cell*, v131, p966, | 169 | 1415 |
| 2 | Sun Q, 2014, *Cell Res*, v24, p1288, doi 10.1038/cr.2014.137 | 78 | 955 |
| 3 | Sun Q, 2014, *Cell Res*, v24, p1299, | 75 | 981 |
| 4 | Krajcovic M, 2011, *Nat Cell Biol*, v13, p324, | 69 | 791 |
| 5 | Florey O, 2011, *Nat Cell Biol*, v13, p1335, | 68 | 777 |
| 6 | Overholtzer M, 2008, *Nat Rev Mol Cell Bio*, v9, p796, | 68 | 764 |
| 7 | Hamann Jc, 2017, *Cell Rep*, v20, p201, | 56 | 623 |
| 8 | Lugini L, 2006, *Cancer Res*, v66, p3629, | 53 | 703 |
| 9 | Durgan J, 2017, *Elife*, v6, | 42 | 523 |
| 10 | Fais S, 2018, *Nat Rev Cancer*, v18, p758, | 41 | 562 |

the top 25 sources with the most intense citation surges, as shown in Figure 6C. Notably, Qiang Sun's 2014 article, "Induction of Entosis by Epithelial Cadherin Expression" (21), ranked highest (intensity = 10.11). Following this, Krajcovic et al. defined a previously unknown mechanism of cytokinesis failure and aneuploid cell formation in human cancers (5), further exploring the role of entosis in this context.

## 3.7 Analysis of keywords

CiteSpace's algorithm was used to detect keyword bursts. Figure 7A displays the top 10 keywords with the most significant bursts. The most frequently cited keyword was "phagocytosis" (intensity = 3.68), followed by "human cancers" (3.38) and "autophagy" (2.62). The keyword "phagocytosis" had the longest burst duration, spanning six years from 2012 to 2017. Notably, the keyword "ferroptosis" has seen a recent surge in citations (2022–2024). Ferroptosis is a novel iron-dependent mode of programmed cell death that differs from apoptosis, necrosis, and autophagy. It is closely linked to the pathophysiological processes of various diseases, including tumors and neurological disorders (22). Given that entosis and ferroptosis are both forms of programmed cell death, their simultaneous appearance in studies related to tumor

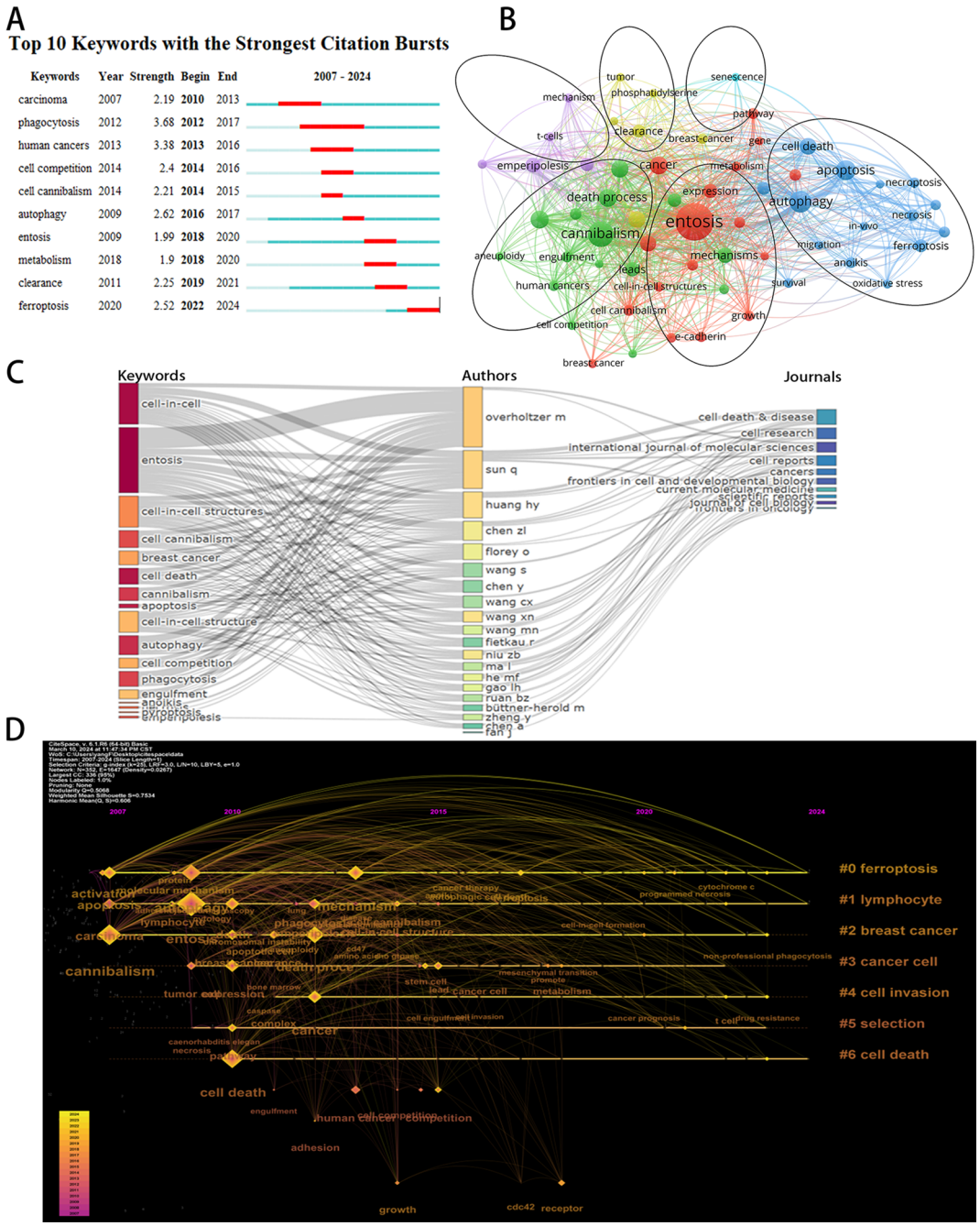


FIGURE 7
**(A)** Top 10 keywords with the strongest citation bursts based on Citespace. **(B)** Overlay visualization of the keywords network based on Vosviewer. **(C)** The three-field plot of the Keywords analysis base on R package "bibliometrix." **(D)** The timeline view of keywords conducted by CiteSpace.

cellular mechanisms suggests that research into entosis's role in tumor development may become a significant area of interest in the future.

Analyzing keyword co-occurrences facilitates the rapid identification of hotspots within the research domain. The leading 20 high-frequency terms in this area are enumerated in Table 5. According to the co-occurrence analysis, the top four keywords identified were: "entosis" (137 occurrences), "cannibalism" (58 occurrences), "autophagy" (42 occurrences), and "apoptosis" (35 occurrences). Cannibalism, autophagy, and apoptosis were mentioned more than 30 times and represent the primary focus of entosis research.

From a total of 1,111 keywords, we excluded those with fewer than five occurrences and selected 59 keywords for cluster analysis using VOSviewer. As illustrated in Figure 7B, the keywords were categorized into six distinct clusters, each representing a unique research pathway. The red cluster includes "entosis," "expression," and "gene," indicating a strong correlation between entosis and the selective expression of genes. The blue cluster encompasses "autophagy," "apoptosis," and "cell death," suggesting a potential

TABLE 5 Top 20 keywords on research of Entosis.

| Rank | Keywords | Occurrences | Rank | Keywords | Occurrences |
|---|---|---|---|---|---|
| 1 | Entosis | 137 | 11 | Death | 21 |
| 2 | Cannibalism | 58 | 12 | Mechanisms | 19 |
| 3 | Autophagy | 42 | 13 | Emperipolesis | 18 |
| 4 | Apoptosis | 35 | 14 | Leads | 16 |
| 5 | Cell-in-cell | 28 | 15 | Expression | 16 |
| 6 | Cancer | 28 | 16 | Tumor-cells | 15 |
| 7 | Death process | 27 | 17 | Lymphocytes | 15 |
| 8 | Phagocytosis | 26 | 18 | Ferroptosis | 14 |
| 9 | Carcinoma | 24 | 19 | Activation | 14 |
| 10 | Cell death | 23 | 20 | Clearance | 13 |

connection between entosis and various forms of cell death, particularly apoptosis. The purple cluster, characterized by terms like "emperipolesis," "lymphocytes," and "nurse cells," indicates a higher incidence of entosis in specific cell types, such as lymphocytes. The green cluster features keywords like "cannibalism," "engulfment," and "death process," emphasizing the concept of cannibalism among similar cells in entosis. Lastly, the orange cluster contains keywords such as "breast cancer," "clearance," and "tumor," highlighting that entosis has been extensively studied in solid tumors, particularly breast cancer.

Figure 7C presents a three-field graph linking authors, keywords, and journals, showcasing the most frequently used keywords and the journals that publish the most in this field. The most common keywords include "CIC," "entosis," "CIC structures," and "cell cannibalism." Authors Sun Q, Overholtzer M, and Huang HY are closely associated with the keywords "entosis" and "CIC," creating strong links. The journal with the most significant connections is *Cell Death & Disease*.

Analyzing the timeline of keywords provides valuable insights into the progress and evolving focus of the research area. The size of the nodes reflects the frequency of keyword appearances within the clusters, with earlier nodes representing keywords that appeared first in the timeline. Figure 7D depicts keywords such as "ferroptosis," "lymphocyte," "breast cancer," "cancer cell," "cell invasion," "selection," and "cell death." The early appearance of "cannibalism" (dating back to 2007) suggests that cancer and apoptosis were among the initial areas of interest in this field. Notably, the frequency of the keyword "drug resistance" has significantly increased recently. This trend may indicate the rapid development of entosis within cancer therapeutics, suggesting that the development of novel drugs aimed at countering cancer cell escape is becoming a prominent research topic.

# 4 Discussion

This investigation used tools such as VOSviewer, CiteSpace, and the Bibliometrix R package to implement sophisticated bibliometric analysis principles and advanced visualization techniques. Our review of entosis and its impact on cancer involved an extensive analysis of annual publications, geographical regions, institutions, contributing and cited authors, academic and peer-reviewed journals, and pertinent keywords, aiming to uncover major research foci and trends in this domain.

In examining geographical areas and institutions, China and the United States emerged as the leading countries in terms of publication output. However, there is a notable lack of international collaboration between these countries. To foster the collective advancement of this field, China must actively engage in strengthening global cooperation. Chinese institutions account for the highest percentage of the top 10 institutions by publication volume. While the development of entosis research requires the exchange and collaboration of experts, these institutions predominantly collaborate with domestic counterparts. We anticipate an increase in cooperation among different countries and institutions to promote collaborative growth in this research area.

Regarding journals and co-citation analysis, *Current Molecular Medicine* ranked first in terms of publication count. In 2024, the top 10 journals had an average IF of 9.86, with *Cell Research* recording the highest IF at 44.10. Notably, 80% of the journals had an IF exceeding 5, and 70% of these journals were categorized as Q1 (JCR). Among the journals cited together, *Nature Reviews Molecular Cell Biology* emerged as the highest in IF at 112.70, while *Cell* was the most frequently cited. Furthermore, 9 out of the top 10 journals frequently cited were classified as Q1. These results indicate that this research area has attracted significant academic attention from prominent journals specializing in cell biology and cancer treatments.

In terms of authorship, Sun, Qiang, and Overholtzer, Michael stand out as the most prolific contributors in the field. The collaboration network among authors (Figure 3C) highlights their ongoing cooperative efforts. Their most cited article, "Competition between Human Cells by Entosis," demonstrates that human cells engage in direct competition through a phagocytic process known as entosis, resulting in their engulfment or cannibalism while alive,

followed by cell death. Our research reveals that the characteristics of the engulfing ("winner") and engulfed ("loser") cells are determined by the phagocytic mechanism governed by RhoA and actomyosin. In heterogeneous populations, tumor cells with high deformability tend to engulf and outcompete neighboring cells with lower deformability. Furthermore, the study found that the activation of the Kras and Rac pathways bestows dominant status on cells by reducing contractile myosin, facilitating the absorption of adjacent cells, which ultimately leads to cell death. The paper also calculates the energy dynamics of CIC formation, highlighting the mechanical distinctions between winning and losing cells as crucial for advancing our understanding of entosis. This information outlines a competitive process in mammalian cells, particularly in human tumors, and serves as a vital guide for examining entosis in human cancer cells.

Within the context of cited authors, Overholtzer, M emerges as the most frequently cited author. He is best known for his article that first introduced the concept of "entosis," providing evidence that it is a prevalent "CIC" phenomenon in human cancers. This foundational article not only established the concept of entosis but also suggested that it is driven by the compaction forces associated with the formation of adherens junctions, occurring without integrin interaction. This mechanism may potentially serve as an inherent tumor-inhibiting force for cells separated from the extracellular matrix.

The significance of the most cited literature and references in this field has been discussed in detail above; therefore, these points will not be reiterated here.

## 4.1 Hotspots and frontiers

Recent research has highlighted that references and keywords experiencing a surge in citations can serve as indicators of trending topics within a specific field. Upon examining the major research areas associated with these frequently cited references and keywords, we identified that current themes in entosis research primarily focus on understanding the biological mechanisms underlying entosis and exploring the potential of inducing entosis in cancer cells as a therapeutic strategy. Notably, references citing the surge in 2014 reported that the expression of exogenous epithelial cadherin proteins (E- or P-cadherin) in human breast tumor cells, which lack endogenous expression of these cadherins, induces entosis and inhibits transformed growth (21).

Keywords are an effective means of quickly grasping the focus and progress within the entosis research field. By employing both keyword clustering analysis and a timeline perspective (see Figure 7), we can discern temporal shifts in research topics. Current trends increasingly concentrate on the potential impact of entosis on tumor cells and the application of entosis to impede cancer progression. This focus reflects a strong interest in the practical implications of entosis research, particularly in uncovering the effects of entosis on the development of tumor and entosis inhibitors. Thus, we can conclude that research on entosis has focused on the following areas:

## 4.2 Hotspots: impact of entosis on tumor development

Entosis is characterized by the dynamic penetration of a living cell (the internalized cell) into an adjacent living cell of a similar type (the host cell), leading to the formation of a CIC structure. While entotic cells typically undergo death, some can escape from the host cell. A small percentage of these cells are capable of division within the host (3). The death of entotic cells occurs through a non-cell-autonomous process, as the live engulfed cells are degraded by autophagy and lysosomal pathways (23). This cell death occurs in the absence of cysteine-3 cleavage and lacks the morphological features associated with apoptosis. Therefore, it has been suggested that entosis should be classified as a novel type IV cell death (24).

Initial research indicated that CIC structures had an anticancer effect primarily by inducing cell death (3, 25). Early experiments demonstrated that the entosis process could inhibit tumor progression by killing tumor cells that had already been isolated from the stroma (5). However, entosis may promote tumor progression by inducing changes in cell ploidy (6). It actively fosters polyploidy through the interruption of cell division, leading to the development of polyploid cells in cultures. Furthermore, there is a correlation between CIC structures and cancer stages; for instance, in lung (26), gastric (27, 28), breast (29), renal (30), and pancreatic cancers (31), CIC structures serve as markers of poor prognosis. A direct comparison of xenograft growth in mice revealed that cells exhibiting greater endodermal activity formed larger tumors, indirectly hinting at a pro-tumorigenic role for the CIC structure (32). As research on entosis has advanced, evidence has accumulated that a significant proportion of cancer cells undergoing entosis are able to escape from host cells (32, 33). It is now widely accepted that host cells provide a safe environment for endocytes, allowing them to evade adverse conditions such as nutrient deprivation, toxic substances, and immune cell attacks (34, 35). In conclusion, entosis is increasingly viewed as promoting the proliferation and metastasis of tumor cells.

## 4.3 Hotspots: inhibitors of entosis

Entosis is triggered by various physiological conditions, including matrix detachment, aberrant mitosis (36), and glucose deprivation (37), Regardless of the initiating mechanism, entotic cells form adherens junctions (AJs) through $Ca^{2+}$/E-cadherin interactions (21). Following the formation of AJs, these cells are engulfed via actin polymerization (38), mechanical ring formation (39), and actomyosin contraction (40–42).

Recent findings indicate that intracellular $Ca^{2+}$ signaling regulates entosis through the SEPTIN-Orai1-$Ca^{2+}$/CaM-MLCK-actomyosin axis (40, 41). Intracellular $Ca^{2+}$ oscillations in entotic cells exhibit spatiotemporal variations during engulfment, mediated by Orai1 $Ca^{2+}$ channels in the plasma membrane (43). SEPTIN controls the polarized distribution of Orai1, leading to local MLCK activation, which results in MLC phosphorylation and actomyosin contraction, ultimately facilitating the internalization of invasive cells (44–46). Notably, $Ca^{2+}$ chelators and inhibitors of SEPTIN, Orai1, and MLCK have been shown to suppress entosis (10).

As the role of entosis in tumor development becomes clearer, investment in research and development of entosis inhibitors is expected to grow, paving the way for future anticancer therapies that target this process.

## 5 Conclusion

In summary, a bibliometric analysis of entosis research reveals a rapidly evolving and dynamic field that reflects our growing understanding of novel modes of cell death and the potential for anticancer therapies to make a significant impact. Key themes identified include "cancer prognosis," "drug resistance," and "cell engulfment." As research in entosis has advanced, there is a noticeable shift toward the perspective that entosis promotes tumor cell proliferation and metastasis, underscoring the current emphasis on the entotic properties of tumor cells. Notably, the emergence of "entosis inhibitors" as a central topic suggests a promising direction for future research, as the pro-cancer effects of entosis continue to be elucidated. The integration of cellular pharmacology, cell biology, and related disciplines may provide a robust impetus for the development of entosis inhibitors. For instance, the identification of Orai1 as a $Ca^{2+}$ channel involved in non-apoptotic cell death and its role in cancer development has facilitated the development of $Ca^{2+}$ chelators, as well as inhibitors targeting SEPTIN, Orai1, and MLCK to inhibit entosis. Consequently, researchers, clinicians, and policymakers should closely monitor this field and support its ongoing advancement, given its significant potential to inhibit tumor cell growth of tumor cells.

## Data availability statement

The original contributions presented in the study are included in the article/supplementary material. Further inquiries can be directed to the corresponding author.

## Author contributions

YX: Conceptualization, Data curation, Investigation, Methodology, Software, Visualization, Writing – original draft. JT: Conceptualization, Investigation, Software, Visualization, Writing – review & editing. XZ: Software, Writing – review & editing. XH: Conceptualization, Writing – review & editing. YT: Project administration, Resources, Writing – review & editing.

## Funding

The author(s) declare financial support was received for the research, authorship, and/or publication of this article. This research was funded by the Zhejiang Traditional Chinese Medicine Science and Technology Program (Special project modernization of Traditional Chinese Medicine) (Grant Number 2022ZX006).

## Acknowledgments

We are grateful to The First Affiliated Hospital of Zhejiang Chinese Medical University for their support of this work and the free software CiteSpace, VOSviewer and R4.3.1.

## Conflict of interest

The authors declare that the research was conducted in the absence of any commercial or financial relationships that could be construed as a potential conflict of interest.

## Publisher's note



## References

1. Le Bot N. Entosis: cell death by invasion. *Nat Cell Biol*. (2007) 9:1346–. doi: 10.1038/ncb1207-1346

2. Mlynarczuk-Bialy I, Dziuba I, Sarnecka A, Platos E, Kowalczyk M, Pels KK, et al. Entosis: from cell biology to clinical cancer pathology. *Cancers*. (2020) 12:2481. doi: 10.3390/cancers12092481

3. Overholtzer M, Mailleux AA, Mouneimne G, Normand G, Schnitt SJ, King RW, et al. A nonapoptotic cell death process, entosis, that occurs by cell-in-cell invasion. *Cell*. (2007) 131:966–79. doi: 10.1016/j.cell.2007.10.040

4. Florey O, Kim SE, Sandoval CP, Haynes CM, Overholtzer M. Autophagy machinery mediates macroendocytic processing and entotic cell death by targeting single membranes. *Nat Cell Biol*. (2011) 13:1335–U118. doi: 10.1038/ncb2363

5. Krajcovic M, Johnson NB, Sun Q, Normand G, Hoover N, Yao E, et al. A non-genetic route to aneuploidy in human cancers. *Nat Cell Biol*. (2011) 13:324–U07. doi: 10.1038/ncb2174

6. Krajcovic M, Overholtzer M. Mechanisms of ploidy increase in human cancers: A new role for cell cannibalism. *Cancer Res*. (2012) 72:1596–601. doi: 10.1158/0008-5472.Can-11-3127

7. Lugini L, Matarrese P, Tinari A, Loznpone F, Federici C, Iessi E, et al. Cannibalism of live lymphocytes by human metastatic but not primary melanoma cells. *Cancer Res*. (2006) 66:3629–38. doi: 10.1158/0008-5472.Can-05-3204

8. Krajcovic M, Krishna S, Akkari L, Joyce JA, Overholtzer M. Mtor regulates phagosome and entotic vacuole fission. *Mol Biol Cell*. (2013) 24:3736–45. doi: 10.1091/mbc.E13-07-0408

9. Hyrossova P, Arago M, Munoz-Pinedo C, Vinals F, Garcia-Roves PM, Escolano C, et al. Glycosylation defects, offset by pepck-M, drive entosis in breast carcinoma cells. *Cell Death Dis*. (2022) 13:730. doi: 10.1038/s41419-022-05177-x

10. Lee AR, Park CY. Orai1 is an entotic $ca^{2+}$ Channel for non-apoptotic cell death, entosis in cancer development. *Adv Sci*. (2023) 10:e2205913. doi: 10.1002/advs.202205913

11. Wang J, Maniruzzaman M. A global bibliometric and visualized analysis of bacteria-mediated cancer therapy. *Drug Discov Today*. (2022) 27:103297. doi: 10.1016/j.drudis.2022.05.023

12. Ellegaard O, Wallin JA. The bibliometric analysis of scholarly production: how great is the impact? *Scientometrics*. (2015) 105:1809–31. doi: 10.1007/s11192-015-1645-z

13. Chen CM. Searching for intellectual turning points: progressive knowledge domain visualization. *Proc Natl Acad Sci USA*. (2004) 101:5303–10. doi: 10.1073/pnas.0307513100

14. van Eck NJ, Waltman L. Software survey: vosviewer, a computer program for bibliometric mapping. *Scientometrics*. (2010) 84:523–38. doi: 10.1007/s11192-009-0146-3

15. Liu F, Chen N, Wang R, Zhang L, Li Y. Visual analysis of allergic rhinitis in children based on web of science and citespace software. *Front Pediatr*. (2022) 10:911293. doi: 10.3389/fped.2022.911293

16. Pan W, Zheng P, Huang J, Mou D, Li Y. A study on the effects of the "Dean" Process on health information. Detection of research hotspots in the field of health information based on the data cleansing "Dean" Process. *Mod Intell*. (2018) 38:73–7. doi: 10.3969/j.issn.1008-0821.2018.10.011

17. Synnestvedt MB, Chen C, Holmes JH. Citespace ii: visualization and knowledge discovery in bibliographic databases. *AMIA Ann Symp Proc*. (2005) 2005:724–8.

18. Di Somma S, Iannuzzi CA, Passaro C, Forte IM, Iannone R, Gigantino V, et al. The oncolytic virus *dl* 922-947 triggers immunogenic cell death in mesothelioma and reduces xenograft growth. *Front Oncol*. (2019) 9:564. doi: 10.3389/fonc.2019.00564

19. Liu B, Zhou C, Ma H, Gong B. Mapping the youth soccer: A bibliometrix analysis using R-tool. *Digit Health*. (2023) 9:20552076231183550. doi: 10.1177/20552076231183550

20. Kroemer G, Galluzzi L, Vandenabeele P, Abrams J, Alnemri ES, Baehrecke EH, et al. Classification of cell death: recommendations of the nomenclature committee on cell death 2009. *Cell Death Differ*. (2009) 16:3–11. doi: 10.1038/cdd.2008.150

21. Sun Q, Cibas ES, Huang H, Hodgson L, Overholtzer M. Induction of entosis by epithelial cadherin expression. *Cell Res*. (2014) 24:1288–98. doi: 10.1038/cr.2014.137

22. Li J, Cao F, Yin H, Huang Z, Lin Z, Mao N, et al. Ferroptosis: past, present and future. *Cell Death Dis*. (2020) 11:88. doi: 10.1038/s41419-020-2298-2

23. Krishna S, Overholtzer M. Mechanisms and consequences of entosis. *Cell Mol Life Sci*. (2016) 73:2379–86. doi: 10.1007/s00018-016-2207-0

24. Martins I, Raza SQ, Voisin L, Dakhli H, Law F, De Jong D, et al. Entosis: the emerging face of non-cell-autonomous type iv programmed death. *BioMed J*. (2017) 40:133–40. doi: 10.1016/j.bj.2017.05.001

25. Florey O, Gammoh N, Kim SE, Jiang X, Overholtzer M. V-atpase and osmotic imbalances activate endolysosomal lc3 lipidation. *Autophagy*. (2015) 11:88–99. doi: 10.4161/15548627.2014.984277

26. Augusto Aguirre L, Montalban-Hernandez K, Avendano-Ortiz J, Marin E, Lozano R, Toledano V, et al. Tumor stem cells fuse with monocytes to form highly invasive tumor-hybrid cells. *Oncoimmunology*. (2020) 9:1773204. doi: 10.1080/2162402x.2020.1773204

27. Houghton J, Stoicov C, Nomura S, Rogers AB, Carlson J, Li HC, et al. Gastric cancer originating from bone marrow-derived cells. *Science*. (2004) 306:1568–71. doi: 10.1126/science.1099513

28. Su Y, Subedee A, Bloushtain-Qimron N, Savova V, Krzystanek M, Li L, et al. Somatic cell fusions reveal extensive heterogeneity in basal-like breast cancer. *Cell Rep*. (2015) 11:1549–63. doi: 10.1016/j.celrep.2015.05.011

29. Dziuba I, Gawel AM, Tyrna P, Machtyl J, Olszanecka M, Pawlik A, et al. Homotypic entosis as a potential novel diagnostic marker in breast cancer. *Int J Mol Sci*. (2023) 24:6819. doi: 10.3390/ijms24076819

30. Kong Y, Liang Y, Wang J. Foci of entotic nuclei in different grades of noninherited renal cell cancers. *IUBMB Life*. (2015) 67:139–44. doi: 10.1002/iub.1354

31. Nitschke C, Markmann B, Konczalla L, Kropidlowski J, Pereira-Veiga T, Scognamiglio P, et al. Circulating cancer associated macrophage-like cells as a potential new prognostic marker in pancreatic ductal adenocarcinoma. *Biomedicines*. (2022) 10:2955. doi: 10.3390/biomedicines10112955

32. Mackay HL, Moore D, Hall C, Birkbak NJ, Jamal-Hanjani M, Karim SA, et al. Genomic instability in mutant P53 cancer cells upon entotic engulfment. *Nat Commun*. (2018) 9:3070. doi: 10.1038/s41467-018-05368-1

33. Fais S, Overholtzer M. Cell-in-cell phenomena in cancer. *Nat Rev Cancer*. (2018) 18:758–66. doi: 10.1038/s41568-018-0073-9

34. Gutwillig A, Santana-Magal N, Farhat-Younis L, Rasoulouniriana D, Madi A, Luxenburg C, et al. Transient cell-in-cell formation underlies tumor relapse and resistance to immunotherapy. *Elife*. (2022) 11:e80315. doi: 10.7554/eLife.80315

35. Liu J, Wang L, Zhang Y, Li S, Sun F, Wang G, et al. Induction of entosis in prostate cancer cells by nintedanib and its therapeutic implications. *Oncol Lett*. (2019) 17:3151–62. doi: 10.3892/ol.2019.9951

36. Durgan J, Tseng YY, Hamann JC, Domart MC, Collinson L, Hall A, et al. Mitosis can drive cell cannibalism through entosis. *Elife*. (2017) 6:e27134. doi: 10.7554/eLife.27134

37. Hamann JC, Surcel A, Chen R, Teragawa C, Albeck JG, Robinson DN, et al. Entosis is induced by glucose starvation. *Cell Rep*. (2017) 20:201–10. doi: 10.1016/j.celrep.2017.06.037

38. Ren W, Zhao W, Cao L, Huang J. Involvement of the actin machinery in programmed cell death. *Front Cell Dev Biol*. (2021) 8:634849. doi: 10.3389/fcell.2020.634849

39. Wang M, Niu Z, Qin H, Ruan B, Zheng Y, Ning X, et al. Mechanical ring interfaces between adherens junction and contractile actomyosin to coordinate entotic cell-in-cell formation. *Cell Rep*. (2020) 32:108071. doi: 10.1016/j.celrep.2020.108071

40. Lioudyno MI, Kozak JA, Penna A, Safrina O, Zhang SL, Sen D, et al. Orai1 and stim1 move to the immunological synapse and are up-regulated during T cell activation. *Proc Natl Acad Sci USA*. (2008) 105:2011–6. doi: 10.1073/pnas.0706122105

41. Yang S, Zhang JJ, Huang XY. Orai1 and stim1 are critical for breast tumor cell migration and metastasis. *Cancer Cell*. (2009) 15:124–34. doi: 10.1016/j.ccr.2008.12.019

42. Sun Q, Cibas ES, Huang H, Hodgson L, Overholtzer M. Induction of entosis by epithelial cadherin expression. *Cell Res*. (2014) 24:1288–98. doi: 10.1038/cr.2014.137

43. Bagur R, Hajnoczky G. Intracellular $ca^{2+}$ Sensing: its role in calcium homeostasis and signaling. *Mol Cell*. (2017) 66:780–8. doi: 10.1016/j.molcel.2017.05.028

44. Hogan PG. The stim1-orai1 microdomain. *Cell Calcium*. (2015) 58:357–67. doi: 10.1016/j.ceca.2015.07.001

45. La Rovere RML, Roest G, Bultynck G, Parys JB. Intracellular $ca^{2+}$ Signaling and $ca^{2+}$ Microdomains in the control of cell survival, apoptosis and autophagy. *Cell Calcium*. (2016) 60:74–87. doi: 10.1016/j.ceca.2016.04.005

46. Sharma S, Quintana A, Findlay GM, Mettlen M, Baust B, Jain M, et al. An sirna screen for nfat activation identifies septins as coordinators of store-operated $ca^{2+}$ Entry. *Nature*. (2013) 499:238–42. doi: 10.1038/nature12229

frontiers | Frontiers in Oncology

TYPE Technology and Code
PUBLISHED 19 February 2025
DOI 10.3389/fonc.2025.1539782



OPEN ACCESS

EDITED BY
Tao Liu,
University of New South Wales, Australia

REVIEWED BY
Lei Bu,
New York University, United States
Yong Li,
The First Affiliated Hospital of Nanchang University, China
Susanna Grigson,
Flinders University, Australia
Deyou Tang,
South China University of Technology, China

*CORRESPONDENCE
Wenjun Deng
wdeng@mgh.harvard.edu
Shanye Yin
shanye.yin@einsteinmed.edu

RECEIVED 04 December 2024
ACCEPTED 31 January 2025
PUBLISHED 19 February 2025

CITATION
Hu E, An J, Gersten AJ, Wu N, Kawachi N, Zhu J, Rosenblatt G, Augustine S, Smith RV, Segall JE, Ostrer H, Amelio AL, Chung CH, Prystowsky MB, Ow TJ, Deng W and Yin S (2025) Virusplot: a web server for viral integration analysis and visualization. *Front. Oncol.* 15:1539782. doi: 10.3389/fonc.2025.1539782



# Virusplot: a web server for viral integration analysis and visualization

Erqiang Hu[1,2,3], Jianhong An[1,2,3], Adam J Gersten[1,4], Nicole Wu[5], Nicole Kawachi[1], Jing Zhu[1], Gregory Rosenblatt[1], Stelby Augustine[4], Richard V. Smith[4], Jeffrey E Segall[1], Harry Ostrer[1], Antonio L Amelio[6,7], Christine H. Chung[7], Michael B. Prystowsky[1], Thomas J. Ow[1,4], Wenjun Deng[8]* and Shanye Yin[1,2,3]*

[1]Department of Pathology, Albert Einstein College of Medicine, Bronx, NY, United States, [2]Einstein Pathology Single-cell & Bioinformatics Laboratory, Bronx, NY, United States, [3]Montefiore Einstein Comprehensive Cancer Center, Albert Einstein College of Medicine, Bronx, NY, United States, [4]Department of Otorhinolaryngology-Head and Neck Surgery, Montefiore Medical Center/Albert Einstein College of Medicine, Bronx, NY, United States, [5]The University of Texas at Austin, Austin, TX, United States, [6]Department of Tumor Microenvironment and Metastasis, H. Lee Moffitt Cancer Center & Research Institute, Tampa, FL, United States, [7]Department of Head and Neck-Endocrine Oncology, H. Lee Moffitt Cancer Center & Research Institute, Tampa, FL, United States, [8]Department of Neurology, Massachusetts General Hospital, Harvard Medical School, Boston, MA, United States

The integration of viral DNA into the human genome is a critical event in the pathogenesis of various cancers. This process leads to genomic instability, disrupts cellular regulatory mechanisms, and activates oncogenes or inactivates tumor suppressor genes. Despite significant advancements in genome sequencing technologies, there remains a notable lack of computational tools, particularly web-based applications, specifically designed for viral integration analysis and visualization. To address this gap, we present virusPlot, a web server with the following functional modules: (i) automatic retrieval of virus genome sequences and their annotation; (ii) visualization of virus integration locations and read counts through a graphical representation that links viral and host genome integration sites, facilitating the interpretation of integration patterns; (iii) analysis of virus integration hotspots using Fisher's exact test; and (iv) integration of various functions into an interactive web platform via shinyapp. VirusPlot efficiently processes and visualizes integration data from viruses and host genomes, providing researchers with an intuitive and user-friendly analytical tool that simplifies the complexity of virus integration analysis.

KEYWORDS

**viral integration, genomic visualization, hotspot analysis, computational biology, bioinformatics tool, host-virus interaction**

# 1 Introduction

Viral insertion into the host genome is a critical event in the viral life cycle of several viruses associated with tumorigenesis (1, 2). Specifically, viruses, such as human papillomavirus (HPV) (3, 4), hepatitis B virus (HBV) (5), Epstein-Barr virus (EBV) (6), and Human T-cell leukemia virus type 1 (HTLV-1) (7), are well-known for their oncogenic potential through this mechanism. The integration of viral DNA can result in genomic alterations that drive malignant transformation, contributing to cancer development and progression (1, 8–12). Understanding the molecular mechanisms of viral integration and its impact on cellular pathways is essential for developing targeted therapies and preventive strategies against virus-associated cancers.

Recent advances in genome sequencing methods have significantly enhanced the detection of viral integration events in tumor genomes. Whole Genome Sequencing (WGS) provides a comprehensive view of the entire tumor genome and allows for the identification of viral integration sites across the genome (3, 13–15). Capture sequencing involves the enrichment of viral sequences and their adjacent host sequences before sequencing, which is highly effective for detecting viral integration sites and mapping the integration landscape with high sensitivity and specificity (14, 16, 17). The development of long-read sequencing technologies offers the advantage of reading longer DNA fragments, which can span entire integration sites and provide more accurate mapping of integration events (18–21). This method is particularly useful for resolving complex integration events and structural variations.

Additionally, tools such as isling (22) and Vseq-Toolkit (23) have been developed for viral integration analysis, along with other tools benchmarked in these studies, providing a foundation for comparative assessments.

Viral integration events are complex and require sophisticated algorithms to accurately detect and interpret insertion sites within the host genome (9). These events can vary significantly in their genomic context, integration frequency, and impact on gene regulation, necessitating specialized tools for comprehensive analysis (1, 3, 9, 14). Currently, most available tools for viral integration analysis are either standalone software or scripts requiring a high level of bioinformatics expertise to operate (24–26). These tools often demand substantial computational resources and can be challenging for researchers without advanced programming skills. Furthermore, effective visualization tools are lacking, which are essential for interpreting the results of viral integration studies, allowing researchers to explore integration sites, their genomic contexts, and potential effects on gene expression and genome stability.

The absence of user-friendly, web-based platforms limits accessibility and hinders the widespread adoption of viral integration studies in the broader research community. To address this, we have developed virusPlot, an all-in-one analysis and visualization software. Key features of virusPlot include the automatic retrieval of virus genome sequences and annotation information, a visualization tool that represents viral integration events by connecting integration sites in the host genome with corresponding positions in the viral genome, and virus integration hotspot analysis using Fisher's exact test to help identify possible integration hotspot regions. Importantly, virusPlot integrates all these functions into an interactive web platform via shinyapp, expanding accessibility to users without technical or computational skills. The integration of interactive, web-based visualization tools can significantly enhance the ability to communicate findings, generate hypotheses, and facilitate collaborative research.

# 2 Methods and functions

We have developed virusPlot, an R package that offers a comprehensive suite of tools for analyzing and visualizing virus integration into the host genome. The user interface and back-end of virusPlot are built using Shiny. Analysis results are displayed on the web page and can be downloaded in various formats, including PDF, PNG, EPS, TXT, and HTML (for more details, refer to the website help pages). The workflow and typical output schema are illustrated in Figures 1–4. Detailed functions and operations for each module are described below.

## 2.1 Automatic retrieval of virus genome

The virusPlot package includes two key functions for retrieving virus genome data: get_virus_genom and get_virus_annotation. The get_virus_genom function automates the process of obtaining viral genomic sequences from the National Center for Biotechnology Information (NCBI) database. By leveraging NCBI's extensive repository, this function provides users with accurate and up-to-date viral sequences for their research. Complementing this, the get_virus_annotation function retrieves gene annotation information for the obtained viral genomes, which is essential for understanding the functional roles of various viral genes and their potential impact on the host organism.

## 2.2 Quality control

To ensure the robustness of the input data analysis, we have incorporated a rigorous quality control mechanism. This mechanism allows users to apply filters based on two adjustable parameters: minimum read number and p-value threshold. For example, users can set a minimum read number (e.g., ≥10 reads) to exclude low-confidence breakpoints supported by insufficient reads, and a p-value threshold (e.g., $p < 0.05$) to ensure statistical significance. These parameters can be fine-tuned based on the specific characteristics of the dataset, such as sequencing depth or experimental design.

We have observed that adjusting these parameters has distinct effects on the dataset:

- Increasing the minimum read number threshold improves the confidence of the retained breakpoints but may reduce

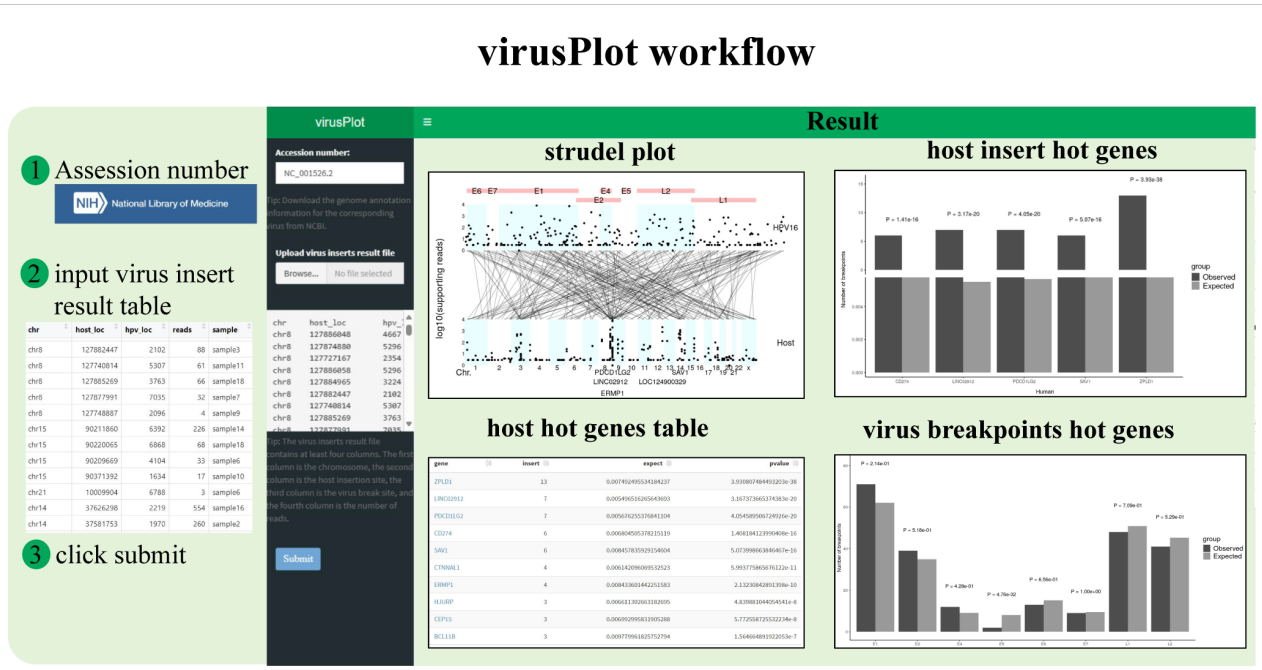


FIGURE 1
Screenshot of the virusPlot web tool. This package encompasses four main functionalities: (i) Automatic retrieval of virus genome information, (ii) Virus integration information visualization, (iii) Virus integration hot spots analysis, hot spots refer to genes with a statistically significant number of viral integration events, identified using Fisher's exact test or Chi-square test, and (iv) a user-friendly web application interface (shinyapp).

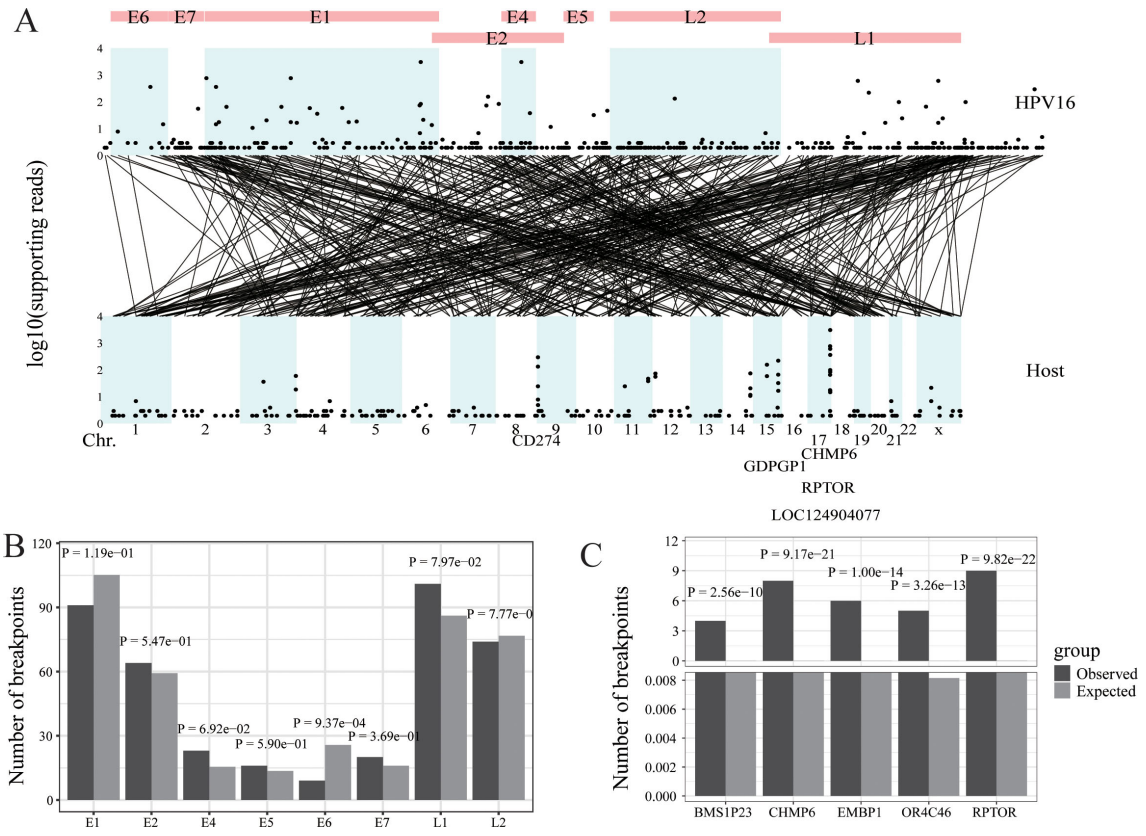


FIGURE 2
HPV integration in oropharyngeal cancer. **(A)** Strudel plot of HPV16 integration information. **(B)** The HPV16 integration hotspot analysis of the HPV16 genome. **(C)** The HPV16 integration hotspot analysis of the host genome.

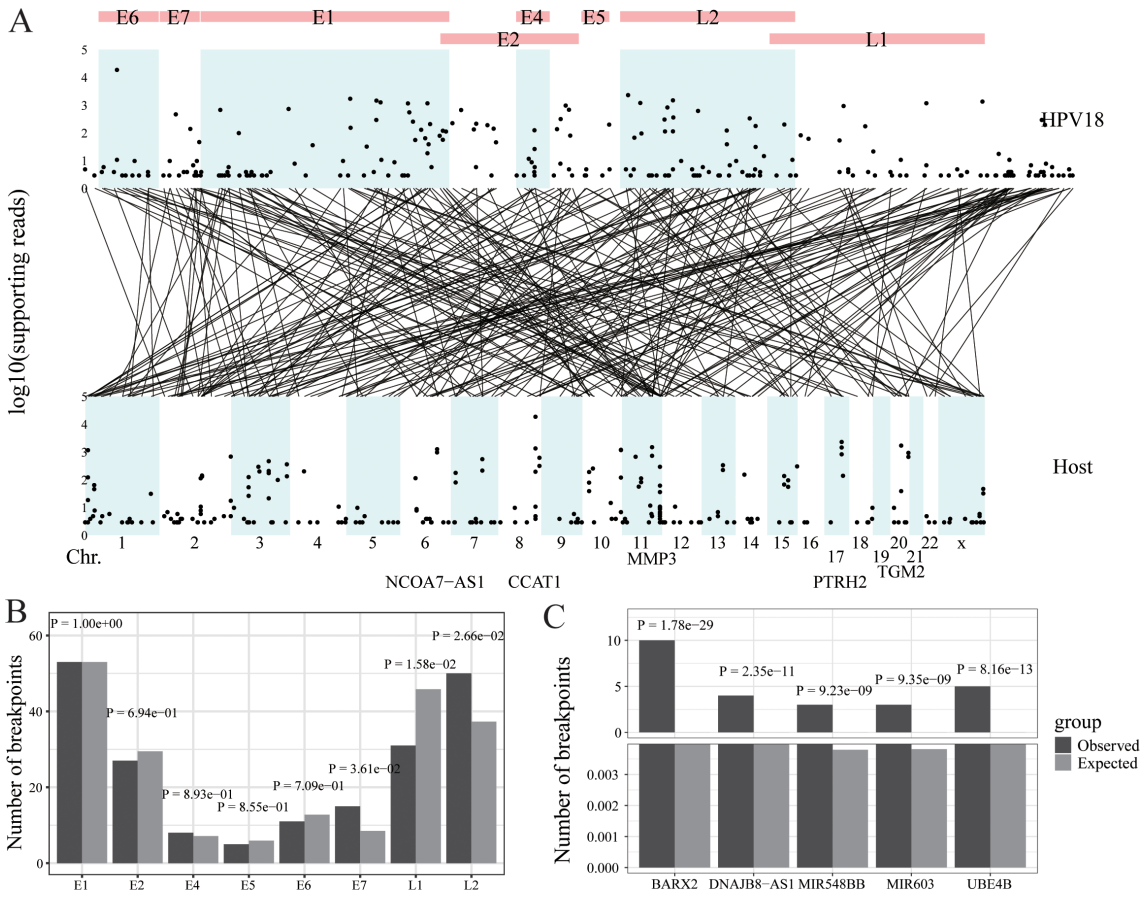


FIGURE 3
HPV integration in cervical cancer. **(A)** Strudel plot of HPV18 integration information. **(B)** The HPV18 integration hotspot analysis of the HPV18 genome. **(C)** The HPV18 integration hotspot analysis of the host genome.

the overall number of breakpoints available for downstream analysis.

- Tightening the p-value threshold enhances statistical rigor but might exclude potentially relevant breakpoints with weaker statistical signals.

## 2.3 Virus integration information visualization

A novel visualization approach, the strudel plot, has been developed within the virusPlot package to graphically represent the complex integration patterns of viruses within host genomes. The strudel plot is a multi-faceted structure that effectively displays integration sites, viral genome breakpoints, and the correspondence between host integration sites and viral breakpoints. The plot is organized into five distinct components:

I. Viral Genome Retrieval: Presents the sequence and annotated information of the viral genome.
II. Viral Integration Sites: Illustrates the positions of viral integration sites along with the number of associated reads.
III. Integration Breakpoints: Maps the breakpoints in both the viral and host genomes.
IV. Host Integration Sites: Shows the positions of integration sites in the host genome along with their respective read counts.
V. Host Gene Hotspots: Identifies the host genes that are hotspots for viral integration.

VirusPlot analyzes viral integration breakpoints irrespective of the completeness of the viral genome at the site. The analysis supports both forward and reverse orientations of the virus and incorporates rearranged fragments by identifying and visualizing integration breakpoints on both the viral and host genomes.

## 2.4 Virus integration hot spots analysis

Viral integration hotspots are pivotal for comprehending virus-induced cancer mechanisms and for devising targeted therapies and preventive strategies. Identifying these hotspots holds promise for

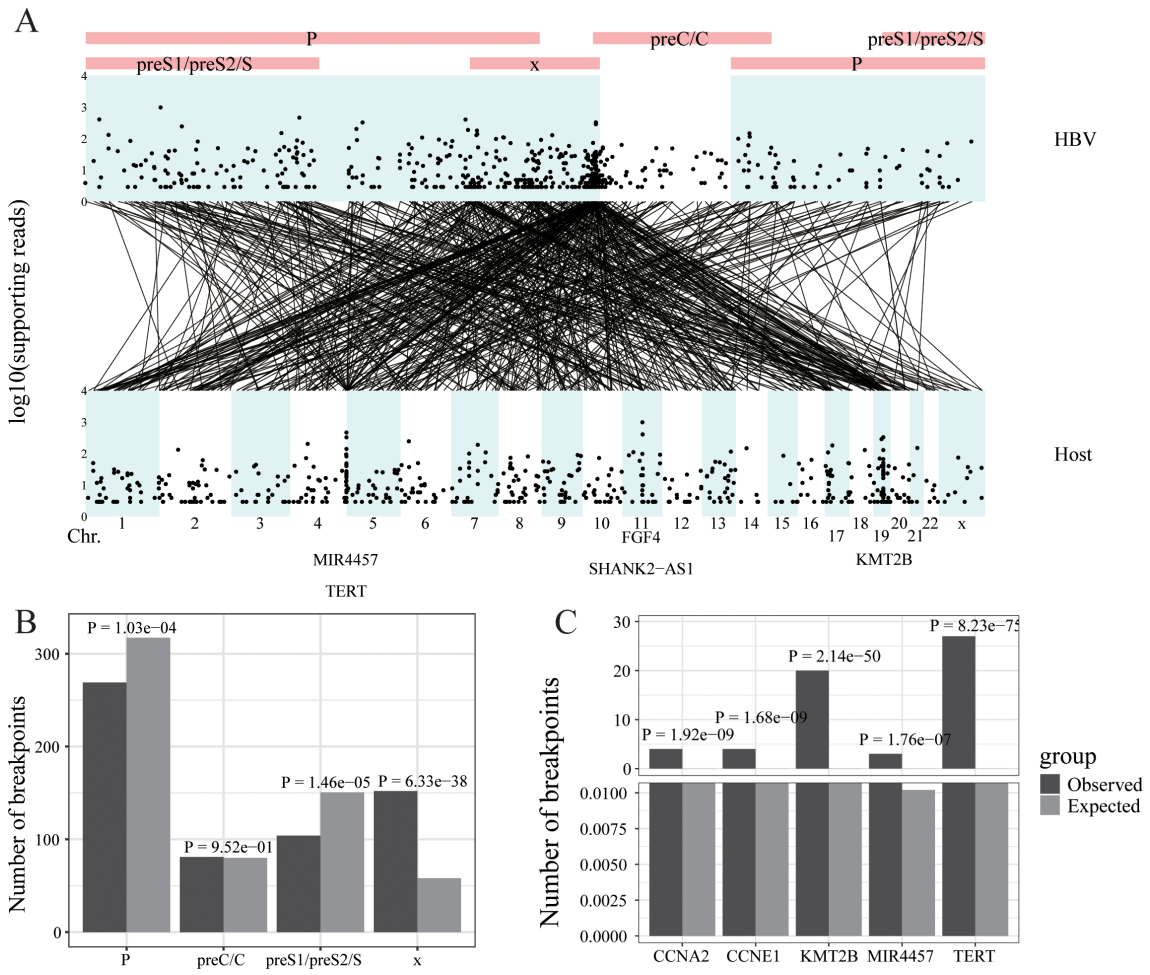


FIGURE 4
HBV integration in liver cancer. **(A)** Strudel plot of HBV integration information. **(B)** The HBV integration hotspot analysis of the HBV genome. **(C)** The HBV integration hotspot analysis of the host genome.

early detection, prognostic insights, and personalized treatment approaches. In the virusPlot package, a robust analysis tool is included for detecting viral integration hotspots within the host genome. A gene is identified as a potential hotspot if the observed number of integration sites significantly exceeds the expected count by chance. This comparison, facilitated by both Fisher's exact and chi-square tests, offers valuable insights into the preferential integration patterns of viruses, critical for deciphering viral persistence mechanisms and pathogenesis. The expected number of integration sites for each genomic region was calculated as follows:

$$\text{Excepted count} = \text{Total observed integrations} \times \frac{\text{Region size (bp)}}{\text{Total genome size (bp)}}$$

Statistical significance was determined using Fisher's exact test and Chi-square test by comparing the observed and expected counts. The p-value threshold for significance was set at 0.05.

The web-based version of VirusPlot processes viral integration data using the hg38 human genome assembly by default. For users of the R package version, the genome assembly can be customized by specifying the TxDb parameter in functions such as get_hot_gene and strudel_plot. This flexibility allows users to work with data aligned to different genome versions, ensuring compatibility with their specific datasets and annotations.

## 2.5 A user-friendly web application interface

To make virusPlot widely accessible and easy to use, we've integrated a shinyapp, providing a user-friendly web interface for accessing all features without the need for coding. This web app simplifies operations, requiring no local setup or specific hardware, as all computations are cloud-based, ensuring compatibility across different systems. Through practical case studies using our own data and published HPV and HBV integration data in various cancers

(i.e., oropharyngeal cancer, cervical cancer and hepatocellular cancer) (Figures 2–4), virusPlot has proven effective in displaying integration sites and identifying hotspots, underscoring virusPlot's utility in simplifying the complex analysis of viral integration and providing valuable insights into the genomic alternations and regulatory disruptions associated with virus-related cancers.

### 2.6 A data security and privacy

VirusPlot employs multiple measures to ensure the security of user data. All data transfers between the user and the server are encrypted using HTTPS. Uploaded data is processed in-memory without being stored permanently on the server, and all data is automatically deleted upon completion of the analysis. The server is hosted on a secure platform with firewalls and regular updates to protect against vulnerabilities.

## 3 Case study

### 3.1 HPV integration in oropharyngeal cancer (Data in this study)

Whole Exome & HPV capture sequencing (WEHS) was performed on 20 head and neck cancer samples. We used the Survirus software (24) to detect HPV16 integration information. This analysis revealed 471 integration sites and 13,007 reads encompassing these sites. The viral integration sites were evenly distributed throughout the HPV16 genome but concentrated in specific chromosomal regions of the host genome, such as chr17, chr9, and chr15. The five genes with the highest number of viral read insertions were CHMP6, RPTOR, LOC124904077, CD274, and GDPGP1 (Figure 2A). Regarding the HPV16 genome, fewer integration sites were observed in the E6 gene compared to random occurrences, while no significant differences were noted for other genes, and no hotspot integration genes were identified (Figure 2B). In the host (human) genome, several hotspots for HPV16 insertion were identified, including BMS1P23, CHMP6, EBMP1, OR4C46, and RPTOR, compared to random occurrences (Figure 2C).

### 3.2 HPV integration in cervical cancer

Ma's Lab conducted DNA sequencing on 39 cervical cancer samples collected from Tongji Hospital in Wuhan and Jingmen No. 2 People's Hospital in Hubei Province, China, between 2007 and 2014 (14). Exfoliated cervical epithelial cells were collected using cervical brushes. The high-throughput Viral Integration Detection (HIVID) (27) was then applied to these samples to detect HPV18 integration information. This analysis identified 241 integration sites and 48,603 reads including these sites. The viral integration sites were evenly distributed across the HPV18 genome and concentrated in specific chromosomal regions of the host genome, such as chr8, chr11, and chr17. The five genes with the highest number of viral read insertions were CCAT1, PTRH2, TGM2, MMP3, and NCOA7-AS1 (Figure 3A). In the HPV18 genome, the actual number of integration sites in the E7 and L2 genes was significantly higher than random, indicating hotspots for integration, while the L1 gene had significantly fewer integration sites than random (Figure 3B). In the host (human) genome, multiple hotspots for HPV18 insertion were identified, including BARX2, DNAJB8-AS1, MIR548BB, MIR603, and UBE4B, compared to random occurrences (Figure 3C).

### 3.3 HBV integration in liver cancer

Wang's Lab performed DNA sequencing on 138 hepatocellular carcinomas (HCCs) collected at the Eastern Hepatobiliary Surgery Hospital in Shanghai from 2009 to 2010 using high-throughput viral integration detection (HIVID) method (28). This analysis identified 546 integration sites and 13,242 reads encompassing these sites. The reads containing viral integration sites were primarily concentrated in the X gene of the HBV genome and on chromosomes chr5, chr11, and chr19 of the host genome. The five genes with the highest number of viral read insertions were MIR4457, TERT, FGF4, SHANK2-AS1, and KM12B (Figure 4A). Regarding the HBV genome, the actual number of integration sites in the X gene was significantly higher than random, indicating hotspots for integration, whereas the PreS1/PreS2/S and P genes had significantly fewer integration sites than random (Figure 4B). In the host (human) genome, multiple hotspots for HBV insertion were identified, including TEAR, KMT2B, CCNE1, CCNA2, and MIR4457, compared to random occurrences (Figure 4C).

## 4 Discussion

The virusPlot platform offers a comprehensive suite of tools and workflows designed to simplify the analysis and visualization of viral integration events within host genomes. Serving as an visualization solution, virusPlot streamlines the process of identifying integration hotspots and understanding the impact of viral integration on cancer development. With its intuitive interface, virusPlot enables researchers, including experimental biologists without computational programming skills, to explore complex viral integration patterns and gain valuable insights into virus-associated cancers. By integrating multiple analytical approaches and statistical tests, virusPlot enhances the analysis of viral integration data, complementing traditional methods and enabling more comprehensive investigations. As sequencing methods continue to evolve and become more cost-effective, an increasing number of viral-associated cancers and viral integration events are expected to be uncovered (1, 20). This expanding dataset of viral-related cancer genomes and integration sites will provide valuable insights into the role of viruses in oncogenesis and facilitate the development of targeted therapies and preventive strategies against virus-associated cancers. We are committed to maintaining the virusPlot platform and continuously updating it with new data

and methods, ensuring its relevance and utility for the research community over the coming years. Through its user-friendly interface and powerful analytical capabilities, virusPlot aims to accelerate discoveries in viral oncology and facilitate the identification of novel cancer pathways and therapeutic targets.

To evaluate the usability of VirusPlot, we compared it with other visualization tools commonly used for integration data, such as Circos (29). Users reported that VirusPlot's interactive interface significantly reduced the complexity of generating visualizations, compared to the manual configurations required by Circos. Furthermore, VirusPlot provides integration-specific features, such as the strudel plot and hotspot analysis, which are not available in these general-purpose tools. Additionally, the web-based accessibility of VirusPlot eliminates the need for local installations, making it a more user-friendly and efficient tool for analyzing viral integration data.

Future updates to virusPlot aim to expand its capabilities by including support for additional genomic data types, such as RNA-seq and long-read sequencing data. Planned features include new visualization tools, such as circular diagrams and VCF diagrams, which are currently under development. We also aim to integrate more advanced statistical modules to accommodate complex integration scenarios, such as those involving rearranged viral genomes.

## Data availability statement

Publicly available datasets were analyzed in this study. This data can be found here: https://github.com/huerqiang/virusPlot.

## Author contributions

SY: Methodology, Project administration, Software, Writing – original draft, Writing – review & editing. EH: Methodology, Software, Visualization, Writing – original draft, Writing – review & editing. JA: Writing – review & editing. AG: Writing – review & editing. NW: Writing – review & editing. NK: Writing – review & editing. JZ: Writing – review & editing. GR: Writing – review & editing. SA: Writing – review & editing. RS: Writing – review & editing. JS: Writing – review & editing. HO: Writing – review & editing. AA: Writing – review & editing. CC: Writing – review & editing. MP: Writing – review & editing. TO: Writing – review & editing. WD: Project administration, Writing – review & editing.

## Funding

The author(s) declare that financial support was received for the research, authorship, and/or publication of this article. This work was in part supported by NIH R01CA291607 (SY), R21 CA267527-01 (SY), the Feldstein Medical Foundation grant (SY), R01INS134819 (WD), Fundings from the Moffitt Cancer Center and State of Florida (AA).

## Conflict of interest

WD and SY hold equity in Yihui Bio, Inc. AA is a Global Advisory Board member and paid consultant for LG Chem Life Sciences Innovation Center.

The remaining authors declare that the research was conducted in the absence of any commercial or financial relationships that could be construed as a potential conflict of interest.

The author(s) declared that they were an editorial board member of Frontiers, at the time of submission. This had no impact on the peer review process and the final decision.

## Generative AI statement

The author(s) declare that no Generative AI was used in the creation of this manuscript.

## Publisher's note



## References

1. Ye R, Wang A, Bu B, Luo P, Deng W, Zhang X, et al. Viral oncogenes, viruses, and cancer: A third-generation sequencing perspective on viral integration into the human genome. *Front Oncol*. (2023) 13:1333812. doi: 10.3389/fonc.2023.1333812

2. Zapatka M, Borozan I, Brewer DS, Iskar M, Grundhoff A, Alawi M, et al. The landscape of viral associations in human cancers. *Nat Genet*. (2020) 52:320–30. doi: 10.1038/s41588-019-0558-9

3. Akagi K, Li J, Broutian TR, Padilla-Nash H, Xiao W, Jiang B, et al. Genome-wide analysis of hpv integration in human cancers reveals recurrent, focal genomic instability. *Genome Res*. (2014) 24:185–99. doi: 10.1101/gr.164806.113

4. Lechner M, Liu J, Masterson L, Fenton TR. Hpv-associated oropharyngeal cancer: epidemiology, molecular biology and clinical management. *Nat Rev Clin Oncol*. (2022) 19:306–27. doi: 10.1038/s41571-022-00603-7

5. Arzumanyan A, Reis HM, Feitelson MA. Pathogenic mechanisms in hbv- and hcv-associated hepatocellular carcinoma. *Nat Rev Cancer*. (2013) 13:123–35. doi: 10.1038/nrc3449

6. Young LS, Yap LF, Murray PG. Epstein-barr virus: more than 50 years old and still providing surprises. *Nat Rev Cancer*. (2016) 16:789–802. doi: 10.1038/nrc.2016.92

7. Matsuoka M, Jeang KT. Human T-cell leukaemia virus type 1 (Htlv-1) infectivity and cellular transformation. *Nat Rev Cancer*. (2007) 7:270–80. doi: 10.1038/nrc2111

8. Williams VM, Filippova M, Soto U, Duerksen-Hughes PJ. Hpv-DNA integration and carcinogenesis: putative roles for inflammation and oxidative stress. *Future Virol*. (2011) 6:45–57. doi: 10.2217/fvl.10.73

9. Symer DE, Akagi K, Geiger HM, Song Y, Li G, Emde AK, et al. Diverse tumorigenic consequences of human papillomavirus integration in primary oropharyngeal cancers. *Genome Res*. (2022) 32:55–70. doi: 10.1101/gr.275911.121

10. Porter VL, Marra MA. The drivers, mechanisms, and consequences of genome instability in hpv-driven cancers. *Cancers (Basel)*. (2022) 14. doi: 10.3390/cancers14194623

11. Kang JJ, Yu Y, Chen L, Zakeri K, Gelblum DY, McBride SM, et al. Consensuses, controversies, and future directions in treatment deintensification for human papillomavirus-associated oropharyngeal cancer. *CA Cancer J Clin*. (2022). doi: 10.3322/caac.21758

12. Sabatini ME, Chiocca S. Human papillomavirus as a driver of head and neck cancers. *Br J Cancer*. (2020) 122:306–14. doi: 10.1038/s41416-019-0602-7

13. Cancer Genome Atlas N. Comprehensive genomic characterization of head and neck squamous cell carcinomas. *Nature*. (2015) 517:576–82. doi: 10.1038/nature14129

14. Hu Z, Zhu D, Wang W, Li W, Jia W, Zeng X, et al. Genome-wide profiling of hpv integration in cervical cancer identifies clustered genomic hot spots and a potential microhomology-mediated integration mechanism. *Nat Genet*. (2015) 47:158–63. doi: 10.1038/ng.3178

15. Muhr LSA, Guerendiain D, Cuschieri K, Sundstrom K. Human papillomavirus detection by whole-genome next-generation sequencing: importance of validation and quality assurance procedures. *Viruses*. (2021) 13. doi: 10.3390/v13071323

16. Pinatti LM, Gu W, Wang Y, Elhossiny A, Bhangale AD, Brummel CV, et al. Searchpv: A novel approach to identify and assemble human papillomavirus-host genomic integration events in cancer. *Cancer*. (2021) 127:3531–40. doi: 10.1002/cncr.33691

17. Liu Y, Lu Z, Xu R, Ke Y. Comprehensive mapping of the human papillomavirus (Hpv) DNA integration sites in cervical carcinomas by hpv capture technology. *Oncotarget*. (2016) 7:5852–64. doi: 10.18632/oncotarget.6809

18. Yang S, Zhao Q, Tang L, Chen Z, Wu Z, Li K, et al. Whole genome assembly of human papillomavirus by nanopore long-read sequencing. *Front Genet*. (2021) 12:798608. doi: 10.3389/fgene.2021.798608

19. Amarasinghe SL, Su S, Dong X, Zappia L, Ritchie ME, Gouil Q. Opportunities and challenges in long-read sequencing data analysis. *Genome Biol*. (2020) 21:30. doi: 10.1186/s13059-020-1935-5

20. Zhou L, Qiu Q, Zhou Q, Li J, Yu M, Li K, et al. Long-read sequencing unveils high-resolution hpv integration and its oncogenic progression in cervical cancer. *Nat Commun*. (2022) 13:2563. doi: 10.1038/s41467-022-30190-1

21. Yang W, Liu Y, Dong R, Liu J, Lang J, Yang J, et al. Accurate detection of hpv integration sites in cervical cancer samples using the nanopore minion sequencer without error correction. *Front Genet*. (2020) 11:660. doi: 10.3389/fgene.2020.00660

22. Scott S, Hallwirth CV, Hartkopf F, Grigson S, Jain Y, Alexander IE, et al. Isling: A tool for detecting integration of wild-type viruses and clinical vectors. *J Mol Biol*. (2022) 434:167408. doi: 10.1016/j.jmb.2021.167408

23. Afzal S, Fronza R, Schmidt M. Vseq-toolkit: comprehensive computational analysis of viral vectors in gene therapy. *Mol Ther Methods Clin Dev*. (2020) 17:752–7. doi: 10.1016/j.omtm.2020.03.024

24. Rajaby R, Zhou Y, Meng Y, Zeng X, Li G, Wu P, et al. Survirus: A repeat-aware virus integration caller. *Nucleic Acids Res*. (2021) 49:e33. doi: 10.1093/nar/gkaa1237

25. Baheti S, Tang X, O'Brien DR, Chia N, Roberts LR, Nelson H, et al. Hgt-id: an efficient and sensitive workflow to detect human-viral insertion sites using next-generation sequencing data. *BMC Bioinf*. (2018) 19:271. doi: 10.1186/s12859-018-2260-9

26. Zeng X, Zhao L, Shen C, Zhou Y, Li G, Sung WK. Hivid2: an accurate tool to detect virus integrations in the host genome. *Bioinformatics*. (2021) 37:1821–7. doi: 10.1093/bioinformatics/btab031

27. Li W, Zeng X, Lee NP, Liu X, Chen S, Guo B, et al. Hivid: an efficient method to detect hbv integration using low coverage sequencing. *Genomics*. (2013) 102:338–44. doi: 10.1016/j.ygeno.2013.07.002

28. Zhao LH, Liu X, Yan HX, Li WY, Zeng X, Yang Y, et al. Genomic and oncogenic preference of hbv integration in hepatocellular carcinoma. *Nat Commun*. (2016) 7:12992. doi: 10.1038/ncomms12992

29. Krzywinski M, Schein J, Birol I, Connors J, Gascoyne R, Horsman D, et al. Circos: an information aesthetic for comparative genomics. *Genome Res*. (2009) 19:1639–45. doi: 10.1101/gr.092759.109

# Frontiers in Oncology

**Advances knowledge of carcinogenesis and tumor progression for better treatment and management**

The third most-cited oncology journal, which highlights research in carcinogenesis and tumor progression, bridging the gap between basic research and applications to imrpove diagnosis, therapeutics and management strategies.

---

## Discover the latest Research Topics

See more →


**Frontiers**

Avenue du Tribunal-Fédéral 34
1005 Lausanne, Switzerland
frontiersin.org

**Contact us**

+41 (0)21 510 17 00
frontiersin.org/about/contact